Elsevier Editorial System(tm) for Gondwana Research
Manuscript Draft

Manuscript Number: GR-D-19-00418R1

Title: Long-lived, Eocene-Miocene stationary magmatism in NW Iran along a transform plate boundary

Article Type: Research Paper

Corresponding Author: Dr. Federico Rossetti,

Corresponding Author's Institution: Università di Roma Tre

First Author: Ahmad Rabiee

Order of Authors: Ahmad Rabiee; Federico Rossetti; Yoshihiro Asahara; Hossein Azizi; Federico Lucci; Michele Lustrino; Reza Nozaem

Abstract: The Eocene-Miocene Mianeh-Hashtroud igneous district in NW Iran is part of the Turkish-Caucasus-Iranian collision zone, a key region to decipher the assembly and differentiation of Gondwana-derived terranes along the Alpine-Himalayan convergence zone. Major inherited tectonic structures control in space and time the Mesozoic-Cenozoic transition from oceanic subduction to continental collision in the region. The geology of the study area is dominated by a polyphase, long-lived magmatic activity, spanning from ~45 to ~6 Ma. The igneous products are subalkaline to alkaline, with intermediate to acidic compositions and a high-K calcalkaline to shoshonitic affinity. Evidence of crustal contamination is attested by inherited zircons in the oldest (Eocene-Oligocene) samples, with ages spanning from Neo-Archean to Paleocene. The Sr-Nd isotopic compositions of the Eocene-Oligocene samples plot close to the Bulk Silicate Earth estimate, whereas the Miocene samples document stronger crustal contamination. The lack of correlation between Nd-Sr isotopes and SiO2 supports a scenario of magma differentiation of different magma batches rather than crustal contamination. Major oxide and Sr-Nd isotopic variation lead us to suggest that magmatism is the consequence of re-melting of earlier underplated (Mesozoic-Tertiary) magmatic products, controlled by amphibole-dominated fractionation processes. Regional scale correlations show long-lived Cenozoic magmatism in NW Iran and Caucasus region, where the main porphyry and epithermal deposits occur. We propose that the Cenozoic collisional magmatism and the associated mineralisation at the junction between NW-Iran and Caucasus was controlled by the activity of a major, lithosphere-scale inherited boundary, transverse to the convergence zone. In such a geodynamic setting, the along-strike segmentation of the lithosphere slab generated asthenospheric melts, their upwelling into the metasomatised supra-subduction mantle wedge and the potential activation of different mantle and crustal sources, with consequent mineral endowment in the region.

Response to Reviewers: Roma, March 15 2020

To: Prof. A. Festa , Editor Gondwana Research

Submission of the revised version manuscript entitled "Long-lived, Eocene-Miocene stationary magmatism in NW Iran along a transform plate boundary" by Ahmad Rabiee, Federico Rossetti, Yoshihiro Asahara, Hossein Azizi, Federico Lucci, Michele Lustrino, Reza Nozaem.

Dear Editor, please find attached the revised version of our manuscript submitted for possible publication in Gondwana Research.

The three reviewers provided constructive comments and remarks that greatly contributed to improve the manuscript. We have carefully followed the reviewers' advice and comments to prepare this revised version. Before presenting the detailed responses to the reviewers' comments, we inform that in order to adapt this revised version to the reviewers' suggestions, we added new materials to the early submitted typescript. These include:

1. Supplementary materials S1: Table of main characteristics of selected porphyry deposits along UDMZ (Iran) and Armenia.
2. Supplementary materials S3: Details of Zircon U-Pb geochronology (zircon characteristics and each analysis).
3. Supplementary materials S4: Probability density and weighted age plots of measured zircons from all collected samples from Mianeh-Hashtroud area.
4. A new Fig. 13a to better support the continues magmatism during the Eocene-Miocene time lapse in the study area;
5. A new 3D petrogenetic model (Fig. 16), where we propose a synthetic geodynamic scenario for the Cenozoic evolution of the Turkish-Iranian-Caucasus collisional boundary and associated magmatism.

Below we provide a point-by-point response to the reviewers' comments and illustrate how these major changes are integrated in the revised version. In the following, the response are typed in italics. Changes in the original text are typed in red to allow tracking the changes. Reference to the text pages refers to the uploaded revised Word file.

Reviewer #1:
One point which could be enhanced in the petrologic model concerns the quantification of crustal contamination. Evidence of crustal contamination is 'attested by inherited zircons', while Miocene samples document a 'stronger crustal contamination' than Oligocene ones. However, the amount of crustal contamination has not be quantified using mixing curves, which the authors could probably have attempted. Can the authors precise that point?
Authors' answer: We have modified the interpretation of our data, reducing the necessity to invoke any strong crustal contamination. A careful check of Sr-Nd isotopic data as well as the overall incompatible element content of Miocene samples do not require any substantially higher degree of interaction with typical upper crustal rocks.
Reviewer #1: Minor comments in the text.
Authors' answer: All comments have been fixed.

Reviewer #2 (H. Rezeau) general comments
H. Rezeau: The authors describe 26 samples, including 12 samples dated from 44.32 Ma to 5.93 Ma covering a total magmatic duration of almost 40 Myr. However, it is not clear how the authors distinguish the undated samples between Eocene, Oligocene and Miocene since the whole-rock geochemistry overlap significantly, especially for Oligocene and Eocene rocks. In addition, the authors claim a continuous magmatism, which I would rather interpret as pulsed magmatism. Indeed, when I look at the

zircon mean age (Fig. 7), there is no obvious continuity/overlapping in age from 44 Ma to 5 Ma, but it rather illustrates snapshot of magmatic pulses at 44-43 Ma, 40-36 Ma, 30-26 Ma, 22 Ma , 14 Ma and 5 Ma. Therefore, I question the co-genetic relationship of these intrusions, which is not fully addressed by the authors in the present manuscript. I rather understand that they use the similar whole-rock geochemistry to propose a similar petrogenetic model for all the rocks emplaced in the Mianeh-Hashtroud study area. However, published study in central to NW Iran and Lesser Caucasus generally demonstrate the evolution of petrogenetic processes through time from the Eocene to Miocene (e.g., Castro et al., 2013; Shafiei et al., 2009; Moritz et al., 2016; H. Rezeau et al., 2017). I encourage the author to reconsider this point because it will significantly improve the strength of the manuscript.
Authors' answer:
Regarding the undated samples
We carried out an extensive field work in the studied area, which results in the production of the geological map shown in Fig. 3, where the different textural and geometrical relationships among intrusive and volcanic rocks are reported. We paid attention to conduct a comprehensive sampling of all the different magmatic rock types, avoiding repeated sampling for geochronology. We are thus confident regarding the relative age estimation of undated samples based on the field relationships, cross cutting relationships and the correlation on rock texture (from coarse- to fine-grained, porphyritic and vitrophyric) within the different magmatic groups (intrusive, hypabyssal and volcanic). For example, the Eocene intrusive rocks show always a granular texture, while the Oligocene rocks are always porphyritic. Regarding Miocene samples, we have only three samples, two of which were dated. The two dated samples are similar each other and are similar to other neighbouring dykes (samples MN05 and MN07).
Regarding the continuity/overlapping in age from 44 Ma to 5 Ma
To answer to the reviewer criticism, we re-organised the text of Section 6, leaving just the necessary info and moving the detailed description of the samples to the Supplementary Material S2-S4. The criteria for age calculation, including categorisation of the zircon types (autocrysts, antecrysts, and xenocrysts/inherited; after Miller et al., 2007) is now provided in Appendix A1 and illustrated for the cumulative samples as probability density plots and weighted mean ages in Supplementary material S4. To better document the continuity of magmatism we prepared a new figure (Fig. 13a), where we present the weighted age distribution of the dated zircons (autocrysts and antecrysts). Based on the age distribution (with 2σ uncertainty) there is a continuous range from ca. 55 (54.8±2.8 Ma) to at least 12 Ma and the magmatism resumes at ~8 Ma. this evidence is consistent with published ages from the Sahand volcano (Richards et al., 2006; Sawada et al., 2016; Lechman et al., 2018).
Regarding the co-genetic relationship of the studied magmatic products
Despite the presence of inherited zircon crystals with ages as old as Proterozoic, the Sr-Nd isotopic ratios of the investigated rocks is surprisingly homogeneous. This feature is increasingly interesting considering the diffuse chemical alteration of the samples (despite we selected only the freshest rocks for whole rock composition) and the wide chemical range of compositions (with SiO2 spanning over ~30 wt% variation). To sum up, the overall similar mineral paragenesis, the common primitive mantle incompatible element-normalized patterns and the restricted variability of Sr-Nd isotopic ratios led us to support to a co-genetic origin among the different magma batches.
H. Rezeau: The classification of the rocks investigated in this study is a main issue for me. The authors use many different ways to name/classify

them (i.e., volcanic rocks, intrusions, hypabyssal, country rocks, Eocene rocks, Oligocene rocks, Miocene rocks, Late Miocene-Quaternary rocks), which make it extremely difficult to follow for the reader. In addition, the authors do not differentiate volcanic from plutonic rocks in the whole-rock geochemistry results neither in the geochemical plots, which is not correct to me. The authors should use the appropriate classification scheme for volcanic and intrusive rocks, and name the rocks accordingly. They should also distinguish the different type of rocks by using two different symbols in the geochemical plots. In the text, I suggested a way to name/describe the rocks, which would help the reader to follow. I think this is a major issue in the present manuscript, which could be easily fixed before resubmission.
Authors’ answer: We agree with the reviewer about the confusion present in the previous version. Following the reviewer's advice, we have modified section 5 to have a consistent nomenclature throughout the text. The rationale in the petrography section (section 5) has been conceived to present the different rock types based on the field evidence that is synthesised in the geological map of the area shown in Fig. 3. It is worth noting that the studied igneous rocks are emplaced within Eocene volcanic country rocks. We would thus maintain the classification separating plutonic, hypabyssal and volcanic rock types (see also answer to the above point) with respect to the Eocene country rocks. We classify the samples based on their ages, since the geochemical fingerprint within the same age group is overlapping, irrespective of the rock type (either intrusive or volcanic).
H. Rezeau: The authors present a “Field and Petrographic observations” section, however they barely (if not at all) refer to it nor use it in the discussion. Petrographic observations provide important information about the sequence of mineral crystallization, which inherently depends on the melt chemistry from which they crystallize. Therefore, I think it is a pity to not take advantage of it. I have provided some detailed comment directly in the attached manuscript about it and how the author could use some observations in the discussion. If the authors do not use it in the discussion, I am questioning the necessity to include a petrography section if it is not relevant for the discussion.
Authors’ answer: The petrographic section is reduced to the essential description of the investigated rocks (see the new section 5). We propose the involvement of specific mineral phases during a fractional crystallization process only qualitatively drafted in the manuscript (due to the not perfect preservation state of the Mianeh samples). Petrography, coupled with geochemistry and geochronology of the investigated rocks and neighbouring Cenozoic magmatism are used to constrain the geodynamic environment of formation. Therefore, although we agree with the reviewer, the description of the sequence of mineral crystallisation is a bit out of the scope of the present manuscript.
H. Rezeau: Regarding the general geodynamic regional model and its implications for the petrogenesis of the investigated magmatic rocks, the authors use broad general geodynamic models from the literature with no proper evidence to support it from their own data. Even if I am not against the proposed scenario, I encourage the authors to be more careful in addressing their model as well as discussing alternative models too. They should rearrange the discussion and reconsider the way they discuss their data with respect to the regional geodynamic evolution. In the present version of the manuscript, I do not see compelling evidence from the data presented in this study to support the final proposed model. Structural field evidence along with geochemical data would be a good combination to support the proposed model.

Authors' answer: We thank the reviewer of his comment that offer us the opportunity to propose a geodynamic reconstruction with a greater detail (see new Fig. 16). We also agree that a more focused discussion on the geodynamic scenario was necessary. Therefore, we revised the relevant discussion on these themes (see the new section 10). We agree that structural data would be a good addition to the data set, but, unfortunately, the large volcanic cover in the area prevents direct field observations on the main deformation structures and feeding zones. However, we are confident that after the exhaustive literature review presented in section 2 and correlation at regional scale, the tectonic/geodynamic scenario to frame the Cenozoic magmatic evolution in the region is quite well constrained. In particular, the inherited structures (transversal from the collisional boundary) provided long-lasting weak zones for magma ascent and accumulation from Eocene to Miocene. Since these structures are likely inherited from a major transform zone (e.g., Barrier and Vrienlink, 2018; Van der Boon et al., 2018; Rolland et al., 2017), we suggest the presence of slab tearing and slab window during the Cenozoic, which provided asthenospheric flow and heat able to generate the long-lasting and almost homogeneous magmatism during Eocene and Oligocene. During Miocene the collision event and thickening changed the geodynamic setting, but the new magma still was able to ascent to this weak zone. These ideas are depicted in the conceptual geodynamic scenario presented in the new Fig. 16.
H. Rezeau: The calculated zircon U-Pb mean ages are presented in Fig. 7 along with the Concordia diagrams generated using Isoplot. For some samples, I can see a spread in ages over 2-4 Ma. The calculation of the weighted mean age is not described in the methods, although the notion of autocrysts and antecrysts is mentioned is the manuscript. It is very important to describe the criteria you have used to include or reject a single measurement from the weighted mean age calculation. I know that Isoplot can do it automatically for you, but I would advise to use a density probability plot to identify one or several sub-population(s) of zircons within sample. This will allow you to select on the youngest family to calculate the crystallization age, generally assumed to be represented by the youngest population. You can include such plots in the supplementary material along with zircon CL images for each sample, which will avoid any question from the readers regarding the calculation of the weighted mean ages used in this study. Furthermore, I also request a plot of the weighted mean age with uncertainties (2s) to illustrate the continuous magmatism versus pulsed magmatism in the area. If the authors agree with my comments, I am sure that it will significantly improve the manuscript and help them to clearly address the temporal magmatic history of the Mianeh-Hashtrood study area.
Authors' answer: We thank the reviewer for his comment that is fully pertinent and offer us the possibility to better explain the scientific rationale adopted on the U-Pb geochronology. We did not use weighted mean age calculation. Since this method does not eliminate some zircon antecrysts, which their ages clearly are out of normal distribution in histogram plots and the probability of the calculated ages are below 0.1 in most of the samples (see supplementary Material S4). Instead we chose the best concordant results in a continuous range, preferably for Concordia age calculation. In particular, zircons results with Pb common should be <20% and Th/U >0.1 were used to calculate Concordia age. To calculate the Concordia ages for some samples (when available), only concordant ages were used. The maximum numbers of datasets in a continuous sorted population (excluding outlier values) which were acceptable by Isoplot to calculate a Concordia age were considered. In the cases where most of ages were discordant (mainly due to Pb common

>5%) the Terra-Wasserburg method was used which provide more reliable ages. For instance, in sample MN76 we eliminated 4 younger and 2 older zircons which are clearly out of the main population. for samples MN10 we only used 18 zircons to be able to provide a Concordia age while the weighted mean average method uses 28 out of 31 dataset but the calculated age is less accurate (MSWD=2.6 , probability =0.000).
Following the Reviewer's advice, we specified the criteria for age calculation, including categorisation of the zircon types (autocrysts, antecrysts, and xenocrysts/inherited; after Miller et al., 2007) that is provided in Appendix A1 and illustrated for the cumulative samples as probability density plots and weighted mean ages in Supplementary material S4. We also prepared a new figure (Fig. 13a), reporting the weighted age distribution of the dated zircons (autocrysts and antecrysts) to better document the continuity of magmatism.
H. Rezeau: In the abstract, at the end of the introduction and in the last section of the discussion, the authors mention briefly the notion of mineral deposits. I am not quite sure why the authors briefly mention it here and there. This is poorly described and also not discussed at all. I would either recommend to clearly describe and stress its importance in the area and then discuss it, or completely remove it from the manuscript.
Authors’ answer: We thank the reviewer for his comment. Following the reviewer's advice, we have expanded the description of the main ore zones in the region (see new section 3 and lines 223-265) Moreover, the new Fig. 2 now contains the distribution of the main porphyry mineralization. A Table is now provided in Supplementary Material S1, showing the characteristics of each deposit. Our main scope is not the metallogeny of the region but the linkage between the porphyry ore localisation with (i) the major tectonic structures, and (ii) the peculiar geodynamic setting we propose. In particular, we propose the Eastern Caucasus-Western Iran Boundary as a long-lived tectonic structure, which acted as a weak zone susceptible to multiple tectonic reactivation, able to focus magmatism as a preferred pathway for magma ascent and emplacement and focused mineralisation during Eocene-Miocene times.
H. Rezeau: I don’t see this abrupt transition, I see similar colors (yellow, light and dark green) on each side of both fault. …..I am not sure what you want to show with the isotherm of the upper mantle, but I am not convinced about its relevance here. See also my comment on Fig. 1.
Authors’ answer: We have strongly modified Fig. 1, reporting the lithospheric thickness variation as reported in the same reference (Priestley et al., 2012). However, considering the continuation of Mianeh-Ardabil fault toward SW (see also Fig. 2), it is well evident that the trace of this fault zone corresponds to a SE-ward transition from thin to thick lithosphere in the region.
Other comments from H.H. Rezeau in the file
Line 47-51 (76-78): We have modified the sentence, following the reviewer’s suggestion.
Line 88: Do you refer to the Moho depth here? If yes, you should mention Shad Manaman et al., 2011 and Fig. 1b.
Authors’ answer: Here we are referring to lithosphere not to the Moho depth.
Lines 109-114: Fixed with additional materials. We also added relevant text in the discussion section and a new Figure.
Lines 157-164: Fixed.
Lines 208-210: We have modified the text following the reviewer’s suggestion.
Lines 267-282: Section 4: We have modified the section following the reviewer’s suggestion.

Lines 293-298: The Paragraph was revised, to avoid any confusion regarding roc classification.
Section 5.4. Here again volcanic rocks but you do not provide an age information. You should consider if you can merge it with 5.1 under volcanic rocks, and then make 2 distinct paragraphs for the Eocene ones and this one. Also why not calling the Eocene Group 1 and this one Group 2, instead of Eocene volcanic country rocks and volcanic rocks. I am sure it will help to clarify and avoid unnecessary subdivision. Same for Intrusions and hypabyssal, which could be merged under a "intrusive rocks" section with two distinct paragraphs, and maybe Group 1 and 2 as well based on the age or other features.
Section 5.2 to 5.4: These sections were modified following the reviewer's suggestion.
H. Rezeau: I would suggest to rearrange the Figure 4 in order to have the Fig.4d as a Fig. 4a, and then modify accordingly.
Authors' answer: Following the Reviewer's advice, we have modified the Figure. Please see the new version in the revised manuscript.
H. Rezeau: Section 6. This section is highly repetitive for each section with a lot of information ……
Authors' answer: We kept the most important features in the section and moved details in Supplementary Material S3.
H. Rezeau: Fig 7a and 7n: Very small and hard to see anything.
Authors' answer: Here we put this image to show examples of general characteristics of zircon autocrysts, antecrysts and inherited ones in CL images in which different categories are shown with distinct colored circles. A larger size is available in Supplementary Material S3
H. Rezeau: You don't show any CL images here, so why referring to Sup. Mat. Here?
Authors' answer: We showed two examples in the Fig. 7. However, we moved the details of this section to Supplementary materials S2 and S3.
H. Rezeau: How do you calculate U-Pb ages?
Authors' answer: We added additional materials on this regard in the Methods and Appendix. Please see also the authors' answer above in general comments.
H. Rezeau: you do not mention it in the method to explain how you calculate the weighted mean age of each sample. …..If you discard some antecryst from the calculation, you also should explain how which basis you decided to exclude them from the calculation of the weighted mean age.
Authors' answer: Please see the authors' answer to the same question above in general comments.
H. Rezeau: What are the evidence for lead loss using LA-ICP-MS technique? I am not convinced that we can accurately estimate lead loss using LA-ICP-MS technique, compared to ID-TIMS technique.
Authors' answer: Zircon structure is not so favorable to retain the radiogenic Pb. Therefore, Pb losses typically occur along cracks generated during dynamic deformation (and crushing). In addition, sometimes during the crushing and polishing, environmental Pb goes inside the existing fractures. Furthermore, chamber environment has some Pb common resulted from shooting to other grains rather than zircon which could cause contamination. In general, if the common Pb is above 20% the dataset would not be appropriate for the age calculation in the LA-ICPMS data. In our calculation, we excluded all datasets with common Pb above 20%.
H. Rezeau: late Miocene-QUATERNARY in diagrams.
Authors' answer: Fixed.
H. Rezeau: In figure 12, Nd-Sr data from H. Rezeau et al., 2017
Authors' answer: Sorry, Fixed.

H. Rezeau: Line 440; No igneous rocks can reach $SiO_2$>76-78 wt%....this high values must illustrate alteration or magmatic-hydrothermal melt/fluid (pegmatitic or something like this). Please check the rock with such high value and eventually remove it from the data set.
Authors' answer: We agree with the reviewer. Some of the Oligocene-early Miocene subvolcanic bodies are affected by secondary silicification. But we would prefer to use these data rather than giving away most of these samples. We have avoided additional comments on rocks with $SiO_2$ >78 wt% and we didn't use the most silicic samples in the discussion.
H. Rezeau: In your Figure 13 the histogram use a bin of 5 Ma, which is a huge interval considering that magmatic system are generally consider to last <0.5 to 1 Ma ….
Authors' answer: Figure 13 is devoted to zircon antecrysts and xenocrysts to show their distribution but not for a continuous magmatism approach. However, the distribution histogram shows some populated clusters which we think it is worth to be noted. Following the Reviewr's Advice we have added the weighted mean age distribution (see new Fig. 13)
H. Rezeau: Lines 513-516; I am not sure this is the right ratio to use to show the calc-alkaline and subduction environment….I think that the enrichment in incompatible trace element in the spider diagram is a better diagnostic, especially if you compare with the average arc crust composition from Rudnick and Gao 2003, I imagine that it should fit perfectly. You could any of LREE/HREE and MREE/HREE, they will show positive values characteristics of subduction zones. The calc-alkaline signature is better showed by your TAS diagram. You should not use the La/Yb ratio as a proof for subduction-related calc-alkaline magmas….
Authors' answer: We have not written that LREE/HREE fractionation in a magma can be used to infer subduction environments. The La/Yb ratio is used in literature, coupled with Sr and Sr/Y ratios to infer an "adakitic" composition of subduction-related melts instead of a "normal calcalkaline" composition. Indeed, adakites are classically interpreted in literature as being derived from eclogite partial melting. Eclogites are plagioclase-free, garnet-bearing lithologies and if induced to partially melt, they produce liquids rich in Sr and poor in Y and Yb (hence the high La/Yb and the low Yb as illustrated in Fig. 14b and the high Sr/Y and the low Y reported in Fig. 14a).
We disagree with the reviewer as concerns the possibility to distinguish calcalkaline signature on the basis of the TAS diagram. TAS diagram cannot be used to distinguish between tholeiitic and calcalkaline affinity.
H. Rezeau: Lines 523; Why not using isotope to discuss crustal contamination???...you should…
Authors' answer: Indeed, we infer that crustal contamination happened at source depths, i.e., it is not a shallow crustal contamination, but, rather, a modification of mantle sources by subduction. This is confirmed by the relatively uniform Sr-Nd isotopic ratios, as already explained in the previous sections.
H. Rezeau: Lines 524; I am not convinced by all these classification diagram between subduction vs. post-collision environments simply because the subduction to collision to post-collision is a continuous process involving similar end-members, but their respective involvement (and their timing) in the generation of arc-related melt is difficult to assess within the evolution of the orogen. Unless you provide clear structural evidence for post-collisional environment, I would assume that it is difficult to differentiate syn-subduction to post-collisional magmatism for I-type igneous rocks. The degree of partial melting of the mantle, the involvement of slab-related fluid vs. melt and the degree of assimilation of old vs. young rocks will impact the melt chemistry and it

is difficult to find a systematic as predicted with these "environment classification plot".
Authors' answer: We agree, but here we are just reporting the output of classical discrimination diagrams for felsic rocks.
H. Rezeau: Lines 577-582; Actually, there many way to explain the enrichment in incompatible element such as variable degree of partial melting in the source (Rezeau et al., 2017), remelting of metasomatized sub-continental lithospheric mantle (Castro et al., 2013), and so on…I think it would be great to propose these different scenario and eventually prefer one over the other based on some evidence presented in this study. For now, you just propose one way to generate this signature, but you do not really show any evidence that support this specific scenario.
H. Rezeau: Lines 583; Do you mean the high concentration of incompatible (HFSE, LILE, LREE) trace elements? If yes, be specific.
Authors' answer: We have deeply modified this paragraph following reviewer's request.
H. Rezeau: Lines 581; what is moderate? With respect to what?
Authors' answer: Moderate simply means not flat neither strongly enriched such as in Ca-carbonatitic melts. In any case we refer to CI chondrite-normalized patterns shown in Fig. 11b.
H. Rezeau: Lines 583-610; by reading this paragraph, I am not sure what do you mean by crustal recycling. Do you mean delamination of the crust, contamination of the source, which is further remelted to generate the Eocene to Miocene magmatism? Or recycling by remelting the lower crust? Or recycling by crustal assimilation? You use the evidence of antecryst, which seems to favor the crustal assimilation. If I did not understand correctly, and if you mean delamination, how the zircon are not fully dissolved at higher temperature and pressure in the mantle? These are all the question you should clarify by rephrasing this part of the discussion.
Authors' answer: The reviewer is correct. In its original version, the manuscript was not sufficiently clear. In the new version of the manuscript, we have tried to clarify our concepts improving the readability of the text (see the new section 9).
H. Rezeau: Lines 607; Is it homogeneous or not? … I am not sure when I look at the TAS diagram, and some incompatible trace element.
Authors' answer: The reviewer is right. We meant the relative homogeneity of incompatible elements rather than major oxides, strongly influenced by fractional crystallization processes, as those shown in Fig. 9.
H. Rezeau: Lines 609; I am not sure about this process to generate large volume of felsic magmatism (see Jagoutz and Klein, 2018). In addition, I would still expect contaminated geochemical signature.
Authors' answer: Jagoutz and Klein deal with the origin of granitoid melts distinguishing two main hypotheses, that referring to sedimentary partial melting and that referring to prolonged fractional crystallization of hydrous basaltic melts, mostly in supra-subduction settings. Our model is much more devoted to an igneous origin of the intermediate-acid Mianeh-Hashtroud rocks. Indeed, we refer the main petrogenetic process to partial melting of a supra-subduction mantle wedge. Magma derived therefrom can induce partial melting in underplated basaltic hydrous mineral-bearing lower crust. Coupled to this mixed mantle and lower crust partial melting is also associated a poorly defined process of fractional crystallization associated to variable (but generally minor) upper crustal assimilation. The model we propose is compatible with the petrogenetic hypothesis favoured by Jagoutz and Klein (2018).

H. Rezeau: Fig. 1 caption; I am not sure how important is this information, since there is no specific correlation with the Moho depth and so on. To my opinion, I think it adds more confusion than clarity. I would prefer if you only show the structure and the Moho depth contours (and eventually the Neogene magmatism matching thin crust), because that's the main focus of the paper.
Authors' answer: We have modified this figure, reporting the lithospheric thickness variation as reported in the same reference (Priestley et al., 2012).

Reviewer #3
Reviewer #3: This manuscript presents important results on the nature, origin, age and geodynamic setting of an intense magmatism which occurred from the Eocene until the end of the Miocene in the NW of the Iranian plateau (at the junction of the Alborz, Talesh and Sanandaj-Sirjan). It is an important contribution on petrology, geochemistry and the dating of volcanic and plutonic rocks in this area. Although I am not a specialist in geochemistry or geochronology methods, it appears that the data processing is of good quality. Except (perhaps) some of the U/Pb geochronology data on zircons which show for some samples very large ellipse error (with 2 sigma level) (Fig. 7).
Authors' answer: The reported uncertainties are common for LA-ICPMS method. In some plots the datasets have been plotted in a narrower window time and hence the ellipses appear to be larger with respect to other plots. For further additional details please refer to answers to Dr. Rezeau above
Reviewer #3: Reading this manuscript, it highlights some points mentioned but not all highlights proposed by the authors. It becomes clear that the history of Cenozoic magmatism in this sector (35 km long and 20 km wide) is very well documented, and the study shows a source of magma is mantle (Metasomatized) with a fusion of the crustal base of an arc.
According to the data presented I think that the results deserve be published. However, the discussion about the geodynamical setting responsible of this long-lived magmatism is not well evidenced. The authors propose the hypothesis about the major role of a tectonic control of the magmatism along a transform boundary between Eastern Caucasus and the Western Iran. Unfortunately, this boundary is not very well documented even if the authors consider the change of thickness of the lithosphere and the crust in this wide region. The figure 1 b do not show a clear boundary beneath the studied region. I think in order to solve this problem a wide study of the Cenozoic magmatism must be performed. But one more time I consider the results are important and will allow in the future to be include in a wide study, a synthesis, about the magmatism of the Caucasus and West Iran.
Authors' answer: We thank the reviewer for his comments that offer us the possibility to re-think and re-organise the discussion section on the geodynamic scenario. We thus re-organised the discussion section (see the new section 10) added a comprehensive model which could help to better finger out our reconstruction (see new Figure 16).
Regarding the Aras fault we agree with the reviewer. Albeit it cannot be traced in Moho contour map, but it could have been an active transform fault during blocks juxtaposing and reorganization which reactivated during collision events. However, the fault is consistent with block boundaries proposed by Reilinger et al., (2006) which has interrupted major structures such as suture lines and likely segmented Talesh-Arasbaran and Lesser Caucasus zones.
Regarding the figure 1b, please refer to the authors' answer to the same question from H. Rezeau above.

Reviewer #3: Comments in the text.
Reviewer #3: Line 81 and (90-94): make the citation of Sahakyan et al., 2017 Geochemistry of the Eocene magmatic rocks from the Lesser Caucasus area (Armenia): evidence of a subduction geodynamic environment Geological Society, London, Special Publications 428 (1), 73-98. This publication describes a recent version about the nature origin and tectonic setting of the huge Eocene magmatism in the Lesser Caucasus, very close from your study area.
Authors' answer: Fixed
Reviewer #3: Also this paper is important and have to be cited: Sugden, et al., 2019. The Thickness of the Mantle Lithosphere and Collision-Related Volcanism in the Lesser Caucasus, Journal of Petrology 60 (2), 199-230
Authors' answer: We agree and cited this paper in the discussion.
Reviewer #3: Line 127: not forget to cite Sosson et al., 2010 (instead of only Rolland et al., 2018) which proposed a reconstruction of the region (fig 13 of this paper) and placed a transform fault as you place it on your figure 1. Also make the citation of Barrier and Vrielynck, 2008. Rolland et al 2018 have used these two papers for their conclusions. The suggestion of Sosson et al (2010) is a hypothesis, and still now this is always a hypothesis. The Aras, or Arax fault is visible at now but there is no evidence which allow to be sure that it is the surface expression of the old transform fault through the Eurasian plate before the collision with the Taurides- Anatolides-Soutn Armenian microplate during the Paleocene-Early Eocene.
Authors' answer: References were fixed. Regarding the Aras fault we agree with the reviewer. It could have been an active transform fault separating the Zagros subduction from the Pontides, likely re-activated during collision events. The fault trace is consistent with block boundaries proposed by Reilinger et al., (2006) for the Turkish-Caucasus-NW Iran collisional boundary
Reviewer #3: line 136: Sorry again you forget the citation Sosson et al., 2010. (read it in detail you will see!)
Authors' answer: References were fixed.
Reviewer #3: Which evidence of a lithospheric fault zone (Aras and Ardabil-Mianeh-Baneh fault system)? The change of the thickness of the lithosphere (figure 1B) is not so sharp, and the faults in surface not very long as they should be if they were crossing all the lithosphere of Eurasia in this region.
Reviewer: The reviewer is rightWe believe that the Mianeh-Ardabil fault can be confidently traced toward SW. Please also refer to the authors' answer to the same question from Dr. H. Rezeau above.
Reviewer #3: Line 512: add as a reference Sahakyan et al., 2017
Authors' answer: Fixed
Reviewer #3: Line 606: I don't understand what do you mean exactly? It seems that there a lot of old zircons in the Eocene rocks, so a lot of crustal contamination during Eocene.
Authors' answer: In order to reconcile the large spread of ages of inherited zircons with the relatively homogeneous Sr and Nd isotopic ratios, as well as the similar interelemental fractionation, we propose that the Mesozoic to Neoarchean inherited zircons occasionally found in the Mianeh-Hashtroud rocks were acquired by partial melting of early underplated rocks at the base of the Iran block lithosphere. We therefore suggest that the inherited zircons originated from crustal wall rocks during magma ascent.
-Line 644: or collision thickening which conduct to the melting of the deep crustal base. ...see also the hypotheses proposed by Sosson et al (2010) for the Lesser Caucasus.

Authors’ answer: Yes, we agree. We modified the text as proposed.
Reviewer #3: Line 662: Rolland 2019 is a review. Again and really I don't like to insist, but the main hypothesis based on facts, data, was made for the lesser Caucasus by Sosson et al., 2010, and then by all our teams. So please don't used the reference Rolland 2019 instead of the work of a big team which published before Rolland 2018. It should be honest to make the good citations please. I'm very surprised to notice that our scientific ethic progressively disappears with the time. The citations must be well used.
Authors’ answer: Sorry, Fixed.
Reviewer #3: Line 692: Please change Rolland 2017 by Barrier and Vrielynck 2008, Sosson et al, 2010.
Authors’ answer: Fixed.

Hoping in the present form the revised manuscript may fulfil criteria for publication in Gondwana Research,

Sincerely,
Federico Rossetti
(on behalf of the co-Authors)

Research Data Related to this Submission
--------------------------------------------------
There are no linked research data sets for this submission. The following reason is given:
Data will be made available on request

Roma, March 15 2020

**To**: Prof. A. Festa , Editor Gondwana Research

**Re**: Submission of the revised version manuscript entitled "*Long-lived, Eocene-Miocene stationary magmatism in NW Iran along a transform plate boundary*" by Ahmad Rabiee, Federico Rossetti, Yoshihiro Asahara, Hossein Azizi, Federico Lucci, Michele Lustrino, Reza Nozaem.

Dear Editor, please find attached the revised version of our manuscript submitted for possible publication in Gondwana Research.

The three reviewers provided constructive comments and remarks that greatly contributed to improve the manuscript. We have carefully followed the reviewers' advice and comments to prepare this revised version.

The Respond to Reviewers letter details how the comments from the Reviewers we addressed in this revised version. Changes in the original text are typed in red to allow tracking the changes. Reference to the text pages refers to the uploaded revised Word file.

Sincerely Yours,

Federico Rossetti

(on behalf of the coauthors)

Roma, March 15 2020

**To**: Prof. A. Festa , Editor Gondwana Research

***S****ubmission of the revised version manuscript entitled "***Long-lived, Eocene-Miocene stationary magmatism in NW Iran along a transform plate boundary***" by Ahmad Rabiee, Federico Rossetti, Yoshihiro Asahara, Hossein Azizi, Federico Lucci, Michele Lustrino, Reza Nozaem.*

Dear Editor, please find attached the revised version of our manuscript submitted for possible publication in Gondwana Research.

The three reviewers provided constructive comments and remarks that greatly contributed to improve the manuscript. We have carefully followed the reviewers' advice and comments to prepare this revised version. Before presenting the detailed responses to the reviewers' comments, we inform that in order to adapt this revised version to the reviewers' suggestions, we added new materials to the early submitted typescript. These include:

1. Supplementary materials S1: Table of main characteristics of selected porphyry deposits along UDMZ (Iran) and Armenia.
2. Supplementary materials S3: Details of Zircon U-Pb geochronology (zircon characteristics and each analysis).
3. Supplementary materials S4: Probability density and weighted age plots of measured zircons from all collected samples from Mianeh-Hashtroud area.
4. A new Fig. 13a to better support the continues magmatism during the Eocene-Miocene time lapse in the study area;
5. A new 3D petrogenetic model (Fig. 16), where we propose a synthetic geodynamic scenario for the Cenozoic evolution of the Turkish-Iranian-Caucasus collisional boundary and associated magmatism.

Below we provide a point-by-point response to the reviewers' comments and illustrate how these major changes are integrated in the revised version. In the following, the response are typed in italics. Changes in the original text are typed in red to allow tracking the changes. Reference to the text pages refers to the uploaded revised Word file.

## Response to Reviewer #1:

One point which could be enhanced in the petrologic model concerns the quantification of crustal contamination. Evidence of crustal contamination is 'attested by inherited zircons', while Miocene samples document a 'stronger crustal contamination' than Oligocene ones. However, the amount of crustal contamination has not be quantified using mixing curves, which the authors could probably have attempted. Can the authors precise that point?

***Authors' answer:*** *We have modified the interpretation of our data, reducing the necessity to invoke any strong crustal contamination. A careful check of Sr-Nd isotopic data as well as the overall incompatible element content of Miocene samples do not require any substantially higher degree of interaction with typical upper crustal rocks.*

**Reviewer #1: Minor comments in the text.**
***Authors' answer:*** *All comments have been fixed.*

## Response to Reviewer #2 (H. Rezeau) general comments

**H. Rezeau:** The authors describe 26 samples, including 12 samples dated from 44.32 Ma to 5.93 Ma covering a total magmatic duration of almost 40 Myr. However, it is not clear how the authors distinguish the **undated samples** between Eocene, Oligocene and Miocene since the whole-rock geochemistry overlap significantly, especially for Oligocene and Eocene rocks. In addition, the authors claim a continuous magmatism, which I would rather interpret as pulsed magmatism. Indeed, when I look at the zircon mean age (Fig. 7), there is no obvious **continuity/overlapping in age from 44 Ma to 5 Ma,** but it rather illustrates snapshot of magmatic pulses at 44-43 Ma, 40-36 Ma, 30-26 Ma, 22 Ma , 14 Ma and 5 Ma. Therefore, I question **the co-genetic relationship** of these intrusions, which is not fully addressed by the authors in the present manuscript. I rather understand that they use the similar whole-rock geochemistry to propose a similar petrogenetic model for all the rocks emplaced in the Mianeh-Hashtroud study area. However, **published study in central to NW Iran and Lesser Caucasus** generally demonstrate the evolution of petrogenetic processes through time from the Eocene to Miocene (e.g., Castro et al., 2013; Shafiei et al., 2009; Moritz et al., 2016; H. Rezeau et al., 2017). I encourage the author to reconsider this point because it will significantly improve the strength of the manuscript.

***Authors' answer:***

***Regarding the undated samples***

*We carried out an extensive field work in the studied area, which results in the production of the geological map shown in Fig. 3, where the different textural and geometrical relationships among intrusive and volcanic rocks are reported. We paid attention to conduct a comprehensive sampling of all the different magmatic rock types, avoiding repeated sampling for geochronology. We are thus confident regarding the relative age estimation of undated samples based on the field relationships, cross cutting relationships and the correlation on rock texture (from coarse- to fine-grained, porphyritic and vitrophyric) within the different magmatic groups (intrusive, hypabyssal and volcanic). For example, the Eocene intrusive rocks show always a granular texture, while the Oligocene rocks are always porphyritic. Regarding Miocene samples, we have only three samples, two of which were dated. The two dated samples are similar each other and are similar to other neighbouring dykes (samples MN05 and MN07).*

***Regarding the continuity/overlapping in age from 44 Ma to 5 Ma***

*To answer to the reviewer criticism, we re-organised the text of Section 6, leaving just the necessary info and moving the detailed description of the samples to the Supplementary Material S2-S4. The criteria for age calculation, including categorisation of the zircon types (autocrysts, antecrysts, and xenocrysts/inherited; after Miller et al., 2007) is now provided in Appendix A1 and illustrated for the cumulative samples as probability density plots and weighted mean ages in Supplementary material S4. To better document the continuity of magmatism we prepared a new figure (Fig. 13a), where we present the weighted age distribution of the dated zircons (autocrysts and antecrysts). Based on the age distribution (with 2σ uncertainty) there is a continuous range from ca. 55 (54.8±2.8 Ma) to at least 12 Ma and the magmatism resumes at ~8 Ma. this evidence is consistent with published ages from the Sahand volcano (Richards et al., 2006; Sawada et al., 2016; Lechman et al., 2018).*

***Regarding the co-genetic relationship of the studied magmatic products***

*Despite the presence of inherited zircon crystals with ages as old as Proterozoic, the Sr-Nd isotopic ratios of the investigated rocks is surprisingly homogeneous. This feature is* *increasingly interesting considering the diffuse chemical alteration of the samples (despite we selected only the freshest rocks for whole rock composition) and the wide chemical range of compositions (with $SiO_2$ spanning over ~30 wt% variation). To sum up, the overall similar mineral paragenesis, the common primitive mantle incompatible element-normalized patterns and the restricted variability of Sr-Nd isotopic ratios led us to support to a co-genetic origin among the different magma batches.*

**H. Rezeau:** The classification of the rocks investigated in this study is a main issue for me. **The authors use many different ways to name/classify** them (i.e., volcanic rocks, intrusions, hypabyssal, country rocks, Eocene rocks, Oligocene rocks, Miocene rocks, Late Miocene-Quaternary rocks), which make it extremely difficult to follow for the reader. In addition, the authors do not differentiate volcanic from plutonic rocks in the whole-rock geochemistry results neither in the geochemical plots, which is not correct to me. The authors should use the appropriate classification scheme for volcanic and intrusive rocks, and name the rocks accordingly. They should also distinguish the different type of rocks by using two different symbols in the geochemical plots. In the text, I suggested a way to name/describe the rocks, which would help the reader to follow. I think this is a major issue in the present manuscript, which could be easily fixed before resubmission.
***Authors' answer:*** *We agree with the reviewer about the confusion present in the previous version. Following the reviewer's advice, we have modified section 5 to have a consistent nomenclature throughout the text. The rationale in the petrography section (section 5) has been conceived to present the different rock types based on the field evidence that is synthesised in the geological map of the area shown in Fig. 3. It is worth noting that the studied igneous rocks are emplaced within Eocene volcanic country rocks. We would thus maintain the classification separating plutonic, hypabyssal and volcanic rock types (see also answer to the above point) with respect to the Eocene country rocks. We classify the samples based on their ages, since the geochemical fingerprint within the same age group is overlapping, irrespective of the rock type (either intrusive or volcanic).*

**H. Rezeau:** The authors present a "Field and Petrographic observations" section, however **they barely (if not at all) refer to it nor use it in the discussion**. Petrographic observations provide important information about the sequence of mineral crystallization, which inherently depends on the melt chemistry from which they crystallize. Therefore, I think it is a pity to not take advantage of it. I have provided some detailed comment directly in the attached manuscript about it and how the author could use some observations in the discussion. If the authors do not use it in the discussion, I am questioning the necessity to include a petrography section if it is not relevant for the discussion.
***Authors' answer:*** *The petrographic section is reduced to the essential description of the investigated rocks (see the new section 5). We propose the involvement of specific mineral phases during a fractional crystallization process only qualitatively drafted in the manuscript (due to the not perfect preservation state of the Mianeh samples). Petrography, coupled with geochemistry and geochronology of the investigated rocks and neighbouring Cenozoic magmatism are used to constrain the geodynamic environment of formation. Therefore, although we agree with the reviewer, the description of the sequence of mineral crystallisation is a bit out of the scope of the present manuscript.*

**H. Rezeau:** Regarding the general geodynamic regional model and its implications for the petrogenesis of the investigated magmatic rocks, the authors use broad general geodynamic models from the literature with no proper evidence to support it from their own data. Even if I am not against the proposed scenario, I encourage the authors to be more careful in addressing their model as well as discussing alternative models too. They should rearrange the discussion and reconsider the way they discuss their data with respect to the regional geodynamic evolution. In the present version of the manuscript, I do not see compelling evidence from the data presented in this study to support the final proposed model. Structural field evidence along with geochemical data would be a good combination to support the proposed model.

***Authors' answer:*** *We thank the reviewer of his comment that offer us the opportunity to propose a geodynamic reconstruction with a greater detail (see new Fig. 16). We also agree that a more focused discussion on the geodynamic scenario was necessary. Therefore, we revised the relevant discussion on these themes (see the new section 10). We agree that structural data would be a good addition to the data set, but, unfortunately, the large volcanic cover in the area prevents direct field observations on the main deformation structures and feeding zones. However, we are confident that after the exhaustive literature review presented in section 2 and correlation at regional scale, the tectonic/geodynamic scenario to frame the Cenozoic magmatic evolution in the region is quite well constrained. In particular, the inherited structures (transversal from the collisional boundary) provided long-lasting weak zones for magma ascent and accumulation from Eocene to Miocene. Since these structures are likely inherited from a major transform zone (e.g., Barrier and Vrienlink, 2018; Van der Boon et al., 2018; Rolland et al., 2017), we suggest the presence of slab tearing and slab window during the Cenozoic, which provided asthenospheric flow and heat able to generate the long-lasting and almost homogeneous magmatism during Eocene and Oligocene. During Miocene the collision event and thickening changed the geodynamic setting, but the new magma still was able to ascent to this weak zone. These ideas are depicted in the conceptual geodynamic scenario presented in the new Fig. 16.*

**H. Rezeau:** The calculated zircon U-Pb mean ages are presented in Fig. 7 along with the Concordia diagrams generated using Isoplot. For some samples, I can see a spread in ages over 2-4 Ma. The calculation of the **weighted mean age is** not described in the methods, although the notion of autocrysts and antecrysts is mentioned is the manuscript. It is very important to describe the criteria you have used to include or reject a single measurement from the weighted mean age calculation. I know that Isoplot can do it automatically for you, but I would advise to use a density probability plot to identify one or several sub-population(s) of zircons within sample. This will allow you to select on the youngest family to calculate the crystallization age, generally assumed to be represented by the youngest population. You can include such plots in the supplementary material along with zircon CL images for each sample, which will avoid any question from the readers regarding the calculation of the weighted mean ages used in this study. Furthermore, I also request a plot of the weighted mean age with uncertainties (2s) to illustrate the continuous magmatism versus pulsed magmatism in the area. If the authors agree with my comments, I am sure that it will significantly improve the manuscript and help them to clearly address the temporal magmatic history of the Mianeh-Hashtrood study area.

***Authors' answer:*** *We thank the reviewer for his comment that is fully pertinent and offer us the possibility to better explain the scientific rationale adopted on the U-Pb geochronology. We did not use weighted mean age calculation. Since this method does not eliminate some zircon antecrysts, which their ages clearly are out of normal distribution in histogram plots and the probability of the calculated ages are below 0.1 in most of the samples (see*

*supplementary Material S4). Instead we chose the best concordant results in a continuous range, preferably for Concordia age calculation. In particular, zircons results with Pb common should be <20% and Th/U >0.1 were used to calculate Concordia age. To calculate the Concordia ages for some samples (when available), only concordant ages were used. The maximum numbers of datasets in a continuous sorted population (excluding outlier values) which were acceptable by Isoplot to calculate a Concordia age were considered. In the cases where most of ages were discordant (mainly due to Pb common >5%) the Terra-Wasserburg method was used which provide more reliable ages. For instance, in sample MN76 we eliminated 4 younger and 2 older zircons which are clearly out of the main population. for samples MN10 we only used 18 zircons to be able to provide a Concordia age while the weighted mean average method uses 28 out of 31 dataset but the calculated age is less accurate (MSWD=2.6 , probability =0.000).*
*Following the Reviewer's advice, we specified the criteria for age calculation, including categorisation of the zircon types (autocrysts, antecrysts, and xenocrysts/inherited; after Miller et al., 2007) that is provided in Appendix A1 and illustrated for the cumulative samples as probability density plots and weighted mean ages in Supplementary material S4. We also prepared a new figure (Fig. 13a), reporting the weighted age distribution of the dated zircons (autocrysts and antecrysts) to better document the continuity of magmatism.*

**H. Rezeau:** In the abstract, at the end of the introduction and in the last section of the discussion, the **authors mention briefly the notion of mineral deposits**. I am not quite sure why the authors briefly mention it here and there. This is poorly described and also not discussed at all. I would either recommend to clearly describe and stress its importance in the area and then discuss it, or completely remove it from the manuscript.
***Authors' answer****: We thank the reviewer for his comment. Following the reviewer's advice, we have expanded the description of the main ore zones in the region (see new section 3 and lines 223-265) Moreover, the new Fig. 2 now contains the distribution of the main porphyry mineralization. A Table is now provided in Supplementary Material S1, showing the characteristics of each deposit. Our main scope is not the metallogeny of the region but the linkage between the porphyry ore localisation with (i) the major tectonic structures, and (ii) the peculiar geodynamic setting we propose. In particular, we propose the Eastern Caucasus-Western Iran Boundary as a long-lived tectonic structure, which acted as a weak zone susceptible to multiple tectonic reactivation, able to focus magmatism as a preferred pathway for magma ascent and emplacement and focused mineralisation during Eocene-Miocene times.*

**H. Rezeau:** I don't see this abrupt transition, I see similar colors (yellow, light and dark green) on each side of both fault. …..I am not sure what you want to show with the isotherm of the upper mantle, but I am not convinced about its relevance here. See also my comment on Fig. 1.
***Authors' answer:*** *We have strongly modified Fig. 1, reporting the lithospheric thickness variation as reported in the same reference (Priestley et al., 2012). However, considering the continuation of Mianeh-Ardabil fault toward SW (see also Fig. 2), it is well evident that the trace of this fault zone corresponds to a SE-ward transition from thin to thick lithosphere in the region.*

**Other comments from H.H. Rezeau in the file**

Line 47-51 (76-78): *We have modified the sentence, following the reviewer's suggestion.*

Line 88: Do you refer to the Moho depth here? If yes, you should mention Shad Manaman et al., 2011 and Fig. 1b.
***Authors' answer:*** *Here we are referring to lithosphere not to the Moho depth.*

Lines 109-114: *Fixed with additional materials. We also added relevant text in the discussion section and a new Figure.*

Lines 157-164: *Fixed.*

Lines 208-210: *We have modified the text following the reviewer's suggestion.*

Lines 267-282: Section 4: *We have modified the section following the reviewer's suggestion.*

Lines 293-298: *The Paragraph was revised, to avoid any confusion regarding roc classification.*

**Section 5.4.** Here again volcanic rocks but you do not provide an age information. You should consider if you can merge it with 5.1 under volcanic rocks, and then make 2 distinct paragraphs for the Eocene ones and this one. Also why not calling the Eocene Group 1 and this one Group 2, instead of Eocene volcanic country rocks and volcanic rocks. I am sure it will help to clarify and avoid unnecessary subdivision. Same for Intrusions and hypabyssal, which could be merged under a "intrusive rocks" section with two distinct paragraphs, and maybe Group 1 and 2 as well based on the age or other features.

*Section 5.2 to 5.4: These sections were modified following the reviewer's suggestion.*

**H. Rezeau:** I would suggest to rearrange the Figure 4 in order to have the Fig.4d as a Fig. 4a, and then modify accordingly.
***Authors' answer:*** *Following the Reviewer's advice, we have modified the Figure. Please see the new version in the revised manuscript.*

**H. Rezeau: Section 6.** This section is highly repetitive for each section with a lot of information ……
***Authors' answer:*** *We kept the most important features in the section and moved details in Supplementary Material S3.*

**H. Rezeau:** Fig 7a and 7n: Very small and hard to see anything.
***Authors' answer:*** *Here we put this image to show examples of general characteristics of zircon autocrysts, antecrysts and inherited ones in CL images in which different categories are shown with distinct colored circles. A larger size is available in Supplementary Material S3*

**H. Rezeau:** You don't show any CL images here, so why referring to Sup. Mat. Here?
***Authors' answer:*** *We showed two examples in the Fig. 7. However, we moved the details of this section to Supplementary materials S2 and S3.*

**H. Rezeau:** How do you calculate U-Pb ages?
***Authors' answer:*** *We added additional materials on this regard in the Methods and Appendix. Please see also the authors' answer above in general comments.*

**H. Rezeau:** you do not mention it in the method to explain how you calculate the weighted mean age of each sample. …..If you discard some antecryst from the calculation, you also

should explain how which basis you decided to exclude them from the calculation of the weighted mean age.
***Authors' answer:*** *Please see the authors' answer to the same question above in general comments.*

**H. Rezeau:** What are the evidence for lead loss using LA-ICP-MS technique? I am not convinced that we can accurately estimate lead loss using LA-ICP-MS technique, compared to ID-TIMS technique.
***Authors' answer:*** *Zircon structure is not so favorable to retain the radiogenic Pb. Therefore, Pb losses typically occur along cracks generated during dynamic deformation (and crushing). In addition, sometimes during the crushing and polishing, environmental Pb goes inside the existing fractures. Furthermore, chamber environment has some Pb common resulted from shooting to other grains rather than zircon which could cause contamination. In general, if the common Pb is above 20% the dataset would not be appropriate for the age calculation in the LA-ICPMS data. In our calculation, we excluded all datasets with common Pb above 20%.*

**H. Rezeau:** late Miocene-QUATERNARY in diagrams.
***Authors' answer:*** *Fixed.*

**H. Rezeau:** In figure 12, Nd-Sr data from H. Rezeau et al., 2017
***Authors' answer:*** *Sorry, Fixed.*

**H. Rezeau: Line 440;** No igneous rocks can reach $SiO_2$>76-78 wt%....this high values must illustrate alteration or magmatic-hydrothermal melt/fluid (pegmatitic or something like this). Please check the rock with such high value and eventually remove it from the data set.
***Authors' answer:*** *We agree with the reviewer. Some of the Oligocene-early Miocene subvolcanic bodies are affected by secondary silicification. But we would prefer to use these data rather than giving away most of these samples. We have avoided additional comments on rocks with $SiO_2$ >78 wt% and we didn't use the most silicic samples in the discussion.*

**H. Rezeau:** In your Figure 13 the histogram use a bin of 5 Ma, which is a huge interval considering that magmatic system are generally consider to last <0.5 to 1 Ma ….
***Authors' answer:*** *Figure 13 is devoted to zircon antecrysts and xenocrysts to show their distribution but not for a continuous magmatism approach. However, the distribution histogram shows some populated clusters which we think it is worth to be noted. Following the Reviewr's Advice we have added the weighted mean age distribution (see new Fig. 13)*

**H. Rezeau: Lines 513-516;** I am not sure this is the right ratio to use to show the calc-alkaline and subduction environment….I think that the enrichment in incompatible trace element in the spider diagram is a better diagnostic, especially if you compare with the average arc crust composition from Rudnick and Gao 2003, I imagine that it should fit perfectly. You could any of LREE/HREE and MREE/HREE, they will show positive values characteristics of subduction zones. The calc-alkaline signature is better showed by your TAS diagram. You should not use the La/Yb ratio as a proof for subduction-related calc-alkaline magmas….
***Authors' answer:*** *We have not written that LREE/HREE fractionation in a magma can be used to infer subduction environments. The La/Yb ratio is used in literature, coupled with Sr and Sr/Y ratios to infer an "adakitic" composition of subduction-related melts instead of a "normal calcalkaline" composition. Indeed, adakites are classically interpreted in literature as being derived from eclogite partial melting. Eclogites are plagioclase-free, garnet-bearing lithologies and if induced to partially melt, they produce liquids rich in Sr and poor in Y and*

*Yb (hence the high La/Yb and the low Yb as illustrated in Fig. 14b and the high Sr/Y and the low Y reported in Fig. 14a).*
*We disagree with the reviewer as concerns the possibility to distinguish calcalkaline signature on the basis of the TAS diagram. TAS diagram cannot be used to distinguish between tholeiitic and calcalkaline affinity.*

**H. Rezeau: Lines 523;** Why not using isotope to discuss crustal contamination???...you should…
***Authors' answer:*** *Indeed, we infer that crustal contamination happened at source depths, i.e., it is not a shallow crustal contamination, but, rather, a modification of mantle sources by subduction. This is confirmed by the relatively uniform Sr-Nd isotopic ratios, as already explained in the previous sections.*

**H. Rezeau: Lines 524;** I am not convinced by all these classification diagram between subduction vs. post-collision environments simply because the subduction to collision to post-collision is a continuous process involving similar end-members, but their respective involvement (and their timing) in the generation of arc-related melt is difficult to assess within the evolution of the orogen. Unless you provide clear structural evidence for post-collisional environment, I would assume that it is difficult to differentiate syn-subduction to post-collisional magmatism for I-type igneous rocks. The degree of partial melting of the mantle, the involvement of slab-related fluid vs. melt and the degree of assimilation of old vs. young rocks will impact the melt chemistry and it is difficult to find a systematic as predicted with these "environment classification plot".
***Authors' answer:*** *We agree, but here we are just reporting the output of classical discrimination diagrams for felsic rocks.*

**H. Rezeau: Lines 577-582;** Actually, there many way to explain the enrichment in incompatible element such as variable degree of partial melting in the source (Rezeau et al., 2017), remelting of metasomatized sub-continental lithospheric mantle (Castro et al., 2013), and so on…I think it would be great to propose these different scenario and eventually prefer one over the other based on some evidence presented in this study. For now, you just propose one way to generate this signature, but you do not really show any evidence that support this specific scenario.
**H. Rezeau: Lines 583;** Do you mean the high concentration of incompatible (HFSE, LILE, LREE) trace elements? If yes, be specific.
***Authors' answer:*** *We have deeply modified this paragraph following reviewer's request.*

**H. Rezeau: Lines 581;** what is moderate? With respect to what?
***Authors' answer:*** *Moderate simply means not flat neither strongly enriched such as in Ca-carbonatitic melts. In any case we refer to CI chondrite-normalized patterns shown in Fig. 11b.*

**H. Rezeau: Lines 583-610;** by reading this paragraph, I am not sure what do you mean by crustal recycling. Do you mean delamination of the crust, contamination of the source, which is further remelted to generate the Eocene to Miocene magmatism? Or recycling by remelting the lower crust? Or recycling by crustal assimilation? You use the evidence of antecryst, which seems to favor the crustal assimilation. If I did not understand correctly, and if you mean delamination, how the zircon are not fully dissolved at higher temperature and pressure in the mantle? These are all the question you should clarify by rephrasing this part of the discussion.

***Authors' answer:*** *The reviewer is correct. In its original version, the manuscript was not sufficiently clear. In the new version of the manuscript, we have tried to clarify our concepts improving the readability of the text (see the new section 9).*

**H. Rezeau: Lines 607;** Is it homogeneous or not? … I am not sure when I look at the TAS diagram, and some incompatible trace element.
***Authors' answer:*** *The reviewer is right. We meant the relative homogeneity of incompatible elements rather than major oxides, strongly influenced by fractional crystallization processes, as those shown in Fig. 9.*

**H. Rezeau: Lines 609;** I am not sure about this process to generate large volume of felsic magmatism (see Jagoutz and Klein, 2018). In addition, I would still expect contaminated geochemical signature.
***Authors' answer:*** *Jagoutz and Klein deal with the origin of granitoid melts distinguishing two main hypotheses, that referring to sedimentary partial melting and that referring to prolonged fractional crystallization of hydrous basaltic melts, mostly in supra-subduction settings. Our model is much more devoted to an igneous origin of the intermediate-acid Mianeh-Hashtroud rocks. Indeed, we refer the main petrogenetic process to partial melting of a supra-subduction mantle wedge. Magma derived therefrom can induce partial melting in underplated basaltic hydrous mineral-bearing lower crust. Coupled to this mixed mantle and lower crust partial melting is also associated a poorly defined process of fractional crystallization associated to variable (but generally minor) upper crustal assimilation. The model we propose is compatible with the petrogenetic hypothesis favoured by Jagoutz and Klein (2018).*

**H. Rezeau: Fig. 1 caption;** I am not sure how important is this information, since there is no specific correlation with the Moho depth and so on. To my opinion, I think it adds more confusion than clarity. I would prefer if you only show the structure and the Moho depth contours (and eventually the Neogene magmatism matching thin crust), because that's the main focus of the paper.
***Authors' answer:*** *We have modified this figure, reporting the lithospheric thickness variation as reported in the same reference (Priestley et al., 2012).*

# Reviewer #3

**Reviewer #3:** This manuscript presents important results on the nature, origin, age and geodynamic setting of an intense magmatism which occurred from the Eocene until the end of the Miocene in the NW of the Iranian plateau (at the junction of the Alborz, Talesh and Sanandaj-Sirjan). It is an important contribution on petrology, geochemistry and the dating of volcanic and plutonic rocks in this area. Although I am not a specialist in geochemistry or geochronology methods, it appears that the data processing is of good quality. Except (perhaps) some of the U/Pb geochronology data on zircons which show for some samples very large ellipse error (with 2 sigma level) (Fig. 7).
***Authors' answer:*** *The reported uncertainties are common for LA-ICPMS method. In some plots the datasets have been plotted in a narrower window time and hence the ellipses appear to be larger with respect to other plots. For further additional details please refer to answers to Dr. Rezeau above*

**Reviewer #3:** Reading this manuscript, it highlights some points mentioned but not all highlights proposed by the authors. It becomes clear that the history of Cenozoic magmatism

in this sector (35 km long and 20 km wide) is very well documented, and the study shows a source of magma is mantle (Metasomatized) with a fusion of the crustal base of an arc.
According to the data presented I think that the results deserve be published. However, the discussion about the geodynamical setting responsible of this long-lived magmatism is not well evidenced. The authors propose the hypothesis about the major role of a tectonic control of the magmatism along a transform boundary between Eastern Caucasus and the Western Iran. Unfortunately, this boundary is not very well documented even if the authors consider the change of thickness of the lithosphere and the crust in this wide region. The figure 1 b do not show a clear boundary beneath the studied region. I think in order to solve this problem a wide study of the Cenozoic magmatism must be performed. But one more time I consider the results are important and will allow in the future to be include in a wide study, a synthesis, about the magmatism of the Caucasus and West Iran.
***Authors' answer:*** *We thank the reviewer for his comments that offer us the possibility to re-think and re-organise the discussion section on the geodynamic scenario. We thus re-organised the discussion section (see the new section 10) added a comprehensive model which could help to better finger out our reconstruction (see new Figure 16).*
*Regarding the Aras fault we agree with the reviewer. Albeit it cannot be traced in Moho contour map, but it could have been an active transform fault during blocks juxtaposing and reorganization which reactivated during collision events. However, the fault is consistent with block boundaries proposed by Reilinger et al., (2006) which has interrupted major structures such as suture lines and likely segmented Talesh-Arasbaran and Lesser Caucasus zones.*
*Regarding the figure 1b, please refer to the authors' answer to the same question from H. Rezeau above.*

**Reviewer #3: Comments in the text.**

**Reviewer #3:** Line 81 and (90-94): make the citation of Sahakyan et al., 2017 Geochemistry of the Eocene magmatic rocks from the Lesser Caucasus area (Armenia): evidence of a subduction geodynamic environment Geological Society, London, Special Publications 428 (1), 73-98. This publication describes a recent version about the nature origin and tectonic setting of the huge Eocene magmatism in the Lesser Caucasus, very close from your study area.
***Authors' answer:*** *Fixed*

**Reviewer #3:** Also this paper is important and have to be cited: Sugden, et al., 2019. The Thickness of the Mantle Lithosphere and Collision-Related Volcanism in the Lesser Caucasus, Journal of Petrology 60 (2), 199-230
***Authors' answer:*** *We agree and cited this paper in the discussion.*

**Reviewer #3: Line 127**: not forget to cite Sosson et al., 2010 (instead of only Rolland et al., 2018) which proposed a reconstruction of the region (fig 13 of this paper) and placed a transform fault as you place it on your figure 1. Also make the citation of Barrier and Vrielynck, 2008. Rolland et al 2018 have used these two papers for their conclusions. The suggestion of Sosson et al (2010) is a hypothesis, and still now this is always a hypothesis. The Aras, or Arax fault is visible at now but there is no evidence which allow to be sure that it is the surface expression of the old transform fault through the Eurasian plate before the collision with the Taurides- Anatolides-Soutn Armenian microplate during the Paleocene-Early Eocene.
***Authors' answer:*** *References were fixed. Regarding the Aras fault we agree with the reviewer. It could have been an active transform fault separating the Zagros subduction from the Pontides, likely re-activated during collision events. The fault trace is consistent with*

*block boundaries proposed by Reilinger et al., (2006) for the Turkish-Caucasus-NW Iran collisional boundary*

**Reviewer #3: line 136**: Sorry again you forget the citation Sosson et al., 2010. (read it in detail you will see!)
***Authors' answer:*** *References were fixed.*

**Reviewer #3:** Which evidence of a lithospheric fault zone (Aras and Ardabil-Mianeh-Baneh fault system)? The change of the thickness of the lithosphere (figure 1B) is not so sharp, and the faults in surface not very long as they should be if they were crossing all the lithosphere of Eurasia in this region.
**Reviewer:** The reviewer is right*We believe that the Mianeh-Ardabil fault can be confidently traced toward SW. Please also refer to the authors' answer to the same question from Dr. H. Rezeau above.*

**Reviewer #3: Line 512:** add as a reference Sahakyan et al., 2017
***Authors' answer:*** *Fixed*

**Reviewer #3: Line 606:** I don't understand what do you mean exactly? It seems that there a lot of old zircons in the Eocene rocks, so a lot of crustal contamination during Eocene.
***Authors' answer:*** *In order to reconcile the large spread of ages of inherited zircons with the relatively homogeneous Sr and Nd isotopic ratios, as well as the similar interelemental fractionation, we propose that the Mesozoic to Neoarchean inherited zircons occasionally found in the Mianeh-Hashtroud rocks were acquired by partial melting of early underplated rocks at the base of the Iran block lithosphere. We therefore suggest that the inherited zircons originated from crustal wall rocks during magma ascent.*

**-Line 644:** or collision thickening which conduct to the melting of the deep crustal base. ...see also the hypotheses proposed by Sosson et al (2010) for the Lesser Caucasus.
***Authors' answer:*** *Yes, we agree. We modified the text as proposed.*

**Reviewer #3:** Line 662: Rolland 2019 is a review. Again and really I don't like to insist, but the main hypothesis based on facts, data, was made for the lesser Caucasus by Sosson et al., 2010, and then by all our teams. So please don't used the reference Rolland 2019 instead of the work of a big team which published before Rolland 2018. It should be honest to make the good citations please. I'm very surprised to notice that our scientific ethic progressively disappears with the time. The citations must be well used.
***Authors' answer:*** *Sorry, Fixed.*

**Reviewer #3:** Line 692: Please change Rolland 2017 by Barrier and Vrielynck 2008, Sosson et al, 2010.
***Authors' answer:*** *Fixed.*

Hoping in the present form the revised manuscript may fulfil criteria for publication in Gondwana Research,

Sincerely,

Federico Rossetti

(on behalf of the co-Authors)

*Graphical Abstract

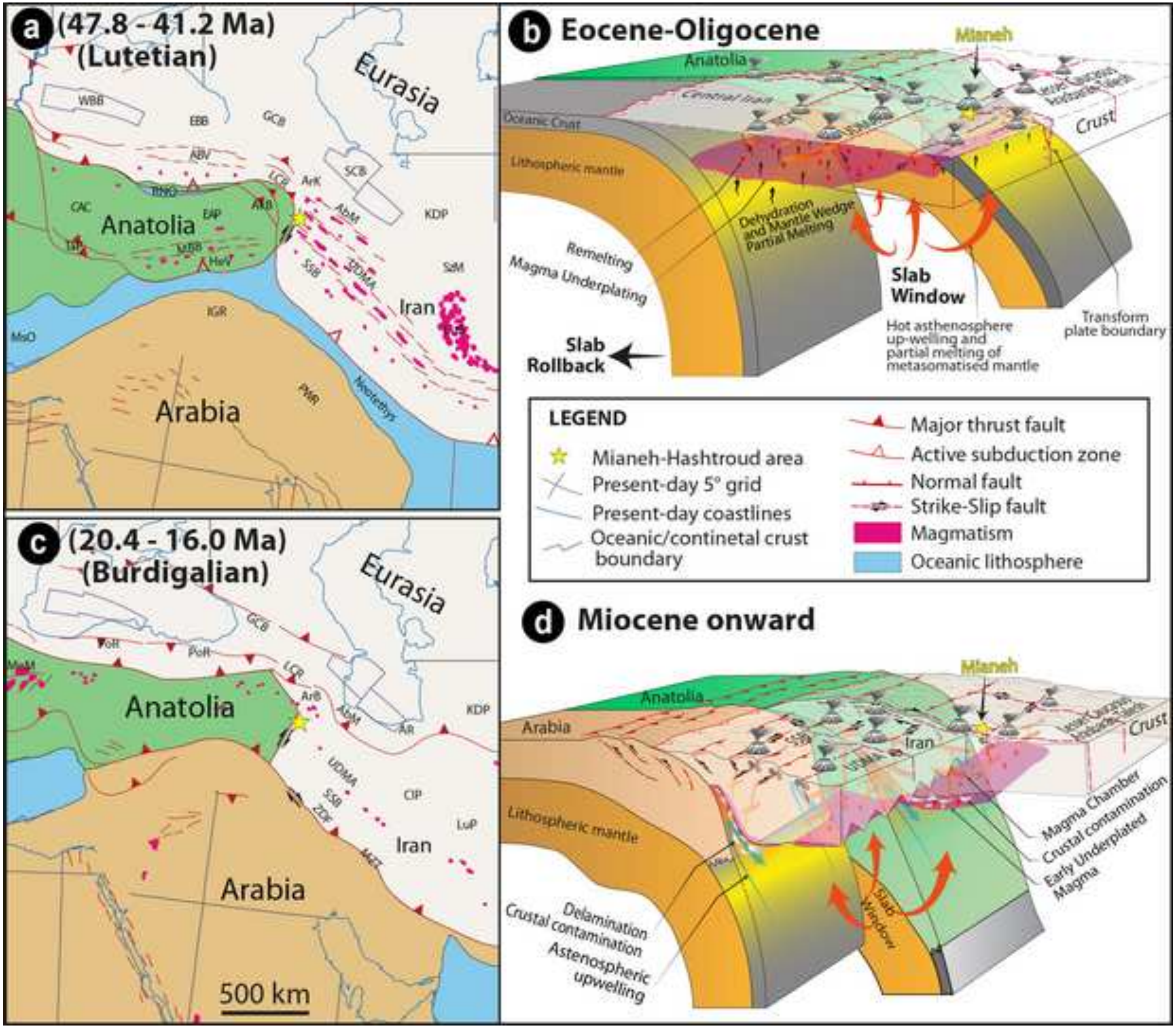

# Highlights

- A long-lived (ca. 40 Myr) stationary history of Cenozoic magmatism is documented
- Metasomatized mantle lithosphere sources, lower arc crust foundering and melting
- Collisional magmatism controlled by major lithosphere-scale tectonic boundaries
-Tectonic reactivation controls the pattern and longevity of the Cenozoic magmatism

# Long-lived, Eocene-Miocene stationary magmatism in NW Iran along a transform plate boundary

Ahmad Rabiee[1], Federico Rossetti[1,*], Yoshihiro Asahara[2], Hossein Azizi[3], Federico Lucci[1], Michele Lustrino[4,5], Reza Nozaem[6]

*[1] Dipartimento di Scienze, Università degli Studi Roma Tre, Roma, Italy*

*[2] Department of Earth and Environmental Sciences, Nagoya University, Nagoya, Japan*

*[3] Mining Department, Faculty of Engineering, University of Kurdistan, Sanandaj, Iran.*

*[4] Dipartimento di Scienze della Terra. Sapienza Università di Roma, P.le A. Moro, 5, 00185, Roma, Italy*

*[5] Istituto di Geologia Ambientale e Geoingegneria, c/o Dipartimento di Scienze della Terra, Sapienza Università di Roma, P.le A. Moro, 5, 00185, Roma, Italy*

*[6] School of Geology, University of Tehran, Tehran, Iran*

** = Corresponding author. E-mail: federico.rossetti@uniroma3.it*

## Abstract

The Eocene-Miocene Mianeh-Hashtroud igneous district in NW Iran is part of the Turkish–Caucasus–Iranian collision zone, a key region to decipher the assembly and differentiation of Gondwana-derived terranes along the Alpine-Himalayan convergence zone. Major inherited tectonic structures control in space and time the Mesozoic-Cenozoic transition from oceanic subduction to continental collision in the region. The geology of the study area is dominated by a polyphase, long-lived magmatic activity, spanning from ~45 to ~6 Ma. The igneous products are subalkaline to alkaline, with intermediate to acidic compositions and a high-K calcalkaline to shoshonitic affinity. Evidence of crustal contamination is attested by inherited zircons in the oldest (Eocene-Oligocene) samples, with ages spanning from Neo-Archean to Paleocene. The Sr-Nd isotopic compositions of the Eocene-Oligocene samples plot close to the Bulk Silicate Earth estimate, whereas the Miocene samples document stronger crustal contamination. The lack of correlation between Nd-Sr isotopes and $SiO_2$ supports a scenario of magma differentiation of different magma batches rather than crustal contamination. Major oxide and Sr-Nd isotopic variation lead us to suggest that magmatism is the consequence of re-melting of earlier underplated (Mesozoic-Tertiary) magmatic products, controlled by amphibole-dominated fractionation processes. Regional scale correlations show long-lived Cenozoic magmatism in NW Iran and Caucasus region, where the main porphyry and epithermal deposits occur. We propose that the Cenozoic collisional magmatism and the associated mineralisation at the junction between NW-Iran and Caucasus was controlled by the activity of a major, lithosphere-scale inherited boundary, transverse to the convergence zone. In such a geodynamic setting, the along-strike segmentation of the lithosphere slab generated asthenospheric melts, their upwelling into the metasomatised supra-subduction mantle wedge and the potential activation of different mantle and crustal sources, with consequent mineral endowment in the region.

## 1. Introduction

Convergent margins are the regions where the bulk of the continental crust forms and differentiates, assisted by magma production during oceanic subduction, continental collision and post-collisional tectonics (Harris et al., 1986; Stern, 2002; 2003; Tatsumi and Kogiso, 2003; 2005; DeCelles et al., 2009; Jagoutz and Klein, 2018). A progressive transition in space and time of the geochemical characteristics of magmatism in collisional settings, from calcalkaline/potassic/ultrapotassic (arc-type) to sodic alkaline (OIB-type) is commonly observed (e.g., Lustrino and Wilson, 2007). This documents the progressive involvement of sub-lithospheric mantle in magma genesis after the vanishing of subduction-related modifications (e.g., Lustrino et al., 2011; Di Giuseppe et al., 2017). This transition is enhanced in collisional zones, where difficulty of the buoyant continental lithosphere to be subducted is commonly associated with crustal thickening, and eventually to crustal and lithosphere delamination (Bird, 1979; Jull and Kelemen, 2001; Lustrino, 2005; Hacker et al., 2015), slab tearing (Faccenna et al., 2005; Rosenbaum et al., 2008; Prelević et al., 2015), slab break-off (von Blanckenburg and Davies, 1995). Scenarios which are prone to convective erosion of the sub-continental mantle (Houseman et al., 1981; Platt and England, 1994), decompressional melting (e.g. Allen et al., 2013a) or small-scale lithospheric keel instabilities (e.g. Kaislaniemi et al., 2014).

All of these processes may result in complex mantle-crust interaction, with the generation of compositionally different magma batches (Duggen et al., 2005; Allen et al., 2013a; van Hunen and Miller, 2015; Di Giuseppe et al., 2017; Kimura, 2017; Rezeau et al., 2018; Agostini et al., 2019). Tracing the spatial and temporal distribution of syn- to post-collisional magmatism can thus provide important information on the geodynamic evolution of convergent plate boundaries and, ultimately, on the spatio-temporal evolution of collisional systems.

The Alpine-Himalayan Belt, extending from the Western Mediterranean through Middle East to Indochina, is a natural laboratory to study the magmatic response to a continuously evolving geodynamic collisional process (Prelević and Seghedi, 2013). Indeed, it records a prolonged history of Mesozoic-Cenozoic accretionary tectonics and continental assembly along the southern margin of Eurasia, accompanied by diffuse syn- to post-collisional magmatism (e.g., Pearce et al., 1990; Keskin, 2003; Köksal et al., 2004; Guo et al., 2006; Şengör et al., 2008; Dilek and Altunkaynak, 2009; Dargahi et al., 2010; Agard et al., 2011; Lustrino et al., 2011; Prelević et al., 2013; Richards, 2015; Schleiffarth et al., 2015; Di Giuseppe et al., 2017; Sahakyan et al., 2017; Sugden et al., 2019).

The Cenozoic Turkish–Caucasus–Iranian collision zone (Fig. 1a) is part of this vast collisional belt (McKenzie, 1972; Allen et al., 2004; Reilinger et al., 2006). This region experienced complex and diachronous collisions involving the Arabia, Eurasia and Anatolia plates, started from Eocene-Oligocene (Allen and Armstrong, 2008; Okay et al., 2010; Ballato et al., 2011; Mouthereau et al., 2012; Madanipour et al., 2013; McQuarrie and van Hinsbergen, 2013; François et al., 2014; Cavazza et al., 2015, 2019; Cowgill et al., 2016; Vincent et al., 2016; Tadayon et al., 2018). The spatio-temporal distribution of collisional magmatism shows punctuated (in space and time) magma production with distinct geochemical characteristics (Berberian and Berberian, 1981; Pearce et al., 1990; Alavi, 1994; Vincent et al., 2005; Keskin et al., 2006; Omrani et al., 2008; Dilek et al., 2010; Verdel et al., 2011; Allen et al., 2013b; Chiu et al., 2013; Neill et al., 2013; Pang et al., 2013a; Neill et al., 2015; Schleiffarth et al., 2015; Shafaii Moghadam et al., 2015; Moritz et al., 2016b; Pang et al., 2016; Di Giuseppe et al., 2018; Lechmann et al., 2018).

Seismic tomography models have documented a variable but in general thin (<50-90 km) lithosphere (with the almost complete absence of the rigid lithospheric mantle) across eastern Anatolia and NW Iran with respect to the Zagros convergence zones (Fig. 1b; Priestley et al., 2012; Delph et al., 2017). The areas with thinner lithosphere and, in particular, the transition from thin to thick lithosphere, correspond to the regions with diffuse late Miocene-Quaternary collisional magmatism (Fig. 1a,b; Kheirkhah et al., 2009; Allen et al., 2013b; Chiu et al., 2013; Kheirkhah et al., 2013; Schleiffarth et al., 2015; Moghadam et al., 2016a; Di Giuseppe et al., 2017; Lechmann et al., 2018). Slab break-off, tearing and fragmentation, assisted by lithospheric mantle delamination, account for the Neogene-Quaternary transition from dominantly calcalkaline to mildly sodic alkaline magmatism (e.g., Faccenna et al., 2007; Göğüş and Pysklywec, 2008; Agard et al., 2011; van Hunen and Allen, 2011; Mouthereau et al., 2012; Allen et al., 2013b; Schildgen et al., 2014; Neill et al., 2015; Delph et al., 2017; Lechmann et al., 2018; Agostini et al., 2019). Furthermore, the presence of one of the major metallogenic region along the Alpine-Himalayan Belt (Richards, 2015) renders the Turkish-Caucasus-Iranian collision zone a suitable region to improve our understanding of the tectonic/geodynamic control on magmatism and associated mineralisation across collisional zones.

In this manuscript, we present whole-rock major and trace element data, U-Pb zircon geochronology and Sr-Nd isotope systematic for the Cenozoic Mianeh-Hashtroud magmatic district located in NW Iran, at the junction between the Cenozoic Urumieh–Dokhtar Magmatic Arc (UDMA), the Alborz-Talesh and the Zangezur–Ordubad magmatic districts (Figs. 1a and 2). The Mianeh-Hashtroud magmatic district (Study area; Figs. 2-3) hosts the unique Oligocene porphyry Mo-only ore deposit (Siah-Kamar) of the Iran region (Nabatian et al., 2017; Rabiee et al., 2019; Simmonds et al., 2019). The Mo-ore forming magmatism shows a metaluminous, high-K calcalkaline to shoshonitic geochemical fingerprint (Khaleghi et al., 2013; Nabatian et al., 2017), but the age and petrological information regarding the Mianeh-Hashtroud magmatic district is still lacking. The integration of the new data with those available from the neighbouring magmatic districts allowed us to shed light into the geodynamic scenario controlling the Cenozoic collisional magmatism and the associated porphyry mineralisation in the region.

## 2. Geodynamic and tectonic evolution

The study area is located within the Turkish-Caucasus-Iranian collision zone (Fig. 1a), a complex tectonic zone made up of a mosaic of continental and obducted oceanic blocks (e.g., Barrier et al., 2018). It results from a long-lasting history of NE-directed oceanic subduction (Paleo- and Neo-Tethys realms), continent-continent collision, as well as intra- and inter-plate deformation during the convergence and subsequent collision of the Arabian plate towards the Eurasian margin (e.g., Stocklin, 1968; McKenzie, 1972; Dewey et al., 1973; Berberian and King, 1981; Stampfli and Borel, 2002; Allen et al., 2004; Copley and Jackson, 2006; Okay et al., 2006; Reilinger et al., 2006; Sosson et al., 2010; Agard et al., 2011; McQuarrie and van Hinsbergen, 2013; Rolland, 2017; Barrier et al., 2018).In particular, during the Cretaceous, two subduction systems developed along the Turkish side to bound the Anatolide-Tauride block, forming the northern Izmir-Ankara-Erzincan suture zone in Anatolia, which can be traced to the east in the Sevan-Akera suture zone (Armenia), and the Bitlis-Pütürge suture zone to the south (Rolland et al., 2012). To the east, on the Iranian side, a single long-lived NE-directed subduction system was instead active along the Zagros convergence zone during Mesozoic until Paleogene (e.g., Agard et al., 2011; Fig. 1a). The Anatolian subduction systems were connected to the Zagros subduction zone through a major transform plate boundary, the Eastern Caucasus-Western Iran Boundary (Sosson et al., 2010; Rolland, 2017; Barrier et al., 2018; Rolland et al., 2020), with surface expression along the Aras Fault (Jackson and McKenzie, 1984; van der Boon et al., 2018; Fig. 1b). This major transform boundary is likely inherited from the late Palaeozoic-early Mesozoic fragmentation of the northern Gondwana Supercontinent, which produced, segmented and then recycled the Neotethyan oceanic lithosphere along the Zagros convergence zone since early Jurassic (Stampfli and Borel, 2002; Barrier et al., 2018). The Aras Fault operated as major transform boundary since Eocene, separating the Eastern Pontides-Caucasus domain from the Talesh-Alborz-Central Iran assembly (Meijers et al., 2017; van der Boon et al., 2018).

The age of Arabia-Eurasia continental collision is still debated, with estimates ranging from Eocene-Oligocene (McQuarrie et al., 2003; Allen and Armstrong, 2008; Agard et al., 2011; Ballato et al., 2011; Mouthereau et al., 2012; Rolland et al., 2012; Madanipour et al., 2013; McQuarrie and van Hinsbergen, 2013; Tadayon et al., 2017; Koshnaw et al., 2018; Tadayon et al., 2018) to Miocene (Guest et al., 2006; Okay et al., 2010; Cavazza et al., 2018). A major episode of basin inversion and rock exhumation, recorded along the Caucasus-Talesh-Alborz during the Eocene-Oligocene boundary, is related to the final closure of the Neotethys oceanic corridor in the Caucasus (e.g., Barrier et al., 2018). This major compressional stage marked the transition from back-arc extension to collisional tectonics in the region (Vincent et al., 2007; Mouthereau et al., 2012; Madanipour et al., 2013; François et al., 2014; Cowgill et al., 2016; Vincent et al., 2016; Rolland, 2017; van der Boon et al., 2018). A further major episode of intracontinental shortening and regional exhumation occurred during early-middle Miocene as documented along the Bitlis–Zagros collisional zone, the Talesh-Alborz and Caucasus regions (Axen et al., 2001; Hessami et al., 2001; Allen et al., 2004; Guest et al., 2006; Mouthereau et al., 2007; Ballato et al., 2008; Morley et al., 2009; Gavillot et al., 2010; Homke et al., 2010; Khadivi et al., 2010; Okay et al., 2010; Sosson et al., 2010; Ballato et al., 2011; Madanipour et al., 2013; François et al., 2014; Cavazza et al., 2018). This latter episode is also referred to the transition from a soft (mostly involving ocean-continent transition margins) to a hard (mature, continent-continent) stage of collision (Ballato et al., 2008; Cowgill et al., 2016). The early-middle Miocene also corresponds to a period of transition from marine to continental sedimentation in the Iranian plateau (Morley et al., 2009) and a major change in the magmatic activity in the region, from dominantly calcalkaline to K-alkaline in composition (Chiu et al., 2013).

The present-day tectonic setting of the region is considered as a consequence of the recent (<5 Ma) regional tectonic reorganisation (Allen et al., 2004; Copley and Jackson, 2006). Active deformation is largely accommodated through shortening to the north (Great Caucasus) and the south (Zagros) of the Turkish-Iranian Plateau, together with the westward escape of the Anatolia plate, accommodated by the dextral North Anatolian and sinistral East Anatolian Fault systems (Jackson and McKenzie, 1988; Jackson et al., 1995; Allen et al., 2004; Talebian and Jackson, 2004; Vernant et al., 2004; Avagyan et al., 2005; Reilinger et al., 2006; Avagyan et al., 2010; Walpersdorf et al., 2014; Tsereteli et al., 2016).

Active tectonics across the Turkish-Caucasus-Iranian Plateau is dominantly accommodated by WNW-ESE dextral shearing along the Chaldoran and Tabriz fault systems (Fig. 1a; Berberian and Arshadi, 1976; Jackson, 1992; Copley and Jackson, 2006; Djamour et al., 2011; Moradi et al., 2011; Moradi et al., 2016; Su et al., 2017). The GPS-derived tectonic boundaries within the collision zone identified four major tectonic blocks delimited by major seismically active zones (Reilinger et al., 2006; Fig. 1a): Anatolia, Caucasus (including Lesser Caucasus-Armenia and Talesh-Arasbaran zones), Alborz and Central Iran (including the Sanandaj-Sirjan Mesozoic and the Urumieh-Dokhtar Cenozoic magmatic zones). These four major blocks are bounded by the remnants of major ophiolite sutures, diachronoulsy structured during the Paleotethyan and Neotethyan closures (Fig 1a; Hässig et al., 2013; Barrier et al., 2018; Naumenko-Dèzes et al., 2020). This evidence supports the fundamental role of structural inheritance in controlling the present tectonic setting and the overall collisional evolution of the entire region.

An abrupt transition in the lithospheric structure and thickness is observed across the Aras Fault and the southward and sub-parallel Mianeh-Ardabil fault zone (Priestley et al., 2012; Fig. 1b), where the study area is located (Fig. 1b). Finally, seismic models of the crustal structure in the region show an abrupt change in the Moho depth across the Tabriz Fault, sharply deepening from ~33 to ~55 km to the NE in a ~50 km NE-SW transect (Taghizadeh-Farahmand et al., 2010; Shad Manaman et al., 2011; Fig. 1b).

## 3. Cenozoic magmatism and mineralisation

The geology of the Turkish-Caucasus-Iranian collision zone is dominated by diffuse exposure of Cenozoic igneous rocks, mostly occurring along the north-western segment of the UDMA (Takab and Mianeh-Hashtroud districts), Alborz, Lesser Caucasus-Arasbaran-Talesh (CAT), and the Naqadeh-Sonqor-Azna (NSA) magmatic zones (Fig. 2). Major magmatic episodes are distributed across the collisional zones during the Eocene-Oligocene and from middle Miocene to Quaternary. The geochemical signature of the collisional magmatism is characterized by a typical but diachronic progression from calcalkaline, shoshonite (Eocene-Oligocene) and adakitic, to dominantly high-K alkaline and minor sodic alkaline magmatism (Miocene-Quaternary; e.g., Vincent et al., 2005; Omrani et al., 2008; Azizi and Moinevaziri, 2009; Aghazadeh et al., 2010; Verdel et al., 2011; Allen et al., 2013b; Castro et al., 2013; Chiu et al., 2013; Neill et al., 2013; Pang et al., 2013a; Neill et al., 2015; Moghadam et al., 2016b; Moritz et al., 2016b; Pang et al., 2016; Rezeau et al., 2017; Lechmann et al., 2018; 2018; Schleiffarth et al., 2018; Shafaii Moghadam et al., 2018). A dominant contribution of a metasomatised sub-continental lithospheric mantle is commonly postulated as the main source for the Neogene-Quaternary magmatism in the region (Kheirkhah et al., 2009; Allen et al., 2013b; Chiu et al., 2013; Kheirkhah et al., 2013; Pang et al., 2013a; Sahakyan et al., 2017; Lechmann et al., 2018; Shafaii Moghadam et al., 2018).

The Cenozoic magmatism is mainly distributed to form roughly parallel linear arrays running NW-SE along the NSA (to the south), the UDMA, and the Alborz-CAT (to the north) magmatic zones (Fig. 2).

Within the NSA magmatic zone, Eocene (~52-34 Ma) tholeiitic to calcalkaline and high-K calcalkaline to shoshonite, dominantly intrusive, magmatic suites are reported (Azizi and Moinevaziri, 2009; Mazhari et al., 2009a; Mazhari et al., 2009b; Mazhari et al., 2010; Azizi et al., 2011; Bea et al., 2011; Mahmoudi et al., 2011; Mazhari et al., 2012; Whitechurch et al., 2013; Ao et al., 2016; Chiu et al., 2017; Nouri et al., 2017; Azizi et al., 2018a; Zhang et al., 2018). Azizi and Moinevaziri (2009) interpreted these igneous rocks as resulting from mantle sources modified during the Paleogene oceanic subduction along an active intra-oceanic arc system during the final closure stage of the Neotethys.

In the north-western UDMA, the Takab zone records a long-lived (Eocene to Miocene) magmatism, ranging from calcalkaline to K-alkaline compositions (Daliran et al., 2013; Heidari et al., 2015; Moghadam et al., 2016a; Shafaii Moghadam et al., 2017; Honarmand et al., 2018). The Takab region hosts important epithermal Miocene Au-Cu-Zn mineralisation systems [Zarshuran, Anguran and Touzlar deposits; e.g.; Mehrabi et al. (1999); Gilg et al. (2006); Daliran (2007); Heidari et al. (2015); Fig. 2 and Supplementary Material S1]. The large Miocene-Quaternary Sahand (~8-0.17 Ma) and Sabalan (~4.5-0.15 Ma) and the smaller Saray (~11 Ma) composite volcanoes (Pang et al., 2013b; Ghalamghash et al., 2016; Lechmann et al., 2018; Ghalamghash et al., 2019; Lustrino et al., 2019b) are the most prominent volcanic structures in the region (Fig. 2), with the Saray volcano marking the first stage of post-collisional magmatism in the Arabia-Eurasia collisional zone (Pang et al., 2013b; Moghadam et al., 2014). The volcanic activity starts with emplacement of high-K basalts to plagioleucitites at Saray (Eslamieh peninsula), followed by trachyandesites to dacites of the two large Sahand and Sabalan, with a variable potassic to high-K calcalkaline and adakitic geochemical signatures. The origin of the igneous activity is referred either to mantle melting triggered by slab roll-back and slab break-off shortly after continental collision (Ghalamghash et al., 2016; 2019) or to lithospheric small scale convection in post-subduction environments (Kaislaniemi et al., 2014).Significantly, the lithosphere structure in the region is characterized by low velocity zones down to upper mantle depths, assumed as the source region of Neogene-Quaternary magmatism of NW Iran (Bavali et al., 2016).

In the Alborz-CAT zone, calcalkaline to alkaline magmatism is documented during the Eocene-Oligocene and is attributed to tapping of a metasomatized mantle source during lithosphere extension in a back-arc setting (Aghazadeh et al., 2011; Castro et al., 2013; Nabatian et al., 2014; Nabatian et al., 2016; Ashrafi et al., 2018; Eskandari et al., 2020). The Oligocene and early Miocene magmatism are more scattered. In particular, igneous rocks largely crop out within the Alborz-CAT zone, and are mostly aligned along, or confined within, the transverse Aras and Mianeh-Ardabil faults (Fig. 2).

The Arasbaran magmatic zone (part of the Alborz-CAT magmatic zone) hosts notable porphyry deposits, mainly associated with Oligocene-Miocene monzonitic and monzodioritic intrusive bodies and showing a concentration and ore enhancement toward the Aras Fault (Fig. 2). The Sungun, Haft Cheshmeh Cu-Mo and the Masjed-Daghi Cu-Au deposits are the most important ones, with molybdenite Re-Os ages of 21 Ma, 27 Ma and 20 Ma, respectively (Aghazadeh et al., 2015). A prolonged and stationary magmatism (mostly with geochemical affinities ranging from calcalkaline to shoshonitic and adakitic) is instead documented in the Lesser Caucasus, where the Meghri-Ordubad composite pluton records ~30 Myr-long activity (Eocene-Miocene; Chiu et al., 2013; Moritz et al., 2016b; Rezeau et al., 2016; 2017; Fig. 2; 2018). The Zangezur-Ordubad region in the Lesser Caucasus host two stages of porphyry Cu-Mo deposits, including the ~49-44 Ma (Agarak, Hanqasar, Aygedzor and Dastakert), and the 27-26 Ma (e.g., Kadjaran) deposits (Moritz et al., 2016a). The prolonged mantle-derived magmatism has been considered as a prerequisite to form fertile magmatic-hydrothermal systems and a key requirement for the formation of economically important porphyry Cu-Mo deposits (Rezeau et al., 2016; 2017). Similarly to the Arasbaran zone, the frequency of occurrence of the porphyry systems increases toward the Aras Fault.

## 4. Materials and methods

The research strategy combines field investigations with laboratory (petrographic, geochemical and geochronological) studies aimed at describing the spatio-temporal and petrological evolution of the Cenozoic magmatic activity within the Mianeh-Hashtroud magmatic complex (Figs. 1a and 2). Fieldwork was based on the 1:250,000 cartography (Amidi et al., 1987; Khodabandeh et al., 1999), with the scope to map and refine the distribution of the main magmatic rock types (Fig. 3). Classification of the different magmatic rocks in plutonic, hypabyssal and volcanic types follows Le Maitre et al. (2005). An extensive sampling of representative lithologies has been then carried out and investigated though whole-rock geochemistry [X-ray fluorescence (XRF) and inductively coupled plasma mass spectrometry (ICPMS) methods], Sr-Nd isotope systematics and laser ablation inductively coupled plasma mass spectrometry (LA-ICP-MS) zircon U-Pb geochronology. The studied samples are listed in Table 1, where their location, age, petrography and geochemical characteristics are reported in detail. The analytical protocols are described in Appendix A1.

The collected data are then compared with the geochronological and geochemical data available from the neighbouring regions, in order to build up a regional synthesis and propose a corresponding geodynamic interpretation.

## 5. Field data and petrography

The revised geological map of the study area is shown in Fig. 3 that includes the new geochronological data presented in this study (see below). The stratigraphy of the area is dominated by a wide exposure of Eocene volcanic rocks (hereafter referred as country rocks), unconformably covered by discontinuous Miocene volcanic and volcano-sedimentary successions and by continental deposits of the Miocene Upper Red Fm. (Amidi et al., 1987; Khodabandeh et al., 1999; Ballato et al., 2017). Pliocene-Quaternary continental sedimentary successions are dominant in the western and eastern sectors of the area (Fig. 3).

The Eocene volcanic country rocks are intruded by a polyphase (Eocene, Oligocene to early Miocene) magmatic suite made up of intrusive (plutonic and hypabyssal) bodies. The main plutonic bodies, usually showing granular texture, crop out to the northwest and centre of the study area, defining a NW-SE-oriented magmatic belt (Figs. 3 and 4a). The Oligocene magmatism is responsible for the Mo endowment in the Siah-Kamar porphyry deposit (Fig. 3; Nabatian et al., 2014; Rabiee et al., 2019; Simmonds et al., 2019). The Mo deposit is associated with diffuse rock alteration, grading from an inner sodic-potassic to an outer propylitic zone formed in the 33-28 Ma time lapse (Rabiee et al., 2019).To the southeast (from Khatoon-Abad to Siah-Kamar), an array of abundant E-W to NE-SW striking microgranular and porphyritic felsic stocks, and dykes intrude the Eocene country rocks (Figs. 3 and 5).

A description of the rocks samples, textural types and mineral paragenesis is reported below.

### *5.1 Eocene volcanic country rocks*

The Eocene volcanic country rocks (samples MN04, MN33, MN37, MN38) are made up of a thick pile of alternating lava flows and pyroclastic beds, variably affected by secondary hydrothermal propylitic alteration (Fig. 4a and 4b-d). Lava flows are intermediate to acid in composition, ranging from basaltic trachyandesite to trachyte (Table 1). They are porphyritic (phenocryst load up to 20 vol%) with hypohyaline textures and fluidal to trachytic fabrics (Fig. 6a). They show a mineral assemblage with phenocrysts dominated by plagioclase together with amphibole and minor clinopyroxene (commonly altered), in a matrix of plagioclase, alkali feldspar, ± amphibole, clinopyroxene and Fe-Ti oxides, plus minor accessory phases such as apatite and zircon, and glass (Fig. 6a).

### *5.2. Plutonic rocks*

Intrusive rocks (samples MN09, MN10A, MN10B, MN10C, MN12, MN67 and MN74; Fig. 4a and 4e-h) are characterized by equigranular to porphyritic holocrystalline hypidiomorphic textures (Fig. 6b-e). Mineral assemblages are typical of metaluminous rocks with plagioclase, alkali feldspar, quartz, amphibole (usually altered), biotite, and minor clinopyroxene (altered). Plagioclase occurs either as coarse-grained crystals (Fig. 6b) or as phenocrysts (Fig. 6e). Based on the modal abundance of minerals (Middlemost, 1994), these intrusive rocks span from monzodiorite to monzonite, syenite and granite (Table 1). Granitoid rocks (samples MN10A; Fig. 6d) host monzonitic enclaves (samples MN10B-C) with porphyritic holocrystalline textures and comparable mineral assemblage (plagioclase, alkali feldspar, quartz, biotite, amphibole and clinopyroxene). Accessory minerals are made of apatite, zircon and Fe-Ti oxides.

### *5.3. Hypabyssal rocks*

Hypabyssal rocks consist of stocks and dykes (samples MN02A, MN02B, MN03, MN45, MN65 and MN76; Fig. 5a). They show typical porphyritic holocrystalline, hypidiomorphic to autoallotriomorphic textures and microcrystalline matrix. (Fig. 5b-c). These subvolcanic rocks span from mafic to felsic compositions and, show a metaluminous assemblage similar to that of intrusive rocks made up of quartz, alkali feldspar, plagioclase, biotite, amphibole, with minor clinopyroxene (Fig. 6f-g-h). Accessory minerals include apatite, zircon and Fe-Ti oxides. These hypabyssal rocks span from monzonite to syenite and granite in composition (Table 1).

### *5.4. Volcanic rocks*

Volcanic rocks (samples MN05, MN07, MN19, MN20, MN35, MN39, MN43, MN44, and MN73) include glass bearing magmatic rocks. This rock group comprises porphyritic to vitrophyric types, with hypohyaline to holohyaline groundmass (Fig. 5a,d-h). Phenocrysts (20-40 % vol.) are subhedral to euhedral plagioclase, alkali feldspars, quartz, biotite, amphibole (seldom altered) and rare, commonly altered, clinopyroxene (Fig. 6i). Rock composition varies from andesite to rhyolite (Table1).

## 6. Zircon U-Pb geochronology

The zircon U-Pb geochronological study was carried out on twelve samples (Table 1 and Fig. 7). Zircons were investigated through backscattered electron and cathodoluminescence (CL) imaging (see Supplementary Material S2), and then analysed through LA-ICP-MS. Analytical results are reported in Table 2, whereas the detailed description for each sample analysis is provided in Supplementary Material S3. In general, the Th/U values are in the range of 0.09-2.79, compatible with an igneous origin (e.g., Rubatto, 2002; Kirkland et al., 2015). Evidence of Pb loss is seen in some zircons resulting in discordant ages but most of the results from oscillatory growth zones show concordant ages. The criteria for age calculation, including categorisation of the zircon types (autocrysts, antecrysts, and xenocrysts/inherited; Miller et al., 2007) is provided in Appendix A1 and illustrated as probability density plots and weighted mean ages in Supplementary material S4.

Below, the basic features of the analysed samples are reported, grouping the results into four age groups: (1) two samples from the Eocene country rocks [MN33 (43.4 ± 2.6 Ma) and MN38 (38.4 ± 1.0 Ma)], collected at the bottom and at the top of the exposed volcanic succession in the Siah-Kamar area (Fig. 3); (2) three samples from the Eocene intrusive bodies exposed in the central [Khatoonabad; samples MN09 (44.32 ± 0.58 Ma), MN67 (40.69 ± 0.88 Ma) and MN10 (36.75 ± 0.62 Ma)] and north-western corner [Dizaj; samples MN45 (30.21 ± 0.41 Ma) and MN76 (28.23 ± 0.88 Ma)] of the study area; (3) four samples from the Oligocene-early Miocene hypabyssal/subvolcanic bodies [samples MN05 (22.6 ± 0.41 Ma), MN39 (28.18 ± 0.80 Ma), MN43 (26.97 ± 0.35 Ma) and MN44 (26.19 ± 0.54 Ma)] from the central and western sectors of the study area (Khatoonabad and Ebak), and (4) one sample (MN35) from the late Miocene volcanic rocks (Ebak area; 5.93 ± 0.24 Ma Fig. 3).

The Eocene volcanic country rocks possess remarkable number of inherited zircons. Inherited zircons are commonly broken, fractured and sub-rounded often showing metamict and complex zoning textures. Sample MN33 show 27 inherited zircons out of a total of 39 measured zircons, which show apparent $^{206}Pb/^{238}U$ ages spanning from Middle Jurassic (167 ± 5 Ma) to Paleo-Proterozoic (2208 ± 49 Ma). Sample MN38 contains inherited zircons showing apparent $^{206}Pb/^{238}U$ ages spanning from Paleocene (63 ± 5 Ma) to Neoarchean (2737 ± 77 Ma; Table 2). A few inherited zircons are also seen in sample MN67 (40.69 ± 0.88 Ma) from a syenite body. They show $^{206}Pb/^{238}U$ ages spanning from Upper Cretaceous (~67 Ma) to Upper Jurassic (~148 Ma; Table 2).

## 7. Geochemistry

The major and trace element compositions of the twenty-six samples analysed in this study are presented in Table 3. The mass loss of ignition (LOI) is mostly below 3 wt%, apart from four samples (LOI = 4-6 wt%) and one sample with LOI = 10.5 wt%. Collectively, the studied samples mostly plot in the alkaline (trachyandesite and trachyte) and the rhyolite fields of the TAS diagram (Fig. 8a), with just a few samples falling in the andesite and dacite fields. In the $K_2O$ vs. $SiO_2$ diagram (Peccerillo and Taylor, 1976), the samples are mostly distributed in the high-K calcalkaline and shoshonitic fields (Fig. 8b). To avoid possible bias caused by post-emplacement fluid-rock interaction during hydrothermal alteration, the classification schemes based on immobile trace elements (Winchester and Floyd, 1977; Hastie et al., 2007) are adopted in this study. In the $SiO_2$ vs. Nb/Y classification proposed by Winchester and Floyd (1977; Fig. 8c), the samples mostly confirm their alkaline nature, with a few of them straddling the subalkaline to alkaline division line, and only two falling in a true alkaline field. In the Th vs. Co classification diagram (Hastie et al., 2007; Fig. 8d) the samples mostly plot in the high-K and shoshonite (HK-SHO) series fields.

None of the investigated rocks shows primitive character (MgO<4 wt%) and all can be interpreted as derivative liquids. Anyway, some general comments on the possible mantle sources can be inferred focusing on the least differentiated compositions (samples with <57 wt% $SiO_2$; 1.6-4.0 wt% MgO). In the following, the description of the geochemical characteristics of the analysed rocks is presented, grouping them into the respective age group.

### *7.1. Eocene rocks*

Eocene rocks (n = 11) show intermediate to acid compositions ($SiO_2$ = 54.27-75.22 wt%), with moderate $Al_2O_3$ (12.52-18.83 wt%), low MgO (0.07-3.97 wt%) and Mg# (Mg/[Mg+$Fe_{tot}$]*100) in the 5-62 range. These samples also show low $TiO_2$ (<1 wt%), coupled with a wide range of CaO (0.43-8.36 wt%), $K_2O$ (2.06-7.78 wt%) and $Na_2O$ (2.92-8.99 wt%; Table 3). Harker diagrams for major elements show negative correlation with $SiO_2$ for $Al_2O_3$, $Fe_2O_{3tot}$, MgO, Mg#, $P_2O_5$ and $TiO_2$, and CaO, whereas $Na_2O$, with the exception of an outlier at ~9 wt% remains nearly constant at ~3-4 wt% within the ~54-75 wt% $SiO_2$ range (Fig. 9). Trace elements show no appreciable trends with $SiO_2$ for many of large ion lithophile elements (LILE) and high field strength elements (HFSE). Negative correlation with $SiO_2$ are observed for Y, V, Eu, Sr, and Dy/Yb, whereas Nb shows a rough correlation with the same parameter. A selection of the key trace elements vs. $SiO_2$ is reported in Fig. 10. Primitive Mantle (PM) normalized (after Lyubetskaya and Korenaga, 2007) patterns of the Eocene samples show several spikes and troughs, with marked enrichments of LILE (such as Ba, Cs, Rb, Th, U, K) and distinctive Pb positive spikes. Some HFSE (Nb, Ta and Ti) define clear troughs, whereas others (Zr and Hf) show no anomaly compared to neighbouring REE with similar incompatibility (Sm and Eu). Phosphorous shows the largest variability, with slightly positive to negative anomalies (Fig. 11a). Middle (MREE) to Heavy (HREE) lanthanides show no appreciable fractionation, with an overall flat pattern and an average $(Dy/Lu)_N$ ratio of ~1.2. This is associated to a mildly fractionated Light (LREE)/HREE ratio [$(La/Lu)_N$ ~10.9] and a limited Eu negative anomaly [(Eu/Eu*) ~0.79]. Overall, the least differentiated Eocene rocks (those with $SiO_2$ <57 wt%) show a relatively uniform character, resembling closely the present-day average global subducting sediment (GloSS; Plank, 2014; Fig. 8). The most evolved compositions ($SiO_2$ >58 wt%) show more spiky patterns, with deeper troughs and higher peaks, mostly related to fractionation apatite, zircon and Fe-Ti oxides.

### *7.2. Oligocene rocks*

Oligocene rocks (n = 13) nearly completely overlap the Eocene rocks in Harker diagrams with negative correlations for $Al_2O_3$, $Fe_2O_{3tot}$, MgO, $TiO_2$, $P_2O_5$ and CaO, whereas no clearly correlation is observed for $Na_2O$ and $K_2O$ contents (Fig. 9). Oligocene rocks show intermediate to acid compositions ($SiO_2$ = 54.9-82.2 wt%), with the highest $SiO_2$ contents likely representing the effect of silicification. Rock compositions with SiO2 >78 wt% are no longer discussed in the text, because silicification is usually associated with alkali mobility (e.g., Lustrino et al., 2010). The main characteristics are variable $Al_2O_3$ content (ranging from 10.2 to 22.7 wt%), low MgO (0.1-3.5 wt%), low $TiO_2$ (<1 wt%) and CaO (0.1-7.8 wt%), with $K_2O$ generally higher than $Na_2O$ (Table 3).

Analogously, trace elements show a negative correlation for Y, Yb and Eu content and the Dy/Yb, whereas Nb and Th correlates with $SiO_2$ (Fig. 10). The least differentiated Oligocene rocks ($SiO_2$ <57 wt%) are characterized by PM-normalized patterns qualitatively indistinguishable from those of the Eocene rocks. The LREE/HREE [average $(La/Lu)_N$ ~20.9] and MREE/HREE values [average $(Dy/Lu)_N$ ~1.4] are slightly higher than the Eocene samples, whereas no substantial Eu anomaly is recorded (Eu/Eu* ~1.01). The most evolved samples ($SiO_2$ >57 wt%) show more spiky patterns and deep negative Eu anomaly (Eu/Eu* ~0.74).

### *7.3. Miocene rocks*

Miocene rocks (n = 3) show intermediate to acid compositions ($SiO_2$ = 56.5-78 wt%), with moderate $Al_2O_3$ (10.6-17 wt%), low MgO (0.1-2 wt%) and Mg# (23-39), low $TiO_2$ (<1 wt%), CaO in the 0.1-3.8 wt% range, and $K_2O$ generally higher than $Na_2O$. The strongly evolved composition found in one early Miocene sample (MN05; $SiO_2$ = ~78 wt%) is characterized by strongly fractionated patterns with deep troughs at P and Ti and with Eu/Eu* = 0.32. The youngest, late Miocene shoshonite (MN35) shows intermediate $SiO_2$ (~56.5 wt%), low MgO (~2 wt%) and high $K_2O/Na_2O$ (~4.6) (Table 3). For what regards major and trace elements, these rocks plot along the same trend shown by the Eocene and Oligocene samples in Harker diagrams (Figs. 9 and 10). PM- and CI chondrite-normalized patterns do not show any peculiarity, closely resembling the GloSS composition (Fig. 11).

## 8. Sr-Nd isotopic ratios

Eighteen selected samples have been analysed for Sr and Nd isotopic ratios. The measured and initial $^{87}Sr/^{86}Sr$ and $^{143}Nd/^{144}Nd$ isotopic ratios, as well as epsilon values for Mianeh-Hashtroud igneous rocks are reported in Table 4. In the $\varepsilon Nd_{(t)}$ vs. $^{87}Sr/^{86}Sr_{(t)}$ isotopic diagram (Fig. 12), most of the Cenozoic igneous rocks analysed in this study plot not far away from BSE and ChUR estimates, with a relatively limited range of $^{87}Sr/^{86}Sr_{(t)}$ (0.70413-0.70524) and $^{143}Nd/^{144}Nd_{(t)}$ (0.51267-0.51274), the latter corresponding to $\varepsilon Nd_{(t)}$ from -1.56 to +3.47. The Eocene and Oligocene rocks overlap almost completely, whereas the Miocene samples show more radiogenic $^{87}Sr/^{86}Sr_{(t)}$ (0.70588-0.70646), but $\varepsilon Nd_{(t)}$ mostly within the lower end range of the older samples (−1.56 to +0.32; Fig. 12). The Nd model ages ($T_{DM}$), as calculated based on the method of Keto and Jacobsen (1987), span from 0.61 to 0.96 Ga (Table 4).

## 9. Discussion

### *9.1. A long-lived stationary magmatism*

The new U-Pb zircon ages presented in this study document a protracted magmatic activity from Eocene (~44 Ma) to late Miocene (~6 Ma). Based on the weighted age distribution of the all measured zircon autocrysts and antecrysts (Miller et al., 2007), a continuous range from ~55 (54.8 ± 2.8 Ma) to ~12 Ma emerges, with a possible magmatic lull at ~12-8 Ma (Fig. 13a), which is consistent with the onset of the eruptive magmatism in nearby Sahand volcano (Richards et al., 2006; Sawada et al., 2016; Lechmann et al., 2018). Zircons possessing ages older than this continuous range are considered as inherited ones (see Appendix A1 and Supplementary Material S4). This evidence suggests the incorporation of zircon antecrysts during successive magmatic injections and growth of newly formed zircons (autocrysts sensu Miller et al., 2007), in a scenario of a long-lived and incremental growth of the Mianeh-Hashtroud magmatic complex during the Eocene-Miocene times.

The dated samples contain abundant inherited zircons populations. Irrespective of the obtained apparent $^{206}Pb/^{238}U$ ages, the Th/U values of the inherited zircons (n = 142) range from 0.1 to 2.7. These values, together with their textural characteristics (oscillatory to sector zoning; Supplementary Material S2) are consistent with a magmatic origin (e.g., Corfu et al., 2003; Kirkland et al., 2015). Both zircon antecrysts and inherited zircons show a major frequency distribution in Cenozoic with respect to pre-Cenozoic times (Fig. 13b-c). The pre-Cenozoic inherited zircons are mainly observed in the Eocene and Oligocene rocks, typically showing a remarkable spread of apparent $^{206}Pb/^{238}U$ ages, from Paleocene (~66-56 Ma) to Neoarchean (~2.6-2.7 Ga; Fig. 13b; Table 2). In particular, the age distribution histogram for inherited zircons in Eocene rocks clusters at ~260-140 Ma (Triassic-Jurassic), ~550-420 Ma (Cambrian-Silurian), and ~1000-700 Ma (early Neoproterozoic), but Proterozoic (up to 2500 Ma) and Neoarchean (2800-2500 Ma) ages are also reported (Fig. 13b). These age span is compatible with ages reported for the Iran basement rocks (Mazhari et al., 2009a; Chiu et al., 2013; Nutman et al., 2014; Ao et al., 2016; Lechmann et al., 2018; Shakerardakani et al., 2019).

A similar scenario of prolonged and stationary incremental growth of a magmatic complex (in terms of both longevity and age of magma production) is documented in the Cenozoic Zangezur-Ordubad magmatic district of Lesser Caucasus (Moritz et al., 2016b; Rezeau et al., 2016; 2017; 2018; Fig. 2). Interestingly, the Zangezur-Ordubad in the Lesser Caucasus, Arasbaran, Takab and the Mianeh-Hashtroud magmatic districts of NW Iran are all located along the transverse tectonic structures of Aras and Ardabil-Mianeh-Baneh fault systems that segment the continental lithosphere of the Iranian plateau (Fig. 2).

### *9.2. Petrological model*

Irrespective of the age and magmatic facies, the PM-normalized patterns of the Mianeh-Hashtroud rocks closely resemble present-day subducting sediments (GloSS; Plank, 2014), average continental crust composition (Rudnick and Gao 2003) and igneous rocks emplaced above active subduction systems (Fig. 11a). The geochemical fingerprints of magmas generated in subduction zones consist in variable LILE enrichment, whose most peculiar features are the positive anomalies at K and Pb together with the HFSE depletion with respect to their neighbouring elements. This likely results from the ability of metasomatic fluids to fractionate elements with different compatibilities in subducted slab-derived components (e.g., Pearce, 1983; Tatsumi et al., 1986; Tatsumi et al., 1991; Hawkesworth et al., 1997; Elburg et al., 2002; Kessel et al., 2005; Kimura, 2017; Sahakyan et al., 2017; Lustrino et al., 2019a; Zheng, 2019). The overall incompatible element fractionation reported in Fig. 11 clearly evidences the subduction-related compositions of the investigated rocks. Taking into consideration the poor Sr enrichment and the relatively high Y and Yb content (coupled with relatively low Sr/Y and La/Yb), the majority of Mianeh-Hashtroud rocks plot within the calcalkaline arc field, supporting a dominant subduction fingerprint of the Mianeh-Hashtroud magmatic suite (Figs. 14a-b).

The enrichment in incompatible trace elements (such as Ba Cs, Th, La, Nd) are significantly higher than those of calcalkaline arc magmas, but comparable with those of continental arc shoshonites (see inset in Fig. 10b). When the least differentiated compositions ($SiO_2$ <57 wt%) are taken into account, the low Ce/Pb (~1.5-6.0) and Nb/U (~2.6-8.9) and the extremely high $(Th/Nb)_N$ ratios (up to ~12.9) are all consistent with crustal contamination or subduction-related metasomatism (Pearce, 2008). In the Th/Yb vs. Nb/Yb diagram (Fig.14c), the same samples plot far from the oceanic mantle array, pointing towards high Th/Yb ratios, close to average crustal values (4.0-7.0; average value 5.3; Rudnick and Gao, 2003) at moderate Nb/Yb (5.3-17.7; Fig. 14c). In the Rb vs. Nb+Y discrimination diagram (Fig.14c) for granitic rocks, the most evolved Mianeh-Hashtroud rocks ($SiO_2$>57 wt%) fall within the volcanic arc granite field, in the transition zone assumed as representative of post-collisional environments (Fig. 14d).

Most of the studied samples show highly evolved compositions, with low MgO contents, Mg# (0.62–0.35) and Cr contents (all but two samples <200 ppm; Table 3), far away from the primitive melt composition expected for melts in equilibrium with the mantle (Kimura, 2017; Schmidt and Jagoutz, 2017; Zheng, 2019). These compositional characteristics suggest that the studied magmatic products experienced significant fractionation after mantle anatexis (e.g., Ulmer et al., 2018). The occurrence of amphibole in the basic products and the negative correlation with differentiation of major oxides, including $Al_2O_3$, $FeO_t$, MgO, CaO, $TiO_2$, and $P_2O_5$, and trace elements such as V, and Y are indeed compatible with amphibole fractionation (Fig. 9). The negative correlation of Dy/Yb with $SiO_2$ (e.g., Klein et al., 1997; Davidson et al., 2007) and of Dy/Dy* $[Dy_N/(La_N^{4/13} x Yb_N^{9/13})]$ vs. Dy/Yb (Davidson et al., 2013) is further compatible with a role of amphibole in the fractionating assemblage (Fig. 10).

The negative correlation of Eu with differentiation (Fig. 10) also suggests a significant role of plagioclase fractionation mainly in the most evolved compositions. Due to the higher partitioning coefficient of middle REE (MREE) with respect to LREE and HREE in amphibole (Davidson et al., 2007), fractional crystallization of amphibole from parental mafic magmas can explain the strongly fractionated REE and the flat HREE patterns of the Mianeh-

Hashtroud magmatic products. In this scenario, the slightly high Sr/Y and $(La/Yb)_N$ of a subset of samples, falling in the adakitic field (Moyen, 2009; Figs. 14a,b), can be thus related to amphibole fractionation during magmatic differentiation (e.g., Macpherson et al., 2006; Li et al., 2009; Moyen, 2009; Dessimoz et al., 2012; Rossetti et al., 2014; Moghadam et al., 2016b), rather than the result of partial melting of the eclogitised subducted oceanic crust.

The Sr and Nd isotopic compositions (Fig. 12) indicate depleted (or not strongly enriched) mantle sources for the Eocene-Oligocene rocks of the Mianeh-Hashtroud area. On the other hand, the Miocene hypabyssal and volcanic rocks document a stronger crustal component in their genesis. This shift towards a more enriched mantle source with decreasing age is in line with the isotopic signature of the Neogene-Quaternary magmatic products of NW Iran Azerbaijan (Lechmann et al., 2018; Fig. 12). The lack of clear correlation between Sr and Nd isotopes vs. $SiO_2$ (Fig. 15) supports a scenario of magmatic differentiation with limited assimilation of radiogenic crustal rocks (i.e., old basement) as the main petrogenetic process. Similar Sr-Nd isotope ratios and magmatic differentiation series dominated by fractional crystallization and limited crustal assimilation are reported from the Mesozoic and Cenozoic Zangezur–Ordubad magmatic district (Mederer et al., 2013; Moritz et al., 2016b; Fig. 12), which could be interpreted with a similar scenario and therefore extended to the Lesser Caucasus region too. This is in line with the studies in Lesser Caucasus by Sugden et al. (2019).

On the other hand, the occurrence of abundant inherited zircons in Eocene magmatic products points to crustal contamination during the melt differentiation and the emplacement in the crust. On this regard, it is worth nothing that the relatively young Nd model ages (0.61 to 0.91 Ga) indicate that the Mianeh-Hashtroud magmatic products originated from juvenile crustal rocks. This hypothesis is corroborated by the compelling evidence of extensive magmatic underplating during Mesozoic-Cenozoic times in Central Iran in the upper-plate of the Neotethyan subduction (e.g., Berberian and King, 1981; Omrani et al., 2008; Azizi and Moinevaziri, 2009; Agard et al., 2011; Verdel et al., 2011; Richards, 2015). It is worth noting that the Sr-Nd isotopic compositions of the Mianeh-Hashtroud igneous rocks overlap those reported for the Jurassic-Cretaceous igneous rocks from the neighbouring Sanandaj-Sirjan zone (ε$Nd_{(t)}$: +2 to +6; Azizi and Asahara, 2013; Azizi et al., 2018b; Fig. 12). We therefore propose that voluminous mafic underplating of arc magmas during the Mesozoic and its successive re-melting was the dominant process leading to the generation of the Cenozoic magmatism in NW Iran (e.g., Chung et al., 2009; Pe-Piper et al., 2009; Jiang et al., 2014). On this regard, melting of LILE- and LREE-enriched and HFSE-depleted lower crustal mafic amphibolite could have contributed to impart the distinctive trace-element characteristics of the Cenozoic igneous rocks of Mianeh-Hashtroud (Fig. 11a), including the moderate fractionation of the REE and the flat HREE pattern (e.g., Pe-Piper et al., 2009; Jiang et al., 2014; Fig. 11b).

Crustal foundering and melting have been also proposed as viable mechanism for the genesis of the Quaternary adakite-like magmatism in Iran (Pang et al., 2016) and for the Miocene-Quaternary magmatism in NW Iran (Lechmann et al., 2018). It is worth noting that the Sr-Nd isotope systematics of the Cenozoic magmatism in NW Iran largely overlaps in space and time, confirming extensive crustal recycling as a viable source of magmatism in the region.

This reconstruction is also compatible with the dominant enriched sources of the Miocene-Quaternary magmatism documented in the Azerbaijan region of NW Iran (Lechmann et al., 2018), which confirm crustal-contaminated heterogeneous magmatic sources through time (Allen et al., 2013b; Lechmann et al., 2018). This hypothesis is also compatible with the scenarios proposed for the collisional to post-collisional Cenozoic high-K calcalkaline and shoshonitic magmatism documented along the entire Alpine-Himalayan convergence zone, such as in the Tibet (Xu et al., 2002; Hou et al., 2004; Wang et al., 2006; Chung et al., 2009; Jiang et al., 2014; Yang et al., 2016), Turkey (Delph et al., 2017) and Mediterranean area (Duggen et al., 2005), as well as the California Arc (Saleeby et al., 2003; Ducea, 2011).

To conclude, the characteristic incompatible element content, the interelemental fractionation in primitive mantle-normalized diagrams, the Sr-Nd isotopic ratios, as well as the Proterozoic- to Mesozoic-age inherited magmatic zircon of the Mianeh-Hashtroud rocks indicate derivation from mantle sources that strongly interacted with crustal lithologies. A derivation from a mantle source that suffered contamination of heterogeneous subducted components would have resulted in much more variable trace element ratios as well as wider Sr-Nd isotopic ratio spreading. On the other hand, much of the variations observed in the Mianeh-Hashtroud rocks are compatible with fractional crystallization processes, with limited crustal interaction/assimilation.

To sum up, in order to reconcile the large spread of ages of inherited zircons with the relatively homogeneous Sr and Nd isotopic ratios, as well as the similar interelemental fractionation, we propose that the Mesozoic to Neoarchean inherited zircons occasionally found in the Mianeh-Hashtroud rocks were acquired by partial melting of early underplated rocks at the base of the Iran block lithosphere.

## 10. Geodynamic synthesis

The geodynamic framework of the Cenozoic Mianeh-Hashtroud magmatism should be referred to the specific tectonic setting recorded in the Turkish-Caucasus-Iranian collision zone during the Eocene-Miocene time lapse (Fig. 16). In particular, we refer to the transition from the Neotethyan oceanic subduction along the Zagros convergence zone to the continental collision along the Caucasus-Talesh-Alborz zone (Vincent et al., 2005; 2007; Barrier and Vrielynck, 2008; Sosson et al., 2010; Mouthereau et al., 2012; Madanipour et al., 2013; François et al., 2014; Cowgill et al., 2016; FVincent et al., 2016; Rolland, 2017; Barrier et al., 2018; van der Boon et al., 2018). This along-strike change in the geodynamic regime was accommodated by a former transform plate boundary, the Eastern Caucasus-Western Iran Boundary (Barrier and Vrielynck, 2008; Sosson et al., 2010; Rolland, 2017; Barrier et al., 2018; van der Boon et al., 2018), that originally linked the Anatolian subduction systems with the Zagros subduction zone through a major transform plate boundary (Fig. 16a).

The waning stage of the Neotethyan oceanic subduction was associated with volcanic flare-up in the upper-plate domain (Central Iran) during the Eocene, from ~55 to 35 Ma (Verdel et al., 2011). This phase is coeval with the transition from an advancing (Cretaceous-

Paleocene) to a retreating plate margin along the Zagros convergence zone (e.g., Agard et al., 2011; Verdel et al., 2011; Moghadam et al., 2016b; Tadayon et al., 2018). Slab hinge retreat and the associated decompression melting of a passively upwelling subduction component-modified asthenosphere were coupled with lithospheric thinning during the transition from compression to back-arc extension in the overriding plate (Verdel et al., 2011; Castro et al., 2013; Moghadam et al., 2016b). Such circumstances resulted in enhanced melting of the subduction-modified mantle wedge (Prelević et al., 2008; Avanzinelli et al., 2009; Tommasini et al., 2011; Allen et al., 2013b; Di Giuseppe et al., 2018), causing voluminous mafic magma production. Under this geodynamic regime, lateral flow of fertile sub-lithospheric mantle is enhanced in slab windows along the transform boundary toward the mantle wedge region (Faccenna et al., 2005; Rosenbaum et al., 2008; van Hunen and Miller, 2015). The upwelling asthenosphere and the associated melts provided the required thermal conditions for lower crustal melting (mostly at the expenses of the Mesozoic Neotethyan arc root) and continuous addition of mantle-derived melts to the crust (Fig. 16b).

From the late Eocene-Oligocene, the overriding plate experienced renewed shortening causing by the onset of continental collision in the upper plate of the Zagros convergence zone. This new tectonic setting induced shortening and incremental crustal thickening in the upper-plate domain, preconditioning to lithospheric keel foundering and delamination from Oligocene-Miocene onward (Fig. 16c). The continuous passive upwelling of asthenosphere material through the slab windows along the transform boundary caused the transition to the dominantly alkaline, magmatism during the Neogene-Quaternary (Allen et al., 2013b; Chiu et al., 2013; Kaislaniemi et al., 2014; Pang et al., 2014; 2016; Lechmann et al., 2018). The thin lithosphere across the north of this major boundary continues to the Anatolia region (Delph et al., 2017), supporting a scenario of over-thickened lithosphere delamination during the continental collision and the thermal erosion of the lower crust induced by the passive asthenosphere upwelling (Fig. 16d).

It is worth nothing that the zone of long-lived stationary magmatism and associated porphyry mineralisation (i.e. the Lesser Caucasus and the Mianeh-Hashtroud areas), are located in the region where an abrupt change of the lithosphere structure and thickness of Moho depths occurs (Fig. 1b and Fig. 2). In particular, the northward thinning of the lithosphere from ~240 to ~100 km (Priestley et al., 2012), broadly corresponds to a set of orogeny-orthogonal, regional NE-SW strike-slip fault systems (Aras Fault to the north and Mianeh-Ardabil Fault to the south). These systems segment the continuity of the regional NW-SE-striking regional tectonic lineament (Figs. 1 and 2). More importantly, this sharp lithosphere discontinuity is localized along the former transform plate boundary, the Eastern Caucasus-Western Iran Boundary (Barrier and Vrielynck, 2008; Sosson et al., 2010; Rolland, 2017; Barrier et al., 2018; van der Boon et al., 2018), that originally linked the Anatolian subduction systems with the Zagros subduction zone through a major transform plate boundary. Therefore, this sharp and prominent lithospheric discontinuity is supposed to be localized along a pre-existing, lithosphere-scale tectonic boundary that have kinematically accommodated the differential deformation transmitted by the adjacent subduction systems to the overriding plates during Mesozoic and Paleogene times.

The occurrence of long-lived magmatic zones and associated ore deposits along the paleo-tectonic boundary separating the Zagros systems from the Caucasus collisional zone may have significant implications for the localisation of the ore deposits in the region. It is in fact suggested that Mianeh-Ardabil and Aras faults localised along this inherited structural zone and have acted as conduits for prolonged magma ascent to the chamber. In this scenario, the intersection of major orogen-parallel and orogen-orthogonal fault systems provided the favourite locations for development of long-lived magma chambers and consequent ore endowment (e. g., Richards, 2000; Chernicoff et al., 2002)

To sum up, we propose that the long-lived Cenozoic stationary igneous activity of the Lesser Caucasus and Mianeh-Hashtroud districts was dominantly localized along a major inherited lithosphere-scale transform boundary along the Eastern Caucasus-Western Iran Boundary. In such a geodynamic setting, segmentation of the Neotethyan oceanic slab generated asthenospheric melt upwelling into the metasomatised supra-subduction mantle wedge with the potential to activate different mantle and crustal sources. This process is able to generate heterogeneous magmatism (Prelević et al., 2013; Kaislaniemi et al., 2014) such as that distributed along the Caucasus-Iranian collision zone (Allen et al., 2013b; Moritz et al., 2016b; Lechmann et al., 2018). The Eastern Caucasus-Western Iran Boundary is thus considered as a long-lived structure, which acted as a weak zone susceptible to multiple tectonic reactivation, able to focus magmatism as a preferred pathway for magma ascent and emplacement and focused mineralisation.

## 11. Conclusions

The results of the present study can be synthesised as follows:

1) A long-lived (>20 Myr) history of igneous activity occurred in the Mianeh-Hashtroud area, from ~45 to 22 Ma, which culminated with Mo porphyry mineralization at ~33-28 in the Siah-Kamar deposit (Rabiee et al., 2019; Simmonds et al., 2019). The igneous activity resumed during latest Miocene (~6 Ma), with emplacement of lava flows.

2) The whole-rock chemistry of the Cenozoic igneous products of the Mianeh-Hashtroud district is characterized by evolved mildly potassic alkaline terms, with shoshonitic serial affinity, mostly with shoshonite to trachyte and rhyolite (plus the plutonic equivalents) compositions. The incompatible element budget of these samples resembles the composition of magmas emplaced above present-day subduction settings, with overall intra-elemental fractionation patters very close to the global subducting sediments (GloSS) and average upper crustal estimates. The variation of major oxides and trace elements with silica is qualitatively compatible with a process involving amphibole and plagioclase fractionation.

3) The initial Sr-Nd isotopic ratios of the Eocene-Oligocene volcanic and plutonic rocks show relatively narrow variation, not far from the BSE and ChUR estimates. The Miocene hypabyssal and the late Miocene volcanic rocks of the area shows more radiogenic $^{87}Sr/^{86}Sr$ (0.7058-0.7059 and 0.7064, respectively) and relatively low $^{143}Nd/^{144}Nd$ (0.51260-0.51263 and 0.512550, respectively).

4) The results of the present study indicate that collisional-stage magmatism originated from subduction-modified metasomatized mantle lithosphere, in a geodynamic environment dominated by a major transform boundary and flow of fertile mantle material along the slab windows.

5) The Cenozoic stationary, long-lived magmatism and associated mineralisation within the Turkish-Caucasus-Iranian collision zone was structurally controlled by the reactivation of the orogen-orthogonal Eastern Caucasus-Western Iran transform boundary.

## Acknowledgments

This paper is dedicated to the memory of Prof. Jeremy Richards. This research is part of the first Author PhD program at the Roma Tre University. The Grant to Department of Science, Roma Tre University (MIUR-Italy Dipartimenti di Eccellenza, ARTICOLO 1, COMMI 314 – 337 LEGGE 232/2016) is gratefully acknowledged. ML acknowledges Ateneo Sapienza funds (2016-2017-2018). We are indebted to K. Yamamoto for support and providing access to the XRF, ICP-MS and LA-ICP-MS facilities at Nagoya University. The constructive reviews of H. Rezeau and two anonymous reviewers greatly contributed to improve the manuscript.

**APPENDIX A1: Analytical techniques**

**XRF and ICP-MS**

Major elements were measured using the conventional X-ray fluorescence (XRF) technique with a Rigaku ZSX Primus II. Glass beads for the XRF analysis were prepared as follows: 0.50 g of the sample powder was mixed with 5.0 g of lithium tetraborate, and the mixture was melted at 1200 °C for 12–17 min with a high-frequency bead sampler (Rigaku Co. Japan). The loss on ignition (LOI) of the sample was measured from the sample powder weight in a quartz glass beaker in the oven at 950 °C for 5 h.

Regarding inductively coupled plasma mass spectrometry (ICP-MS) analysis, powdered samples were prepared in a two stage decomposition method using HF+$HClO_4$ at high pressure-temperature condition. About 0.1 g of powdered samples were dissolved in a covered Teflon beaker using 2 ml HF (38%) and 0.5–1 ml $HClO_4$ (70%) at 120–140 °C on a hotplate until the powder was dissolved. The dissolved samples were dried at 150 °C on the hotplate with infrared lamps. The dried samples were dissolved in 10 ml of 6 M and the 2.4 M HCl and moved to a PE centrifuge tube. After centrifuging the sample solution, the supernatant was moved to the PTFE beaker, and the residue was moved into a small sealed PTFE vessel. After drying the wet residue on a hotplate, 0.5-0.7 ml of HF (38%) and 0.5 ml of $HClO_4$ (70%) were added. The small sealed PTFE vessel was set in an outer PTFE vessel, and the outer vessel was inserted into a stainless steel jacket. The steel-jacketed PTFE bomb was kept in an oven at 180 °C for 2–3 days to completely dissolve the residual minerals. The second decomposed fraction was dried on a hotplate and dissolved in 6 M and the 2.4 M HCl. This solution was mixed with the supernatant in the PTFE beaker and weighted. The solution was divided into two aliquots at a ratio of 1:9. The first aliquot (10%: Fraction A) was used for the ICP-MS analysis for trace and REEs and the second (90%: Fraction B) was used for the column chemistry to extract Sr and Nd for natural Sr–Nd isotopes. The Fraction A dried on hotplate with IR lamp and then was dissolved in 15 ml 2M $HNO_3$. About 5-10 was used to measure Hf and Ta and the rest of the sample was diluted 10 times more to measure other trace and REE. The concentrations of trace elements, including REEs, were analyzed using ICP-MS device (Agilent 7700x).

Fraction B was loaded to a calibrated cation exchange column (AG50W-X8, 200–400 mesh) using HCl eluent (2.4 and 6 M) to separate Sr. Fraction B2 was then loaded in another specialized calibrated cation exchange column using HIBA eluent (0.2- 0.4 M) to separate Nd.

**Sr-Nd isotope**

To extract Sr and Nd from the samples, routine cation exchange column chemistry methods were followed. Fraction B from the dissolved samples (above section) was loaded to a calibrated cation exchange column (AG50W-X8, 200–400 mesh) using HCl eluent (2.4 and 6 M) to collect Sr and REE fraction. The REE fraction then loaded in another specialized calibrated cation exchange column using HIBA (hydroxyiso butyric acid) eluent (0.2- 0.4 M) to separate Nd fraction. Sr and Nd bearing fractions were dried inside a specially equipped drier and then dissolved in roughly calculated amount of pure water and appropriate amount of dissolved. Sr and Nd samples (~0.1-0.2 μg) then were loaded on Ta single and Re triple filaments with 2 M $H_3PO_4$, respectively. NBS987 and JNdi-1 (Tanaka et al., 2000) were adopted as standards for natural Sr and Nd isotope ratios, respectively. The isotope ratios of Sr and Nd were then measured using a VG Sector 54-30 and GVI IsoProbe Thermal ionization mass spectrometers (TIMS) at Nagoya University. The mass fractionations were corrected for measured Nd and Sr isotope ratios based on $^{143}Nd/^{144}Nd = 0.7219$ and $^{87}Sr/^{86}Sr = 0.1194$, respectively. Averages and 1SE for isotope ratio standards, were $^{143}Nd/^{144}Nd = 0.512115 \pm 0.000080$ (n = 4), and $^{87}Sr/^{86}Sr = 0.7102527 \pm 0.0000095$ (n = 4). Moreover two standard samples of JG-1a (granite) and JA-1 (andesite; (Imai et al., 1995) were used which the result show the analytical errors below 5% for most of the elements and less than 10% for the rest.

**Zircon U-Pb Geochronology**

The zircon U-Pb geochronology study was carried out at the Department of Earth and Environmental Sciences of Nagoya University. Twelve samples were selected for zircon grains separation. About 5 kg (more than 10 kg for volcanic rock samples) for each sample were collected, crushed and the heavy mineral fraction were recovered. Except to monzonitic subvolcanic samples, sufficient zircon grains were available in the case of intrusive and subvolcanic samples but only few zircon grains were found in volcanic samples in which some of them were useless due to the small grain size (<30 μm) or to the strongly fractured crystal structure. Petrographic investigation was devoted to identify the possible presence of inclusions inside zircon grains. Cathodoluminescence (CL) and Back Scatter Electron (BSE) imaging were used first to gather information on the grain texture and internal growth and/or alteration zoning. Zircon grains with intense fracturing and inclusions were avoided. The zircon grains were analyzed by laser ablation inductively coupled plasma mass spectrometry LA-ICP-MS (Agilent 7700XICPMS machine connected with NWR213 (Electro Scientific Industries) laser ablation system (Kouchi et al., 2015). A standard glass (NIST SRM 610) and two zircon standards, named 91500 (1059 Ma, Wiedenbeck et al., 1995) and OD-3 (33.1 Ma, Iwano et al., 2013) were used. Blanks, the zircon standards, and the standard glass were measured at the beginning and ending of each measurement cycle. Eight points were measured in each cycle. The ISOPLOT V4.15 software (Ludwig, 2011) was utilized to calculate the Concordia, statistics and to prepare the age plots. Correction for the common Pb was performed using $^{204}Pb$ intensity (Cox and Wilton, 2006) and value of common Pb was assumed by Stacey and Kramers (1975) model. The results with common Pb values above 20% and Th/U <0.1 were eliminated from calculations. Preferably, Concordia age was calculated for a maximum number of concordant results in a continuous range. Where some results from main population yielded discordant ages, then a Terra-Wasserburg method was used.

The continuous distributed ages (with 2σ uncertainty) of measured zircons which lie in an almost normally distributed population are considered as zircons autocrysts from which the age of the sample is calculated (Supplementary Material S4). Zircons possessing ages between sample's age and the oldest Eocene igneous rock are considered as antecrysts. Zircons which show older ages with a significant gap from the oldest sample are xenocrysts or inherited ones (Miller et al., 2007; also see Supplementary Material S4).

## References

Agard, P., Omrani, J., Jolivet, L., Whitechurch, H., Vrielynck, B., Spakman, W., MoniÉ, P., Meyer, B., Wortel, R., 2011. Zagros orogeny: a subduction-dominated process. Geological Magazine 148, 692-725.

Aghazadeh, M., Castro, A., Badrzadeh, Z., Vogt, K., 2011. Post-collisional polycyclic plutonism from the Zagros hinterland: the Shaivar Dagh plutonic complex, Alborz belt, Iran. Geological Magazine 148, 980-1008.

Aghazadeh, M., Castro, A., Omran, N.R., Emami, M.H., Moinvaziri, H., Badrzadeh, Z., 2010. The gabbro (shoshonitic)–monzonite–granodiorite association of Khankandi pluton, Alborz Mountains, NW Iran. Journal of Asian Earth Sciences 38, 199-219.

Aghazadeh, M., Hou, Z., Badrzadeh, Z., Zhou, L., 2015. Temporal–spatial distribution and tectonic setting of porphyry copper deposits in Iran: Constraints from zircon U–Pb and molybdenite Re–Os geochronology. Ore Geology Reviews 70, 385-406.

Agostini, S., Savasçin, M.Y., Di Giuseppe, P., Di Stefano, F., Karaoglu, O., Lustrino, M., Manetti, P., Ersoy, Y., Kurum, S., Onal, A.O., 2019. Neogene volcanism in Elazig-Tunceli area (eastern Anatolia): geochronological and petrological constraints. Italian Journal of Geosciences, in press, https://doi.org/10.3301/IJG.2019.3318.

Alavi, M., 1994. Tectonics of the Zagros orogenic belt of Iran: new data and interpretations. Tectonophysics 229, 211-238.

Allen, M., Jackson, J., Walker, R., 2004. Late Cenozoic reorganization of the Arabia-Eurasia collision and the comparison of short-term and long-term deformation rates. Tectonics 23, TC2008, doi:2010.1029/2003TC001530.

Allen, M., Kheirkhah, M., Neill, I., Emami, M., McLeod, C., 2013a. Generation of arc and within-plate chemical signatures in collision zone magmatism: Quaternary lavas from Kurdistan province, Iran. Journal of Petrology 54, 887-911.

Allen, M., Kheirkhah, M., Neill, I., Emami, M.H., McLeod, C., 2013b. Generation of Arc and Within-plate Chemical Signatures in Collision Zone Magmatism: Quaternary Lavas from Kurdistan Province, Iran.

Allen, M.B., Armstrong, H.A., 2008. Arabia–Eurasia collision and the forcing of mid-Cenozoic global cooling. Palaeogeography, Palaeoclimatology, Palaeoecology 265, 52-58.

Amidi, M., Alavi Tehrani, M., Lotfi, P., Haghipour, A., Sabzehei, M., Behroozi, A., Lescuyer, J., Riou, R., 1987. Geological map of Mianeh. Geological Survey of Iran, Tehran.

Ao, S., Xiao, W., Jafari, M.K., Talebian, M., Chen, L., Wan, B., Ji, W., Zhang, Z., 2016. U–Pb zircon ages, field geology and geochemistry of the Kermanshah ophiolite (Iran): From continental rifting at 79 Ma to oceanic core complex at ca. 36 Ma in the southern Neo-Tethys. Gondwana Research 31, 305-318.

Ashrafi, N., Jahangiri, A., Hasebe, N., Eby, G.N., 2018. Petrology, geochemistry and geodynamic setting of Eocene-Oligocene alkaline intrusions from the Alborz-Azerbaijan magmatic belt, NW Iran. Geochemistry 78, 432-461.

Avagyan, A., Sosson, M., Karakhanian, A., Philip, H., Rebai, S., Rolland, Y., Melkonyan, R., Davtyan, V., 2010. Recent tectonic stress evolution in the Lesser Caucasus and adjacent regions. Geological Society, London, Special Publications 340, 393.

Avagyan, A., Sosson, M., Philip, H., Karakhanian, A., Rolland, Y., Melkonyan, R., Rebaï, S., Davtyan, V., 2005. Neogene to Quaternary stress field evolution in Lesser Caucasus and adjacent regions using fault kinematics analysis and volcanic cluster data. Geodinamica Acta 18, 401-416.

Avanzinelli, R., Lustrino, M., Mattei, M., Melluso, L., Conticelli, S., 2009. Potassic and ultrapotassic magmatism in the circum-Tyrrhenian region: Significance of carbonated pelitic vs. pelitic sediment recycling at destructive plate margins. Lithos 113, 213-227.

Axen, G.J., Lam, P.S., Grove, M., Stockli, D.F., Hassanzadeh, J., 2001. Exhumation of the west-central Alborz Mountains, Iran, Caspian subsidence, and collision-related tectonics. Geology 29, 559-562.

Azizi, H., Asahara, Y., 2013. Juvenile granite in the Sanandaj–Sirjan Zone, NW Iran: Late Jurassic–Early Cretaceous arc–continent collision. International Geology Review 55, 1523-1540.

Azizi, H., Asahara, Y., Mehrabi, B., Chung, S.L., 2011. Geochronological and geochemical constraints on the petrogenesis of high-K granite from the Suffi abad area, Sanandaj-Sirjan Zone, NW Iran. Chemie der Erde - Geochemistry 71, 363-376.

Azizi, H., Hadad, S., Stern, R.J., Asahara, Y., 2018a. Age, geochemistry, and emplacement of the ~40-Ma Baneh granite–appinite complex in a transpressional tectonic regime, Zagros suture zone, northwest Iran. International Geology Review 61, 95-223.

Azizi, H., Lucci, F., Stern, R.J., Hasannejad, S., Asahara, Y., 2018b. The Late Jurassic Panjeh submarine volcano in the northern Sanandaj-Sirjan Zone, northwest Iran: Mantle plume or active margin? Lithos 308-309, 364-380.
Azizi, H., Moinevaziri, H., 2009. Review of the tectonic setting of Cretaceous to Quaternary volcanism in northwestern Iran. Journal of Geodynamics 47, 167-179.
Ballato, P., Cifelli, F., Heidarzadeh, G., Ghassemi, M.R., Wickert, A.D., Hassanzadeh, J., Dupont-Nivet, G., Balling, P., Sudo, M., Zeilinger, G., 2017. Tectono-sedimentary evolution of the northern Iranian Plateau: insights from middle–late Miocene foreland-basin deposits. Basin Research 29, 417-446.
Ballato, P., Nowaczyk, N.R., Landgraf, A., Strecker, M.R., Friedrich, A., Tabatabaei, S.H., 2008. Tectonic control on sedimentary facies pattern and sediment accumulation rates in the Miocene foreland basin of the southern Alborz mountains, northern Iran. Tectonics 27, TC6001, doi:6010.1029/2008TC002278.
Ballato, P., Uba, C.E., Landgraf, A., Strecker, M.R., Sudo, M., Stockli, D.F., Friedrich, A., Tabatabaei, S.H., 2011. Arabia-Eurasia continental collision: Insights from late Tertiary foreland-basin evolution in the Alborz Mountains, northern Iran. Bulletin 123, 106-131.
Barrier, E., Vrielynck, B., 2008. Palaeotectonic maps of the Middle East. Atlas of 14.
Barrier, E., Vrielynck, B., Brouillet, J., Brunet, M., 2018. Paleotectonic Reconstruction of the Central Tethyan Realm. Tectonono-Sedimentary-Palinspastic maps from Late Permian to Pliocene. CCGM/CGMW, Paris. CCGM/CGMW Paris: France.
Bavali, K., Motaghi, K., Sobouti, F., Ghods, A., Abbasi, M., Priestley, K., Mortezanejad, G., Rezaeian, M., 2016. Lithospheric structure beneath NW Iran using regional and teleseismic travel-time tomography. Physics of the Earth and Planetary Interiors 253, 97-107.
Bea, F., Mazhari, A., Montero, P., Amini, S., Ghalamghash, J., 2011. Zircon dating, Sr and Nd isotopes, and element geochemistry of the Khalifan pluton, NW Iran: Evidence for Variscan magmatism in a supposedly Cimmerian superterrane. Journal of Asian Earth Sciences 40, 172-179.
Berberian, F., Berberian, M., 1981. Tectono-plutonic episodes in Iran. Zagros Hindu Kush Himalaya Geodynamic Evolution 3, 5-32.
Berberian, M., Arshadi, S., 1976. On the evidence of the youngest activity of the North Tabriz Fault and the seismicity of Tabriz City, pp. 397-418.
Berberian, M., King, G., 1981. Towards a paleogeography and tectonic evolution of Iran. Canadian Journal of Earth Sciences 18, 210-265.
Bird, P., 1979. Continental delamination and the Colorado Plateau. Journal of Geophysical Research: Solid Earth 84, 7561-7571.
Castro, A., Aghazadeh, M., Badrzadeh, Z., Chichorro, M., 2013. Late Eocene–Oligocene post-collisional monzonitic intrusions from the Alborz magmatic belt, NW Iran. An example of monzonite magma generation from a metasomatized mantle source. Lithos 180-181, 109-127.
Cavazza, W., Albino, I., Galoyan, G., Zattin, M., Cattò, S., 2019. Continental accretion and incremental deformation in the thermochronologic evolution of the Lesser Caucasus. Geoscience Frontiers 10, 2189-2202.
Cavazza, W., Albino, I., Zattin, M., Galoyan, G., Imamverdiyev, N., Melkonyan, R., 2015. Thermochronometric evidence for Miocene tectonic reactivation of the Sevan-Akera suture zone (Lesser Caucasus): A far-field tectonic effect of the Arabia-Eurasia collision?
Cavazza, W., Cattò, S., Zattin, M., Okay, A.I., Reiners, P., 2018. Thermochronology of the Miocene Arabia-Eurasia collision zone of southeastern Turkey. Geosphere 14, 2277-2293.
Chernicoff, C.J., Richards, J.P., Zappettini, E.O., 2002. Crustal lineament control on magmatism and mineralization in northwestern Argentina: geological, geophysical, and remote sensing evidence. Ore Geology Reviews 21, 127-155.
Chiu, H.-Y., Chung, S.-L., Zarrinkoub, M.H., Melkonyan, R., Pang, K.-N., Lee, H.-Y., Wang, K.-L., Mohammadi, S.S., Khatib, M.M., 2017. Zircon Hf isotopic constraints on magmatic

and tectonic evolution in Iran: Implications for crustal growth in the Tethyan orogenic belt. Journal of Asian Earth Sciences 145, 652-669.

Chiu, H.-Y., Chung, S.-L., Zarrinkoub, M.H., Mohammadi, S.S., Khatib, M.M., Iizuka, Y., 2013. Zircon U–Pb age constraints from Iran on the magmatic evolution related to Neotethyan subduction and Zagros orogeny. Lithos 162, 70-87.

Chung, S.-L., Chu, M.-F., Ji, J., O'Reilly, S.Y., Pearson, N.J., Liu, D., Lee, T.-Y., Lo, C.-H., 2009. The nature and timing of crustal thickening in Southern Tibet: Geochemical and zircon Hf isotopic constraints from postcollisional adakites. Tectonophysics 477, 36-48.

Copley, A., Jackson, J., 2006. Active tectonics of the Turkish-Iranian Plateau. Tectonics 25, TC6006, doi:6010.1029/2005TC001906.

Corfu, F., Hanchar, J.M., Hoskin, P.W.O., Kinny, P., 2003. Atlas of Zircon Textures. Reviews in Mineralogy and Geochemistry 53, 469-500.

Cowgill, E., Forte, A.M., Niemi, N., Avdeev, B., Tye, A., Trexler, C., Javakhishvili, Z., Elashvili, M., Godoladze, T., 2016. Relict basin closure and crustal shortening budgets during continental collision: An example from Caucasus sediment provenance. Tectonics 35, 2918-2947.

Cox, R.A., Wilton, D.H., 2006. U–Pb dating of perovskite by LA-ICP-MS: an example from the Oka carbonatite, Quebec, Canada. Chemical Geology 235, 21-32.

Daliran, F., 2007. The carbonate rock-hosted epithermal gold deposit of Agdarreh, Takab geothermal field, NW Iran—hydrothermal alteration and mineralisation. Mineralium Deposita 43, 383-404.

Daliran, F., Pride, K., Walther, J., Berner, Z.A., Bakker, R.J., 2013. The Angouran Zn (Pb) deposit, NW Iran: Evidence for a two stage, hypogene zinc sulfide–zinc carbonate mineralization. Ore Geology Reviews 53, 373-402.

Dargahi, S., Arvin, M., Pan, Y., Babaei, A., 2010. Petrogenesis of post-collisional A-type granitoids from the Urumieh–Dokhtar magmatic assemblage, Southwestern Kerman, Iran: Constraints on the Arabian–Eurasian continental collision. Lithos 115, 190-204.

Davidson, J., Turner, S., Handley, H., Macpherson, C., Dosseto, A., 2007. Amphibole “sponge” in arc crust? Geology 35, 787-790.

Davidson, J., Turner, S., Plank, T., 2013. Dy/Dy*: Variations Arising from Mantle Sources and Petrogenetic Processes. Journal of Petrology 54, 525-537.

DeCelles, P.G., Ducea, M.N., Kapp, P., Zandt, G., 2009. Cyclicity in Cordilleran orogenic systems. Nature Geoscience 2, 251-257.

Defant, M.J., Drummond, M.S., 1990. Derivation of some modern arc magmas by melting of young subducted lithosphere. Nature 347, 662-665.

Delph, J., Abgarmi, B., M. Ward, K., Beck, S., Özacar, A., Zandt, G., Sandvol, E., Turkelli, N., Kalafat, D., 2017. The effects of subduction termination on the continental lithosphere: Linking volcanism, deformation, surface uplift, and slab tearing in central Anatolia.

Dessimoz, M., Müntener, O., Ulmer, P., 2012. A case for hornblende dominated fractionation of arc magmas: the Chelan Complex (Washington Cascades). Contributions to Mineralogy and Petrology 163, 567-589.

Dewey, J.F., Pitman, W.C., III, Ryan, W.B.F., Bonnin, J., 1973. Plate Tectonics and the Evolution of the Alpine System. GSA Bulletin 84, 3137-3180.

Di Giuseppe, P., Agostini, S., Lustrino, M., Karaoğlu, Ö., Savaşçın, M.Y., Manetti, P., Ersoy, Y., 2017. Transition from compression to strike-slip tectonics revealed by Miocene–Pleistocene volcanism west of the Karlıova triple junction (East Anatolia). Journal of Petrology 58, 2055-2087.

Di Giuseppe, P., Agostini, S., Manetti, P., Savaşçın, M.Y., Conticelli, S., 2018. Sub-lithospheric origin of Na-alkaline and calc-alkaline magmas in a post-collisional tectonic regime: Sr-Nd-Pb isotopes in recent monogenetic volcanism of Cappadocia, Central Turkey. Lithos 316-317, 304-322.

Dilek, Y., Altunkaynak, Ş., 2009. Geochemical and temporal evolution of Cenozoic magmatism in western Turkey: mantle response to collision, slab break-off, and

lithospheric tearing in an orogenic belt. Geological Society, London, Special Publications 311, 213-233.
Dilek, Y., Imamverdiyev, N., Altunkaynak, Ş., 2010. Geochemistry and tectonics of Cenozoic volcanism in the Lesser Caucasus (Azerbaijan) and the peri-Arabian region: collision-induced mantle dynamics and its magmatic fingerprint. International Geology Review 52, 536-578.
Djamour, Y., Vernant, P., Nankali, H.R., Tavakoli, F., 2011. NW Iran-eastern Turkey present-day kinematics: results from the Iranian permanent GPS network. Earth and Planetary Science Letters 307, 27-34.
Ducea, M.N., 2011. Fingerprinting orogenic delamination. Geology 39, 191-192.
Duggen, S., Hoernle, K., van den Bogaard, P., Garbe-Schönberg, D., 2005. Post-collisional transition from subduction-to intraplate-type magmatism in the westernmost Mediterranean: evidence for continental-edge delamination of subcontinental lithosphere. Journal of Petrology 46, 1155-1201.
Elburg, M.A., van Bergen, M., Hoogewerff, J., Foden, J., Vroon, P., Zulkarnain, I., Nasution, A., 2002. Geochemical trends across an arc-continent collision zone: magma sources and slab-wedge transfer processes below the Pantar Strait volcanoes, Indonesia. Geochimica et Cosmochimica Acta 66, 2771-2789.
Eskandari, A., Deevsalar, R., De Rosa, R., Shinjo, R., Donato, P., Neill, I., 2020. Geochemical and isotopic constraints on the evolution of magma plumbing system at Damavand Volcano, N Iran. Lithos 354-355, 105274.
Faccenna, C., Civetta, L., D'Antonio, M., Funiciello, F., Margheriti, L., Piromallo, C., 2005. Constraints on mantle circulation around the deforming Calabrian slab. Geophysical Research Letters 32, L06311, doi:06310.01029/02004GL021874.
Faccenna, C., Funiciello, F., Civetta, L., D'Antonio, M., Moroni, M., Piromallo, C., 2007. Slab disruption, mantle circulation, and the opening of the Tyrrhenian basins.
François, T., Burov, E., Agard, P., Meyer, B., 2014. Buildup of a dynamically supported orogenic plateau: Numerical modeling of the Zagros/Central Iran case study. Geochemistry, Geophysics, Geosystems 15, 2632-2654.
Gavillot, Y., Axen, G.J., Stockli, D.F., Horton, B.K., Fakhari, M.D., 2010. Timing of thrust activity in the High Zagros fold-thrust belt, Iran, from (U-Th)/He thermochronometry. Tectonics 29, TC4025,doi:4010.1029/2009TC002484.
Ghalamghash, J., Mousavi, S.Z., Hassanzadeh, J., Schmitt, A.K., 2016. Geology, zircon geochronology, and petrogenesis of Sabalan volcano (northwestern Iran). Journal of Volcanology and Geothermal Research 327, 192-207.
Ghalamghash, J., Schmitt, A., Chaharlang, R., 2019. Age and compositional evolution of Sahand volcano in the context of post-collisional magmatism in northwestern Iran: Evidence for time-transgressive magmatism away from the collisional suture. Lithos 344, 265-279.
Gilg, H.A., Boni, M., Balassone, G., Allen, C.R., Banks, D., Moore, F., 2006. Marble-hosted sulfide ores in the Angouran Zn-(Pb–Ag) deposit, NW Iran: interaction of sedimentary brines with a metamorphic core complex. Mineralium Deposita 41, 1-16.
Göğüş, O., Pysklywec, R., 2008. Mantle lithosphere delamination driving plateau uplift and synconvergent extension in Eastern Anatolia. Geology 36, 723-726.
Guest, B., Stockli, D.F., Grove, M., Axen, G.J., Lam, P.S., Hassanzadeh, J., 2006. Thermal histories from the central Alborz Mountains, northern Iran: implications for the spatial and temporal distribution of deformation in northern Iran. Geological Society of America Bulletin 118, 1507-1521.
Guo, Z., Wilson, M., Liu, J., Mao, Q., 2006. Post-collisional, Potassic and Ultrapotassic Magmatism of the Northern Tibetan Plateau: Constraints on Characteristics of the Mantle Source, Geodynamic Setting and Uplift Mechanisms. Journal of Petrology 47, 1177-1220.
Hacker, B.R., Kelemen, P.B., Behn, M.D., 2015. Continental Lower Crust. Annual Review of Earth and Planetary Sciences 43, 167-205.

Harris, N.B.W., Pearce, J.A., Tindle, A.G., 1986. Geochemical characteristics of collision-zone magmatism. Geological Society, London, Special Publications 19, 67-81.

Hässig, M., Rolland, Y., Sosson, M., Galoyan, G., Sahakyan, L., Topuz, G., Çelik, Ö.F., Avagyan, A., Müller, C., 2013. Linking the NE Anatolian and Lesser Caucasus ophiolites: evidence for large-scale obduction of oceanic crust and implications for the formation of the Lesser Caucasus-Pontides Arc. Geodinamica Acta 26, 311-330.

Hastie, A.R., Kerr, A.C., Pearce, J.A., Mitchell, S.F., 2007. Classification of Altered Volcanic Island Arc Rocks using Immobile Trace Elements: Development of the Th–Co Discrimination Diagram. Journal of Petrology 48, 2341-2357.

Hawkesworth, C.J., Turner, S.P., McDermott, F., Peate, D.W., van Calsteren, P., 1997. U-Th Isotopes in Arc Magmas: Implications for Element Transfer from the Subducted Crust. Science 276, 551.

Heidari, S.M., Daliran, F., Paquette, J.-L., Gasquet, D., 2015. Geology, timing, and genesis of the high sulfidation Au (–Cu) deposit of Touzlar, NW Iran. Ore Geology Reviews 65, 460-486.

Hessami, K., Koyi, H.A., Talbot, C.J., Tabasi, H., Shabanian, E., 2001. Progressive unconformities within an evolving foreland fold–thrust belt, Zagros Mountains. Journal of the Geological Society 158, 969-981.

Homke, S., Vergés, J., Van Der Beek, P., Fernàndez, M., Saura, E., Barbero, L., Badics, B., Labrin, E., 2010. Insights in the exhumation history of the NW Zagros from bedrock and detrital apatite fission-track analysis: evidence for a long-lived orogeny. Basin Research 22, 659-680.

Honarmand, M., Xiao, W., Nabatian, G., Blades, M.L., dos Santos, M.C., Collins, A.S., Ao, S., 2018. Zircon U-Pb-Hf isotopes, bulk-rock geochemistry and Sr-Nd-Pb isotopes from late Neoproterozoic basement in the Mahneshan area, NW Iran: Implications for Ediacaran active continental margin along the northern Gondwana and constraints on the late Oligocene crustal anatexis. Gondwana Research 57, 48-76.

Hou, Z.Q., Gao, Y.F., Qu, X.M., Rui, Z.Y., Mo, X.X., 2004. Origin of adakitic intrusives generated during mid-Miocene east–west extension in southern Tibet. Earth and Planetary Science Letters 220, 139-155.

Houseman, G.A., McKenzie, D.P., Molnar, P., 1981. Convective instability of a thickened boundary layer and its relevance for the thermal evolution of continental convergent belts. Journal of Geophysical Research: Solid Earth 86, 6115-6132.

Hubner, H., 1969. Geological map of Iran. National Iranian Oil Company, Tehran.

Imai, N., Terashima, S., Itoh, S., Ando, A., 1995. 1994 compilation values for GSJ reference samples,"Igneous rock series". Geochemical Journal 29, 91-95.

Iwano, H., Orihashi, Y., Hirata, T., Ogasawara, M., Danhara, T., Horie, K., Hasebe, N., Sueoka, S., Tamura, A., Hayasaka, Y., 2013. An inter-laboratory evaluation of OD-3 zircon for use as a secondary U–Pb dating standard. Island Arc 22, 382-394.

Jackson, J., 1992. Partionning of strike-slip and convergent motion between Eurasia and Arabia in Eastern Turkey and the Caucasus. Journal of Geophysical Research 971, 12471-12479.

Jackson, J., Haines, J., Holt, W., 1995. The accommodation of Arabia-Eurasia plate convergence in Iran. Journal of Geophysical Research: Solid Earth 100, 15205-15219.

Jackson, J., McKenzie, D., 1984. Active tectonics of the Alpine—Himalayan Belt between western Turkey and Pakistan. Geophysical Journal International 77, 185-264.

Jackson, J., McKenzie, D., 1988. The relationship between plate motions and seismic moment tensors, and the rates of active deformation in the Mediterranean and Middle East. Geophysical Journal International 93, 45-73.

Jagoutz, O., Klein, B., 2018. On the importance of crystallization-differentiation for the generation of $SiO_2$-rich melts and the compositional build-up of arc (and continental) crust. American Journal of Science 318, 29-63.

Jiang, Z.-Q., Wang, Q., Wyman, D.A., Li, Z.-X., Yang, J.-H., Shi, X.-B., Ma, L., Tang, G.-J., Gou, G.-N., Jia, X.-H., Guo, H.-F., 2014. Transition from oceanic to continental lithosphere subduction in southern Tibet: Evidence from the Late Cretaceous–Early

Oligocene (~91–30Ma) intrusive rocks in the Chanang–Zedong area, southern Gangdese. Lithos 196-197, 213-231.

Jull, M., Kelemen, P.B., 2001. On the conditions for lower crustal convective instability. Journal of Geophysical Research: Solid Earth 106, 6423-6446.

Kaislaniemi, L., Van Hunen, J., Allen, M., Neill, I., 2014. Sublithospheric small-scale convection—a mechanism for collision zone magmatism. Geology 42, 291-294.

Keskin, M., 2003. Magma generation by slab steepening and breakoff beneath a subduction-accretion complex: An alternative model for collision-related volcanism in Eastern Anatolia, Turkey. Geophysical Research Letters 30, 8046, doi:8010.1029/2003GL018019.

Keskin, M., Pearce, J., Kempton, P., Greenwood, 2006. Magma-crust interactions and magma plumbing in a post-collision setting: geochemical evidence from the Erzurum-Kars Plateau, Eastern Turkey. In: Dilek,Y. and Pavlides, S. (eds) Postcollisional tectonics and magmatism in the Mediterranean region and Asia. Special Paper of the Geological Society of America 409, 475-505.

Kessel, R., Schmidt, M.W., Ulmer, P., Pettke, T., 2005. Trace element signature of subduction-zone fluids, melts and supercritical liquids at 120–180 km depth. Nature 437, 724.

Keto, L.S., Jacobsen, S.B., 1987. Nd and Sr isotopic variations of Early Paleozoic oceans. Earth and Planetary Science Letters 84, 27-41.

Khadivi, S., Mouthereau, F., Larrasoaña, J., Vergés, J., Lacombe, O., Khademi, E., Beamud, E., Melinte-Dobrinescu, M., Suc, J.-P., 2010. Magnetochronology of synorogenic Miocene foreland sediments in the Fars arc of the Zagros Folded Belt (SW Iran). Basin Research 22, 918-932.

Khaleghi, F., Hosseinzadeh, G., Rasa, I., Moayyed, M., 2013. Geological and Geochemical Characteristics of the Syah Kamar Porphyry Molybdenum Deposit , West of Mianeh , NW Iran. ULUM-I ZAMIN 88, 187-196.

Kheirkhah, M., Allen, M., Emami, M.H., 2009. Quaternary syn-collision magmatism from the Iran/Turkey borderlands. Journal of Volcanology and Geothermal Research 182, 1-12.

Kheirkhah, M., Neill, I., Allen, M.B., Ajdari, K., 2013. Small-volume melts of lithospheric mantle during continental collision: Late Cenozoic lavas of Mahabad, NW Iran. Journal of Asian Earth Sciences 74, 37-49.

Khodabandeh, A.A., Amini Azar, R., Faridi, M., 1999. Geological map of the Mianeh quadrangle. Geological Survey of Iran and Mining Exploration, Tehran.

Kimura, J.-I., 2017. Modeling chemical geodynamics of subduction zones using the Arc Basalt Simulator version 5. Geosphere 13, 992-1025.

Kirkland, C., Smithies, R., Taylor, R., Evans, N., McDonald, B., 2015. Zircon Th/U ratios in magmatic environs. Lithos 212, 397-414.

Klein, M., Stosch, H.G., Seck, H.A., 1997. Partitioning of high field-strength and rare-earth elements between amphibole and quartz-dioritic to tonalitic melts: an experimental study. Chemical Geology 138, 257-271.

Köksal, S., Romer, R.L., Göncüoglu, M.C., Toksoy-Köksal, F., 2004. Timing of post-collisional H-type to A-type granitic magmatism: U–Pb titanite ages from the Alpine central Anatolian granitoids (Turkey). International Journal of Earth Sciences 93, 974-989.

Koshnaw, R.I., Stockli, D.F., Schlunegger, F., 2018. Timing of the Arabia-Eurasia continental collision—Evidence from detrital zircon U-Pb geochronology of the Red Bed Series strata of the northwest Zagros hinterland, Kurdistan region of Iraq. Geology 47, 47-50.

Kouchi, Y., Obara, H., Fujimoto, T., Orihashi, Y., Haruta, Y., Yamamoto, K., 2015. Zircon U–Pb dating by 213 nm Nd. YAG laser ablation inductively coupled plasma mass spectrometry. Optimization of the analytical condition to use NIST SRM 610 for Pb/U fractionation correction. Chikyu Kagaku 49, 19-35.

Le Maitre, R.W., Streckeisen, A., Zanettin, B., Le Bas, M., Bonin, B., Bateman, P., 2005. Igneous rocks: a classification and glossary of terms: recommendations of the

International Union of Geological Sciences Subcommission on the Systematics of Igneous Rocks. Cambridge University Press.
Lechmann, A., Burg, J.-P., Ulmer, P., Guillong, M., Faridi, M., 2018. Metasomatized mantle as the source of Mid-Miocene-Quaternary volcanism in NW-Iranian Azerbaijan: Geochronological and geochemical evidence. Lithos 304-307, 311-328.
Li, J.-W., Zhao, X.-F., Zhou, M.-F., Ma, C.-Q., de Souza, Z.S., Vasconcelos, P., 2009. Late Mesozoic magmatism from the Daye region, eastern China: U–Pb ages, petrogenesis, and geodynamic implications. Contributions to Mineralogy and Petrology 157, 383-409.
Ludwig, K., 2011. Isoplot v. 4.15: A Geochronological Toolkit for Microsoft Excel. Berkeley Geochronology Center Special Publication 4, 75.
Lustrino, M., 2005. How the delamination and detachment of lower crust can influence basaltic magmatism. Earth-Science Reviews 72, 21-38.
Lustrino, M., Abbas, H., Agostini, S., Caggiati, M., Carminati, E., Gianolla, P., 2019a. Origin of Triassic magmatism of the Southern Alps (Italy): constraints from geochemistry and Sr-Nd-Pb isotopic ratios. Gondwana Research 75, 218-238.
Lustrino, M., Duggen, S., Rosenberg, C.L., 2011. The Central-Western Mediterranean: Anomalous igneous activity in an anomalous collisional tectonic setting. Earth-Science Reviews 104, 1-40.
Lustrino, M., Fedele, L., Agostini, S., Prelević, D., Salari, G., 2019b. Leucitites within and around the Mediterranean area. Lithos 324, 216-233.
Lustrino, M., Marrazzo, M., Melluso, L., Tassinari, C.C., Brotzu, P., Gomes, C.B., Morbidelli, L., Ruberti, E., 2010. Petrogenesis of Early Cretaceous silicic volcanism in SE Uruguay: The role of mantle and crustal sources. Geochemical Journal 44, 1-22.
Lustrino, M., Wilson, M., 2007. The circum-Mediterranean anorogenic Cenozoic igneous province. Earth-Science Reviews 81, 1-65.
Lyubetskaya, T., Korenaga, J., 2007. Chemical composition of Earth's primitive mantle and its variance: 1. Method and results. Journal of Geophysical Research: Solid Earth 112.
Macpherson, C.G., Dreher, S.T., Thirlwall, M.F., 2006. Adakites without slab melting: High pressure differentiation of island arc magma, Mindanao, the Philippines. Earth and Planetary Science Letters 243, 581-593.
Madanipour, S., Ehlers, T.A., Yassaghi, A., Rezaeian, M., Enkelmann, E., Bahroudi, A., 2013. Synchronous deformation on orogenic plateau margins: Insights from the Arabia–Eurasia collision. Tectonophysics 608, 440-451.
Mahmoudi, S., Corfu, F., Masoudi, F., Mehrabi, B., Mohajjel, M., 2011. U–Pb dating and emplacement history of granitoid plutons in the northern Sanandaj–Sirjan Zone, Iran. Journal of Asian Earth Sciences 41, 238-249.
Mazhari, S.A., Amini, S., Ghalamghash, J., Bea, F., 2009a. Petrogenesis of granitic unit of Naqadeh complex, Sanandaj–Sirjan Zone, NW Iran. Arabian Journal of Geosciences 4, 59-67.
Mazhari, S.A., Amini, S., Ghalamghash, J., Bea, F., 2010. The origin of mafic rocks in the Naqadeh intrusive complex, Sanandaj-Sirjan Zone, NW Iran. Arabian Journal of Geosciences 4, 1207-1214.
Mazhari, S.A., Bea, F., Amini, S., Ghalamghash, J., Molina, J.F., Montero, P., Scarrow, J.H., Williams, I.S., 2009b. The Eocene bimodal Piranshahr massif of the Sanandaj-Sirjan Zone, NW Iran: a marker of the end of the collision in the Zagros orogen. Journal of the Geological Society 166, 53-69.
Mazhari, S.A., Hajalilou, B., Bea, F., 2012. Evaluation of Syenite as Feldspar Source: Piranshahr Pluton, NW of Iran. Natural Resources Research 21, 279-283.
McKenzie, D., 1972. Active Tectonics of the Mediterranean Region. Geophysical Journal International 30, 109-185.
McQuarrie, N., Stock, J.M., Verdel, C., Wernicke, B.P., 2003. Cenozoic evolution of Neotethys and implications for the causes of plate motions. Geophysical Research Letters 30, 2036, doi:2010.1029/2003GL017992.

McQuarrie, N., van Hinsbergen, D.J., 2013. Retrodeforming the Arabia-Eurasia collision zone: Age of collision versus magnitude of continental subduction. Geology 41, 315-318.

Mederer, J., Moritz, R., Ulianov, A., Chiaradia, M., 2013. Middle Jurassic to Cenozoic evolution of arc magmatism during Neotethys subduction and arc-continent collision in the Kapan Zone, southern Armenia. Lithos 177, 61-78.

Mehrabi, B., Yardley, B., Cann, J., 1999. Sediment-hosted disseminated gold mineralisation at Zarshuran, NW Iran. Mineralium Deposita 34, 673-696.

Meijers, M.J.M., Smith, B., Pastor-Galán, D., Degenaar, R., Sadradze, N., Adamia, S., Sahakyan, L., Avagyan, A., Sosson, M., Rolland, Y., Langereis, C.G., Müller, C., 2017. Progressive orocline formation in the Eastern Pontides–Lesser Caucasus. Geological Society, London, Special Publications 428, 117-143.

Middlemost, E.A., 1994. Naming materials in the magma/igneous rock system. Earth-Science Reviews 37, 215-224.

Miller, J.S., Matzel, J.E.P., Miller, C.F., Burgess, S.D., Miller, R.B., 2007. Zircon growth and recycling during the assembly of large, composite arc plutons. Journal of Volcanology and Geothermal Research 167, 282-299.

Moghadam, H.S., Ghorbani, G., Khedr, M.Z., Fazlnia, N., Chiaradia, M., Eyuboglu, Y., Santosh, M., Francisco, C.G., Martinez, M.L., Gourgaud, A., 2014. Late Miocene K-rich volcanism in the Eslamieh Peninsula (Saray), NW Iran: implications for geodynamic evolution of the Turkish–Iranian High Plateau. Gondwana Research 26, 1028-1050.

Moghadam, H.S., Li, X.-H., Stern, R.J., Ghorbani, G., Bakhshizad, F., 2016a. Zircon U–Pb ages and Hf–O isotopic composition of migmatites from the Zanjan–Takab complex, NW Iran: Constraints on partial melting of metasediments. Lithos 240-243, 34-48.

Moghadam, H.S., Rossetti, F., Lucci, F., Chiaradia, M., Gerdes, A., Martinez, M.L., Ghorbani, G., Nasrabady, M., 2016b. The calc-alkaline and adakitic volcanism of the Sabzevar structural zone (NE Iran): implications for the Eocene magmatic flare-up in Central Iran. Lithos 248, 517-535.

Moradi, A.S., Hatzfeld, D., Tatar, M., 2011. Microseismicity and seismotectonics of the North Tabriz fault (Iran). Tectonophysics 506, 22-30.

Moradi, R., Boomeri, M., Bagheri, S., Nakashima, K., 2016. Mineral chemistry of igneous rocks in the Lar Cu-Mo prospect, southeastern part of Iran: implications for P, T, and ƒO2. Turkish Journal of Earth Sciences 25, 418-433.

Moritz, R., Melkonyan, R., Selby, D., Popkhadze, N., Gugushvili, V., Tayan, R., Ramazanov, V., 2016a. Metallogeny of the Lesser Caucasus: from arc construction to post-collision evolution, Special publications of the Society of Economic Geologists. Society of Economic Geologists, pp. 157-192.

Moritz, R., Rezeau, H., Ovtcharova, M., Tayan, R., Melkonyan, R., Hovakimyan, S., Ramazanov, V., Selby, D., Ulianov, A., Chiaradia, M., 2016b. Long-lived, stationary magmatism and pulsed porphyry systems during Tethyan subduction to post-collision evolution in the southernmost Lesser Caucasus, Armenia and Nakhitchevan. Gondwana Research 37, 465-503.

Morley, C.K., Kongwung, B., Julapour, A.A., Abdolghafourian, M., Hajian, M., Waples, D., Warren, J., Otterdoom, H., Srisuriyon, K., Kazemi, H., 2009. Structural development of a major late Cenozoic basin and transpressional belt in central Iran: The Central Basin in the Qom-Saveh area. Geosphere 5, 325-362.

Mouthereau, F., Lacombe, O., Vergés, J., 2012. Building the Zagros collisional orogen: Timing, strain distribution and the dynamics of Arabia/Eurasia plate convergence. Tectonophysics 532-535, 27-60.

Mouthereau, F., Tensi, J., Bellahsen, N., Lacombe, O., De Boisgrollier, T., Kargar, S., 2007. Tertiary sequence of deformation in a thin-skinned/thick-skinned collision belt: The Zagros Folded Belt (Fars, Iran). Tectonics 26, TC5006, doi:5010.1029/2007TC002098.

Moyen, J.-F., 2009. High Sr/Y and La/Yb ratios: The meaning of the “adakitic signature”. Lithos 112, 556-574.

Nabatian, G., Ghaderi, M., Neubauer, F., Honarmand, M., Liu, X., Dong, Y., Jiang, S.-Y., von Quadt, A., Bernroider, M., 2014. Petrogenesis of Tarom high-potassic granitoids in the Alborz–Azarbaijan belt, Iran: Geochemical, U–Pb zircon and Sr–Nd–Pb isotopic constraints. Lithos 184-187, 324-345.

Nabatian, G., Jiang, S.-Y., Honarmand, M., Neubauer, F., 2016. Zircon U–Pb ages, geochemical and Sr–Nd–Pb–Hf isotopic constraints on petrogenesis of the Tarom-Olya pluton, Alborz magmatic belt, NW Iran. Lithos 244, 43-58.

Nabatian, G., Wan, B., Honarmand, M., 2017. Whole rock geochemistry, molybdenite Re-Os geochronology, stable isotope and fluid inclusion investigations of the Siah-Kamar deposit, western Alborz-Azarbayjan: New constrains on the porphyry Mo deposit in Iran. Ore Geology Reviews 91, 638-659.

Naumenko-Dèzes, M.O., Rolland, Y., Lamarque, G., Duclaux, G., Gallet, S., Bascou, J., Ménot, R.P., 2020. Petrochronology of the Terre Adélie Craton (East Antarctica) evidences a long-lasting Proterozoic (1.7–1.5 Ga) tectono-metamorphic evolution — Insights for the connections with the Gawler Craton and Laurentia. Gondwana Research 81, 21-57.

Neill, I., Meliksetian, K., Allen, M., Navasardyan, G., Karapetyan, S., 2013. Pliocene-Quaternary volcanic rocks of NW Armenia: Magmatism and lithospheric dynamics within an active orogenic plateau. Lithos 180-181, 200-215.

Neill, I., Meliksetian, K., Allen, M., Navasardyan, G., Kuiper, K.F., 2015. Petrogenesis of mafic collision zone magmatism: The Armenian sector of the Turkish-Iranian Plateau. Chemical Geology 403, 24-41.

Nouri, F., Asahara, Y., Azizi, H., Yamamoto, K., Tsuboi, M., 2017. Geochemistry and petrogenesis of the Eocene back arc mafic rocks in the Zagros suture zone, northern Noorabad, western Iran. Chemie der Erde - Geochemistry 77, 517-533.

Nutman, A.P., Mohajjel, M., Bennett, V.C., Fergusson, C.L., 2014. Gondwanan Eoarchean–Neoproterozoic ancient crustal material in Iran and Turkey: zircon U–Pb–Hf isotopic evidence. Canadian Journal of Earth Sciences 51, 272-285.

Okay, A., Tuysuz, O., Satır, M., Ozkan-Altiner, S., Altiner, D., Sherlock, S., Eren, R., 2006. Cretaceous and Triassic subduction-accretion, high-pressure–low-temperature metamorphism, and continental growth in the Central Pontides, Turkey. Geological Society of America Bulletin 118, 1247-1269.

Okay, A.I., Zattin, M., Cavazza, W., 2010. Apatite fission-track data for the Miocene Arabia-Eurasia collision. Geology 38, 35-38.

Omrani, J., Agard, P., Whitechurch, H., Benoit, M., Prouteau, G., Jolivet, L., 2008. Arc-magmatism and subduction history beneath the Zagros Mountains, Iran: A new report of adakites and geodynamic consequences. Lithos 106, 380-398.

Pang, K.-N., Chung, S.-L., Zarrinkoub, M., Li, X.-H., Lee, H.-Y., Lin, T.-H., Chiu, H.-Y., 2016. New age and geochemical constraints on the origin of Quaternary adakite-like lavas in the Arabia-Eurasia collision zone. Lithos 264, 348-359.

Pang, K.-N., Chung, S.-L., Zarrinkoub, M.H., Chiu, H.-Y., Li, X.-H., 2014. On the magmatic record of the Makran arc, southeastern Iran: Insights from zircon U-Pb geochronology and bulk-rock geochemistry. Geochemistry, Geophysics, Geosystems 15, 2151-2169.

Pang, K.-N., Chung, S.-L., Zarrinkoub, M.H., Khatib, M.M., Mohammadi, S.S., Chiu, H.-Y., Chu, C.-H., Lee, H.-Y., Lo, C.-H., 2013a. Eocene–Oligocene post-collisional magmatism in the Lut–Sistan region, eastern Iran: Magma genesis and tectonic implications. Lithos 180-181, 234-251.

Pang, K.N., Chung, S.L., Zarrinkoub, M.H., Lin, Y.C., Lee, H.Y., Lo, C.H., Khatib, M.M., 2013b. Iranian ultrapotassic volcanism at~ 11 Ma signifies the initiation of post-collisional magmatism in the A rabia–E urasia collision zone. Terra Nova 25, 405-413.

Pe-Piper, G., Piper, D.J.W., Koukouvelas, I., Dolansky, L.M., Kokkalas, S., 2009. Postorogenic shoshonitic rocks and their origin by melting underplated basalts: The Miocene of Limnos, GreeceShoshonites from melting underplated basalt, Greece. GSA Bulletin 121, 39-54.

Pearce, J., 1983. Role of the sub-continental lithosphere in magma genesis at active continental margin.

Pearce, J.A., 2008. Geochemical fingerprinting of oceanic basalts with applications to ophiolite classification and the search for Archean oceanic crust. Lithos 100, 14-48.

Pearce, J.A., Bender, J.F., De Long, S.E., Kidd, W.S.F., Low, P.J., Güner, Y., Saroglu, F., Yilmaz, Y., Moorbath, S., Mitchell, J.G., 1990. Genesis of collision volcanism in Eastern Anatolia, Turkey. Journal of Volcanology and Geothermal Research 44, 189-229.

Pearce, J.A., Harris, N.B.W., Tindle, A.G., 1984. Trace Element Discrimination Diagrams for the Tectonic Interpretation of Granitic Rocks. Journal of Petrology 25, 956-983.

Peccerillo, A., Taylor, S., 1976. Geochemistry of Eocene calc-alkaline volcanic rocks from the Kastamonu area, northern Turkey. Contributions to Mineralogy and Petrology 58, 63-81.

Plank, T., 2014. The chemical composition of subducting sediments. Treatise on geochemistry 4, 607-629.

Platt, J., England, P., 1994. Convective removal of lithosphere beneath mountain belts-Thermal and mechanical consequences. American Journal of Science 294, 307-336.

Prelević, D., Akal, C., Romer, R.L., Mertz-Kraus, R., Helvacı, C., 2015. Magmatic Response to Slab Tearing: Constraints from the Afyon Alkaline Volcanic Complex, Western Turkey. Journal of Petrology 56, 527-562.

Prelević, D., Foley, S.F., Romer, R., Conticelli, S., 2008. Mediterranean Tertiary lamproites derived from multiple source components in postcollisional geodynamics. Geochimica et Cosmochimica Acta 72, 2125-2156.

Prelević, D., Jacob, D.E., Foley, S.F., 2013. Recycling plus: A new recipe for the formation of Alpine–Himalayan orogenic mantle lithosphere. Earth and Planetary Science Letters 362, 187-197.

Prelević, D., Seghedi, I., 2013. Magmatic response to the post-accretionary orogenesis within Alpine–Himalayan belt—Preface. Lithos, 1-4.

Priestley, K., McKenzie, D., Barron, J., Tatar, M., Debayle, E., 2012. The Zagros core: Deformation of the continental lithospheric mantle. Geochemistry, Geophysics, Geosystems 13, Q11014, doi:11010.11029/12012GC004435.

Rabiee, A., Rossetti, F., Tecce, F., Asahara, Y., Azizi, H., Glodny, J., Lucci, F., Nozaem, R., Opitz, J., Selby, D., 2019. Multiphase magma intrusion, ore-enhancement and hydrothermal carbonatisation in the Siah-Kamar porphyry Mo deposit, Urumieh-Dokhtar magmatic zone, NW Iran. Ore Geology Reviews 110, 102930.

Reilinger, R., McClusky, S., Vernant, P., Lawrence, S., Ergintav, S., Cakmak, R., Ozener, H., Kadirov, F., Guliev, I., Stepanyan, R., Nadariya, M., Hahubia, G., Mahmoud, S., Sakr, K., ArRajehi, A., Paradissis, D., Al-Aydrus, A., Prilepin, M., Guseva, T., Evren, E., Dmitrotsa, A., Filikov, S.V., Gomez, F., Al-Ghazzi, R., Karam, G., 2006. GPS constraints on continental deformation in the Africa-Arabia-Eurasia continental collision zone and implications for the dynamics of plate interactions. Journal of Geophysical Research: Solid Earth 111, B05411, doi:05410.01029/02005JB004051.

Rezeau, H., Leuthold, J., Tayan, R., Hovakimyan, S., Ulianov, A., Kouzmanov, K., Moritz, R., 2018. Incremental Growth of Mid-to Upper-Crustal Magma Bodies During Arabia–Eurasia Convergence and Collision: A Petrological Study of the Calc-Alkaline to Shoshonitic Meghri–Ordubad Pluton (Southern Armenia and Nakhitchevan, Lesser Caucasus). Journal of Petrology 59, 931-966.

Rezeau, H., Moritz, R., Leuthold, J., Hovakimyan, S., Tayan, R., Chiaradia, M., 2017. 30 Myr of Cenozoic magmatism along the Tethyan margin during Arabia–Eurasia accretionary orogenesis (Meghri–Ordubad pluton, southernmost Lesser Caucasus). Lithos 288-289, 108-124.

Rezeau, H., Moritz, R., Wotzlaw, J.-F., Tayan, R., Melkonyan, R., Ulianov, A., Selby, D., d'Abzac, F.-X., Stern, R.A., 2016. Temporal and genetic link between incremental pluton assembly and pulsed porphyry Cu-Mo formation in accretionary orogens. Geology 44, 627-630.

Richards, J., 2000. Lineaments revisited. SEG newsletter 42, 14-20.

Richards, J.P., 2015. Tectonic, magmatic, and metallogenic evolution of the Tethyan orogen: From subduction to collision. Ore Geology Reviews 70, 323-345.
Richards, J.P., Wilkinson, D., Ullrich, T., 2006. Geology of the Sari Gunay epithermal gold deposit, northwest Iran. Economic Geology 101, 1455-1496.
Rolland, Y., 2017. Caucasus collisional history: Review of data from East Anatolia to West Iran. Gondwana Research 49, 130-146.
Rolland, Y., Hässig, M., Bosch, D., Bruguier, O., Melis, R., Galoyan, G., Topuz, G., Sahakyan, L., Avagyan, A., Sosson, M., 2020. The East Anatolia–Lesser Caucasus ophiolite: An exceptional case of large-scale obduction, synthesis of data and numerical modelling. Geoscience Frontiers 11, 83-108.
Rolland, Y., Perincek, D., Kaymakci, N., Sosson, M., Barrier, E., Avagyan, A., 2012. Evidence for ~80–75Ma subduction jump during Anatolide–Tauride–Armenian block accretion and ~48Ma Arabia–Eurasia collision in Lesser Caucasus–East Anatolia. Journal of Geodynamics 56-57, 76-85.
Rosenbaum, G., Gasparon, M., Lucente, F.P., Peccerillo, A., Miller, M.S., 2008. Kinematics of slab tear faults during subduction segmentation and implications for Italian magmatism. Tectonics 27, TC2008, doi:2010.1029/2007TC002143.
Rossetti, F., Nasrabady, M., Theye, T., Gerdes, A., Monié, P., Lucci, F., Vignaroli, G., 2014. Adakite differentiation and emplacement in a subduction channel: The late Paleocene Sabzevar magmatism (NE Iran). Bulletin 126, 317-343.
Rubatto, D., 2002. Zircon trace element geochemistry: partitioning with garnet and the link between U–Pb ages and metamorphism. Chemical Geology 184, 123-138.
Rudnick, R., Gao, S., 2003. Composition of the continental crust. Treatise Geochem. 3, 1–64. Elsevier.
Sahakyan, L., Bosch, D., Sosson, M., Avagyan, A., Galoyan, G., Rolland, Y., Bruguier, O., Stepanyan, Z., Galland, B., Vardanyan, S., 2017. Geochemistry of the Eocene magmatic rocks from the Lesser Caucasus area (Armenia): evidence of a subduction geodynamic environment. Geological Society, London, Special Publications 428, 73-98.
Saleeby, J., Ducea, M., Clemens-Knott, D., 2003. Production and loss of high-density batholithic root, southern Sierra Nevada, California. Tectonics 22, 1064, doi:1010.1029/2002TC001374.
Sawada, Y., Zaree, G.R., Sakai, T., Itaya, T., Yagi, K., Imaizumi, M., Ataabadi, M.M., Fortelius, M., 2016. K–Ar ages and petrology of the late Miocene pumices from the Maragheh Formation, northwest Iran. Palaeobiodiversity and Palaeoenvironments 96, 399-431.
Schildgen, T., Yıldırım, C., Cosentino, D., Strecker, M., 2014. Linking slab break-off, Hellenic trench retreat, and uplift of the Central and Eastern Anatolian plateaus. Earth-Science Reviews 128, 147-168.
Schleiffarth, W.K., Darin, M.H., Reid, M.R., Umhoefer, P.J., 2018. Dynamics of episodic Late Cretaceous–Cenozoic magmatism across Central to Eastern Anatolia: New insights from an extensive geochronology compilation. Geosphere 14, 1990-2008.
Schleiffarth, W.K., Reid, M.R., Cosca, M.A., 2015. Ages, distribution, and evolution of Miocene basalts, East-Central Anatolia. In AGU Fall Meeting Abstracts.
Schmidt, M.W., Jagoutz, O., 2017. The global systematics of primitive arc melts. Geochemistry, Geophysics, Geosystems 18, 2817-2854.
Şengör, A.M.C., Özeren, M.S., Keskin, M., Sakınç, M., Özbakır, A.D., Kayan, İ., 2008. Eastern Turkish high plateau as a small Turkic-type orogen: Implications for post-collisional crust-forming processes in Turkic-type orogens. Earth-Science Reviews 90, 1-48.
Shad Manaman, N., Shomali, H., Koyi, H., 2011. New constraints on upper-mantle S-velocity structure and crustal thickness of the Iranian plateau using partitioned waveform inversion. Geophysical Journal International 184, 247-267.
Shafaii Moghadam, H., Griffin, W., Kirchenbaur, M., Garbe-Schönberg, D., Khedr, M., Kimura, J.-I., Stern, B., Ghorbani, G., Murphy, R., Y. O'Reilly, S., Arai, S., Maghdour-

Mashhour, R., 2018. Roll-Back, Extension and Mantle Upwelling Triggered Eocene Potassic Magmatism in NW Iran. Journal of Petrology 59, 1417-1465.
Shafaii Moghadam, H., Griffin, W.L., Li, X.-H., Santos, J.F., Karsli, O., Stern, R.J., Ghorbani, G., Gain, S., Murphy, R., O'Reilly, S.Y., 2017. Crustal evolution of NW Iran: Cadomian arcs, Archean fragments and the Cenozoic magmatic flare-up. Journal of Petrology 58, 2143-2190.
Shafaii Moghadam, H., Li, X.-H., Stern, B., Ghorbani, G., Bakhshizad, F., 2015. Zircon U-Pb ages and Hf-O isotopic composition of migmatite from the Zanjan-Takab complex, NW Iran: Constraints on partial melting of metasedimentary rocks.
Shakerardakani, F., Li, X.-H., Ling, X.-X., Li, J., Tang, G.-Q., Liu, Y., Monfaredi, B., 2019. Evidence for Archean crust in Iran provided by ca 2.7 Ga zircon xenocrysts within amphibolites from the Sanandaj–Sirjan zone, Zagros orogen. Precambrian Research 332, 105390.
Simmonds, V., Moazzen, M., Selby, D., 2019. U-Pb zircon and Re-Os molybdenite age of the Siah Kamar porphyry molybdenum deposit, NW Iran. International Geology Review 61, 1786-7802.
Sosson, M., Rolland, Y., Müller, C., Danelian, T., Melkonyan, R., Kekelia, S., Adamia, S., Babazadeh, V., Kangarli, T., Avagyan, A., 2010. Subductions, obduction and collision in the Lesser Caucasus (Armenia, Azerbaijan, Georgia), new insights. Geological Society, London, Special Publications 340, 329-352.
Stacey, J.t., Kramers, J., 1975. Approximation of terrestrial lead isotope evolution by a two-stage model. Earth and Planetary Science Letters 26, 207-221.
Stampfli, G.M., Borel, G., 2002. A plate tectonic model for the Paleozoic and Mesozoic constrained by dynamic plate boundaries and restored synthetic oceanic isochrons. Earth and Planetary Science Letters 196, 17-33.
Stern, R.J., 2002. Subduction zones. Reviews of Geophysics 40, 3-1-3-38.
Stern, R.J., Fouch, M.J., Klemperer, S.L., 2003. An overview of the Izu-Bonin-Mariana subduction factory. Inside the subduction factory, 175-222.
Stocklin, J., 1968. Structural history and tectonics of Iran: a review. American Association of Petroleum Geologists Bulletin 52, 1229-1258.
Su, Z., Wang, E.-C., Hu, J.-C., Talebian, M., Karimzadeh, S., 2017. Quantifying the Termination Mechanism Along the North Tabriz-North Mishu Fault Zone of Northwestern Iran via Small Baseline PS-InSAR and GPS Decomposition. IEEE Journal of Selected Topics in Applied Earth Observations and Remote Sensing 10, 130-144.
Sugden, P., Savov, I., Wilson, M., Meliksetian, K., Navasardyan, G., Halama, R., 2019. The Thickness of the Mantle Lithosphere and Collision-Related Volcanism in the Lesser Caucasus. Journal of Petrology 60, 199-230.
Sun, S.s., McDonough, W.F., 1989. Chemical and isotopic systematics of oceanic basalts: implications for mantle composition and processes. Geological Society, London, Special Publications 42, 313-345.
Tadayon, M., Rossetti, F., Zattin, M., Calzolari, G., Nozaem, R., Salvini, F., Faccenna, C., Khodabakhshi, P., 2018. The long-term evolution of the Doruneh Fault region (Central Iran): A key to understanding the spatio-temporal tectonic evolution in the hinterland of the Zagros convergence zone. Geological Journal 54, 1454-1479.
Tadayon, M., Rossetti, F., Zattin, M., Nozaem, R., Calzolari, G., Madanipour, S., Salvini, F., 2017. The Post-Eocene Evolution of the Doruneh Fault Region (Central Iran): The Intraplate Response to the Reorganization of the Arabia-Eurasia Collision Zone. Tectonics 36, 3038-3064.
Taghizadeh-Farahmand, F., Sodoudi, F., Afsari, N., Ghassemi, M.R., 2010. Lithospheric structure of NW Iran from P and S receiver functions. Journal of seismology 14, 823-836.
Talebian, M., Jackson, J., 2004. A reappraisal of earthquake focal mechanisms and active shortening in the Zagros mountains of Iran. Geophysical Journal International 156, 506-526.

Tanaka, T., Togashi, S., Kamioka, H., Amakawa, H., Kagami, H., Hamamoto, T., Yuhara, M., Orihashi, Y., Yoneda, S., Shimizu, H., 2000. JNdi-1: a neodymium isotopic reference in consistency with LaJolla neodymium. Chemical Geology 168, 279-281.
Tatsumi, Y., 2005. The subduction factory: how it operates in the evolving Earth. GSA today 15, 4-10.
Tatsumi, Y., Hamilton, D.L., Nesbitt, R.W., 1986. Chemical characteristics of fluid phase released from a subducted lithosphere and origin of arc magmas: Evidence from high-pressure experiments and natural rocks. Journal of Volcanology and Geothermal Research 29, 293-309.
Tatsumi, Y., Kogiso, T., 2003. The subduction factory: its role in the evolution of the Earth's crust and mantle. Geological Society, London, Special Publications 219, 55-80.
Tatsumi, Y., Murasaki, M., Arsadi, E.M., Nonda, S., 1991. Geochemistry of Quaternary lavas from NE Sulawesi: transfer of subduction components into the mantle wedge. Contributions to Mineralogy and Petrology 107, 137-149.
Tommasini, S., Avanzinelli, R., Conticelli, S., 2011. The Th/La and Sm/La conundrum of the Tethyan realm lamproites. Earth and Planetary Science Letters 301, 469-478.
Tsereteli, N., Tibaldi, A., Alania, V., Gventsadse, A., Enukidze, O., Varazanashvili, O., Müller, B.I.R., 2016. Active tectonics of central-western Caucasus, Georgia. Tectonophysics 691, 328-344.
Ulmer, P., Kaegi, R., Müntener, O., 2018. Experimentally derived intermediate to silica-rich arc magmas by fractional and equilibrium crystallization at 1· 0 GPa: An evaluation of phase relationships, compositions, liquid lines of descent and oxygen fugacity. Journal of Petrology 59, 11-58.
van der Boon, A., van Hinsbergen, D.J.J., Rezaeian, M., Gürer, D., Honarmand, M., Pastor-Galán, D., Krijgsman, W., Langereis, C.G., 2018. Quantifying Arabia–Eurasia convergence accommodated in the Greater Caucasus by paleomagnetic reconstruction. Earth and Planetary Science Letters 482, 454-469.
van Hunen, J., Allen, M., 2011. Continental collision and slab break-off: A comparison of 3-D numerical models with observations. Earth and Planetary Science Letters 302, 27-37.
van Hunen, J., Miller, M.S., 2015. Collisional Processes and Links to Episodic Changes in Subduction Zones. Elements 11, 119-124.
Verdel, C., Wernicke, B.P., Hassanzadeh, J., Guest, B., 2011. A Paleogene extensional arc flare-up in Iran. Tectonics 30, TC3008, doi:3010.1029/2010TC002809.
Vernant, P., Nilforoushan, F., Hatzfeld, D., Abbassi, M.R., Vigny, C., Masson, F., Nankali, H., Martinod, J., Ashtiani, A., Bayer, R., Tavakoli, F., Chéry, J., 2004. Present-day crustal deformation and plate kinematics in the Middle East constrained by GPS measurements in Iran and northern Oman. Geophysical Journal International 157, 381-398.
Vincent, S., Allen, M., D. Ismail-Zadeh, A., Flecker, R., Foland, K., Simmons, M., 2005. Insights from the Talysh of Azerbaijan into the Paleogene evolution of the South Caspian region. Geological Society of America Bulletin 117, 1513-1533.
Vincent, S.J., Braham, W., Lavrishchev, V.A., Maynard, J.R., Harland, M., 2016. The formation and inversion of the western Greater Caucasus Basin and the uplift of the western Greater Caucasus: Implications for the wider Black Sea region. Tectonics 35, 2948-2962.
Vincent, S.J., Morton, A.C., Carter, A., Gibbs, S., Barabadze, T.G., 2007. Oligocene uplift of the Western Greater Caucasus: an effect of initial Arabia–Eurasia collision. Terra Nova 19, 160-166.
von Blanckenburg, F., Davies, J.H., 1995. Slab breakoff: A model for syncollisional magmatism and tectonics in the Alps. Tectonics 14, 120-131.
Walpersdorf, A., Manighetti, I., Mousavi, Z., Tavakoli, F., Vergnolle, M., Jadidi, A., Hatzfeld, D., Aghamohammadi, A., Bigot, A., Djamour, Y., 2014. Present-day kinematics and fault slip rates in eastern Iran, derived from 11 years of GPS data. Journal of Geophysical Research: Solid Earth 119, 1359-1383.
Wang, Q., Wyman, D.A., Xu, J.-F., Zhao, Z.-H., Jian, P., Xiong, X.-L., Bao, Z.-W., Li, C.-F., Bai, Z.-H., 2006. Petrogenesis of Cretaceous adakitic and shoshonitic igneous rocks in

the Luzong area, Anhui Province (eastern China): Implications for geodynamics and Cu–Au mineralization. Lithos 89, 424-446.
Whitechurch, H., Omrani, J., Agard, P., Humbert, F., Montigny, R., Jolivet, L., 2013. Evidence for Paleocene–Eocene evolution of the foot of the Eurasian margin (Kermanshah ophiolite, SW Iran) from back-arc to arc: Implications for regional geodynamics and obduction. Lithos 182-183, 11-32.
Whitney, D.L., Evans, B.W., 2010. Abbreviations for names of rock-forming minerals. American Mineralogist 95, 185-187.
Wiedenbeck, M., Alle, P., Corfu, F., Griffin, W., Meier, M., Oberli, F.v., Quadt, A.v., Roddick, J., Spiegel, W., 1995. Three natural zircon standards for U-Th-Pb, Lu-Hf, trace element and REE analyses. Geostandards newsletter 19, 1-23.
Winchester, J.A., Floyd, P.A., 1977. Geochemical discrimination of different magma series and their differentiation products using immobile elements. Chemical Geology 20, 325-343.
Xu, J.-F., Shinjo, R., Defant, M.J., Wang, Q., Rapp, R.P., 2002. Origin of Mesozoic adakitic intrusive rocks in the Ningzhen area of east China: Partial melting of delaminated lower continental crust? Geology 30, 1111-1114.
Yang, Z., Hou, Z., Chang, Z., Li, Q., Liu, Y., Qu, H., Sun, M., Xu, B., 2016. Cospatial Eocene and Miocene granitoids from the Jiru Cu deposit in Tibet: Petrogenesis and implications for the formation of collisional and postcollisional porphyry Cu systems in continental collision zones. Lithos 245, 243-257.
Zhang, Z., Xiao, W., Ji, W., Majidifard, M.R., Rezaeian, M., Talebian, M., Xiang, D., Chen, L., Wan, B., Ao, S., Esmaeili, R., 2018. Geochemistry, zircon U-Pb and Hf isotope for granitoids, NW Sanandaj-Sirjan zone, Iran: Implications for Mesozoic-Cenozoic episodic magmatism during Neo-Tethyan lithospheric subduction. Gondwana Research 62, 227-245.
Zheng, Y.-F., 2019. Subduction zone geochemistry. Geoscience Frontiers 10, 1223-1254.

Fig. 1. (a) Simplified tectonic map of NW Iran, Arabia, Caucasus and Anatolia, also showing the distribution of Iran Eocene-Oligocene and Neogene-Quaternary igneous rocks and the main ophiolitic mélange outcrops (modified after Hubner, 1969), (micro-) plate boundaries (modified after Reilinger et al., 2006), suture zones and fault distribution (modified after Richards, 2015). (b) The background colours show the surface wave tomographic model at 125 km depth of upper mantle (Priestley et al., 2012). A significant change in the lithosphere structure is observed across the Mianeh-Ardabil fault. The contours are the Moho depth across the Iranian plateau (redrawn after Shad Manaman et al., 2011) showing an abrupt change in the Moho depth across the Tabriz Fault, thickening to the NE. Significant changes are also observed along Mianeh-Ardabil Fault. Abbreviations: F., Fault; ZOMZ, Zangezur-Ordubad volcano-plutonic zone; SbV, Sabalan Volcano; ShV, Sahand Volcano.

Fig. 2. Simplified geological map showing the magmatic zones of NW Iran (modified from Hubner, 1969) and southern Armenia (including the Zangezur-Ordubad volcano-plutonic zone (ZOMZ) and the Meghri-Ordubad pluton (MOP) assemblage; Moritz et al., 2016). The black rectangle indicates the study area. See the Supplementary Material S1 for detail characteristics of each deposit.

Fig. 3. Simplified geological map of the Mianeh-Hashtroud area (modified after Amidi et al., 1987). The analysed samples together with their U-Pb zircon ages (Ma ± 2σ error) are also shown. Ages of samples #01, 03, 19 and 31 are from Rabiee et al. (2019).

Fig. 4. (a) Satellite image (Google Earth) of the central sector of the study area, showing the distribution of the Eocene and Miocene intrusions and samples locations. (b) Eocene volcanic country rocks. (c) Strongly plagioclase-phyric and (c) pyroxene-phyric structure of Eocene volcanic country rocks. (e-h) Hand specimens of the studied Eocene intrusive rocks. (e) Biotite-bearing monzonite. (f) Syenite mainly containing k-feldspar (pinkish) and plagioclase. (g) A close-up view of quartz monzonite body showing a miarolithic cavity in the contact zone with the monzonite body. (h) A close-up view of the microgranular granite body with minor weathered biotite grains. The sampling sites of the investigated rocks are reported in Figure 3.

Fig. 5. (a) Panorama view from east of the area (Ebak-SiahKamar) showing the outcrops of Eocene country rocks intruded by the Oligocene subvolcanic bodies. (b) and (c) close views showing granular and porphyritic textures from two Oligocene monzonite bodies. (d to f) Hand specimens from the Oligocene volcanic rocks showing a porphyritic hypohyaline texture. (g) and (h) altered rhyolitic porphyry dike. The sampling sites of the investigated rocks are reported in Figure 3. Kfs = Alkali feldspar; Bt = Biotite; Pl = Plagioclase; Qz = Quartz.

Fig. 6. Microphotographs of representative magmatic rocks from Mianeh-Hashtroud area. The sample ID is shown on each picture. (a) MN04 Eocene country rock: trachyte showing plagioclase phenocrysts in a groundmass mad of plagioclase microliths; (b) MN09 Eocene monzodiorite showing equigranular-holocrystalline texture made of plagioclase, amphibole and magnetite; (c) MN12 Eocene quartz monzonite with equigranular-holocrystalline texture showing plagioclase, alkali feldspar, quartz and biotite as major crystals; (d) MN10A Eocene granite characterised by porphyritic-holocrystalline texture with microgranular groundmass made up of alkali feldspar, quartz and biotite; (e) MN10C Eocene monzonite enclave in the granite (MN10A) showing porphyritic-holocrystalline texture and plagioclase, alkali feldspar, amphibole ± clinopyroxene as major crystals; (f) MN45 Oligocene monzonite with equigranular-holocrystalline texture with plagioclase alkali feldspar, amphibole and biotite as major crystals; (g) MN65 Oligocene monzonite, hypabyssal porphyritic-holocrystalline texture containing clinopyroxene and plagioclase phenocrysts (h) MN76 Oligocene hypabyssal granite, porphyritic-holocrystalline texture with microgranular groundmass made up of alkali feldspar, quartz and biotite; (i) MN19 Oligocene dacite dome showing a vitrophyric texture, with glassy groundmass containing sub-rounded, resorbed and fractured quartz abd okaguickase phenocrysts and minor biotite and amphibole. All images are in crossed-polarised light.

Fig. 7. U-Pb Concordia diagrams and probability age distribution plot as obtained from the cumulative $^{206}Pb/^{238}U$ age data from the zircon grains recovered from the studied magmatic rock samples. See

also Table 2 for the corresponding analytical results and the Supplementary Material S2 for the complete textural characteristics of the analysed zircon grains.

Fig. 8. (a) Total alkali vs. silica (TAS) diagram (Le Maitre et al. 2005) for the Cenozoic igneous rocks of the Mianeh-Hashtroud district. The volcanic rock name have been used also for the plutonic and the hypabyssal samples. (b) $K_2O$ vs. $SiO_2$ diagram (Peccerillo and Taylor, 1976). HK-CA: high-K calcalkaline; MK-CA: medium-K calcalkaline, LK, low-K. (c) $SiO_2$ vs. Nb/Y diagram (Winchester and Floyd, 1977). A: andesites; AB: Alkali basalts; B: Basalts; BA: Basaltic andesites; BSN, NEP: Basanite, Nephelinite; BTA: Basaltic trachyandesite; COM, PAN: Commendite, Pantellerite; PH: phonolite; R: Rhyolite; R, D: Rhyolite, Dacite; T: Trachyte; TA: Trachy-andesite (d) Th vs. Co diagram (Hastie et al., 2007). B: Basalts; BA/A: Basaltic andesites, Andesites; D/R: Dacite, Rhyolite; CA: Calcalkaline; IAT: Island Arc Tholeiite; H-K: high-K; SHO: Shoshonite. Data from this study are compared with those available from the neighbouring regions.

Fig. 9. Harker diagrams for selected major oxides (in wt%) using $SiO_2$ as differentiation index.

Fig. 10. Harker diagrams for selected trace elements (in ppm) using $SiO_2$ as differentiation index. Grt = garnet; Amp = amphibole.

Fig. 11. (a) Primitive mantle-*normalized* (after Lyubetskaya and Korenaga, 2007) incompatible element diagram for the Cenozoic Mianeh-Hashtroud igneous rocks. The inset shows the plot for the least differentiated compositions ($SiO_2$ <57 wt%) compared with patterns for oceanic island basalts (OIB; after Sun and McDonough, 1989), continental arc calcalkaline and shoshonite magmatism (Cascade arc), island arc magmatism (Izu-Bonin-Marianna (IBM) arc), the Emeishan large igneous province (ELIP) and average continental crust (Rudnick and Gao, 2003). (b) Chondrite-normalised (after Sun and McDonough, 1989) REE diagram for the Cenozoic Mianeh-Hashtroud igneous rocks. The inset shows the same diagram for the least differentiated compositions ($SiO_2$ <57 wt%) as in (a). Data sources: GEOROC (http://georoc.mpch-mainz.gwdg.de/georoc/).

Fig. 12. $\varepsilon Nd_{(t)}$ vs. $(^{87}Sr/^{86}Sr)_t$ diagram of the Mianeh-Hashtroud district igneous rocks. The data are compared with those of Mesozoic and Cenozoic Lesser Caucasus igneous rocks (Mederer et al., 2013 and Moritz et al., 2016, respectively), Quaternary volcanic rocks (NW Iran; Allen et al., 2013), Neogene-Quaternary Azerbaijan volcanic rocks (NW Iran; Lechman et al., 2018), and Jurassic-Cretaceous igneous rocks of the northern Sanandaj Sirjan Zone (Azizi and Asahara, 2013; Azizi et al. 2018). BSE = Bulk Silicate Earth; ChUR = Chondritic Uniform Reservoir.

Fig. 13. (a) Weighted age distribution of all measured zircon autocrysts and antecrysts from Mianeh-Hashtroud area (including four samples mentioned in Fig. 3 caption from Rabiee et al., 2019); (b and c) Relative age frequency distribution for zircons antecrysts and xenocrysts (inherited) recovered from the studied samples.

Fig. 14. (a) Sr/Y vs. Y and (b) $(La/Yb)_N$ vs $Yb_N$ diagrams for the Cenozoic Mianeh-Hashtroud igneous rocks together with literature analyses of NW Iran Cenozoic igneous rocks. These rocks plot almost completely in the “normal” calcalkaline arcs field as defined by Defant and Drummond (1990). (c) Th/Yb vs. Nb/Yb diagram (Pearce (2008) for the least differentiated ($SiO_2$ <57 wt%) Mianeh-Hashtroud rocks. Data sources for Izu Bonin Mariana (IBM), Emeishan Large Igneous Province (ELIP), Ocean Island Basalts (OIB) and Cascade continental arc are from GEOROC (http://georoc.mpch-mainz.gwdg.de/georoc); (d) Rb vs. (Y+Nb) diagram (Pearce et al. (1984) for the most differentiated ($SiO_2$ >57 wt%) rocks showing the fields of ocean ridge (ORG), volcanic arc (VAG), syn-collisional (syn-COLG), and within-plate (WPG) granitic rocks.

Fig. 15. (a) ($^{87}Sr/^{86}Sr)_t$ vs. $SiO_2$ and (b) $\varepsilon Nd_{(t)}$ vs. $SiO_2$ diagrams of Mianeh-Hashtroud Cenozoic igneous rocks. No correlation between Sr and Nd isotopic ratios is observed with the degree of evolution of the melts.

Fig. 16. Geodynamic reconstruction of the Turkish–Caucasus–Iranian collisional zone of Tethyan belt (after Barrier et al. (2018). (a), (c) Paleogeographic scenarios. (b), (d) Geodynamic scenarios (not to scale; location of structures is only indicative). All abbreviations and tectonic domain names are after Barrier et al. (2018): AbM: Alborz Margins (and Talesh); ABV: Artvin-Bolnisi Volcanic Arc; ArB: Arasbaran Belt; Ark: Arkevan Formation; CAC: Central Anatolian Complex; CIP: Central Iranian Platform; EBB: Eastern Black-Sea Basin; EHT: Esfahan-Hamadan Trough; GCB: Greater Caucasus Basin; GKF: Great Kevir fault; HeV: Helete Volcanic arc; ION: Izmir-Ankara-Ercinjan Ophiolite Nappes; KDP: Kopeh Dagh Platform; KON: Khoy ophiolite nappe; LCR: Lesser Caucasus range (including Zangezur-Ordubad volcano-plutonic zone;ZOMZ); LuB: Lut Block; LuP: Lut Platform; MeM: Menderes massif; MsO: Mesogea Ocean; MZT: Main Zagros thrust; PAM: Peri-Arabian massif; PMA: Pontides Magmatic Arc; PoR: Pontides range; RNO: Remnant Neo-Tethys Ocean; SaT: Sanandaj Trough; SCB: South-Caspianbasin; SFB: Srednogorie Fold-Belt; SrB: Sirjan block; SSB: Sanandaj-Sirjan block; SsB: Sistan Basin; SzB: Sabzevar Basin; SzM: Sabzevar Massif; TaP: Taurus platform; UDMA: Urumieh-Dokhtar Magmatic Arc; WBB: Western Black-Sea Basin; ZDF: Zagros deformation front.

# Long-lived, Eocene-Miocene stationary magmatism in NW Iran along a transform plate boundary

Ahmad Rabiee[1], Federico Rossetti[1,*], Yoshihiro Asahara[2], Hossein Azizi[3], Federico Lucci[1], Michele Lustrino[4,5], Reza Nozaem[6]

*[1] Dipartimento di Scienze, Università degli Studi Roma Tre, Roma, Italy*

*[2] Department of Earth and Environmental Sciences, Nagoya University, Nagoya, Japan*

*[3] Mining Department, Faculty of Engineering, University of Kurdistan, Sanandaj, Iran.*

*[4] Dipartimento di Scienze della Terra. Sapienza Università di Roma, P.le A. Moro, 5, 00185, Roma, Italy*

*[5] Istituto di Geologia Ambientale e Geoingegneria, c/o Dipartimento di Scienze della Terra, Sapienza Università di Roma, P.le A. Moro, 5, 00185, Roma, Italy*

*[6] School of Geology, University of Tehran, Tehran, Iran*

** = Corresponding author. E-mail: federico.rossetti@uniroma3.it*

## Abstract

The Eocene-Miocene Mianeh-Hashtroud igneous district in NW Iran is part of the Turkish–Caucasus–Iranian collision zone, a key region to decipher the assembly and differentiation of Gondwana-derived terranes along the Alpine-Himalayan convergence zone. Major inherited tectonic structures control in space and time the Mesozoic-Cenozoic transition from oceanic subduction to continental collision in the region. The geology of the study area is dominated by a polyphase, long-lived magmatic activity, spanning from ~45 to ~6 Ma. The igneous products are subalkaline to alkaline, with intermediate to acidic compositions and a high-K calcalkaline to shoshonitic affinity. Evidence of crustal contamination is attested by inherited zircons in the oldest (Eocene-Oligocene) samples, with ages spanning from Neo-Archean to Paleocene. The Sr-Nd isotopic compositions of the Eocene-Oligocene samples plot close to the Bulk Silicate Earth estimate, whereas the Miocene samples document stronger crustal contamination. The lack of correlation between Nd-Sr isotopes and $SiO_2$ supports a scenario of magma differentiation of different magma batches rather than crustal contamination. Major oxide and Sr-Nd isotopic variation lead us to suggest that magmatism is the consequence of re-melting of earlier underplated (Mesozoic-Tertiary) magmatic products, controlled by amphibole-dominated fractionation processes. Regional scale correlations show long-lived Cenozoic magmatism in NW Iran and Caucasus region, where the main porphyry and epithermal deposits occur. We propose that the Cenozoic collisional magmatism and the associated mineralisation at the junction between NW-Iran and Caucasus was controlled by the activity of a major, lithosphere-scale inherited boundary, transverse to the convergence zone. In such a geodynamic setting, the along-strike segmentation of the lithosphere slab generated asthenospheric melts, their upwelling into the metasomatised supra-subduction mantle wedge and the potential activation of different mantle and crustal sources, with consequent mineral endowment in the region.

## 1. Introduction

Convergent margins are the regions where the bulk of the continental crust forms and differentiates, assisted by magma production during oceanic subduction, continental collision and post-collisional tectonics (Harris et al., 1986; Stern, 2002; 2003; Tatsumi and Kogiso, 2003; 2005; DeCelles et al., 2009; Jagoutz and Klein, 2018). A progressive transition in space and time of the geochemical characteristics of magmatism in collisional settings, from calcalkaline/potassic/ultrapotassic (arc-type) to sodic alkaline (OIB-type) is commonly observed (e.g., Lustrino and Wilson, 2007). This documents the progressive involvement of sub-lithospheric mantle in magma genesis after the vanishing of subduction-related modifications (e.g., Lustrino et al., 2011; Di Giuseppe et al., 2017). This transition is enhanced in collisional zones, where difficulty of the buoyant continental lithosphere to be subducted is commonly associated with crustal thickening, and eventually to crustal and lithosphere delamination (Bird, 1979; Jull and Kelemen, 2001; Lustrino, 2005; Hacker et al., 2015), slab tearing (Faccenna et al., 2005; Rosenbaum et al., 2008; Prelević et al., 2015), slab break-off (von Blanckenburg and Davies, 1995). Scenarios which are prone to convective erosion of the sub-continental mantle (Houseman et al., 1981; Platt and England, 1994), decompressional melting (e.g. Allen et al., 2013a) or small-scale lithospheric keel instabilities (e.g. Kaislaniemi et al., 2014).

All of these processes may result in complex mantle-crust interaction, with the generation of compositionally different magma batches (Duggen et al., 2005; Allen et al., 2013a; van Hunen and Miller, 2015; Di Giuseppe et al., 2017; Kimura, 2017; Rezeau et al., 2018; Agostini et al., 2019). Tracing the spatial and temporal distribution of syn- to post-collisional magmatism can thus provide important information on the geodynamic evolution of convergent plate boundaries and, ultimately, on the spatio-temporal evolution of collisional systems.

The Alpine-Himalayan Belt, extending from the Western Mediterranean through Middle East to Indochina, is a natural laboratory to study the magmatic response to a continuously evolving geodynamic collisional process (Prelević and Seghedi, 2013). Indeed, it records a prolonged history of Mesozoic-Cenozoic accretionary tectonics and continental assembly along the southern margin of Eurasia, accompanied by diffuse syn- to post-collisional magmatism (e.g., Pearce et al., 1990; Keskin, 2003; Köksal et al., 2004; Guo et al., 2006; Şengör et al., 2008; Dilek and Altunkaynak, 2009; Dargahi et al., 2010; Agard et al., 2011; Lustrino et al., 2011; Prelević et al., 2013; Richards, 2015; Schleiffarth et al., 2015; Di Giuseppe et al., 2017; Sahakyan et al., 2017; Sugden et al., 2019).

The Cenozoic Turkish–Caucasus–Iranian collision zone (Fig. 1a) is part of this vast collisional belt (McKenzie, 1972; Allen et al., 2004; Reilinger et al., 2006). This region experienced complex and diachronous collisions involving the Arabia, Eurasia and Anatolia plates, started from Eocene-Oligocene (Allen and Armstrong, 2008; Okay et al., 2010; Ballato et al., 2011; Mouthereau et al., 2012; Madanipour et al., 2013; McQuarrie and van Hinsbergen, 2013; François et al., 2014; Cavazza et al., 2015, 2019; Cowgill et al., 2016; Vincent et al., 2016; Tadayon et al., 2018). The spatio-temporal distribution of collisional magmatism shows punctuated (in space and time) magma production with distinct geochemical characteristics (Berberian and Berberian, 1981; Pearce et al., 1990; Alavi, 1994; Vincent et al., 2005; Keskin et al., 2006; Omrani et al., 2008; Dilek et al., 2010; Verdel et al., 2011; Allen et al., 2013b; Chiu et al., 2013; Neill et al., 2013; Pang et al., 2013a; Neill et al., 2015; Schleiffarth et al., 2015; Shafaii Moghadam et al., 2015; Moritz et al., 2016b; Pang et al., 2016; Di Giuseppe et al., 2018; Lechmann et al., 2018).

Seismic tomography models have documented a variable but in general thin (<50-90 km) lithosphere (with the almost complete absence of the rigid lithospheric mantle) across eastern Anatolia and NW Iran with respect to the Zagros convergence zones (Fig. 1b; Priestley et al., 2012; Delph et al., 2017). The areas with thinner lithosphere and, in particular, the transition from thin to thick lithosphere, correspond to the regions with diffuse late Miocene-Quaternary collisional magmatism (Fig. 1a,b; Kheirkhah et al., 2009; Allen et al., 2013b; Chiu et al., 2013; Kheirkhah et al., 2013; Schleiffarth et al., 2015; Moghadam et al., 2016a; Di Giuseppe et al., 2017; Lechmann et al., 2018). Slab break-off, tearing and fragmentation, assisted by lithospheric mantle delamination, account for the Neogene-Quaternary transition from dominantly calcalkaline to mildly sodic alkaline magmatism (e.g., Faccenna et al., 2007; Göğüş and Pysklywec, 2008; Agard et al., 2011; van Hunen and Allen, 2011; Mouthereau et al., 2012; Allen et al., 2013b; Schildgen et al., 2014; Neill et al., 2015; Delph et al., 2017; Lechmann et al., 2018; Agostini et al., 2019). Furthermore, the presence of one of the major metallogenic region along the Alpine-Himalayan Belt (Richards, 2015) renders the Turkish-Caucasus-Iranian collision zone a suitable region to improve our understanding of the tectonic/geodynamic control on magmatism and associated mineralisation across collisional zones.

In this manuscript, we present whole-rock major and trace element data, U-Pb zircon geochronology and Sr-Nd isotope systematic for the Cenozoic Mianeh-Hashtroud magmatic district located in NW Iran, at the junction between the Cenozoic Urumieh–Dokhtar Magmatic Arc (UDMA), the Alborz-Talesh and the Zangezur–Ordubad magmatic districts (Figs. 1a and 2). The Mianeh-Hashtroud magmatic district (Study area; Figs. 2-3) hosts the unique Oligocene porphyry Mo-only ore deposit (Siah-Kamar) of the Iran region (Nabatian et al., 2017; Rabiee et al., 2019; Simmonds et al., 2019). The Mo-ore forming magmatism shows a metaluminous, high-K calcalkaline to shoshonitic geochemical fingerprint (Khaleghi et al., 2013; Nabatian et al., 2017), but the age and petrological information regarding the Mianeh-Hashtroud magmatic district is still lacking. The integration of the new data with those available from the neighbouring magmatic districts allowed us to shed light into the geodynamic scenario controlling the Cenozoic collisional magmatism and the associated porphyry mineralisation in the region.

## 2. Geodynamic and tectonic evolution

The study area is located within the Turkish-Caucasus-Iranian collision zone (Fig. 1a), a complex tectonic zone made up of a mosaic of continental and obducted oceanic blocks (e.g., Barrier et al., 2018). It results from a long-lasting history of NE-directed oceanic subduction (Paleo- and Neo-Tethys realms), continent-continent collision, as well as intra- and inter-plate deformation during the convergence and subsequent collision of the Arabian plate towards the Eurasian margin (e.g., Stocklin, 1968; McKenzie, 1972; Dewey et al., 1973; Berberian and King, 1981; Stampfli and Borel, 2002; Allen et al., 2004; Copley and Jackson, 2006; Okay et al., 2006; Reilinger et al., 2006; Sosson et al., 2010; Agard et al., 2011; McQuarrie and van Hinsbergen, 2013; Rolland, 2017; Barrier et al., 2018).In particular, during the Cretaceous, two subduction systems developed along the Turkish side to bound the Anatolide-Tauride block, forming the northern Izmir-Ankara-Erzincan suture zone in Anatolia, which can be traced to the east in the Sevan-Akera suture zone (Armenia), and the Bitlis-Pütürge suture zone to the south (Rolland et al., 2012). To the east, on the Iranian side, a single long-lived NE-directed subduction system was instead active along the Zagros convergence zone during Mesozoic until Paleogene (e.g., Agard et al., 2011; Fig. 1a). The Anatolian subduction systems were connected to the Zagros subduction zone through a major transform plate boundary, the Eastern Caucasus-Western Iran Boundary (Sosson et al., 2010; Rolland, 2017; Barrier et al., 2018; Rolland et al., 2020), with surface expression along the Aras Fault (Jackson and McKenzie, 1984; van der Boon et al., 2018; Fig. 1b). This major transform boundary is likely inherited from the late Palaeozoic-early Mesozoic fragmentation of the northern Gondwana Supercontinent, which produced, segmented and then recycled the Neotethyan oceanic lithosphere along the Zagros convergence zone since early Jurassic (Stampfli and Borel, 2002; Barrier et al., 2018). The Aras Fault operated as major transform boundary since Eocene, separating the Eastern Pontides-Caucasus domain from the Talesh-Alborz-Central Iran assembly (Meijers et al., 2017; van der Boon et al., 2018).

The age of Arabia-Eurasia continental collision is still debated, with estimates ranging from Eocene-Oligocene (McQuarrie et al., 2003; Allen and Armstrong, 2008; Agard et al., 2011; Ballato et al., 2011; Mouthereau et al., 2012; Rolland et al., 2012; Madanipour et al., 2013; McQuarrie and van Hinsbergen, 2013; Tadayon et al., 2017; Koshnaw et al., 2018; Tadayon et al., 2018) to Miocene (Guest et al., 2006; Okay et al., 2010; Cavazza et al., 2018). A major episode of basin inversion and rock exhumation, recorded along the Caucasus-Talesh-Alborz during the Eocene-Oligocene boundary, is related to the final closure of the Neotethys oceanic corridor in the Caucasus (e.g., Barrier et al., 2018). This major compressional stage marked the transition from back-arc extension to collisional tectonics in the region (Vincent et al., 2007; Mouthereau et al., 2012; Madanipour et al., 2013; François et al., 2014; Cowgill et al., 2016; Vincent et al., 2016; Rolland, 2017; van der Boon et al., 2018). A further major episode of intracontinental shortening and regional exhumation occurred during early-middle Miocene as documented along the Bitlis–Zagros collisional zone, the Talesh-Alborz and Caucasus regions (Axen et al., 2001; Hessami et al., 2001; Allen et al., 2004; Guest et al., 2006; Mouthereau et al., 2007; Ballato et al., 2008; Morley et al., 2009; Gavillot et al., 2010; Homke et al., 2010; Khadivi et al., 2010; Okay et al., 2010; Sosson et al., 2010; Ballato et al., 2011; Madanipour et al., 2013; François et al., 2014; Cavazza et al., 2018). This latter episode is also referred to the transition from a soft (mostly involving ocean-continent transition margins) to a hard (mature, continent-continent) stage of collision (Ballato et al., 2008; Cowgill et al., 2016). The early-middle Miocene also corresponds to a period of transition from marine to continental sedimentation in the Iranian plateau (Morley et al., 2009) and a major change in the magmatic activity in the region, from dominantly calcalkaline to K-alkaline in composition (Chiu et al., 2013).

The present-day tectonic setting of the region is considered as a consequence of the recent (<5 Ma) regional tectonic reorganisation (Allen et al., 2004; Copley and Jackson, 2006). Active deformation is largely accommodated through shortening to the north (Great Caucasus) and the south (Zagros) of the Turkish-Iranian Plateau, together with the westward escape of the Anatolia plate, accommodated by the dextral North Anatolian and sinistral East Anatolian Fault systems (Jackson and McKenzie, 1988; Jackson et al., 1995; Allen et al., 2004; Talebian and Jackson, 2004; Vernant et al., 2004; Avagyan et al., 2005; Reilinger et al., 2006; Avagyan et al., 2010; Walpersdorf et al., 2014; Tsereteli et al., 2016).

Active tectonics across the Turkish-Caucasus-Iranian Plateau is dominantly accommodated by WNW-ESE dextral shearing along the Chaldoran and Tabriz fault systems (Fig. 1a; Berberian and Arshadi, 1976; Jackson, 1992; Copley and Jackson, 2006; Djamour et al., 2011; Moradi et al., 2011; Moradi et al., 2016; Su et al., 2017). The GPS-derived tectonic boundaries within the collision zone identified four major tectonic blocks delimited by major seismically active zones (Reilinger et al., 2006; Fig. 1a): Anatolia, Caucasus (including Lesser Caucasus-Armenia and Talesh-Arasbaran zones), Alborz and Central Iran (including the Sanandaj-Sirjan Mesozoic and the Urumieh-Dokhtar Cenozoic magmatic zones). These four major blocks are bounded by the remnants of major ophiolite sutures, diachronoulsy structured during the Paleotethyan and Neotethyan closures (Fig 1a; Hässig et al., 2013; Barrier et al., 2018; Naumenko-Dèzes et al., 2020). This evidence supports the fundamental role of structural inheritance in controlling the present tectonic setting and the overall collisional evolution of the entire region.

An abrupt transition in the lithospheric structure and thickness is observed across the Aras Fault and the southward and sub-parallel Mianeh-Ardabil fault zone (Priestley et al., 2012; Fig. 1b), where the study area is located (Fig. 1b). Finally, seismic models of the crustal structure in the region show an abrupt change in the Moho depth across the Tabriz Fault, sharply deepening from ~33 to ~55 km to the NE in a ~50 km NE-SW transect (Taghizadeh-Farahmand et al., 2010; Shad Manaman et al., 2011; Fig. 1b).

## 3. Cenozoic magmatism and mineralisation

The geology of the Turkish-Caucasus-Iranian collision zone is dominated by diffuse exposure of Cenozoic igneous rocks, mostly occurring along the north-western segment of the UDMA (Takab and Mianeh-Hashtroud districts), Alborz, Lesser Caucasus-Arasbaran-Talesh (CAT), and the Naqadeh-Sonqor-Azna (NSA) magmatic zones (Fig. 2). Major magmatic episodes are distributed across the collisional zones during the Eocene-Oligocene and from middle Miocene to Quaternary. The geochemical signature of the collisional magmatism is characterized by a typical but diachronic progression from calcalkaline, shoshonite (Eocene-Oligocene) and adakitic, to dominantly high-K alkaline and minor sodic alkaline magmatism (Miocene-Quaternary; e.g., Vincent et al., 2005; Omrani et al., 2008; Azizi and Moinevaziri, 2009; Aghazadeh et al., 2010; Verdel et al., 2011; Allen et al., 2013b; Castro et al., 2013; Chiu et al., 2013; Neill et al., 2013; Pang et al., 2013a; Neill et al., 2015; Moghadam et al., 2016b; Moritz et al., 2016b; Pang et al., 2016; Rezeau et al., 2017; Lechmann et al., 2018; 2018; Schleiffarth et al., 2018; Shafaii Moghadam et al., 2018). A dominant contribution of a metasomatised sub-continental lithospheric mantle is commonly postulated as the main source for the Neogene-Quaternary magmatism in the region (Kheirkhah et al., 2009; Allen et al., 2013b; Chiu et al., 2013; Kheirkhah et al., 2013; Pang et al., 2013a; Sahakyan et al., 2017; Lechmann et al., 2018; Shafaii Moghadam et al., 2018).

The Cenozoic magmatism is mainly distributed to form roughly parallel linear arrays running NW-SE along the NSA (to the south), the UDMA, and the Alborz-CAT (to the north) magmatic zones (Fig. 2).

Within the NSA magmatic zone, Eocene (~52-34 Ma) tholeiitic to calcalkaline and high-K calcalkaline to shoshonite, dominantly intrusive, magmatic suites are reported (Azizi and Moinevaziri, 2009; Mazhari et al., 2009a; Mazhari et al., 2009b; Mazhari et al., 2010; Azizi et al., 2011; Bea et al., 2011; Mahmoudi et al., 2011; Mazhari et al., 2012; Whitechurch et al., 2013; Ao et al., 2016; Chiu et al., 2017; Nouri et al., 2017; Azizi et al., 2018a; Zhang et al., 2018). Azizi and Moinevaziri (2009) interpreted these igneous rocks as resulting from mantle sources modified during the Paleogene oceanic subduction along an active intra-oceanic arc system during the final closure stage of the Neotethys.

In the north-western UDMA, the Takab zone records a long-lived (Eocene to Miocene) magmatism, ranging from calcalkaline to K-alkaline compositions (Daliran et al., 2013; Heidari et al., 2015; Moghadam et al., 2016a; Shafaii Moghadam et al., 2017; Honarmand et al., 2018). The Takab region hosts important epithermal Miocene Au-Cu-Zn mineralisation systems [Zarshuran, Anguran and Touzlar deposits; e.g.; Mehrabi et al. (1999); Gilg et al. (2006); Daliran (2007); Heidari et al. (2015); Fig. 2 and Supplementary Material S1]. The large Miocene-Quaternary Sahand (~8-0.17 Ma) and Sabalan (~4.5-0.15 Ma) and the smaller Saray (~11 Ma) composite volcanoes (Pang et al., 2013b; Ghalamghash et al., 2016; Lechmann et al., 2018; Ghalamghash et al., 2019; Lustrino et al., 2019b) are the most prominent volcanic structures in the region (Fig. 2), with the Saray volcano marking the first stage of post-collisional magmatism in the Arabia-Eurasia collisional zone (Pang et al., 2013b; Moghadam et al., 2014). The volcanic activity starts with emplacement of high-K basalts to plagioleucitites at Saray (Eslamieh peninsula), followed by trachyandesites to dacites of the two large Sahand and Sabalan, with a variable potassic to high-K calcalkaline and adakitic geochemical signatures. The origin of the igneous activity is referred either to mantle melting triggered by slab roll-back and slab break-off shortly after continental collision (Ghalamghash et al., 2016; 2019) or to lithospheric small scale convection in post-subduction environments (Kaislaniemi et al., 2014).Significantly, the lithosphere structure in the region is characterized by low velocity zones down to upper mantle depths, assumed as the source region of Neogene-Quaternary magmatism of NW Iran (Bavali et al., 2016).

In the Alborz-CAT zone, calcalkaline to alkaline magmatism is documented during the Eocene-Oligocene and is attributed to tapping of a metasomatized mantle source during lithosphere extension in a back-arc setting (Aghazadeh et al., 2011; Castro et al., 2013; Nabatian et al., 2014; Nabatian et al., 2016; Ashrafi et al., 2018; Eskandari et al., 2020). The Oligocene and early Miocene magmatism are more scattered. In particular, igneous rocks largely crop out within the Alborz-CAT zone, and are mostly aligned along, or confined within, the transverse Aras and Mianeh-Ardabil faults (Fig. 2).

The Arasbaran magmatic zone (part of the Alborz-CAT magmatic zone) hosts notable porphyry deposits, mainly associated with Oligocene-Miocene monzonitic and monzodioritic intrusive bodies and showing a concentration and ore enhancement toward the Aras Fault (Fig. 2). The Sungun, Haft Cheshmeh Cu-Mo and the Masjed-Daghi Cu-Au deposits are the most important ones, with molybdenite Re-Os ages of 21 Ma, 27 Ma and 20 Ma, respectively (Aghazadeh et al., 2015). A prolonged and stationary magmatism (mostly with geochemical affinities ranging from calcalkaline to shoshonitic and adakitic) is instead documented in the Lesser Caucasus, where the Meghri-Ordubad composite pluton records ~30 Myr-long activity (Eocene-Miocene; Chiu et al., 2013; Moritz et al., 2016b; Rezeau et al., 2016; 2017; Fig. 2; 2018). The Zangezur-Ordubad region in the Lesser Caucasus host two stages of porphyry Cu-Mo deposits, including the ~49-44 Ma (Agarak, Hanqasar, Aygedzor and Dastakert), and the 27-26 Ma (e.g., Kadjaran) deposits (Moritz et al., 2016a). The prolonged mantle-derived magmatism has been considered as a prerequisite to form fertile magmatic-hydrothermal systems and a key requirement for the formation of economically important porphyry Cu-Mo deposits (Rezeau et al., 2016; 2017). Similarly to the Arasbaran zone, the frequency of occurrence of the porphyry systems increases toward the Aras Fault.

## 4. Materials and methods

The research strategy combines field investigations with laboratory (petrographic, geochemical and geochronological) studies aimed at describing the spatio-temporal and petrological evolution of the Cenozoic magmatic activity within the Mianeh-Hashtroud magmatic complex (Figs. 1a and 2). Fieldwork was based on the 1:250,000 cartography (Amidi et al., 1987; Khodabandeh et al., 1999), with the scope to map and refine the distribution of the main magmatic rock types (Fig. 3). Classification of the different magmatic rocks in plutonic, hypabyssal and volcanic types follows Le Maitre et al. (2005). An extensive sampling of representative lithologies has been then carried out and investigated though whole-rock geochemistry [X-ray fluorescence (XRF) and inductively coupled plasma mass spectrometry (ICPMS) methods], Sr-Nd isotope systematics and laser ablation inductively coupled plasma mass spectrometry (LA-ICP-MS) zircon U-Pb geochronology. The studied samples are listed in Table 1, where their location, age, petrography and geochemical characteristics are reported in detail. The analytical protocols are described in Appendix A1.

The collected data are then compared with the geochronological and geochemical data available from the neighbouring regions, in order to build up a regional synthesis and propose a corresponding geodynamic interpretation.

## 5. Field data and petrography

The revised geological map of the study area is shown in Fig. 3 that includes the new geochronological data presented in this study (see below). The stratigraphy of the area is dominated by a wide exposure of Eocene volcanic rocks (hereafter referred as country rocks), unconformably covered by discontinuous Miocene volcanic and volcano-sedimentary successions and by continental deposits of the Miocene Upper Red Fm. (Amidi et al., 1987; Khodabandeh et al., 1999; Ballato et al., 2017). Pliocene-Quaternary continental sedimentary successions are dominant in the western and eastern sectors of the area (Fig. 3).

The Eocene volcanic country rocks are intruded by a polyphase (Eocene, Oligocene to early Miocene) magmatic suite made up of intrusive (plutonic and hypabyssal) bodies. The main plutonic bodies, usually showing granular texture, crop out to the northwest and centre of the study area, defining a NW-SE-oriented magmatic belt (Figs. 3 and 4a). The Oligocene magmatism is responsible for the Mo endowment in the Siah-Kamar porphyry deposit (Fig. 3; Nabatian et al., 2014; Rabiee et al., 2019; Simmonds et al., 2019). The Mo deposit is associated with diffuse rock alteration, grading from an inner sodic-potassic to an outer propylitic zone formed in the 33-28 Ma time lapse (Rabiee et al., 2019).To the southeast (from Khatoon-Abad to Siah-Kamar), an array of abundant E-W to NE-SW striking microgranular and porphyritic felsic stocks, and dykes intrude the Eocene country rocks (Figs. 3 and 5).

A description of the rocks samples, textural types and mineral paragenesis is reported below.

### 5.1 Eocene volcanic country rocks

The Eocene volcanic country rocks (samples MN04, MN33, MN37, MN38) are made up of a thick pile of alternating lava flows and pyroclastic beds, variably affected by secondary hydrothermal propylitic alteration (Fig. 4a and 4b-d). Lava flows are intermediate to acid in composition, ranging from basaltic trachyandesite to trachyte (Table 1). They are porphyritic (phenocryst load up to 20 vol%) with hypohyaline textures and fluidal to trachytic fabrics (Fig. 6a). They show a mineral assemblage with phenocrysts dominated by plagioclase together with amphibole and minor clinopyroxene (commonly altered), in a matrix of plagioclase, alkali feldspar, ± amphibole, clinopyroxene and Fe-Ti oxides, plus minor accessory phases such as apatite and zircon, and glass (Fig. 6a).

### 5.2. Plutonic rocks

Intrusive rocks (samples MN09, MN10A, MN10B, MN10C, MN12, MN67 and MN74; Fig. 4a and 4e-h) are characterized by equigranular to porphyritic holocrystalline hypidiomorphic textures (Fig. 6b-e). Mineral assemblages are typical of metaluminous rocks with plagioclase, alkali feldspar, quartz, amphibole (usually altered), biotite, and minor clinopyroxene (altered). Plagioclase occurs either as coarse-grained crystals (Fig. 6b) or as phenocrysts (Fig. 6e). Based on the modal abundance of minerals (Middlemost, 1994), these intrusive rocks span from monzodiorite to monzonite, syenite and granite (Table 1). Granitoid rocks (samples MN10A; Fig. 6d) host monzonitic enclaves (samples MN10B-C) with porphyritic holocrystalline textures and comparable mineral assemblage (plagioclase, alkali feldspar, quartz, biotite, amphibole and clinopyroxene). Accessory minerals are made of apatite, zircon and Fe-Ti oxides.

### 5.3. Hypabyssal rocks

Hypabyssal rocks consist of stocks and dykes (samples MN02A, MN02B, MN03, MN45, MN65 and MN76; Fig. 5a). They show typical porphyritic holocrystalline, hypidiomorphic to autoallotriomorphic textures and microcrystalline matrix. (Fig. 5b-c). These subvolcanic rocks span from mafic to felsic compositions and, show a metaluminous assemblage similar to that of intrusive rocks made up of quartz, alkali feldspar, plagioclase, biotite, amphibole, with minor clinopyroxene (Fig. 6f-g-h). Accessory minerals include apatite, zircon and Fe-Ti oxides. These hypabyssal rocks span from monzonite to syenite and granite in composition (Table 1).

### *5.4. Volcanic rocks*

Volcanic rocks (samples MN05, MN07, MN19, MN20, MN35, MN39, MN43, MN44, and MN73) include glass bearing magmatic rocks. This rock group comprises porphyritic to vitrophyric types, with hypohyaline to holohyaline groundmass (Fig. 5a,d-h). Phenocrysts (20-40 % vol.) are subhedral to euhedral plagioclase, alkali feldspars, quartz, biotite, amphibole (seldom altered) and rare, commonly altered, clinopyroxene (Fig. 6i). Rock composition varies from andesite to rhyolite (Table1).

## 6. Zircon U-Pb geochronology

The zircon U-Pb geochronological study was carried out on twelve samples (Table 1 and Fig. 7). Zircons were investigated through backscattered electron and cathodoluminescence (CL) imaging (see Supplementary Material S2), and then analysed through LA-ICP-MS. Analytical results are reported in Table 2, whereas the detailed description for each sample analysis is provided in Supplementary Material S3. In general, the Th/U values are in the range of 0.09-2.79, compatible with an igneous origin (e.g., Rubatto, 2002; Kirkland et al., 2015). Evidence of Pb loss is seen in some zircons resulting in discordant ages but most of the results from oscillatory growth zones show concordant ages. The criteria for age calculation, including categorisation of the zircon types (autocrysts, antecrysts, and xenocrysts/inherited; Miller et al., 2007) is provided in Appendix A1 and illustrated as probability density plots and weighted mean ages in Supplementary material S4.

Below, the basic features of the analysed samples are reported, grouping the results into four age groups: (1) two samples from the Eocene country rocks [MN33 (43.4 ± 2.6 Ma) and MN38 (38.4 ± 1.0 Ma)], collected at the bottom and at the top of the exposed volcanic succession in the Siah-Kamar area (Fig. 3); (2) three samples from the Eocene intrusive bodies exposed in the central [Khatoonabad; samples MN09 (44.32 ± 0.58 Ma), MN67 (40.69 ± 0.88 Ma) and MN10 (36.75 ± 0.62 Ma)] and north-western corner [Dizaj; samples MN45 (30.21 ± 0.41 Ma) and MN76 (28.23 ± 0.88 Ma)] of the study area; (3) four samples from the Oligocene-early Miocene hypabyssal/subvolcanic bodies [samples MN05 (22.6 ± 0.41 Ma), MN39 (28.18 ± 0.80 Ma), MN43 (26.97 ± 0.35 Ma) and MN44 (26.19 ± 0.54 Ma)] from the central and western sectors of the study area (Khatoonabad and Ebak), and (4) one sample (MN35) from the late Miocene volcanic rocks (Ebak area; 5.93 ± 0.24 Ma Fig. 3).

The Eocene volcanic country rocks possess remarkable number of inherited zircons. Inherited zircons are commonly broken, fractured and sub-rounded often showing metamict and complex zoning textures. Sample MN33 show 27 inherited zircons out of a total of 39 measured zircons, which show apparent $^{206}Pb/^{238}U$ ages spanning from Middle Jurassic (167 ± 5 Ma) to Paleo-Proterozoic (2208 ± 49 Ma). Sample MN38 contains inherited zircons showing apparent $^{206}Pb/^{238}U$ ages spanning from Paleocene (63 ± 5 Ma) to Neoarchean (2737 ± 77 Ma; Table 2). A few inherited zircons are also seen in sample MN67 (40.69 ± 0.88 Ma) from a syenite body. They show $^{206}Pb/^{238}U$ ages spanning from Upper Cretaceous (~67 Ma) to Upper Jurassic (~148 Ma; Table 2).

## 7. Geochemistry

The major and trace element compositions of the twenty-six samples analysed in this study are presented in Table 3. The mass loss of ignition (LOI) is mostly below 3 wt%, apart from four samples (LOI = 4-6 wt%) and one sample with LOI = 10.5 wt%. Collectively, the studied samples mostly plot in the alkaline (trachyandesite and trachyte) and the rhyolite fields of the TAS diagram (Fig. 8a), with just a few samples falling in the andesite and dacite fields. In the $K_2O$ vs. $SiO_2$ diagram (Peccerillo and Taylor, 1976), the samples are mostly distributed in the high-K calcalkaline and shoshonitic fields (Fig. 8b). To avoid possible bias caused by post-emplacement fluid-rock interaction during hydrothermal alteration, the classification schemes based on immobile trace elements (Winchester and Floyd, 1977; Hastie et al., 2007) are adopted in this study. In the $SiO_2$ vs. Nb/Y classification proposed by Winchester and Floyd (1977; Fig. 8c), the samples mostly confirm their alkaline nature, with a few of them straddling the subalkaline to alkaline division line, and only two falling in a true alkaline field. In the Th vs. Co classification diagram (Hastie et al., 2007; Fig. 8d) the samples mostly plot in the high-K and shoshonite (HK-SHO) series fields.

None of the investigated rocks shows primitive character (MgO<4 wt%) and all can be interpreted as derivative liquids. Anyway, some general comments on the possible mantle sources can be inferred focusing on the least differentiated compositions (samples with <57 wt% $SiO_2$; 1.6-4.0 wt% MgO). In the following, the description of the geochemical characteristics of the analysed rocks is presented, grouping them into the respective age group.

### *7.1. Eocene rocks*

Eocene rocks (n = 11) show intermediate to acid compositions ($SiO_2$ = 54.27-75.22 wt%), with moderate $Al_2O_3$ (12.52-18.83 wt%), low MgO (0.07-3.97 wt%) and Mg# (Mg/[Mg+$Fe_{tot}$]*100) in the 5-62 range. These samples also show low $TiO_2$ (<1 wt%), coupled with a wide range of CaO (0.43-8.36 wt%), $K_2O$ (2.06-7.78 wt%) and $Na_2O$ (2.92-8.99 wt%; Table 3). Harker diagrams for major elements show negative correlation with $SiO_2$ for $Al_2O_3$, $Fe_2O_{3tot}$, MgO, Mg#, $P_2O_5$ and $TiO_2$, and CaO, whereas $Na_2O$, with the exception of an outlier at ~9 wt% remains nearly constant at ~3-4 wt% within the ~54-75 wt% $SiO_2$ range (Fig. 9). Trace elements show no appreciable trends with $SiO_2$ for many of large ion lithophile elements (LILE) and high field strength elements (HFSE). Negative correlation with $SiO_2$ are observed for Y, V, Eu, Sr, and Dy/Yb, whereas Nb shows a rough correlation with the same parameter. A selection of the key trace elements vs. $SiO_2$ is reported in Fig. 10.

Primitive Mantle (PM) normalized (after Lyubetskaya and Korenaga, 2007) patterns of the Eocene samples show several spikes and troughs, with marked enrichments of LILE (such as Ba, Cs, Rb, Th, U, K) and distinctive Pb positive spikes. Some HFSE (Nb, Ta and Ti) define clear troughs, whereas others (Zr and Hf) show no anomaly compared to neighbouring REE with similar incompatibility (Sm and Eu). Phosphorous shows the largest variability, with slightly positive to negative anomalies (Fig. 11a). Middle (MREE) to Heavy (HREE) lanthanides show no appreciable fractionation, with an overall flat pattern and an average $(Dy/Lu)_N$ ratio of ~1.2. This is associated to a mildly fractionated Light (LREE)/HREE ratio [$(La/Lu)_N$ ~10.9] and a limited Eu negative anomaly [(Eu/Eu*) ~0.79]. Overall, the least differentiated Eocene rocks (those with $SiO_2$ <57 wt%) show a relatively uniform character, resembling closely the present-day average global subducting sediment (GloSS; Plank, 2014; Fig. 8). The most evolved compositions ($SiO_2$ >58 wt%) show more spiky patterns, with deeper troughs and higher peaks, mostly related to fractionation apatite, zircon and Fe-Ti oxides.

### *7.2. Oligocene rocks*

Oligocene rocks (n = 13) nearly completely overlap the Eocene rocks in Harker diagrams with negative correlations for $Al_2O_3$, $Fe_2O_{3tot}$, MgO, $TiO_2$, $P_2O_5$ and CaO, whereas no clearly correlation is observed for $Na_2O$ and $K_2O$ contents (Fig. 9). Oligocene rocks show intermediate to acid compositions ($SiO_2$ = 54.9-82.2 wt%), with the highest $SiO_2$ contents likely representing the effect of silicification. Rock compositions with SiO2 >78 wt% are no longer discussed in the text, because silicification is usually associated with alkali mobility (e.g., Lustrino et al., 2010). The main characteristics are variable $Al_2O_3$ content (ranging from 10.2 to 22.7 wt%), low MgO (0.1-3.5 wt%), low $TiO_2$ (<1 wt%) and CaO (0.1-7.8 wt%), with $K_2O$ generally higher than $Na_2O$ (Table 3).

Analogously, trace elements show a negative correlation for Y, Yb and Eu content and the Dy/Yb, whereas Nb and Th correlates with $SiO_2$ (Fig. 10). The least differentiated Oligocene rocks ($SiO_2$ <57 wt%) are characterized by PM-normalized patterns qualitatively indistinguishable from those of the Eocene rocks. The LREE/HREE [average $(La/Lu)_N$ ~20.9] and MREE/HREE values [average $(Dy/Lu)_N$ ~1.4] are slightly higher than the Eocene samples, whereas no substantial Eu anomaly is recorded (Eu/Eu* ~1.01). The most evolved samples ($SiO_2$ >57 wt%) show more spiky patterns and deep negative Eu anomaly (Eu/Eu* ~0.74).

### *7.3. Miocene rocks*

Miocene rocks (n = 3) show intermediate to acid compositions ($SiO_2$ = 56.5-78 wt%), with moderate $Al_2O_3$ (10.6-17 wt%), low MgO (0.1-2 wt%) and Mg# (23-39), low $TiO_2$ (<1 wt%), CaO in the 0.1-3.8 wt% range, and $K_2O$ generally higher than $Na_2O$. The strongly evolved composition found in one early Miocene sample (MN05; $SiO_2$ = ~78 wt%) is characterized by strongly fractionated patterns with deep troughs at P and Ti and with Eu/Eu* = 0.32. The youngest, late Miocene shoshonite (MN35) shows intermediate $SiO_2$ (~56.5 wt%), low MgO (~2 wt%) and high $K_2O/Na_2O$ (~4.6) (Table 3). For what regards major and trace elements, these rocks plot along the same trend shown by the Eocene and Oligocene samples in Harker diagrams (Figs. 9 and 10). PM- and CI chondrite-normalized patterns do not show any peculiarity, closely resembling the GloSS composition (Fig. 11).

## 8. Sr-Nd isotopic ratios

Eighteen selected samples have been analysed for Sr and Nd isotopic ratios. The measured and initial $^{87}Sr/^{86}Sr$ and $^{143}Nd/^{144}Nd$ isotopic ratios, as well as epsilon values for Mianeh-Hashtroud igneous rocks are reported in Table 4. In the $\varepsilon Nd_{(t)}$ vs. $^{87}Sr/^{86}Sr_{(t)}$ isotopic diagram (Fig. 12), most of the Cenozoic igneous rocks analysed in this study plot not far away from BSE and ChUR estimates, with a relatively limited range of $^{87}Sr/^{86}Sr_{(t)}$ (0.70413-0.70524) and $^{143}Nd/^{144}Nd_{(t)}$ (0.51267-0.51274), the latter corresponding to $\varepsilon Nd_{(t)}$ from -1.56 to +3.47. The Eocene and Oligocene rocks overlap almost completely, whereas the Miocene samples show more radiogenic $^{87}Sr/^{86}Sr_{(t)}$ (0.70588-0.70646), but $\varepsilon Nd_{(t)}$ mostly within the lower end range of the older samples (−1.56 to +0.32; Fig. 12). The Nd model ages ($T_{DM}$), as calculated based on the method of Keto and Jacobsen (1987), span from 0.61 to 0.96 Ga (Table 4).

## 9. Discussion

### *9.1. A long-lived stationary magmatism*

The new U-Pb zircon ages presented in this study document a protracted magmatic activity from Eocene (~44 Ma) to late Miocene (~6 Ma). Based on the weighted age distribution of the all measured zircon autocrysts and antecrysts (Miller et al., 2007), a continuous range from ~55 (54.8 ± 2.8 Ma) to ~12 Ma emerges, with a possible magmatic lull at ~12-8 Ma (Fig. 13a), which is consistent with the onset of the eruptive magmatism in nearby Sahand volcano (Richards et al., 2006; Sawada et al., 2016; Lechmann et al., 2018). Zircons possessing ages older than this continuous range are considered as inherited ones (see Appendix A1 and Supplementary Material S4). This evidence suggests the incorporation of zircon antecrysts during successive magmatic injections and growth of newly formed zircons (autocrysts sensu Miller et al., 2007), in a scenario of a long-lived and incremental growth of the Mianeh-Hashtroud magmatic complex during the Eocene-Miocene times.

The dated samples contain abundant inherited zircons populations. Irrespective of the obtained apparent $^{206}Pb/^{238}U$ ages, the Th/U values of the inherited zircons (n = 142) range from 0.1 to 2.7. These values, together with their textural characteristics (oscillatory to sector zoning; Supplementary Material S2) are consistent with a magmatic origin (e.g., Corfu et al., 2003; Kirkland et al., 2015). Both zircon antecrysts and inherited zircons show a major frequency distribution in Cenozoic with respect to pre-Cenozoic times (Fig. 13b-c). The pre-Cenozoic inherited zircons are mainly observed in the Eocene and Oligocene rocks, typically showing a remarkable spread of apparent $^{206}Pb/^{238}U$ ages, from Paleocene (~66-56 Ma) to Neoarchean (~2.6-2.7 Ga; Fig. 13b; Table 2). In particular, the age distribution histogram for inherited zircons in Eocene rocks clusters at ~260-140 Ma (Triassic-Jurassic), ~550-420 Ma (Cambrian-Silurian), and ~1000-700 Ma (early Neoproterozoic), but Proterozoic (up to 2500 Ma) and Neoarchean (2800-2500 Ma) ages are also reported (Fig. 13b). These age span is compatible with ages reported for the Iran basement rocks (Mazhari et al., 2009a; Chiu et al., 2013; Nutman et al., 2014; Ao et al., 2016; Lechmann et al., 2018; Shakerardakani et al., 2019).

A similar scenario of prolonged and stationary incremental growth of a magmatic complex (in terms of both longevity and age of magma production) is documented in the Cenozoic Zangezur-Ordubad magmatic district of Lesser Caucasus (Moritz et al., 2016b; Rezeau et al., 2016; 2017; 2018; Fig. 2). Interestingly, the Zangezur-Ordubad in the Lesser Caucasus, Arasbaran, Takab and the Mianeh-Hashtroud magmatic districts of NW Iran are all located along the transverse tectonic structures of Aras and Ardabil-Mianeh-Baneh fault systems that segment the continental lithosphere of the Iranian plateau (Fig. 2).

### *9.2. Petrological model*

Irrespective of the age and magmatic facies, the PM-normalized patterns of the Mianeh-Hashtroud rocks closely resemble present-day subducting sediments (GloSS; Plank, 2014), average continental crust composition (Rudnick and Gao 2003) and igneous rocks emplaced above active subduction systems (Fig. 11a). The geochemical fingerprints of magmas generated in subduction zones consist in variable LILE enrichment, whose most peculiar features are the positive anomalies at K and Pb together with the HFSE depletion with respect to their neighbouring elements. This likely results from the ability of metasomatic fluids to fractionate elements with different compatibilities in subducted slab-derived components (e.g., Pearce, 1983; Tatsumi et al., 1986; Tatsumi et al., 1991; Hawkesworth et al., 1997; Elburg et al., 2002; Kessel et al., 2005; Kimura, 2017; Sahakyan et al., 2017; Lustrino et al., 2019a; Zheng, 2019). The overall incompatible element fractionation reported in Fig. 11 clearly evidences the subduction-related compositions of the investigated rocks. Taking into consideration the poor Sr enrichment and the relatively high Y and Yb content (coupled with relatively low Sr/Y and La/Yb), the majority of Mianeh-Hashtroud rocks plot within the calcalkaline arc field, supporting a dominant subduction fingerprint of the Mianeh-Hashtroud magmatic suite (Figs. 14a-b).

The enrichment in incompatible trace elements (such as Ba Cs, Th, La, Nd) are significantly higher than those of calcalkaline arc magmas, but comparable with those of continental arc shoshonites (see inset in Fig. 10b). When the least differentiated compositions ($SiO_2$ <57 wt%) are taken into account, the low Ce/Pb (~1.5-6.0) and Nb/U (~2.6-8.9) and the extremely high $(Th/Nb)_N$ ratios (up to ~12.9) are all consistent with crustal contamination or subduction-related metasomatism (Pearce, 2008). In the Th/Yb vs. Nb/Yb diagram (Fig.14c), the same samples plot far from the oceanic mantle array, pointing towards high Th/Yb ratios, close to average crustal values (4.0-7.0; average value 5.3; Rudnick and Gao, 2003) at moderate Nb/Yb (5.3-17.7; Fig. 14c). In the Rb vs. Nb+Y discrimination diagram (Fig.14c) for granitic rocks, the most evolved Mianeh-Hashtroud rocks ($SiO_2$>57 wt%) fall within the volcanic arc granite field, in the transition zone assumed as representative of post-collisional environments (Fig. 14d).

Most of the studied samples show highly evolved compositions, with low MgO contents, Mg# (0.62–0.35) and Cr contents (all but two samples <200 ppm; Table 3), far away from the primitive melt composition expected for melts in equilibrium with the mantle (Kimura, 2017; Schmidt and Jagoutz, 2017; Zheng, 2019). These compositional characteristics suggest that the studied magmatic products experienced significant fractionation after mantle anatexis (e.g., Ulmer et al., 2018). The occurrence of amphibole in the basic products and the negative correlation with differentiation of major oxides, including $Al_2O_3$, $FeO_t$, MgO, CaO, $TiO_2$, and $P_2O_5$, and trace elements such as V, and Y are indeed compatible with amphibole fractionation (Fig. 9). The negative correlation of Dy/Yb with $SiO_2$ (e.g., Klein et al., 1997; Davidson et al., 2007) and of Dy/Dy* $[Dy_N/(La_N^{4/13} x Yb_N^{9/13})]$ vs. Dy/Yb (Davidson et al., 2013) is further compatible with a role of amphibole in the fractionating assemblage (Fig. 10).

The negative correlation of Eu with differentiation (Fig. 10) also suggests a significant role of plagioclase fractionation mainly in the most evolved compositions. Due to the higher partitioning coefficient of middle REE (MREE) with respect to LREE and HREE in amphibole (Davidson et al., 2007), fractional crystallization of amphibole from parental mafic magmas can explain the strongly fractionated REE and the flat HREE patterns of the Mianeh-

Hashtroud magmatic products. In this scenario, the slightly high Sr/Y and $(La/Yb)_N$ of a subset of samples, falling in the adakitic field (Moyen, 2009; Figs. 14a,b), can be thus related to amphibole fractionation during magmatic differentiation (e.g., Macpherson et al., 2006; Li et al., 2009; Moyen, 2009; Dessimoz et al., 2012; Rossetti et al., 2014; Moghadam et al., 2016b), rather than the result of partial melting of the eclogitised subducted oceanic crust.

The Sr and Nd isotopic compositions (Fig. 12) indicate depleted (or not strongly enriched) mantle sources for the Eocene-Oligocene rocks of the Mianeh-Hashtroud area. On the other hand, the Miocene hypabyssal and volcanic rocks document a stronger crustal component in their genesis. This shift towards a more enriched mantle source with decreasing age is in line with the isotopic signature of the Neogene-Quaternary magmatic products of NW Iran Azerbaijan (Lechmann et al., 2018; Fig. 12). The lack of clear correlation between Sr and Nd isotopes vs. $SiO_2$ (Fig. 15) supports a scenario of magmatic differentiation with limited assimilation of radiogenic crustal rocks (i.e., old basement) as the main petrogenetic process. Similar Sr-Nd isotope ratios and magmatic differentiation series dominated by fractional crystallization and limited crustal assimilation are reported from the Mesozoic and Cenozoic Zangezur–Ordubad magmatic district (Mederer et al., 2013; Moritz et al., 2016b; Fig. 12), which could be interpreted with a similar scenario and therefore extended to the Lesser Caucasus region too. This is in line with the studies in Lesser Caucasus by Sugden et al. (2019).

On the other hand, the occurrence of abundant inherited zircons in Eocene magmatic products points to crustal contamination during the melt differentiation and the emplacement in the crust. On this regard, it is worth nothing that the relatively young Nd model ages (0.61 to 0.91 Ga) indicate that the Mianeh-Hashtroud magmatic products originated from juvenile crustal rocks. This hypothesis is corroborated by the compelling evidence of extensive magmatic underplating during Mesozoic-Cenozoic times in Central Iran in the upper-plate of the Neotethyan subduction (e.g., Berberian and King, 1981; Omrani et al., 2008; Azizi and Moinevaziri, 2009; Agard et al., 2011; Verdel et al., 2011; Richards, 2015). It is worth noting that the Sr-Nd isotopic compositions of the Mianeh-Hashtroud igneous rocks overlap those reported for the Jurassic-Cretaceous igneous rocks from the neighbouring Sanandaj-Sirjan zone (ε$Nd_{(t)}$: +2 to +6; Azizi and Asahara, 2013; Azizi et al., 2018b; Fig. 12). We therefore propose that voluminous mafic underplating of arc magmas during the Mesozoic and its successive re-melting was the dominant process leading to the generation of the Cenozoic magmatism in NW Iran (e.g., Chung et al., 2009; Pe-Piper et al., 2009; Jiang et al., 2014). On this regard, melting of LILE- and LREE-enriched and HFSE-depleted lower crustal mafic amphibolite could have contributed to impart the distinctive trace-element characteristics of the Cenozoic igneous rocks of Mianeh-Hashtroud (Fig. 11a), including the moderate fractionation of the REE and the flat HREE pattern (e.g., Pe-Piper et al., 2009; Jiang et al., 2014; Fig. 11b).

Crustal foundering and melting have been also proposed as viable mechanism for the genesis of the Quaternary adakite-like magmatism in Iran (Pang et al., 2016) and for the Miocene-Quaternary magmatism in NW Iran (Lechmann et al., 2018). It is worth noting that the Sr-Nd isotope systematics of the Cenozoic magmatism in NW Iran largely overlaps in space and time, confirming extensive crustal recycling as a viable source of magmatism in the region.

This reconstruction is also compatible with the dominant enriched sources of the Miocene-Quaternary magmatism documented in the Azerbaijan region of NW Iran (Lechmann et al., 2018), which confirm crustal-contaminated heterogeneous magmatic sources through time (Allen et al., 2013b; Lechmann et al., 2018). This hypothesis is also compatible with the scenarios proposed for the collisional to post-collisional Cenozoic high-K calcalkaline and shoshonitic magmatism documented along the entire Alpine-Himalayan convergence zone, such as in the Tibet (Xu et al., 2002; Hou et al., 2004; Wang et al., 2006; Chung et al., 2009; Jiang et al., 2014; Yang et al., 2016), Turkey (Delph et al., 2017) and Mediterranean area (Duggen et al., 2005), as well as the California Arc (Saleeby et al., 2003; Ducea, 2011).

To conclude, the characteristic incompatible element content, the interelemental fractionation in primitive mantle-normalized diagrams, the Sr-Nd isotopic ratios, as well as the Proterozoic- to Mesozoic-age inherited magmatic zircon of the Mianeh-Hashtroud rocks indicate derivation from mantle sources that strongly interacted with crustal lithologies. A derivation from a mantle source that suffered contamination of heterogeneous subducted components would have resulted in much more variable trace element ratios as well as wider Sr-Nd isotopic ratio spreading. On the other hand, much of the variations observed in the Mianeh-Hashtroud rocks are compatible with fractional crystallization processes, with limited crustal interaction/assimilation.

To sum up, in order to reconcile the large spread of ages of inherited zircons with the relatively homogeneous Sr and Nd isotopic ratios, as well as the similar interelemental fractionation, we propose that the Mesozoic to Neoarchean inherited zircons occasionally found in the Mianeh-Hashtroud rocks were acquired by partial melting of early underplated rocks at the base of the Iran block lithosphere.

## 10. Geodynamic synthesis

The geodynamic framework of the Cenozoic Mianeh-Hashtroud magmatism should be referred to the specific tectonic setting recorded in the Turkish-Caucasus-Iranian collision zone during the Eocene-Miocene time lapse (Fig. 16). In particular, we refer to the transition from the Neotethyan oceanic subduction along the Zagros convergence zone to the continental collision along the Caucasus-Talesh-Alborz zone (Vincent et al., 2005; 2007; Barrier and Vrielynck, 2008; Sosson et al., 2010; Mouthereau et al., 2012; Madanipour et al., 2013; François et al., 2014; Cowgill et al., 2016; FVincent et al., 2016; Rolland, 2017; Barrier et al., 2018; van der Boon et al., 2018). This along-strike change in the geodynamic regime was accommodated by a former transform plate boundary, the Eastern Caucasus-Western Iran Boundary (Barrier and Vrielynck, 2008; Sosson et al., 2010; Rolland, 2017; Barrier et al., 2018; van der Boon et al., 2018), that originally linked the Anatolian subduction systems with the Zagros subduction zone through a major transform plate boundary (Fig. 16a).

The waning stage of the Neotethyan oceanic subduction was associated with volcanic flare-up in the upper-plate domain (Central Iran) during the Eocene, from ~55 to 35 Ma (Verdel et al., 2011). This phase is coeval with the transition from an advancing (Cretaceous-

Paleocene) to a retreating plate margin along the Zagros convergence zone (e.g., Agard et al., 2011; Verdel et al., 2011; Moghadam et al., 2016b; Tadayon et al., 2018). Slab hinge retreat and the associated decompression melting of a passively upwelling subduction component-modified asthenosphere were coupled with lithospheric thinning during the transition from compression to back-arc extension in the overriding plate (Verdel et al., 2011; Castro et al., 2013; Moghadam et al., 2016b). Such circumstances resulted in enhanced melting of the subduction-modified mantle wedge (Prelević et al., 2008; Avanzinelli et al., 2009; Tommasini et al., 2011; Allen et al., 2013b; Di Giuseppe et al., 2018), causing voluminous mafic magma production. Under this geodynamic regime, lateral flow of fertile sub-lithospheric mantle is enhanced in slab windows along the transform boundary toward the mantle wedge region (Faccenna et al., 2005; Rosenbaum et al., 2008; van Hunen and Miller, 2015). The upwelling asthenosphere and the associated melts provided the required thermal conditions for lower crustal melting (mostly at the expenses of the Mesozoic Neotethyan arc root) and continuous addition of mantle-derived melts to the crust (Fig. 16b).

From the late Eocene-Oligocene, the overriding plate experienced renewed shortening causing by the onset of continental collision in the upper plate of the Zagros convergence zone. This new tectonic setting induced shortening and incremental crustal thickening in the upper-plate domain, preconditioning to lithospheric keel foundering and delamination from Oligocene-Miocene onward (Fig. 16c). The continuous passive upwelling of asthenosphere material through the slab windows along the transform boundary caused the transition to the dominantly alkaline, magmatism during the Neogene-Quaternary (Allen et al., 2013b; Chiu et al., 2013; Kaislaniemi et al., 2014; Pang et al., 2014; 2016; Lechmann et al., 2018). The thin lithosphere across the north of this major boundary continues to the Anatolia region (Delph et al., 2017), supporting a scenario of over-thickened lithosphere delamination during the continental collision and the thermal erosion of the lower crust induced by the passive asthenosphere upwelling (Fig. 16d).

It is worth nothing that the zone of long-lived stationary magmatism and associated porphyry mineralisation (i.e. the Lesser Caucasus and the Mianeh-Hashtroud areas), are located in the region where an abrupt change of the lithosphere structure and thickness of Moho depths occurs (Fig. 1b and Fig. 2). In particular, the northward thinning of the lithosphere from ~240 to ~100 km (Priestley et al., 2012), broadly corresponds to a set of orogeny-orthogonal, regional NE-SW strike-slip fault systems (Aras Fault to the north and Mianeh-Ardabil Fault to the south). These systems segment the continuity of the regional NW-SE-striking regional tectonic lineament (Figs. 1 and 2). More importantly, this sharp lithosphere discontinuity is localized along the former transform plate boundary, the Eastern Caucasus-Western Iran Boundary (Barrier and Vrielynck, 2008; Sosson et al., 2010; Rolland, 2017; Barrier et al., 2018; van der Boon et al., 2018), that originally linked the Anatolian subduction systems with the Zagros subduction zone through a major transform plate boundary. Therefore, this sharp and prominent lithospheric discontinuity is supposed to be localized along a pre-existing, lithosphere-scale tectonic boundary that have kinematically accommodated the differential deformation transmitted by the adjacent subduction systems to the overriding plates during Mesozoic and Paleogene times.

The occurrence of long-lived magmatic zones and associated ore deposits along the paleo-tectonic boundary separating the Zagros systems from the Caucasus collisional zone may have significant implications for the localisation of the ore deposits in the region. It is in fact suggested that Mianeh-Ardabil and Aras faults localised along this inherited structural zone and have acted as conduits for prolonged magma ascent to the chamber. In this scenario, the intersection of major orogen-parallel and orogen-orthogonal fault systems provided the favourite locations for development of long-lived magma chambers and consequent ore endowment (e. g., Richards, 2000; Chernicoff et al., 2002)

To sum up, we propose that the long-lived Cenozoic stationary igneous activity of the Lesser Caucasus and Mianeh-Hashtroud districts was dominantly localized along a major inherited lithosphere-scale transform boundary along the Eastern Caucasus-Western Iran Boundary. In such a geodynamic setting, segmentation of the Neotethyan oceanic slab generated asthenospheric melt upwelling into the metasomatised supra-subduction mantle wedge with the potential to activate different mantle and crustal sources. This process is able to generate heterogeneous magmatism (Prelević et al., 2013; Kaislaniemi et al., 2014) such as that distributed along the Caucasus-Iranian collision zone (Allen et al., 2013b; Moritz et al., 2016b; Lechmann et al., 2018). The Eastern Caucasus-Western Iran Boundary is thus considered as a long-lived structure, which acted as a weak zone susceptible to multiple tectonic reactivation, able to focus magmatism as a preferred pathway for magma ascent and emplacement and focused mineralisation.

## 11. Conclusions

The results of the present study can be synthesised as follows:

1) A long-lived (>20 Myr) history of igneous activity occurred in the Mianeh-Hashtroud area, from ~45 to 22 Ma, which culminated with Mo porphyry mineralization at ~33-28 in the Siah-Kamar deposit (Rabiee et al., 2019; Simmonds et al., 2019). The igneous activity resumed during latest Miocene (~6 Ma), with emplacement of lava flows.

2) The whole-rock chemistry of the Cenozoic igneous products of the Mianeh-Hashtroud district is characterized by evolved mildly potassic alkaline terms, with shoshonitic serial affinity, mostly with shoshonite to trachyte and rhyolite (plus the plutonic equivalents) compositions. The incompatible element budget of these samples resembles the composition of magmas emplaced above present-day subduction settings, with overall intra-elemental fractionation patters very close to the global subducting sediments (GloSS) and average upper crustal estimates. The variation of major oxides and trace elements with silica is qualitatively compatible with a process involving amphibole and plagioclase fractionation.

3) The initial Sr-Nd isotopic ratios of the Eocene-Oligocene volcanic and plutonic rocks show relatively narrow variation, not far from the BSE and ChUR estimates. The Miocene hypabyssal and the late Miocene volcanic rocks of the area shows more radiogenic $^{87}Sr/^{86}Sr$ (0.7058-0.7059 and 0.7064, respectively) and relatively low $^{143}Nd/^{144}Nd$ (0.51260-0.51263 and 0.512550, respectively).

4) The results of the present study indicate that collisional-stage magmatism originated from subduction-modified metasomatized mantle lithosphere, in a geodynamic environment dominated by a major transform boundary and flow of fertile mantle material along the slab windows.

5) The Cenozoic stationary, long-lived magmatism and associated mineralisation within the Turkish-Caucasus-Iranian collision zone was structurally controlled by the reactivation of the orogen-orthogonal Eastern Caucasus-Western Iran transform boundary.

## Acknowledgments

This paper is dedicated to the memory of Prof. Jeremy Richards. This research is part of the first Author PhD program at the Roma Tre University. The Grant to Department of Science, Roma Tre University (MIUR-Italy Dipartimenti di Eccellenza, ARTICOLO 1, COMMI 314 – 337 LEGGE 232/2016) is gratefully acknowledged. ML acknowledges Ateneo Sapienza funds (2016-2017-2018). We are indebted to K. Yamamoto for support and providing access to the XRF, ICP-MS and LA-ICP-MS facilities at Nagoya University. The constructive reviews of H. Rezeau and two anonymous reviewers greatly contributed to improve the manuscript.

**APPENDIX A1: Analytical techniques**

**XRF and ICP-MS**

Major elements were measured using the conventional X-ray fluorescence (XRF) technique with a Rigaku ZSX Primus II. Glass beads for the XRF analysis were prepared as follows: 0.50 g of the sample powder was mixed with 5.0 g of lithium tetraborate, and the mixture was melted at 1200 °C for 12–17 min with a high-frequency bead sampler (Rigaku Co. Japan). The loss on ignition (LOI) of the sample was measured from the sample powder weight in a quartz glass beaker in the oven at 950 °C for 5 h.

Regarding inductively coupled plasma mass spectrometry (ICP-MS) analysis, powdered samples were prepared in a two stage decomposition method using $HF+HClO_4$ at high pressure-temperature condition. About 0.1 g of powdered samples were dissolved in a covered Teflon beaker using 2 ml HF (38%) and 0.5–1 ml $HClO_4$ (70%) at 120–140 °C on a hotplate until the powder was dissolved. The dissolved samples were dried at 150 °C on the hotplate with infrared lamps. The dried samples were dissolved in 10 ml of 6 M and the 2.4 M HCl and moved to a PE centrifuge tube. After centrifuging the sample solution, the supernatant was moved to the PTFE beaker, and the residue was moved into a small sealed PTFE vessel. After drying the wet residue on a hotplate, 0.5-0.7 ml of HF (38%) and 0.5 ml of $HClO_4$ (70%) were added. The small sealed PTFE vessel was set in an outer PTFE vessel, and the outer vessel was inserted into a stainless steel jacket. The steel-jacketed PTFE bomb was kept in an oven at 180 °C for 2–3 days to completely dissolve the residual minerals. The second decomposed fraction was dried on a hotplate and dissolved in 6 M and the 2.4 M HCl. This solution was mixed with the supernatant in the PTFE beaker and weighted. The solution was divided into two aliquots at a ratio of 1:9. The first aliquot (10%: Fraction A) was used for the ICP-MS analysis for trace and REEs and the second (90%: Fraction B) was used for the column chemistry to extract Sr and Nd for natural Sr–Nd isotopes. The Fraction A dried on hotplate with IR lamp and then was dissolved in 15 ml 2M $HNO_3$. About 5-10 was used to measure Hf and Ta and the rest of the sample was diluted 10 times more to measure other trace and REE. The concentrations of trace elements, including REEs, were analyzed using ICP-MS device (Agilent 7700x).

Fraction B was loaded to a calibrated cation exchange column (AG50W-X8, 200–400 mesh) using HCl eluent (2.4 and 6 M) to separate Sr. Fraction B2 was then loaded in another specialized calibrated cation exchange column using HIBA eluent (0.2- 0.4 M) to separate Nd.

**Sr-Nd isotope**

To extract Sr and Nd from the samples, routine cation exchange column chemistry methods were followed. Fraction B from the dissolved samples (above section) was loaded to a calibrated cation exchange column (AG50W-X8, 200–400 mesh) using HCl eluent (2.4 and 6 M) to collect Sr and REE fraction. The REE fraction then loaded in another specialized calibrated cation exchange column using HIBA (hydroxyiso butyric acid) eluent (0.2- 0.4 M) to separate Nd fraction. Sr and Nd bearing fractions were dried inside a specially equipped drier and then dissolved in roughly calculated amount of pure water and appropriate amount of dissolved. Sr and Nd samples (~0.1-0.2 μg) then were loaded on Ta single and Re triple filaments with 2 M $H_3PO_4$, respectively. NBS987 and JNdi-1 (Tanaka et al., 2000) were adopted as standards for natural Sr and Nd isotope ratios, respectively. The isotope ratios of Sr and Nd were then measured using a VG Sector 54-30 and GVI IsoProbe Thermal ionization mass spectrometers (TIMS) at Nagoya University. The mass fractionations were corrected for measured Nd and Sr isotope ratios based on $^{143}Nd/^{144}Nd = 0.7219$ and $^{87}Sr/^{86}Sr = 0.1194$, respectively. Averages and 1SE for isotope ratio standards, were $^{143}Nd/^{144}Nd = 0.512115 \pm 0.000080$ (n = 4), and $^{87}Sr/^{86}Sr = 0.7102527 \pm 0.0000095$ (n = 4). Moreover two standard samples of JG-1a (granite) and JA-1 (andesite; (Imai et al., 1995) were used which the result show the analytical errors below 5% for most of the elements and less than 10% for the rest.

**Zircon U-Pb Geochronology**

The zircon U-Pb geochronology study was carried out at the Department of Earth and Environmental Sciences of Nagoya University. Twelve samples were selected for zircon grains separation. About 5 kg (more than 10 kg for volcanic rock samples) for each sample were collected, crushed and the heavy mineral fraction were recovered. Except to monzonitic subvolcanic samples, sufficient zircon grains were available in the case of intrusive and subvolcanic samples but only few zircon grains were found in volcanic samples in which some of them were useless due to the small grain size (<30 μm) or to the strongly fractured crystal structure. Petrographic investigation was devoted to identify the possible presence of inclusions inside zircon grains. Cathodoluminescence (CL) and Back Scatter Electron (BSE) imaging were used first to gather information on the grain texture and internal growth and/or alteration zoning. Zircon grains with intense fracturing and inclusions were avoided. The zircon grains were analyzed by laser ablation inductively coupled plasma mass spectrometry LA-ICP-MS (Agilent 7700XICPMS machine connected with NWR213 (Electro Scientific Industries) laser ablation system (Kouchi et al., 2015). A standard glass (NIST SRM 610) and two zircon standards, named 91500 (1059 Ma, Wiedenbeck et al., 1995) and OD-3 (33.1 Ma, Iwano et al., 2013) were used. Blanks, the zircon standards, and the standard glass were measured at the beginning and ending of each measurement cycle. Eight points were measured in each cycle. The ISOPLOT V4.15 software (Ludwig, 2011) was utilized to calculate the Concordia, statistics and to prepare the age plots. Correction for the common Pb was performed using $^{204}Pb$ intensity (Cox and Wilton, 2006) and value of common Pb was assumed by Stacey and Kramers (1975) model. The results with common Pb values above 20% and Th/U <0.1 were eliminated from calculations. Preferably, Concordia age was calculated for a maximum number of concordant results in a continuous range. Where some results from main population yielded discordant ages, then a Terra-Wasserburg method was used.

The continuous distributed ages (with 2$\sigma$ uncertainty) of measured zircons which lie in an almost normally distributed population are considered as zircons autocrysts from which the age of the sample is calculated (Supplementary Material S4). Zircons possessing ages between sample's age and the oldest Eocene igneous rock are considered as antecrysts. Zircons which show older ages with a significant gap from the oldest sample are xenocrysts or inherited ones (Miller et al., 2007; also see Supplementary Material S4).

## References


Agard, P., Omrani, J., Jolivet, L., Whitechurch, H., Vrielynck, B., Spakman, W., MoniÉ, P., Meyer, B., Wortel, R., 2011. Zagros orogeny: a subduction-dominated process. Geological Magazine 148, 692-725.

Aghazadeh, M., Castro, A., Badrzadeh, Z., Vogt, K., 2011. Post-collisional polycyclic plutonism from the Zagros hinterland: the Shaivar Dagh plutonic complex, Alborz belt, Iran. Geological Magazine 148, 980-1008.

Aghazadeh, M., Castro, A., Omran, N.R., Emami, M.H., Moinvaziri, H., Badrzadeh, Z., 2010. The gabbro (shoshonitic)–monzonite–granodiorite association of Khankandi pluton, Alborz Mountains, NW Iran. Journal of Asian Earth Sciences 38, 199-219.

Aghazadeh, M., Hou, Z., Badrzadeh, Z., Zhou, L., 2015. Temporal–spatial distribution and tectonic setting of porphyry copper deposits in Iran: Constraints from zircon U–Pb and molybdenite Re–Os geochronology. Ore Geology Reviews 70, 385-406.

Agostini, S., Savasçin, M.Y., Di Giuseppe, P., Di Stefano, F., Karaoglu, O., Lustrino, M., Manetti, P., Ersoy, Y., Kurum, S., Onal, A.O., 2019. Neogene volcanism in Elazig-Tunceli area (eastern Anatolia): geochronological and petrological constraints. Italian Journal of Geosciences, in press, https://doi.org/10.3301/IJG.2019.3318.

Alavi, M., 1994. Tectonics of the Zagros orogenic belt of Iran: new data and interpretations. Tectonophysics 229, 211-238.

Allen, M., Jackson, J., Walker, R., 2004. Late Cenozoic reorganization of the Arabia-Eurasia collision and the comparison of short-term and long-term deformation rates. Tectonics 23, TC2008, doi:2010.1029/2003TC001530.

Allen, M., Kheirkhah, M., Neill, I., Emami, M., McLeod, C., 2013a. Generation of arc and within-plate chemical signatures in collision zone magmatism: Quaternary lavas from Kurdistan province, Iran. Journal of Petrology 54, 887-911.

Allen, M., Kheirkhah, M., Neill, I., Emami, M.H., McLeod, C., 2013b. Generation of Arc and Within-plate Chemical Signatures in Collision Zone Magmatism: Quaternary Lavas from Kurdistan Province, Iran.

Allen, M.B., Armstrong, H.A., 2008. Arabia–Eurasia collision and the forcing of mid-Cenozoic global cooling. Palaeogeography, Palaeoclimatology, Palaeoecology 265, 52-58.

Amidi, M., Alavi Tehrani, M., Lotfi, P., Haghipour, A., Sabzehei, M., Behroozi, A., Lescuyer, J., Riou, R., 1987. Geological map of Mianeh. Geological Survey of Iran, Tehran.

Ao, S., Xiao, W., Jafari, M.K., Talebian, M., Chen, L., Wan, B., Ji, W., Zhang, Z., 2016. U–Pb zircon ages, field geology and geochemistry of the Kermanshah ophiolite (Iran): From continental rifting at 79 Ma to oceanic core complex at ca. 36 Ma in the southern Neo-Tethys. Gondwana Research 31, 305-318.

Ashrafi, N., Jahangiri, A., Hasebe, N., Eby, G.N., 2018. Petrology, geochemistry and geodynamic setting of Eocene-Oligocene alkaline intrusions from the Alborz-Azerbaijan magmatic belt, NW Iran. Geochemistry 78, 432-461.

Avagyan, A., Sosson, M., Karakhanian, A., Philip, H., Rebai, S., Rolland, Y., Melkonyan, R., Davtyan, V., 2010. Recent tectonic stress evolution in the Lesser Caucasus and adjacent regions. Geological Society, London, Special Publications 340, 393.

Avagyan, A., Sosson, M., Philip, H., Karakhanian, A., Rolland, Y., Melkonyan, R., Rebaï, S., Davtyan, V., 2005. Neogene to Quaternary stress field evolution in Lesser Caucasus and adjacent regions using fault kinematics analysis and volcanic cluster data. Geodinamica Acta 18, 401-416.

Avanzinelli, R., Lustrino, M., Mattei, M., Melluso, L., Conticelli, S., 2009. Potassic and ultrapotassic magmatism in the circum-Tyrrhenian region: Significance of carbonated pelitic vs. pelitic sediment recycling at destructive plate margins. Lithos 113, 213-227.

Axen, G.J., Lam, P.S., Grove, M., Stockli, D.F., Hassanzadeh, J., 2001. Exhumation of the west-central Alborz Mountains, Iran, Caspian subsidence, and collision-related tectonics. Geology 29, 559-562.

Azizi, H., Asahara, Y., 2013. Juvenile granite in the Sanandaj–Sirjan Zone, NW Iran: Late Jurassic–Early Cretaceous arc–continent collision. International Geology Review 55, 1523-1540.

Azizi, H., Asahara, Y., Mehrabi, B., Chung, S.L., 2011. Geochronological and geochemical constraints on the petrogenesis of high-K granite from the Suffi abad area, Sanandaj-Sirjan Zone, NW Iran. Chemie der Erde - Geochemistry 71, 363-376.

Azizi, H., Hadad, S., Stern, R.J., Asahara, Y., 2018a. Age, geochemistry, and emplacement of the ~40-Ma Baneh granite–appinite complex in a transpressional tectonic regime, Zagros suture zone, northwest Iran. International Geology Review 61, 95-223.

Azizi, H., Lucci, F., Stern, R.J., Hasannejad, S., Asahara, Y., 2018b. The Late Jurassic Panjeh submarine volcano in the northern Sanandaj-Sirjan Zone, northwest Iran: Mantle plume or active margin? Lithos 308-309, 364-380.

Azizi, H., Moinevaziri, H., 2009. Review of the tectonic setting of Cretaceous to Quaternary volcanism in northwestern Iran. Journal of Geodynamics 47, 167-179.

Ballato, P., Cifelli, F., Heidarzadeh, G., Ghassemi, M.R., Wickert, A.D., Hassanzadeh, J., Dupont-Nivet, G., Balling, P., Sudo, M., Zeilinger, G., 2017. Tectono-sedimentary evolution of the northern Iranian Plateau: insights from middle–late Miocene foreland-basin deposits. Basin Research 29, 417-446.

Ballato, P., Nowaczyk, N.R., Landgraf, A., Strecker, M.R., Friedrich, A., Tabatabaei, S.H., 2008. Tectonic control on sedimentary facies pattern and sediment accumulation rates in the Miocene foreland basin of the southern Alborz mountains, northern Iran. Tectonics 27, TC6001, doi:6010.1029/2008TC002278.

Ballato, P., Uba, C.E., Landgraf, A., Strecker, M.R., Sudo, M., Stockli, D.F., Friedrich, A., Tabatabaei, S.H., 2011. Arabia-Eurasia continental collision: Insights from late Tertiary foreland-basin evolution in the Alborz Mountains, northern Iran. Bulletin 123, 106-131.

Barrier, E., Vrielynck, B., 2008. Palaeotectonic maps of the Middle East. Atlas of 14.

Barrier, E., Vrielynck, B., Brouillet, J., Brunet, M., 2018. Paleotectonic Reconstruction of the Central Tethyan Realm. Tectonono-Sedimentary-Palinspastic maps from Late Permian to Pliocene. CCGM/CGMW, Paris. CCGM/CGMW Paris: France.

Bavali, K., Motaghi, K., Sobouti, F., Ghods, A., Abbasi, M., Priestley, K., Mortezanejad, G., Rezaeian, M., 2016. Lithospheric structure beneath NW Iran using regional and teleseismic travel-time tomography. Physics of the Earth and Planetary Interiors 253, 97-107.

Bea, F., Mazhari, A., Montero, P., Amini, S., Ghalamghash, J., 2011. Zircon dating, Sr and Nd isotopes, and element geochemistry of the Khalifan pluton, NW Iran: Evidence for Variscan magmatism in a supposedly Cimmerian superterrane. Journal of Asian Earth Sciences 40, 172-179.

Berberian, F., Berberian, M., 1981. Tectono-plutonic episodes in Iran. Zagros Hindu Kush Himalaya Geodynamic Evolution 3, 5-32.

Berberian, M., Arshadi, S., 1976. On the evidence of the youngest activity of the North Tabriz Fault and the seismicity of Tabriz City, pp. 397-418.

Berberian, M., King, G., 1981. Towards a paleogeography and tectonic evolution of Iran. Canadian Journal of Earth Sciences 18, 210-265.

Bird, P., 1979. Continental delamination and the Colorado Plateau. Journal of Geophysical Research: Solid Earth 84, 7561-7571.

Castro, A., Aghazadeh, M., Badrzadeh, Z., Chichorro, M., 2013. Late Eocene–Oligocene post-collisional monzonitic intrusions from the Alborz magmatic belt, NW Iran. An example of monzonite magma generation from a metasomatized mantle source. Lithos 180-181, 109-127.

Cavazza, W., Albino, I., Galoyan, G., Zattin, M., Cattò, S., 2019. Continental accretion and incremental deformation in the thermochronologic evolution of the Lesser Caucasus. Geoscience Frontiers 10, 2189-2202.

Cavazza, W., Albino, I., Zattin, M., Galoyan, G., Imamverdiyev, N., Melkonyan, R., 2015. Thermochronometric evidence for Miocene tectonic reactivation of the Sevan-Akera suture zone (Lesser Caucasus): A far-field tectonic effect of the Arabia-Eurasia collision?

Cavazza, W., Cattò, S., Zattin, M., Okay, A.I., Reiners, P., 2018. Thermochronology of the Miocene Arabia-Eurasia collision zone of southeastern Turkey. Geosphere 14, 2277-2293.

Chernicoff, C.J., Richards, J.P., Zappettini, E.O., 2002. Crustal lineament control on magmatism and mineralization in northwestern Argentina: geological, geophysical, and remote sensing evidence. Ore Geology Reviews 21, 127-155.

Chiu, H.-Y., Chung, S.-L., Zarrinkoub, M.H., Melkonyan, R., Pang, K.-N., Lee, H.-Y., Wang, K.-L., Mohammadi, S.S., Khatib, M.M., 2017. Zircon Hf isotopic constraints on magmatic and tectonic evolution in Iran: Implications for crustal growth in the Tethyan orogenic belt. Journal of Asian Earth Sciences 145, 652-669.

Chiu, H.-Y., Chung, S.-L., Zarrinkoub, M.H., Mohammadi, S.S., Khatib, M.M., Iizuka, Y., 2013. Zircon U–Pb age constraints from Iran on the magmatic evolution related to Neotethyan subduction and Zagros orogeny. Lithos 162, 70-87.

Chung, S.-L., Chu, M.-F., Ji, J., O'Reilly, S.Y., Pearson, N.J., Liu, D., Lee, T.-Y., Lo, C.-H., 2009. The nature and timing of crustal thickening in Southern Tibet: Geochemical and zircon Hf isotopic constraints from postcollisional adakites. Tectonophysics 477, 36-48.

Copley, A., Jackson, J., 2006. Active tectonics of the Turkish-Iranian Plateau. Tectonics 25, TC6006, doi:6010.1029/2005TC001906.

Corfu, F., Hanchar, J.M., Hoskin, P.W.O., Kinny, P., 2003. Atlas of Zircon Textures. Reviews in Mineralogy and Geochemistry 53, 469-500.

Cowgill, E., Forte, A.M., Niemi, N., Avdeev, B., Tye, A., Trexler, C., Javakhishvili, Z., Elashvili, M., Godoladze, T., 2016. Relict basin closure and crustal shortening budgets during continental collision: An example from Caucasus sediment provenance. Tectonics 35, 2918-2947.

Cox, R.A., Wilton, D.H., 2006. U–Pb dating of perovskite by LA-ICP-MS: an example from the Oka carbonatite, Quebec, Canada. Chemical Geology 235, 21-32.

Daliran, F., 2007. The carbonate rock-hosted epithermal gold deposit of Agdarreh, Takab geothermal field, NW Iran—hydrothermal alteration and mineralisation. Mineralium Deposita 43, 383-404.

Daliran, F., Pride, K., Walther, J., Berner, Z.A., Bakker, R.J., 2013. The Angouran Zn (Pb) deposit, NW Iran: Evidence for a two stage, hypogene zinc sulfide–zinc carbonate mineralization. Ore Geology Reviews 53, 373-402.

Dargahi, S., Arvin, M., Pan, Y., Babaei, A., 2010. Petrogenesis of post-collisional A-type granitoids from the Urumieh–Dokhtar magmatic assemblage, Southwestern Kerman, Iran: Constraints on the Arabian–Eurasian continental collision. Lithos 115, 190-204.

Davidson, J., Turner, S., Handley, H., Macpherson, C., Dosseto, A., 2007. Amphibole “sponge” in arc crust? Geology 35, 787-790.

Davidson, J., Turner, S., Plank, T., 2013. Dy/Dy*: Variations Arising from Mantle Sources and Petrogenetic Processes. Journal of Petrology 54, 525-537.

DeCelles, P.G., Ducea, M.N., Kapp, P., Zandt, G., 2009. Cyclicity in Cordilleran orogenic systems. Nature Geoscience 2, 251-257.

Defant, M.J., Drummond, M.S., 1990. Derivation of some modern arc magmas by melting of young subducted lithosphere. Nature 347, 662-665.

Delph, J., Abgarmi, B., M. Ward, K., Beck, S., Özacar, A., Zandt, G., Sandvol, E., Turkelli, N., Kalafat, D., 2017. The effects of subduction termination on the continental lithosphere: Linking volcanism, deformation, surface uplift, and slab tearing in central Anatolia.

Dessimoz, M., Müntener, O., Ulmer, P., 2012. A case for hornblende dominated fractionation of arc magmas: the Chelan Complex (Washington Cascades). Contributions to Mineralogy and Petrology 163, 567-589.

Dewey, J.F., Pitman, W.C., III, Ryan, W.B.F., Bonnin, J., 1973. Plate Tectonics and the Evolution of the Alpine System. GSA Bulletin 84, 3137-3180.

Di Giuseppe, P., Agostini, S., Lustrino, M., Karaoğlu, Ö., Savaşçın, M.Y., Manetti, P., Ersoy, Y., 2017. Transition from compression to strike-slip tectonics revealed by Miocene–Pleistocene volcanism west of the Karlıova triple junction (East Anatolia). Journal of Petrology 58, 2055-2087.

Di Giuseppe, P., Agostini, S., Manetti, P., Savaşçın, M.Y., Conticelli, S., 2018. Sub-lithospheric origin of Na-alkaline and calc-alkaline magmas in a post-collisional tectonic regime: Sr-Nd-Pb isotopes in recent monogenetic volcanism of Cappadocia, Central Turkey. Lithos 316-317, 304-322.

Dilek, Y., Altunkaynak, Ş., 2009. Geochemical and temporal evolution of Cenozoic magmatism in western Turkey: mantle response to collision, slab break-off, and lithospheric tearing in an orogenic belt. Geological Society, London, Special Publications 311, 213-233.

Dilek, Y., Imamverdiyev, N., Altunkaynak, Ş., 2010. Geochemistry and tectonics of Cenozoic volcanism in the Lesser Caucasus (Azerbaijan) and the peri-Arabian region: collision-induced mantle dynamics and its magmatic fingerprint. International Geology Review 52, 536-578.

Djamour, Y., Vernant, P., Nankali, H.R., Tavakoli, F., 2011. NW Iran-eastern Turkey present-day kinematics: results from the Iranian permanent GPS network. Earth and Planetary Science Letters 307, 27-34.

Ducea, M.N., 2011. Fingerprinting orogenic delamination. Geology 39, 191-192.

Duggen, S., Hoernle, K., van den Bogaard, P., Garbe-Schönberg, D., 2005. Post-collisional transition from subduction-to intraplate-type magmatism in the westernmost Mediterranean: evidence for continental-edge delamination of subcontinental lithosphere. Journal of Petrology 46, 1155-1201.

Elburg, M.A., van Bergen, M., Hoogewerff, J., Foden, J., Vroon, P., Zulkarnain, I., Nasution, A., 2002. Geochemical trends across an arc-continent collision zone: magma sources and slab-wedge transfer processes below the Pantar Strait volcanoes, Indonesia. Geochimica et Cosmochimica Acta 66, 2771-2789.

Eskandari, A., Deevsalar, R., De Rosa, R., Shinjo, R., Donato, P., Neill, I., 2020. Geochemical and isotopic constraints on the evolution of magma plumbing system at Damavand Volcano, N Iran. Lithos 354-355, 105274.

Faccenna, C., Civetta, L., D'Antonio, M., Funiciello, F., Margheriti, L., Piromallo, C., 2005. Constraints on mantle circulation around the deforming Calabrian slab. Geophysical Research Letters 32, L06311, doi:06310.01029/02004GL021874.

Faccenna, C., Funiciello, F., Civetta, L., D'Antonio, M., Moroni, M., Piromallo, C., 2007. Slab disruption, mantle circulation, and the opening of the Tyrrhenian basins.

François, T., Burov, E., Agard, P., Meyer, B., 2014. Buildup of a dynamically supported orogenic plateau: Numerical modeling of the Zagros/Central Iran case study. Geochemistry, Geophysics, Geosystems 15, 2632-2654.

Gavillot, Y., Axen, G.J., Stockli, D.F., Horton, B.K., Fakhari, M.D., 2010. Timing of thrust activity in the High Zagros fold-thrust belt, Iran, from (U-Th)/He thermochronometry. Tectonics 29, TC4025,doi:4010.1029/2009TC002484.

Ghalamghash, J., Mousavi, S.Z., Hassanzadeh, J., Schmitt, A.K., 2016. Geology, zircon geochronology, and petrogenesis of Sabalan volcano (northwestern Iran). Journal of Volcanology and Geothermal Research 327, 192-207.

Ghalamghash, J., Schmitt, A., Chaharlang, R., 2019. Age and compositional evolution of Sahand volcano in the context of post-collisional magmatism in northwestern Iran: Evidence for time-transgressive magmatism away from the collisional suture. Lithos 344, 265-279.

Gilg, H.A., Boni, M., Balassone, G., Allen, C.R., Banks, D., Moore, F., 2006. Marble-hosted sulfide ores in the Angouran Zn-(Pb–Ag) deposit, NW Iran: interaction of sedimentary brines with a metamorphic core complex. Mineralium Deposita 41, 1-16.

Göğüş, O., Pysklywec, R., 2008. Mantle lithosphere delamination driving plateau uplift and synconvergent extension in Eastern Anatolia. Geology 36, 723-726.

Guest, B., Stockli, D.F., Grove, M., Axen, G.J., Lam, P.S., Hassanzadeh, J., 2006. Thermal histories from the central Alborz Mountains, northern Iran: implications for the spatial and temporal distribution of deformation in northern Iran. Geological Society of America Bulletin 118, 1507-1521.

Guo, Z., Wilson, M., Liu, J., Mao, Q., 2006. Post-collisional, Potassic and Ultrapotassic Magmatism of the Northern Tibetan Plateau: Constraints on Characteristics of the Mantle Source, Geodynamic Setting and Uplift Mechanisms. Journal of Petrology 47, 1177-1220.

Hacker, B.R., Kelemen, P.B., Behn, M.D., 2015. Continental Lower Crust. Annual Review of Earth and Planetary Sciences 43, 167-205.

Harris, N.B.W., Pearce, J.A., Tindle, A.G., 1986. Geochemical characteristics of collision-zone magmatism. Geological Society, London, Special Publications 19, 67-81.

Hässig, M., Rolland, Y., Sosson, M., Galoyan, G., Sahakyan, L., Topuz, G., Çelik, Ö.F., Avagyan, A., Müller, C., 2013. Linking the NE Anatolian and Lesser Caucasus ophiolites: evidence for large-scale obduction of oceanic crust and implications for the formation of the Lesser Caucasus-Pontides Arc. Geodinamica Acta 26, 311-330.

Hastie, A.R., Kerr, A.C., Pearce, J.A., Mitchell, S.F., 2007. Classification of Altered Volcanic Island Arc Rocks using Immobile Trace Elements: Development of the Th–Co Discrimination Diagram. Journal of Petrology 48, 2341-2357.

Hawkesworth, C.J., Turner, S.P., McDermott, F., Peate, D.W., van Calsteren, P., 1997. U-Th Isotopes in Arc Magmas: Implications for Element Transfer from the Subducted Crust. Science 276, 551.

Heidari, S.M., Daliran, F., Paquette, J.-L., Gasquet, D., 2015. Geology, timing, and genesis of the high sulfidation Au (–Cu) deposit of Touzlar, NW Iran. Ore Geology Reviews 65, 460-486.

Hessami, K., Koyi, H.A., Talbot, C.J., Tabasi, H., Shabanian, E., 2001. Progressive unconformities within an evolving foreland fold–thrust belt, Zagros Mountains. Journal of the Geological Society 158, 969-981.

Homke, S., Vergés, J., Van Der Beek, P., Fernàndez, M., Saura, E., Barbero, L., Badics, B., Labrin, E., 2010. Insights in the exhumation history of the NW Zagros from bedrock and detrital apatite fission-track analysis: evidence for a long-lived orogeny. Basin Research 22, 659-680.

Honarmand, M., Xiao, W., Nabatian, G., Blades, M.L., dos Santos, M.C., Collins, A.S., Ao, S., 2018. Zircon U-Pb-Hf isotopes, bulk-rock geochemistry and Sr-Nd-Pb isotopes from late Neoproterozoic basement in the Mahneshan area, NW Iran: Implications for Ediacaran active continental margin along the northern Gondwana and constraints on the late Oligocene crustal anatexis. Gondwana Research 57, 48-76.

Hou, Z.Q., Gao, Y.F., Qu, X.M., Rui, Z.Y., Mo, X.X., 2004. Origin of adakitic intrusives generated during mid-Miocene east–west extension in southern Tibet. Earth and Planetary Science Letters 220, 139-155.

Houseman, G.A., McKenzie, D.P., Molnar, P., 1981. Convective instability of a thickened boundary layer and its relevance for the thermal evolution of continental convergent belts. Journal of Geophysical Research: Solid Earth 86, 6115-6132.

Hubner, H., 1969. Geological map of Iran. National Iranian Oil Company, Tehran.

Imai, N., Terashima, S., Itoh, S., Ando, A., 1995. 1994 compilation values for GSJ reference samples,“Igneous rock series”. Geochemical Journal 29, 91-95.

Iwano, H., Orihashi, Y., Hirata, T., Ogasawara, M., Danhara, T., Horie, K., Hasebe, N., Sueoka, S., Tamura, A., Hayasaka, Y., 2013. An inter-laboratory evaluation of OD-3 zircon for use as a secondary U–Pb dating standard. Island Arc 22, 382-394.

Jackson, J., 1992. Partionning of strike-slip and convergent motion between Eurasia and Arabia in Eastern Turkey and the Caucasus. Journal of Geophysical Research 971, 12471-12479.

Jackson, J., Haines, J., Holt, W., 1995. The accommodation of Arabia-Eurasia plate convergence in Iran. Journal of Geophysical Research: Solid Earth 100, 15205-15219.

Jackson, J., McKenzie, D., 1984. Active tectonics of the Alpine—Himalayan Belt between western Turkey and Pakistan. Geophysical Journal International 77, 185-264.

Jackson, J., McKenzie, D., 1988. The relationship between plate motions and seismic moment tensors, and the rates of active deformation in the Mediterranean and Middle East. Geophysical Journal International 93, 45-73.

Jagoutz, O., Klein, B., 2018. On the importance of crystallization-differentiation for the generation of $SiO_2$-rich melts and the compositional build-up of arc (and continental) crust. American Journal of Science 318, 29-63.

Jiang, Z.-Q., Wang, Q., Wyman, D.A., Li, Z.-X., Yang, J.-H., Shi, X.-B., Ma, L., Tang, G.-J., Gou, G.-N., Jia, X.-H., Guo, H.-F., 2014. Transition from oceanic to continental lithosphere subduction in southern Tibet: Evidence from the Late Cretaceous–Early

Oligocene (~91–30Ma) intrusive rocks in the Chanang–Zedong area, southern Gangdese. Lithos 196-197, 213-231.
Jull, M., Kelemen, P.B., 2001. On the conditions for lower crustal convective instability. Journal of Geophysical Research: Solid Earth 106, 6423-6446.
Kaislaniemi, L., Van Hunen, J., Allen, M., Neill, I., 2014. Sublithospheric small-scale convection—a mechanism for collision zone magmatism. Geology 42, 291-294.
Keskin, M., 2003. Magma generation by slab steepening and breakoff beneath a subduction-accretion complex: An alternative model for collision-related volcanism in Eastern Anatolia, Turkey. Geophysical Research Letters 30, 8046, doi:8010.1029/2003GL018019.
Keskin, M., Pearce, J., Kempton, P., Greenwood, 2006. Magma-crust interactions and magma plumbing in a post-collision setting: geochemical evidence from the Erzurum-Kars Plateau, Eastern Turkey. In: Dilek,Y. and Pavlides, S. (eds) Postcollisional tectonics and magmatism in the Mediterranean region and Asia. Special Paper of the Geological Society of America 409, 475-505.
Kessel, R., Schmidt, M.W., Ulmer, P., Pettke, T., 2005. Trace element signature of subduction-zone fluids, melts and supercritical liquids at 120–180 km depth. Nature 437, 724.
Keto, L.S., Jacobsen, S.B., 1987. Nd and Sr isotopic variations of Early Paleozoic oceans. Earth and Planetary Science Letters 84, 27-41.
Khadivi, S., Mouthereau, F., Larrasoaña, J., Vergés, J., Lacombe, O., Khademi, E., Beamud, E., Melinte-Dobrinescu, M., Suc, J.-P., 2010. Magnetochronology of synorogenic Miocene foreland sediments in the Fars arc of the Zagros Folded Belt (SW Iran). Basin Research 22, 918-932.
Khaleghi, F., Hosseinzadeh, G., Rasa, I., Moayyed, M., 2013. Geological and Geochemical Characteristics of the Syah Kamar Porphyry Molybdenum Deposit , West of Mianeh , NW Iran. ULUM-I ZAMIN 88, 187-196.
Kheirkhah, M., Allen, M., Emami, M.H., 2009. Quaternary syn-collision magmatism from the Iran/Turkey borderlands. Journal of Volcanology and Geothermal Research 182, 1-12.
Kheirkhah, M., Neill, I., Allen, M.B., Ajdari, K., 2013. Small-volume melts of lithospheric mantle during continental collision: Late Cenozoic lavas of Mahabad, NW Iran. Journal of Asian Earth Sciences 74, 37-49.
Khodabandeh, A.A., Amini Azar, R., Faridi, M., 1999. Geological map of the Mianeh quadrangle. Geological Survey of Iran and Mining Exploration, Tehran.
Kimura, J.-I., 2017. Modeling chemical geodynamics of subduction zones using the Arc Basalt Simulator version 5. Geosphere 13, 992-1025.
Kirkland, C., Smithies, R., Taylor, R., Evans, N., McDonald, B., 2015. Zircon Th/U ratios in magmatic environs. Lithos 212, 397-414.
Klein, M., Stosch, H.G., Seck, H.A., 1997. Partitioning of high field-strength and rare-earth elements between amphibole and quartz-dioritic to tonalitic melts: an experimental study. Chemical Geology 138, 257-271.
Köksal, S., Romer, R.L., Göncüoglu, M.C., Toksoy-Köksal, F., 2004. Timing of post-collisional H-type to A-type granitic magmatism: U–Pb titanite ages from the Alpine central Anatolian granitoids (Turkey). International Journal of Earth Sciences 93, 974-989.
Koshnaw, R.I., Stockli, D.F., Schlunegger, F., 2018. Timing of the Arabia-Eurasia continental collision—Evidence from detrital zircon U-Pb geochronology of the Red Bed Series strata of the northwest Zagros hinterland, Kurdistan region of Iraq. Geology 47, 47-50.
Kouchi, Y., Obara, H., Fujimoto, T., Orihashi, Y., Haruta, Y., Yamamoto, K., 2015. Zircon U–Pb dating by 213 nm Nd. YAG laser ablation inductively coupled plasma mass spectrometry. Optimization of the analytical condition to use NIST SRM 610 for Pb/U fractionation correction. Chikyu Kagaku 49, 19-35.
Le Maitre, R.W., Streckeisen, A., Zanettin, B., Le Bas, M., Bonin, B., Bateman, P., 2005. Igneous rocks: a classification and glossary of terms: recommendations of the

International Union of Geological Sciences Subcommission on the Systematics of Igneous Rocks. Cambridge University Press.
Lechmann, A., Burg, J.-P., Ulmer, P., Guillong, M., Faridi, M., 2018. Metasomatized mantle as the source of Mid-Miocene-Quaternary volcanism in NW-Iranian Azerbaijan: Geochronological and geochemical evidence. Lithos 304-307, 311-328.
Li, J.-W., Zhao, X.-F., Zhou, M.-F., Ma, C.-Q., de Souza, Z.S., Vasconcelos, P., 2009. Late Mesozoic magmatism from the Daye region, eastern China: U–Pb ages, petrogenesis, and geodynamic implications. Contributions to Mineralogy and Petrology 157, 383-409.
Ludwig, K., 2011. Isoplot v. 4.15: A Geochronological Toolkit for Microsoft Excel. Berkeley Geochronology Center Special Publication 4, 75.
Lustrino, M., 2005. How the delamination and detachment of lower crust can influence basaltic magmatism. Earth-Science Reviews 72, 21-38.
Lustrino, M., Abbas, H., Agostini, S., Caggiati, M., Carminati, E., Gianolla, P., 2019a. Origin of Triassic magmatism of the Southern Alps (Italy): constraints from geochemistry and Sr-Nd-Pb isotopic ratios. Gondwana Research 75, 218-238.
Lustrino, M., Duggen, S., Rosenberg, C.L., 2011. The Central-Western Mediterranean: Anomalous igneous activity in an anomalous collisional tectonic setting. Earth-Science Reviews 104, 1-40.
Lustrino, M., Fedele, L., Agostini, S., Prelević, D., Salari, G., 2019b. Leucitites within and around the Mediterranean area. Lithos 324, 216-233.
Lustrino, M., Marrazzo, M., Melluso, L., Tassinari, C.C., Brotzu, P., Gomes, C.B., Morbidelli, L., Ruberti, E., 2010. Petrogenesis of Early Cretaceous silicic volcanism in SE Uruguay: The role of mantle and crustal sources. Geochemical Journal 44, 1-22.
Lustrino, M., Wilson, M., 2007. The circum-Mediterranean anorogenic Cenozoic igneous province. Earth-Science Reviews 81, 1-65.
Lyubetskaya, T., Korenaga, J., 2007. Chemical composition of Earth's primitive mantle and its variance: 1. Method and results. Journal of Geophysical Research: Solid Earth 112.
Macpherson, C.G., Dreher, S.T., Thirlwall, M.F., 2006. Adakites without slab melting: High pressure differentiation of island arc magma, Mindanao, the Philippines. Earth and Planetary Science Letters 243, 581-593.
Madanipour, S., Ehlers, T.A., Yassaghi, A., Rezaeian, M., Enkelmann, E., Bahroudi, A., 2013. Synchronous deformation on orogenic plateau margins: Insights from the Arabia–Eurasia collision. Tectonophysics 608, 440-451.
Mahmoudi, S., Corfu, F., Masoudi, F., Mehrabi, B., Mohajjel, M., 2011. U–Pb dating and emplacement history of granitoid plutons in the northern Sanandaj–Sirjan Zone, Iran. Journal of Asian Earth Sciences 41, 238-249.
Mazhari, S.A., Amini, S., Ghalamghash, J., Bea, F., 2009a. Petrogenesis of granitic unit of Naqadeh complex, Sanandaj–Sirjan Zone, NW Iran. Arabian Journal of Geosciences 4, 59-67.
Mazhari, S.A., Amini, S., Ghalamghash, J., Bea, F., 2010. The origin of mafic rocks in the Naqadeh intrusive complex, Sanandaj-Sirjan Zone, NW Iran. Arabian Journal of Geosciences 4, 1207-1214.
Mazhari, S.A., Bea, F., Amini, S., Ghalamghash, J., Molina, J.F., Montero, P., Scarrow, J.H., Williams, I.S., 2009b. The Eocene bimodal Piranshahr massif of the Sanandaj-Sirjan Zone, NW Iran: a marker of the end of the collision in the Zagros orogen. Journal of the Geological Society 166, 53-69.
Mazhari, S.A., Hajalilou, B., Bea, F., 2012. Evaluation of Syenite as Feldspar Source: Piranshahr Pluton, NW of Iran. Natural Resources Research 21, 279-283.
McKenzie, D., 1972. Active Tectonics of the Mediterranean Region. Geophysical Journal International 30, 109-185.
McQuarrie, N., Stock, J.M., Verdel, C., Wernicke, B.P., 2003. Cenozoic evolution of Neotethys and implications for the causes of plate motions. Geophysical Research Letters 30, 2036, doi:2010.1029/2003GL017992.

McQuarrie, N., van Hinsbergen, D.J., 2013. Retrodeforming the Arabia-Eurasia collision zone: Age of collision versus magnitude of continental subduction. Geology 41, 315-318.

Mederer, J., Moritz, R., Ulianov, A., Chiaradia, M., 2013. Middle Jurassic to Cenozoic evolution of arc magmatism during Neotethys subduction and arc-continent collision in the Kapan Zone, southern Armenia. Lithos 177, 61-78.

Mehrabi, B., Yardley, B., Cann, J., 1999. Sediment-hosted disseminated gold mineralisation at Zarshuran, NW Iran. Mineralium Deposita 34, 673-696.

Meijers, M.J.M., Smith, B., Pastor-Galán, D., Degenaar, R., Sadradze, N., Adamia, S., Sahakyan, L., Avagyan, A., Sosson, M., Rolland, Y., Langereis, C.G., Müller, C., 2017. Progressive orocline formation in the Eastern Pontides–Lesser Caucasus. Geological Society, London, Special Publications 428, 117-143.

Middlemost, E.A., 1994. Naming materials in the magma/igneous rock system. Earth-Science Reviews 37, 215-224.

Miller, J.S., Matzel, J.E.P., Miller, C.F., Burgess, S.D., Miller, R.B., 2007. Zircon growth and recycling during the assembly of large, composite arc plutons. Journal of Volcanology and Geothermal Research 167, 282-299.

Moghadam, H.S., Ghorbani, G., Khedr, M.Z., Fazlnia, N., Chiaradia, M., Eyuboglu, Y., Santosh, M., Francisco, C.G., Martinez, M.L., Gourgaud, A., 2014. Late Miocene K-rich volcanism in the Eslamieh Peninsula (Saray), NW Iran: implications for geodynamic evolution of the Turkish–Iranian High Plateau. Gondwana Research 26, 1028-1050.

Moghadam, H.S., Li, X.-H., Stern, R.J., Ghorbani, G., Bakhshizad, F., 2016a. Zircon U–Pb ages and Hf–O isotopic composition of migmatites from the Zanjan–Takab complex, NW Iran: Constraints on partial melting of metasediments. Lithos 240-243, 34-48.

Moghadam, H.S., Rossetti, F., Lucci, F., Chiaradia, M., Gerdes, A., Martinez, M.L., Ghorbani, G., Nasrabady, M., 2016b. The calc-alkaline and adakitic volcanism of the Sabzevar structural zone (NE Iran): implications for the Eocene magmatic flare-up in Central Iran. Lithos 248, 517-535.

Moradi, A.S., Hatzfeld, D., Tatar, M., 2011. Microseismicity and seismotectonics of the North Tabriz fault (Iran). Tectonophysics 506, 22-30.

Moradi, R., Boomeri, M., Bagheri, S., Nakashima, K., 2016. Mineral chemistry of igneous rocks in the Lar Cu-Mo prospect, southeastern part of Iran: implications for P, T, and $fO_2$. Turkish Journal of Earth Sciences 25, 418-433.

Moritz, R., Melkonyan, R., Selby, D., Popkhadze, N., Gugushvili, V., Tayan, R., Ramazanov, V., 2016a. Metallogeny of the Lesser Caucasus: from arc construction to post-collision evolution, Special publications of the Society of Economic Geologists. Society of Economic Geologists, pp. 157-192.

Moritz, R., Rezeau, H., Ovtcharova, M., Tayan, R., Melkonyan, R., Hovakimyan, S., Ramazanov, V., Selby, D., Ulianov, A., Chiaradia, M., 2016b. Long-lived, stationary magmatism and pulsed porphyry systems during Tethyan subduction to post-collision evolution in the southernmost Lesser Caucasus, Armenia and Nakhitchevan. Gondwana Research 37, 465-503.

Morley, C.K., Kongwung, B., Julapour, A.A., Abdolghafourian, M., Hajian, M., Waples, D., Warren, J., Otterdoom, H., Srisuriyon, K., Kazemi, H., 2009. Structural development of a major late Cenozoic basin and transpressional belt in central Iran: The Central Basin in the Qom-Saveh area. Geosphere 5, 325-362.

Mouthereau, F., Lacombe, O., Vergés, J., 2012. Building the Zagros collisional orogen: Timing, strain distribution and the dynamics of Arabia/Eurasia plate convergence. Tectonophysics 532-535, 27-60.

Mouthereau, F., Tensi, J., Bellahsen, N., Lacombe, O., De Boisgrollier, T., Kargar, S., 2007. Tertiary sequence of deformation in a thin-skinned/thick-skinned collision belt: The Zagros Folded Belt (Fars, Iran). Tectonics 26, TC5006, doi:5010.1029/2007TC002098.

Moyen, J.-F., 2009. High Sr/Y and La/Yb ratios: The meaning of the “adakitic signature”. Lithos 112, 556-574.

Nabatian, G., Ghaderi, M., Neubauer, F., Honarmand, M., Liu, X., Dong, Y., Jiang, S.-Y., von Quadt, A., Bernroider, M., 2014. Petrogenesis of Tarom high-potassic granitoids in the Alborz–Azarbaijan belt, Iran: Geochemical, U–Pb zircon and Sr–Nd–Pb isotopic constraints. Lithos 184-187, 324-345.

Nabatian, G., Jiang, S.-Y., Honarmand, M., Neubauer, F., 2016. Zircon U–Pb ages, geochemical and Sr–Nd–Pb–Hf isotopic constraints on petrogenesis of the Tarom-Olya pluton, Alborz magmatic belt, NW Iran. Lithos 244, 43-58.

Nabatian, G., Wan, B., Honarmand, M., 2017. Whole rock geochemistry, molybdenite Re-Os geochronology, stable isotope and fluid inclusion investigations of the Siah-Kamar deposit, western Alborz-Azarbayjan: New constrains on the porphyry Mo deposit in Iran. Ore Geology Reviews 91, 638-659.

Naumenko-Dèzes, M.O., Rolland, Y., Lamarque, G., Duclaux, G., Gallet, S., Bascou, J., Ménot, R.P., 2020. Petrochronology of the Terre Adélie Craton (East Antarctica) evidences a long-lasting Proterozoic (1.7–1.5 Ga) tectono-metamorphic evolution — Insights for the connections with the Gawler Craton and Laurentia. Gondwana Research 81, 21-57.

Neill, I., Meliksetian, K., Allen, M., Navasardyan, G., Karapetyan, S., 2013. Pliocene-Quaternary volcanic rocks of NW Armenia: Magmatism and lithospheric dynamics within an active orogenic plateau. Lithos 180-181, 200-215.

Neill, I., Meliksetian, K., Allen, M., Navasardyan, G., Kuiper, K.F., 2015. Petrogenesis of mafic collision zone magmatism: The Armenian sector of the Turkish-Iranian Plateau. Chemical Geology 403, 24-41.

Nouri, F., Asahara, Y., Azizi, H., Yamamoto, K., Tsuboi, M., 2017. Geochemistry and petrogenesis of the Eocene back arc mafic rocks in the Zagros suture zone, northern Noorabad, western Iran. Chemie der Erde - Geochemistry 77, 517-533.

Nutman, A.P., Mohajjel, M., Bennett, V.C., Fergusson, C.L., 2014. Gondwanan Eoarchean–Neoproterozoic ancient crustal material in Iran and Turkey: zircon U–Pb–Hf isotopic evidence. Canadian Journal of Earth Sciences 51, 272-285.

Okay, A., Tuysuz, O., Satır, M., Ozkan-Altiner, S., Altiner, D., Sherlock, S., Eren, R., 2006. Cretaceous and Triassic subduction-accretion, high-pressure–low-temperature metamorphism, and continental growth in the Central Pontides, Turkey. Geological Society of America Bulletin 118, 1247-1269.

Okay, A.I., Zattin, M., Cavazza, W., 2010. Apatite fission-track data for the Miocene Arabia-Eurasia collision. Geology 38, 35-38.

Omrani, J., Agard, P., Whitechurch, H., Benoit, M., Prouteau, G., Jolivet, L., 2008. Arc-magmatism and subduction history beneath the Zagros Mountains, Iran: A new report of adakites and geodynamic consequences. Lithos 106, 380-398.

Pang, K.-N., Chung, S.-L., Zarrinkoub, M., Li, X.-H., Lee, H.-Y., Lin, T.-H., Chiu, H.-Y., 2016. New age and geochemical constraints on the origin of Quaternary adakite-like lavas in the Arabia-Eurasia collision zone. Lithos 264, 348-359.

Pang, K.-N., Chung, S.-L., Zarrinkoub, M.H., Chiu, H.-Y., Li, X.-H., 2014. On the magmatic record of the Makran arc, southeastern Iran: Insights from zircon U-Pb geochronology and bulk-rock geochemistry. Geochemistry, Geophysics, Geosystems 15, 2151-2169.

Pang, K.-N., Chung, S.-L., Zarrinkoub, M.H., Khatib, M.M., Mohammadi, S.S., Chiu, H.-Y., Chu, C.-H., Lee, H.-Y., Lo, C.-H., 2013a. Eocene–Oligocene post-collisional magmatism in the Lut–Sistan region, eastern Iran: Magma genesis and tectonic implications. Lithos 180-181, 234-251.

Pang, K.N., Chung, S.L., Zarrinkoub, M.H., Lin, Y.C., Lee, H.Y., Lo, C.H., Khatib, M.M., 2013b. Iranian ultrapotassic volcanism at~ 11 Ma signifies the initiation of post-collisional magmatism in the A rabia–E urasia collision zone. Terra Nova 25, 405-413.

Pe-Piper, G., Piper, D.J.W., Koukouvelas, I., Dolansky, L.M., Kokkalas, S., 2009. Postorogenic shoshonitic rocks and their origin by melting underplated basalts: The Miocene of Limnos, GreeceShoshonites from melting underplated basalt, Greece. GSA Bulletin 121, 39-54.

Pearce, J., 1983. Role of the sub-continental lithosphere in magma genesis at active continental margin.
Pearce, J.A., 2008. Geochemical fingerprinting of oceanic basalts with applications to ophiolite classification and the search for Archean oceanic crust. Lithos 100, 14-48.
Pearce, J.A., Bender, J.F., De Long, S.E., Kidd, W.S.F., Low, P.J., Güner, Y., Saroglu, F., Yilmaz, Y., Moorbath, S., Mitchell, J.G., 1990. Genesis of collision volcanism in Eastern Anatolia, Turkey. Journal of Volcanology and Geothermal Research 44, 189-229.
Pearce, J.A., Harris, N.B.W., Tindle, A.G., 1984. Trace Element Discrimination Diagrams for the Tectonic Interpretation of Granitic Rocks. Journal of Petrology 25, 956-983.
Peccerillo, A., Taylor, S., 1976. Geochemistry of Eocene calc-alkaline volcanic rocks from the Kastamonu area, northern Turkey. Contributions to Mineralogy and Petrology 58, 63-81.
Plank, T., 2014. The chemical composition of subducting sediments. Treatise on geochemistry 4, 607-629.
Platt, J., England, P., 1994. Convective removal of lithosphere beneath mountain belts-Thermal and mechanical consequences. American Journal of Science 294, 307-336.
Prelević, D., Akal, C., Romer, R.L., Mertz-Kraus, R., Helvacı, C., 2015. Magmatic Response to Slab Tearing: Constraints from the Afyon Alkaline Volcanic Complex, Western Turkey. Journal of Petrology 56, 527-562.
Prelević, D., Foley, S.F., Romer, R., Conticelli, S., 2008. Mediterranean Tertiary lamproites derived from multiple source components in postcollisional geodynamics. Geochimica et Cosmochimica Acta 72, 2125-2156.
Prelević, D., Jacob, D.E., Foley, S.F., 2013. Recycling plus: A new recipe for the formation of Alpine–Himalayan orogenic mantle lithosphere. Earth and Planetary Science Letters 362, 187-197.
Prelević, D., Seghedi, I., 2013. Magmatic response to the post-accretionary orogenesis within Alpine–Himalayan belt—Preface. Lithos, 1-4.
Priestley, K., McKenzie, D., Barron, J., Tatar, M., Debayle, E., 2012. The Zagros core: Deformation of the continental lithospheric mantle. Geochemistry, Geophysics, Geosystems 13, Q11014, doi:11010.11029/12012GC004435.
Rabiee, A., Rossetti, F., Tecce, F., Asahara, Y., Azizi, H., Glodny, J., Lucci, F., Nozaem, R., Opitz, J., Selby, D., 2019. Multiphase magma intrusion, ore-enhancement and hydrothermal carbonatisation in the Siah-Kamar porphyry Mo deposit, Urumieh-Dokhtar magmatic zone, NW Iran. Ore Geology Reviews 110, 102930.
Reilinger, R., McClusky, S., Vernant, P., Lawrence, S., Ergintav, S., Cakmak, R., Ozener, H., Kadirov, F., Guliev, I., Stepanyan, R., Nadariya, M., Hahubia, G., Mahmoud, S., Sakr, K., ArRajehi, A., Paradissis, D., Al-Aydrus, A., Prilepin, M., Guseva, T., Evren, E., Dmitrotsa, A., Filikov, S.V., Gomez, F., Al-Ghazzi, R., Karam, G., 2006. GPS constraints on continental deformation in the Africa-Arabia-Eurasia continental collision zone and implications for the dynamics of plate interactions. Journal of Geophysical Research: Solid Earth 111, B05411, doi:05410.01029/02005JB004051.
Rezeau, H., Leuthold, J., Tayan, R., Hovakimyan, S., Ulianov, A., Kouzmanov, K., Moritz, R., 2018. Incremental Growth of Mid-to Upper-Crustal Magma Bodies During Arabia–Eurasia Convergence and Collision: A Petrological Study of the Calc-Alkaline to Shoshonitic Meghri–Ordubad Pluton (Southern Armenia and Nakhitchevan, Lesser Caucasus). Journal of Petrology 59, 931-966.
Rezeau, H., Moritz, R., Leuthold, J., Hovakimyan, S., Tayan, R., Chiaradia, M., 2017. 30 Myr of Cenozoic magmatism along the Tethyan margin during Arabia–Eurasia accretionary orogenesis (Meghri–Ordubad pluton, southernmost Lesser Caucasus). Lithos 288-289, 108-124.
Rezeau, H., Moritz, R., Wotzlaw, J.-F., Tayan, R., Melkonyan, R., Ulianov, A., Selby, D., d'Abzac, F.-X., Stern, R.A., 2016. Temporal and genetic link between incremental pluton assembly and pulsed porphyry Cu-Mo formation in accretionary orogens. Geology 44, 627-630.
Richards, J., 2000. Lineaments revisited. SEG newsletter 42, 14-20.

Richards, J.P., 2015. Tectonic, magmatic, and metallogenic evolution of the Tethyan orogen: From subduction to collision. Ore Geology Reviews 70, 323-345.

Richards, J.P., Wilkinson, D., Ullrich, T., 2006. Geology of the Sari Gunay epithermal gold deposit, northwest Iran. Economic Geology 101, 1455-1496.

Rolland, Y., 2017. Caucasus collisional history: Review of data from East Anatolia to West Iran. Gondwana Research 49, 130-146.

Rolland, Y., Hässig, M., Bosch, D., Bruguier, O., Melis, R., Galoyan, G., Topuz, G., Sahakyan, L., Avagyan, A., Sosson, M., 2020. The East Anatolia–Lesser Caucasus ophiolite: An exceptional case of large-scale obduction, synthesis of data and numerical modelling. Geoscience Frontiers 11, 83-108.

Rolland, Y., Perincek, D., Kaymakci, N., Sosson, M., Barrier, E., Avagyan, A., 2012. Evidence for ~80–75Ma subduction jump during Anatolide–Tauride–Armenian block accretion and ~48Ma Arabia–Eurasia collision in Lesser Caucasus–East Anatolia. Journal of Geodynamics 56-57, 76-85.

Rosenbaum, G., Gasparon, M., Lucente, F.P., Peccerillo, A., Miller, M.S., 2008. Kinematics of slab tear faults during subduction segmentation and implications for Italian magmatism. Tectonics 27, TC2008, doi:2010.1029/2007TC002143.

Rossetti, F., Nasrabady, M., Theye, T., Gerdes, A., Monié, P., Lucci, F., Vignaroli, G., 2014. Adakite differentiation and emplacement in a subduction channel: The late Paleocene Sabzevar magmatism (NE Iran). Bulletin 126, 317-343.

Rubatto, D., 2002. Zircon trace element geochemistry: partitioning with garnet and the link between U–Pb ages and metamorphism. Chemical Geology 184, 123-138.

Rudnick, R., Gao, S., 2003. Composition of the continental crust. Treatise Geochem. 3, 1–64. Elsevier.

Sahakyan, L., Bosch, D., Sosson, M., Avagyan, A., Galoyan, G., Rolland, Y., Bruguier, O., Stepanyan, Z., Galland, B., Vardanyan, S., 2017. Geochemistry of the Eocene magmatic rocks from the Lesser Caucasus area (Armenia): evidence of a subduction geodynamic environment. Geological Society, London, Special Publications 428, 73-98.

Saleeby, J., Ducea, M., Clemens-Knott, D., 2003. Production and loss of high-density batholithic root, southern Sierra Nevada, California. Tectonics 22, 1064, doi:1010.1029/2002TC001374.

Sawada, Y., Zaree, G.R., Sakai, T., Itaya, T., Yagi, K., Imaizumi, M., Ataabadi, M.M., Fortelius, M., 2016. K–Ar ages and petrology of the late Miocene pumices from the Maragheh Formation, northwest Iran. Palaeobiodiversity and Palaeoenvironments 96, 399-431.

Schildgen, T., Yıldırım, C., Cosentino, D., Strecker, M., 2014. Linking slab break-off, Hellenic trench retreat, and uplift of the Central and Eastern Anatolian plateaus. Earth-Science Reviews 128, 147-168.

Schleiffarth, W.K., Darin, M.H., Reid, M.R., Umhoefer, P.J., 2018. Dynamics of episodic Late Cretaceous–Cenozoic magmatism across Central to Eastern Anatolia: New insights from an extensive geochronology compilation. Geosphere 14, 1990-2008.

Schleiffarth, W.K., Reid, M.R., Cosca, M.A., 2015. Ages, distribution, and evolution of Miocene basalts, East-Central Anatolia. In AGU Fall Meeting Abstracts.

Schmidt, M.W., Jagoutz, O., 2017. The global systematics of primitive arc melts. Geochemistry, Geophysics, Geosystems 18, 2817-2854.

Şengör, A.M.C., Özeren, M.S., Keskin, M., Sakınç, M., Özbakır, A.D., Kayan, İ., 2008. Eastern Turkish high plateau as a small Turkic-type orogen: Implications for post-collisional crust-forming processes in Turkic-type orogens. Earth-Science Reviews 90, 1-48.

Shad Manaman, N., Shomali, H., Koyi, H., 2011. New constraints on upper-mantle S-velocity structure and crustal thickness of the Iranian plateau using partitioned waveform inversion. Geophysical Journal International 184, 247-267.

Shafaii Moghadam, H., Griffin, W., Kirchenbaur, M., Garbe-Schönberg, D., Khedr, M., Kimura, J.-I., Stern, B., Ghorbani, G., Murphy, R., Y. O'Reilly, S., Arai, S., Maghdour-

Mashhour, R., 2018. Roll-Back, Extension and Mantle Upwelling Triggered Eocene Potassic Magmatism in NW Iran. Journal of Petrology 59, 1417-1465.

Shafaii Moghadam, H., Griffin, W.L., Li, X.-H., Santos, J.F., Karsli, O., Stern, R.J., Ghorbani, G., Gain, S., Murphy, R., O'Reilly, S.Y., 2017. Crustal evolution of NW Iran: Cadomian arcs, Archean fragments and the Cenozoic magmatic flare-up. Journal of Petrology 58, 2143-2190.

Shafaii Moghadam, H., Li, X.-H., Stern, B., Ghorbani, G., Bakhshizad, F., 2015. Zircon U-Pb ages and Hf-O isotopic composition of migmatite from the Zanjan-Takab complex, NW Iran: Constraints on partial melting of metasedimentary rocks.

Shakerardakani, F., Li, X.-H., Ling, X.-X., Li, J., Tang, G.-Q., Liu, Y., Monfaredi, B., 2019. Evidence for Archean crust in Iran provided by ca 2.7 Ga zircon xenocrysts within amphibolites from the Sanandaj–Sirjan zone, Zagros orogen. Precambrian Research 332, 105390.

Simmonds, V., Moazzen, M., Selby, D., 2019. U-Pb zircon and Re-Os molybdenite age of the Siah Kamar porphyry molybdenum deposit, NW Iran. International Geology Review 61, 1786-7802.

Sosson, M., Rolland, Y., Müller, C., Danelian, T., Melkonyan, R., Kekelia, S., Adamia, S., Babazadeh, V., Kangarli, T., Avagyan, A., 2010. Subductions, obduction and collision in the Lesser Caucasus (Armenia, Azerbaijan, Georgia), new insights. Geological Society, London, Special Publications 340, 329-352.

Stacey, J.t., Kramers, J., 1975. Approximation of terrestrial lead isotope evolution by a two-stage model. Earth and Planetary Science Letters 26, 207-221.

Stampfli, G.M., Borel, G., 2002. A plate tectonic model for the Paleozoic and Mesozoic constrained by dynamic plate boundaries and restored synthetic oceanic isochrons. Earth and Planetary Science Letters 196, 17-33.

Stern, R.J., 2002. Subduction zones. Reviews of Geophysics 40, 3-1-3-38.

Stern, R.J., Fouch, M.J., Klemperer, S.L., 2003. An overview of the Izu-Bonin-Mariana subduction factory. Inside the subduction factory, 175-222.

Stocklin, J., 1968. Structural history and tectonics of Iran: a review. American Association of Petroleum Geologists Bulletin 52, 1229-1258.

Su, Z., Wang, E.-C., Hu, J.-C., Talebian, M., Karimzadeh, S., 2017. Quantifying the Termination Mechanism Along the North Tabriz-North Mishu Fault Zone of Northwestern Iran via Small Baseline PS-InSAR and GPS Decomposition. IEEE Journal of Selected Topics in Applied Earth Observations and Remote Sensing 10, 130-144.

Sugden, P., Savov, I., Wilson, M., Meliksetian, K., Navasardyan, G., Halama, R., 2019. The Thickness of the Mantle Lithosphere and Collision-Related Volcanism in the Lesser Caucasus. Journal of Petrology 60, 199-230.

Sun, S.s., McDonough, W.F., 1989. Chemical and isotopic systematics of oceanic basalts: implications for mantle composition and processes. Geological Society, London, Special Publications 42, 313-345.

Tadayon, M., Rossetti, F., Zattin, M., Calzolari, G., Nozaem, R., Salvini, F., Faccenna, C., Khodabakhshi, P., 2018. The long-term evolution of the Doruneh Fault region (Central Iran): A key to understanding the spatio-temporal tectonic evolution in the hinterland of the Zagros convergence zone. Geological Journal 54, 1454-1479.

Tadayon, M., Rossetti, F., Zattin, M., Nozaem, R., Calzolari, G., Madanipour, S., Salvini, F., 2017. The Post-Eocene Evolution of the Doruneh Fault Region (Central Iran): The Intraplate Response to the Reorganization of the Arabia-Eurasia Collision Zone. Tectonics 36, 3038-3064.

Taghizadeh-Farahmand, F., Sodoudi, F., Afsari, N., Ghassemi, M.R., 2010. Lithospheric structure of NW Iran from P and S receiver functions. Journal of seismology 14, 823-836.

Talebian, M., Jackson, J., 2004. A reappraisal of earthquake focal mechanisms and active shortening in the Zagros mountains of Iran. Geophysical Journal International 156, 506-526.

Tanaka, T., Togashi, S., Kamioka, H., Amakawa, H., Kagami, H., Hamamoto, T., Yuhara, M., Orihashi, Y., Yoneda, S., Shimizu, H., 2000. JNdi-1: a neodymium isotopic reference in consistency with LaJolla neodymium. Chemical Geology 168, 279-281.

Tatsumi, Y., 2005. The subduction factory: how it operates in the evolving Earth. GSA today 15, 4-10.

Tatsumi, Y., Hamilton, D.L., Nesbitt, R.W., 1986. Chemical characteristics of fluid phase released from a subducted lithosphere and origin of arc magmas: Evidence from high-pressure experiments and natural rocks. Journal of Volcanology and Geothermal Research 29, 293-309.

Tatsumi, Y., Kogiso, T., 2003. The subduction factory: its role in the evolution of the Earth's crust and mantle. Geological Society, London, Special Publications 219, 55-80.

Tatsumi, Y., Murasaki, M., Arsadi, E.M., Nonda, S., 1991. Geochemistry of Quaternary lavas from NE Sulawesi: transfer of subduction components into the mantle wedge. Contributions to Mineralogy and Petrology 107, 137-149.

Tommasini, S., Avanzinelli, R., Conticelli, S., 2011. The Th/La and Sm/La conundrum of the Tethyan realm lamproites. Earth and Planetary Science Letters 301, 469-478.

Tsereteli, N., Tibaldi, A., Alania, V., Gventsadse, A., Enukidze, O., Varazanashvili, O., Müller, B.I.R., 2016. Active tectonics of central-western Caucasus, Georgia. Tectonophysics 691, 328-344.

Ulmer, P., Kaegi, R., Müntener, O., 2018. Experimentally derived intermediate to silica-rich arc magmas by fractional and equilibrium crystallization at 1· 0 GPa: An evaluation of phase relationships, compositions, liquid lines of descent and oxygen fugacity. Journal of Petrology 59, 11-58.

van der Boon, A., van Hinsbergen, D.J.J., Rezaeian, M., Gürer, D., Honarmand, M., Pastor-Galán, D., Krijgsman, W., Langereis, C.G., 2018. Quantifying Arabia–Eurasia convergence accommodated in the Greater Caucasus by paleomagnetic reconstruction. Earth and Planetary Science Letters 482, 454-469.

van Hunen, J., Allen, M., 2011. Continental collision and slab break-off: A comparison of 3-D numerical models with observations. Earth and Planetary Science Letters 302, 27-37.

van Hunen, J., Miller, M.S., 2015. Collisional Processes and Links to Episodic Changes in Subduction Zones. Elements 11, 119-124.

Verdel, C., Wernicke, B.P., Hassanzadeh, J., Guest, B., 2011. A Paleogene extensional arc flare-up in Iran. Tectonics 30, TC3008, doi:3010.1029/2010TC002809.

Vernant, P., Nilforoushan, F., Hatzfeld, D., Abbassi, M.R., Vigny, C., Masson, F., Nankali, H., Martinod, J., Ashtiani, A., Bayer, R., Tavakoli, F., Chéry, J., 2004. Present-day crustal deformation and plate kinematics in the Middle East constrained by GPS measurements in Iran and northern Oman. Geophysical Journal International 157, 381-398.

Vincent, S., Allen, M., D. Ismail-Zadeh, A., Flecker, R., Foland, K., Simmons, M., 2005. Insights from the Talysh of Azerbaijan into the Paleogene evolution of the South Caspian region. Geological Society of America Bulletin 117, 1513-1533.

Vincent, S.J., Braham, W., Lavrishchev, V.A., Maynard, J.R., Harland, M., 2016. The formation and inversion of the western Greater Caucasus Basin and the uplift of the western Greater Caucasus: Implications for the wider Black Sea region. Tectonics 35, 2948-2962.

Vincent, S.J., Morton, A.C., Carter, A., Gibbs, S., Barabadze, T.G., 2007. Oligocene uplift of the Western Greater Caucasus: an effect of initial Arabia–Eurasia collision. Terra Nova 19, 160-166.

von Blanckenburg, F., Davies, J.H., 1995. Slab breakoff: A model for syncollisional magmatism and tectonics in the Alps. Tectonics 14, 120-131.

Walpersdorf, A., Manighetti, I., Mousavi, Z., Tavakoli, F., Vergnolle, M., Jadidi, A., Hatzfeld, D., Aghamohammadi, A., Bigot, A., Djamour, Y., 2014. Present-day kinematics and fault slip rates in eastern Iran, derived from 11 years of GPS data. Journal of Geophysical Research: Solid Earth 119, 1359-1383.

Wang, Q., Wyman, D.A., Xu, J.-F., Zhao, Z.-H., Jian, P., Xiong, X.-L., Bao, Z.-W., Li, C.-F., Bai, Z.-H., 2006. Petrogenesis of Cretaceous adakitic and shoshonitic igneous rocks in the Luzong area, Anhui Province (eastern China): Implications for geodynamics and Cu–Au mineralization. Lithos 89, 424-446.

Whitechurch, H., Omrani, J., Agard, P., Humbert, F., Montigny, R., Jolivet, L., 2013. Evidence for Paleocene–Eocene evolution of the foot of the Eurasian margin (Kermanshah ophiolite, SW Iran) from back-arc to arc: Implications for regional geodynamics and obduction. Lithos 182-183, 11-32.

Whitney, D.L., Evans, B.W., 2010. Abbreviations for names of rock-forming minerals. American Mineralogist 95, 185-187.

Wiedenbeck, M., Alle, P., Corfu, F., Griffin, W., Meier, M., Oberli, F.v., Quadt, A.v., Roddick, J., Spiegel, W., 1995. Three natural zircon standards for U-Th-Pb, Lu-Hf, trace element and REE analyses. Geostandards newsletter 19, 1-23.

Winchester, J.A., Floyd, P.A., 1977. Geochemical discrimination of different magma series and their differentiation products using immobile elements. Chemical Geology 20, 325-343.

Xu, J.-F., Shinjo, R., Defant, M.J., Wang, Q., Rapp, R.P., 2002. Origin of Mesozoic adakitic intrusive rocks in the Ningzhen area of east China: Partial melting of delaminated lower continental crust? Geology 30, 1111-1114.

Yang, Z., Hou, Z., Chang, Z., Li, Q., Liu, Y., Qu, H., Sun, M., Xu, B., 2016. Cospatial Eocene and Miocene granitoids from the Jiru Cu deposit in Tibet: Petrogenesis and implications for the formation of collisional and postcollisional porphyry Cu systems in continental collision zones. Lithos 245, 243-257.

Zhang, Z., Xiao, W., Ji, W., Majidifard, M.R., Rezaeian, M., Talebian, M., Xiang, D., Chen, L., Wan, B., Ao, S., Esmaeili, R., 2018. Geochemistry, zircon U-Pb and Hf isotope for granitoids, NW Sanandaj-Sirjan zone, Iran: Implications for Mesozoic-Cenozoic episodic magmatism during Neo-Tethyan lithospheric subduction. Gondwana Research 62, 227-245.

Zheng, Y.-F., 2019. Subduction zone geochemistry. Geoscience Frontiers 10, 1223-1254.

Fig. 1. (a) Simplified tectonic map of NW Iran, Arabia, Caucasus and Anatolia, also showing the distribution of Iran Eocene-Oligocene and Neogene-Quaternary igneous rocks and the main ophiolitic mélange outcrops (modified after Hubner, 1969), (micro-) plate boundaries (modified after Reilinger et al., 2006), suture zones and fault distribution (modified after Richards, 2015). (b) The background colours show the surface wave tomographic model at 125 km depth of upper mantle (Priestley et al., 2012). A significant change in the lithosphere structure is observed across the Mianeh-Ardabil fault. The contours are the Moho depth across the Iranian plateau (redrawn after Shad Manaman et al., 2011) showing an abrupt change in the Moho depth across the Tabriz Fault, thickening to the NE. Significant changes are also observed along Mianeh-Ardabil Fault. Abbreviations: F., Fault; ZOMZ, Zangezur-Ordubad volcano-plutonic zone; SbV, Sabalan Volcano; ShV, Sahand Volcano.

Fig. 2. Simplified geological map showing the magmatic zones of NW Iran (modified from Hubner, 1969) and southern Armenia (including the Zangezur-Ordubad volcano-plutonic zone (ZOMZ) and the Meghri-Ordubad pluton (MOP) assemblage; Moritz et al., 2016). The black rectangle indicates the study area. See the Supplementary Material S1 for detail characteristics of each deposit.

Fig. 3. Simplified geological map of the Mianeh-Hashtroud area (modified after Amidi et al., 1987). The analysed samples together with their U-Pb zircon ages (Ma ± 2$\sigma$ error) are also shown. Ages of samples #01, 03, 19 and 31 are from Rabiee et al. (2019).

Fig. 4. (a) Satellite image (Google Earth) of the central sector of the study area, showing the distribution of the Eocene and Miocene intrusions and samples locations. (b) Eocene volcanic country rocks. (c) Strongly plagioclase-phyric and (c) pyroxene-phyric structure of Eocene volcanic country rocks. (e-h) Hand specimens of the studied Eocene intrusive rocks. (e) Biotite-bearing monzonite. (f) Syenite mainly containing k-feldspar (pinkish) and plagioclase. (g) A close-up view of quartz monzonite body showing a miarolithic cavity in the contact zone with the monzonite body. (h) A close-up view of the microgranular granite body with minor weathered biotite grains. The sampling sites of the investigated rocks are reported in Figure 3.

Fig. 5. (a) Panorama view from east of the area (Ebak-SiahKamar) showing the outcrops of Eocene country rocks intruded by the Oligocene subvolcanic bodies. (b) and (c) close views showing granular and porphyritic textures from two Oligocene monzonite bodies. (d to f) Hand specimens from the Oligocene volcanic rocks showing a porphyritic hypohyaline texture. (g) and (h) altered rhyolitic porphyry dike. The sampling sites of the investigated rocks are reported in Figure 3. Kfs = Alkali feldspar; Bt = Biotite; Pl = Plagioclase; Qz = Quartz.

Fig. 6. Microphotographs of representative magmatic rocks from Mianeh-Hashtroud area. The sample ID is shown on each picture. (a) MN04 Eocene country rock: trachyte showing plagioclase phenocrysts in a groundmass mad of plagioclase microliths; (b) MN09 Eocene monzodiorite showing equigranular-holocrystalline texture made of plagioclase, amphibole and magnetite; (c) MN12 Eocene quartz monzonite with equigranular-holocrystalline texture showing plagioclase, alkali feldspar, quartz and biotite as major crystals; (d) MN10A Eocene granite characterised by porphyritic-holocrystalline texture with microgranular groundmass made up of alkali feldspar, quartz and biotite; (e) MN10C Eocene monzonite enclave in the granite (MN10A) showing porphyritic-holocrystalline texture and plagioclase, alkali feldspar, amphibole ± clinopyroxene as major crystals; (f) MN45 Oligocene monzonite with equigranular-holocrystalline texture with plagioclase alkali feldspar, amphibole and biotite as major crystals; (g) MN65 Oligocene monzonite, hypabyssal porphyritic-holocrystalline texture containing clinopyroxene and plagioclase phenocrysts (h) MN76 Oligocene hypabyssal granite, porphyritic-holocrystalline texture with microgranular groundmass made up of alkali feldspar, quartz and biotite; (i) MN19 Oligocene dacite dome showing a vitrophyric texture, with glassy groundmass containing sub-rounded, resorbed and fractured quartz abd okaguickase phenocrysts and minor biotite and amphibole. All images are in crossed-polarised light.

Fig. 7. U-Pb Concordia diagrams and probability age distribution plot as obtained from the cumulative $^{206}Pb/^{238}U$ age data from the zircon grains recovered from the studied magmatic rock samples. See

also Table 2 for the corresponding analytical results and the Supplementary Material S2 for the complete textural characteristics of the analysed zircon grains.

Fig. 8. (a) Total alkali vs. silica (TAS) diagram (Le Maitre et al. 2005) for the Cenozoic igneous rocks of the Mianeh-Hashtroud district. The volcanic rock name have been used also for the plutonic and the hypabyssal samples. (b) $K_2O$ vs. $SiO_2$ diagram (Peccerillo and Taylor, 1976). HK-CA: high-K calcalkaline; MK-CA: medium-K calcalkaline, LK, low-K. (c) $SiO_2$ vs. Nb/Y diagram (Winchester and Floyd, 1977). A: andesites; AB: Alkali basalts; B: Basalts; BA: Basaltic andesites; BSN, NEP: Basanite, Nephelinite; BTA: Basaltic trachyandesite; COM, PAN: Commendite, Pantellerite; PH: phonolite; R: Rhyolite; R, D: Rhyolite, Dacite; T: Trachyte; TA: Trachy-andesite (d) Th vs. Co diagram (Hastie et al., 2007). B: Basalts; BA/A: Basaltic andesites, Andesites; D/R: Dacite, Rhyolite; CA: Calcalkaline; IAT: Island Arc Tholeiite; H-K: high-K; SHO: Shoshonite. Data from this study are compared with those available from the neighbouring regions.

Fig. 9. Harker diagrams for selected major oxides (in wt%) using $SiO_2$ as differentiation index.

Fig. 10. Harker diagrams for selected trace elements (in ppm) using $SiO_2$ as differentiation index. Grt = garnet; Amp = amphibole.

Fig. 11. (a) Primitive mantle-*normalized* (after Lyubetskaya and Korenaga, 2007) incompatible element diagram for the Cenozoic Mianeh-Hashtroud igneous rocks. The inset shows the plot for the least differentiated compositions ($SiO_2$ <57 wt%) compared with patterns for oceanic island basalts (OIB; after Sun and McDonough, 1989), continental arc calcalkaline and shoshonite magmatism (Cascade arc), island arc magmatism (Izu-Bonin-Marianna (IBM) arc), the Emeishan large igneous province (ELIP) and average continental crust (Rudnick and Gao, 2003). (b) Chondrite-normalised (after Sun and McDonough, 1989) REE diagram for the Cenozoic Mianeh-Hashtroud igneous rocks. The inset shows the same diagram for the least differentiated compositions ($SiO_2$ <57 wt%) as in (a). Data sources: GEOROC (http://georoc.mpch-mainz.gwdg.de/georoc/).

Fig. 12. $\varepsilon Nd_{(t)}$ vs. $(^{87}Sr/^{86}Sr)_t$ diagram of the Mianeh-Hashtroud district igneous rocks. The data are compared with those of Mesozoic and Cenozoic Lesser Caucasus igneous rocks (Mederer et al., 2013 and Moritz et al., 2016, respectively), Quaternary volcanic rocks (NW Iran; Allen et al., 2013), Neogene-Quaternary Azerbaijan volcanic rocks (NW Iran; Lechman et al., 2018), and Jurassic-Cretaceous igneous rocks of the northern Sanandaj Sirjan Zone (Azizi and Asahara, 2013; Azizi et al. 2018). BSE = Bulk Silicate Earth; ChUR = Chondritic Uniform Reservoir.

Fig. 13. (a) Weighted age distribution of all measured zircon autocrysts and antecrysts from Mianeh-Hashtroud area (including four samples mentioned in Fig. 3 caption from Rabiee et al., 2019); (b and c) Relative age frequency distribution for zircons antecrysts and xenocrysts (inherited) recovered from the studied samples.

Fig. 14. (a) Sr/Y vs. Y and (b) $(La/Yb)_N$ vs $Yb_N$ diagrams for the Cenozoic Mianeh-Hashtroud igneous rocks together with literature analyses of NW Iran Cenozoic igneous rocks. These rocks plot almost completely in the “normal” calcalkaline arcs field as defined by Defant and Drummond (1990). (c) Th/Yb vs. Nb/Yb diagram (Pearce (2008) for the least differentiated ($SiO_2$ <57 wt%) Mianeh-Hashtroud rocks. Data sources for Izu Bonin Mariana (IBM), Emeishan Large Igneous Province (ELIP), Ocean Island Basalts (OIB) and Cascade continental arc are from GEOROC (http://georoc.mpch-mainz.gwdg.de/georoc); (d) Rb vs. (Y+Nb) diagram (Pearce et al. (1984) for the most differentiated ($SiO_2$ >57 wt%) rocks showing the fields of ocean ridge (ORG), volcanic arc (VAG), syn-collisional (syn-COLG), and within-plate (WPG) granitic rocks.

Fig. 15. (a) $(^{87}Sr/^{86}Sr)_t$ vs. $SiO_2$ and (b) $\varepsilon Nd_{(t)}$ vs. $SiO_2$ diagrams of Mianeh-Hashtroud Cenozoic igneous rocks. No correlation between Sr and Nd isotopic ratios is observed with the degree of evolution of the melts.

Fig. 16. Geodynamic reconstruction of the Turkish–Caucasus–Iranian collisional zone of Tethyan belt (after Barrier et al. (2018). (a), (c) Paleogeographic scenarios. (b), (d) Geodynamic scenarios (not to scale; location of structures is only indicative). All abbreviations and tectonic domain names are after Barrier et al. (2018): AbM: Alborz Margins (and Talesh); ABV: Artvin-Bolnisi Volcanic Arc; ArB: Arasbaran Belt; Ark: Arkevan Formation; CAC: Central Anatolian Complex; CIP: Central Iranian Platform; EBB: Eastern Black-Sea Basin; EHT: Esfahan-Hamadan Trough; GCB: Greater Caucasus Basin; GKF: Great Kevir fault; HeV: Helete Volcanic arc; ION: Izmir-Ankara-Ercinjan Ophiolite Nappes; KDP: Kopeh Dagh Platform; KON: Khoy ophiolite nappe; LCR: Lesser Caucasus range (including Zangezur-Ordubad volcano-plutonic zone;ZOMZ); LuB: Lut Block; LuP: Lut Platform; MeM: Menderes massif; MsO: Mesogea Ocean; MZT: Main Zagros thrust; PAM: Peri-Arabian massif; PMA: Pontides Magmatic Arc; PoR: Pontides range; RNO: Remnant Neo-Tethys Ocean; SaT: Sanandaj Trough; SCB: South-Caspianbasin; SFB: Srednogorie Fold-Belt; SrB: Sirjan block; SSB: Sanandaj-Sirjan block; SsB: Sistan Basin; SzB: Sabzevar Basin; SzM: Sabzevar Massif; TaP: Taurus platform; UDMA: Urumieh-Dokhtar Magmatic Arc; WBB: Western Black-Sea Basin; ZDF: Zagros deformation front.

***Declaration of Interest Statement**

**Declaration of interests**

☒ The authors declare that they have no known competing financial interests or personal relationships that could have appeared to influence the work reported in this paper.

☐The authors declare the following financial interests/personal relationships which may be considered as potential competing interests:

| |
|---|
| Federico Rossetti<br>(on behalf of the co-authors) |

*Credit Author Statement

**Ahmad Rabiee**: Conceptualization, Methodology, Software, Investigation, Data curation, Validation, Writing - Original draft preparation, Writing - Review & Editing. **Federico Rossetti**: Supervision, Conceptualization, Methodology, Investigation, Validation, Writing - Review & Editing. **Yoshihiro Asahara**: Conceptualization**,** Methodology, Resources, Validation, Writing - Review & Editing**.** **Hossein Azizi:** Conceptualization, Methodology, Investigation, Validation, Writing - Review & Editing. **Federico Lucci**: Conceptualization, Methodology, Investigation, Validation, Writing - Review & Editing. **Michele Lustrino**: Conceptualization**,** Methodology, Validation, Writing- Reviewing and Editing. **Reza Nozaem**: Conceptualization**,** Investigation, Writing - Review & Editing

Supplementary Material S1

Click here to download e-component: Supplementary material S1.docx

Supplementary Material S2

Click here to download e-component: Supplementary material S2.jpg

**Supplementary Material S3**

**Click here to download e-component: Supplementary material S3.docx**

**Supplementary Materia S4**

**Click here to download e-component: Supplementary material S4.jpg**

Figure 1

Click here to download high resolution image

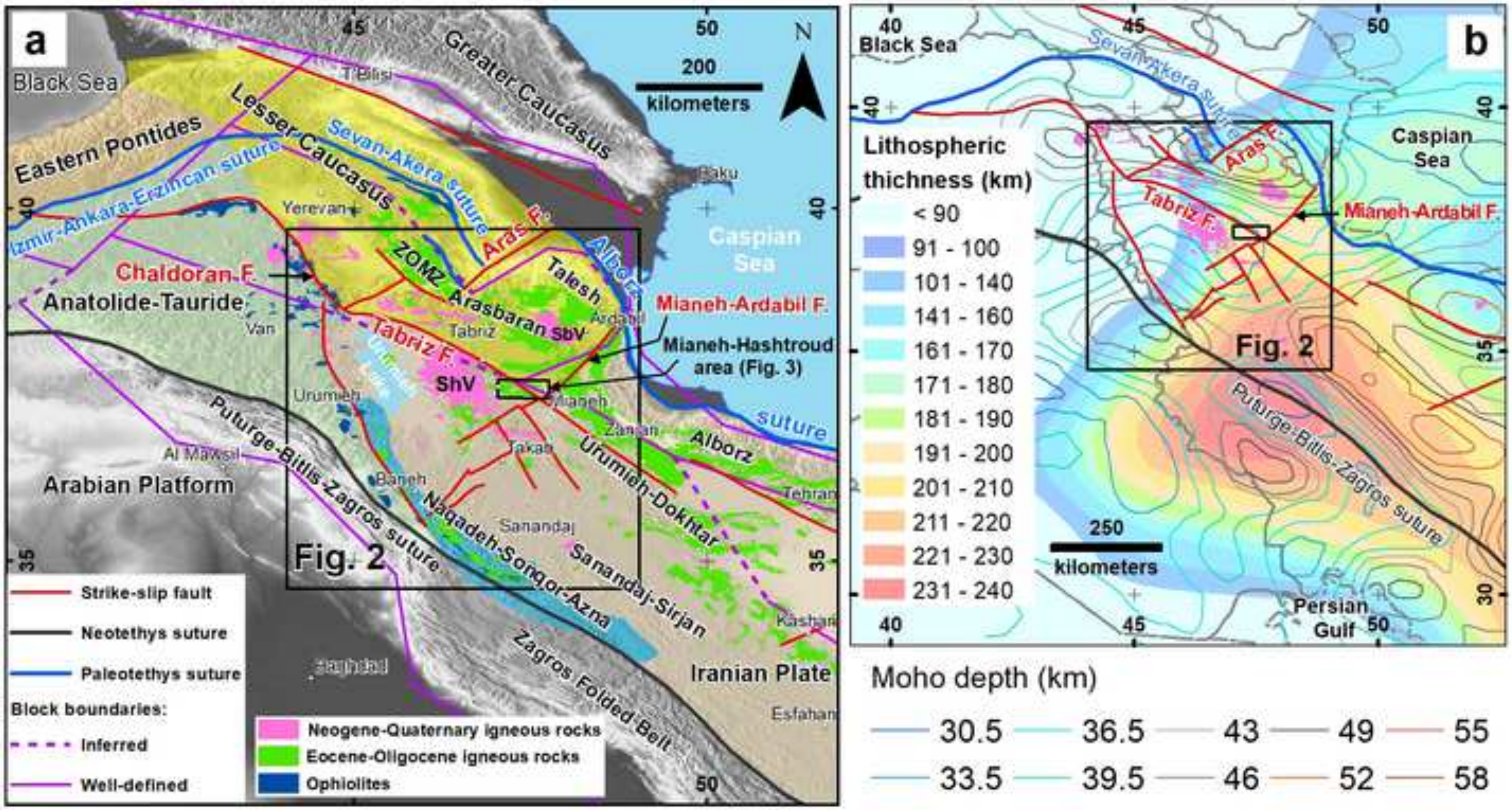

Figure 2
Click here to download high resolution image

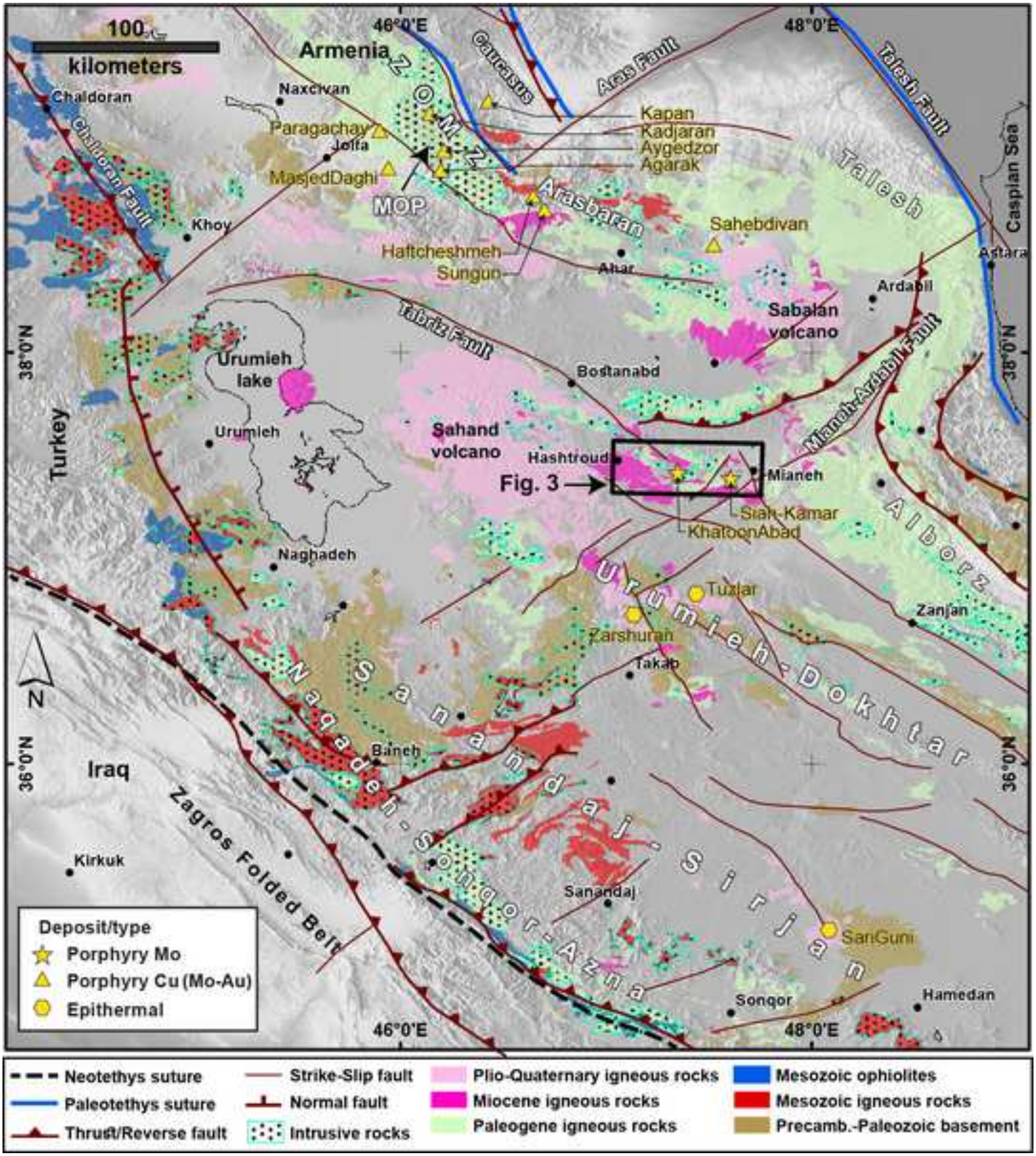

Figure 3
Click here to download high resolution image

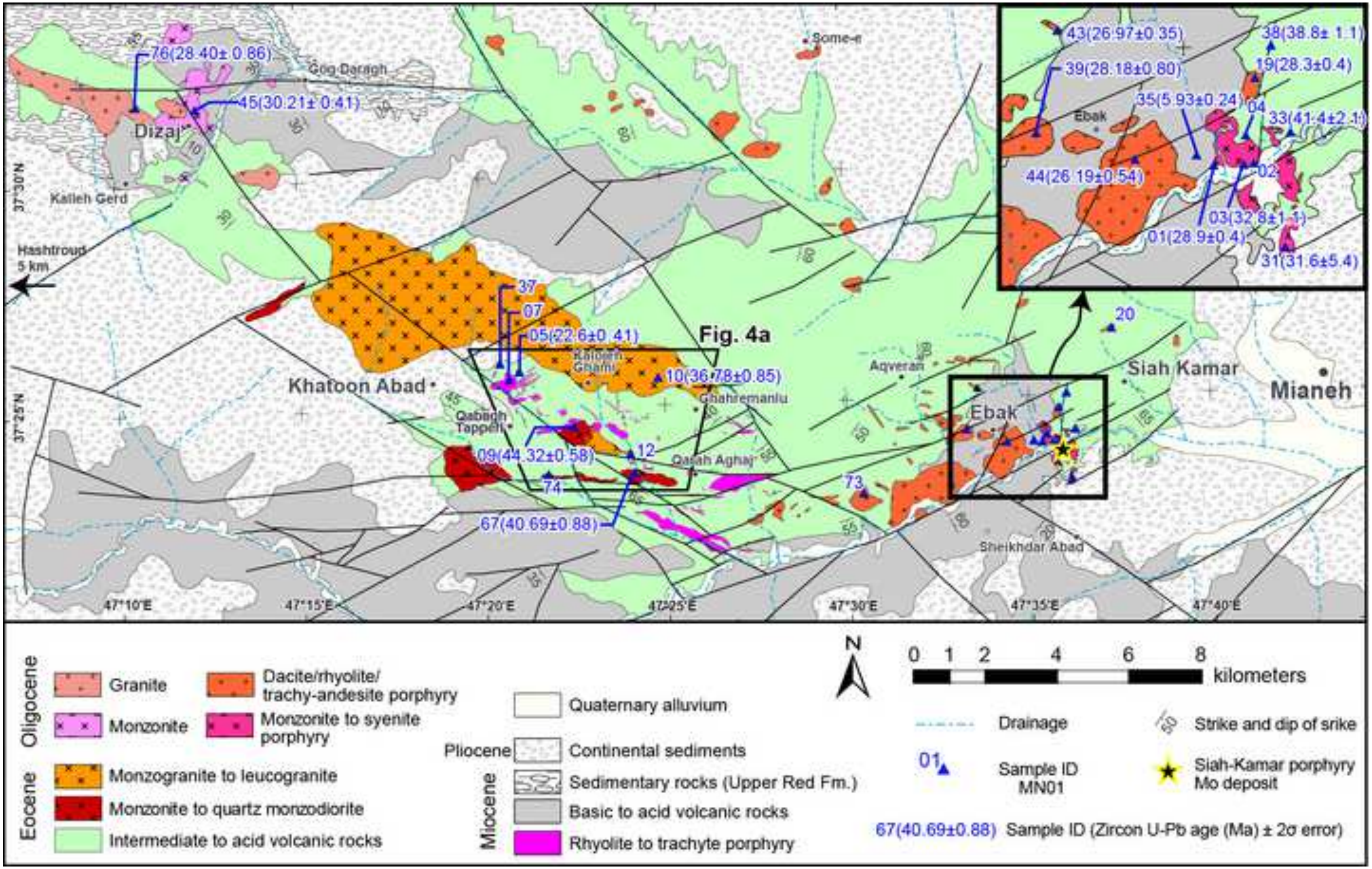

Figure 4

Click here to download high resolution image

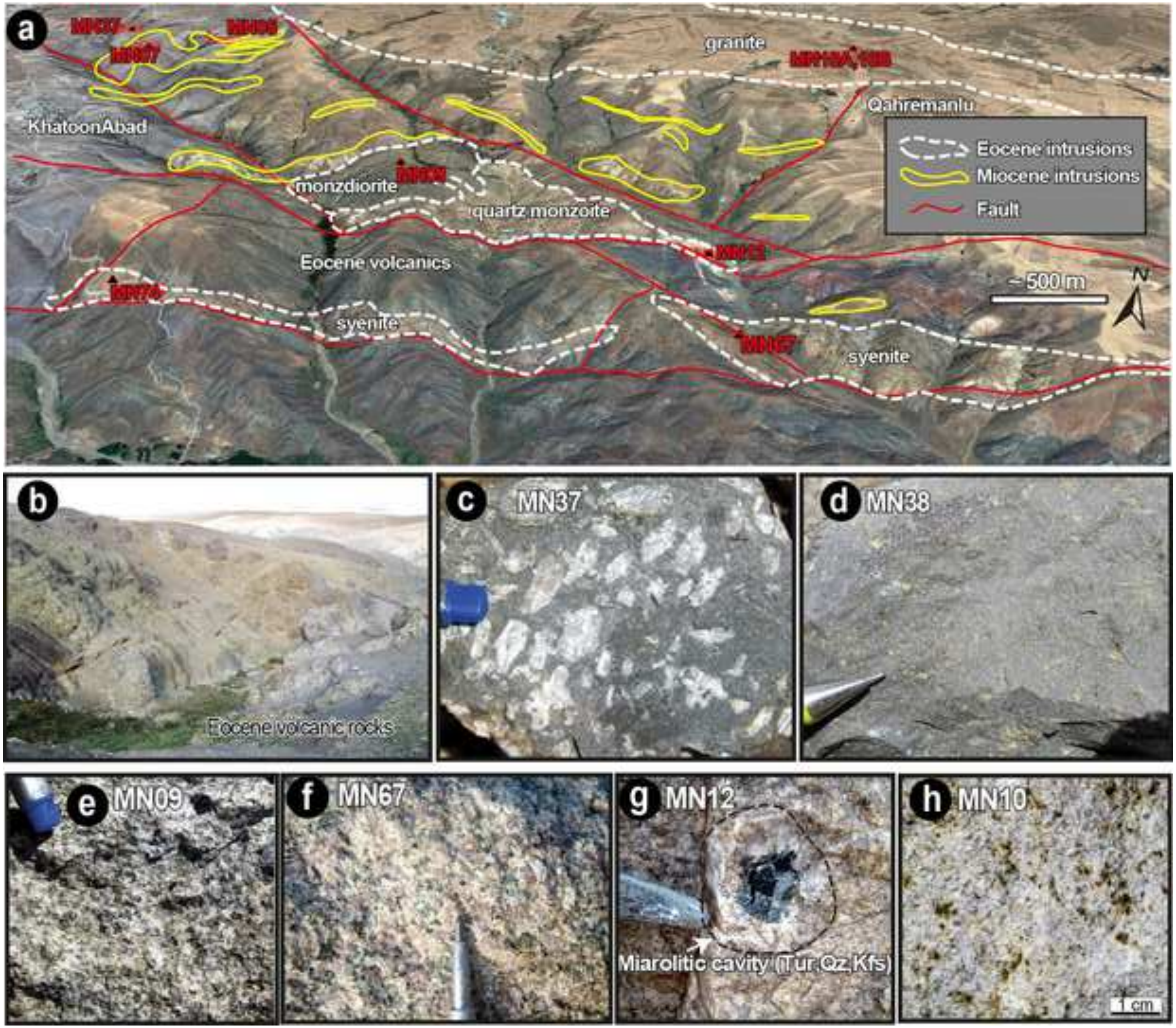

Figure 5
Click here to download high resolution image

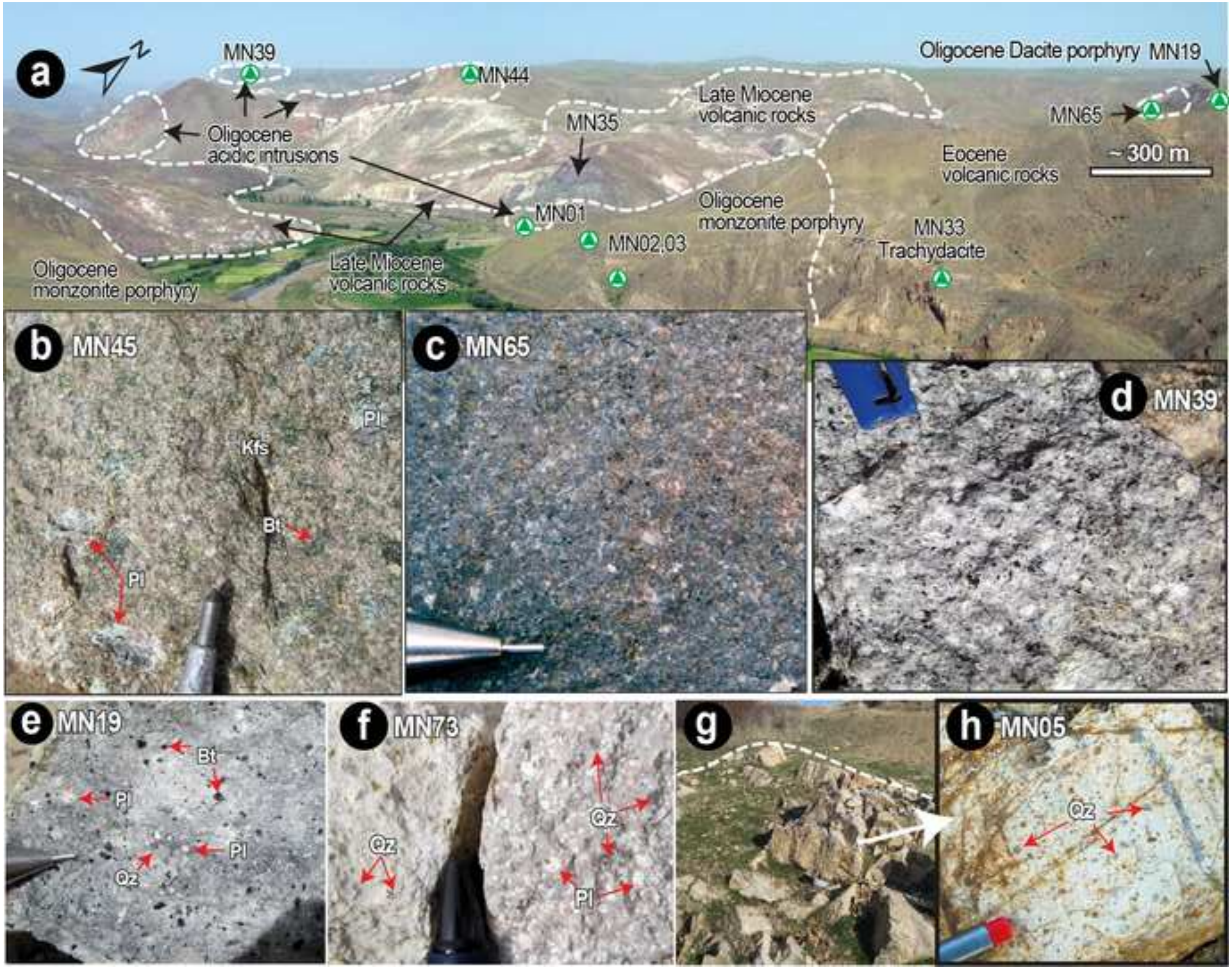

Figure 6
Click here to download high resolution image

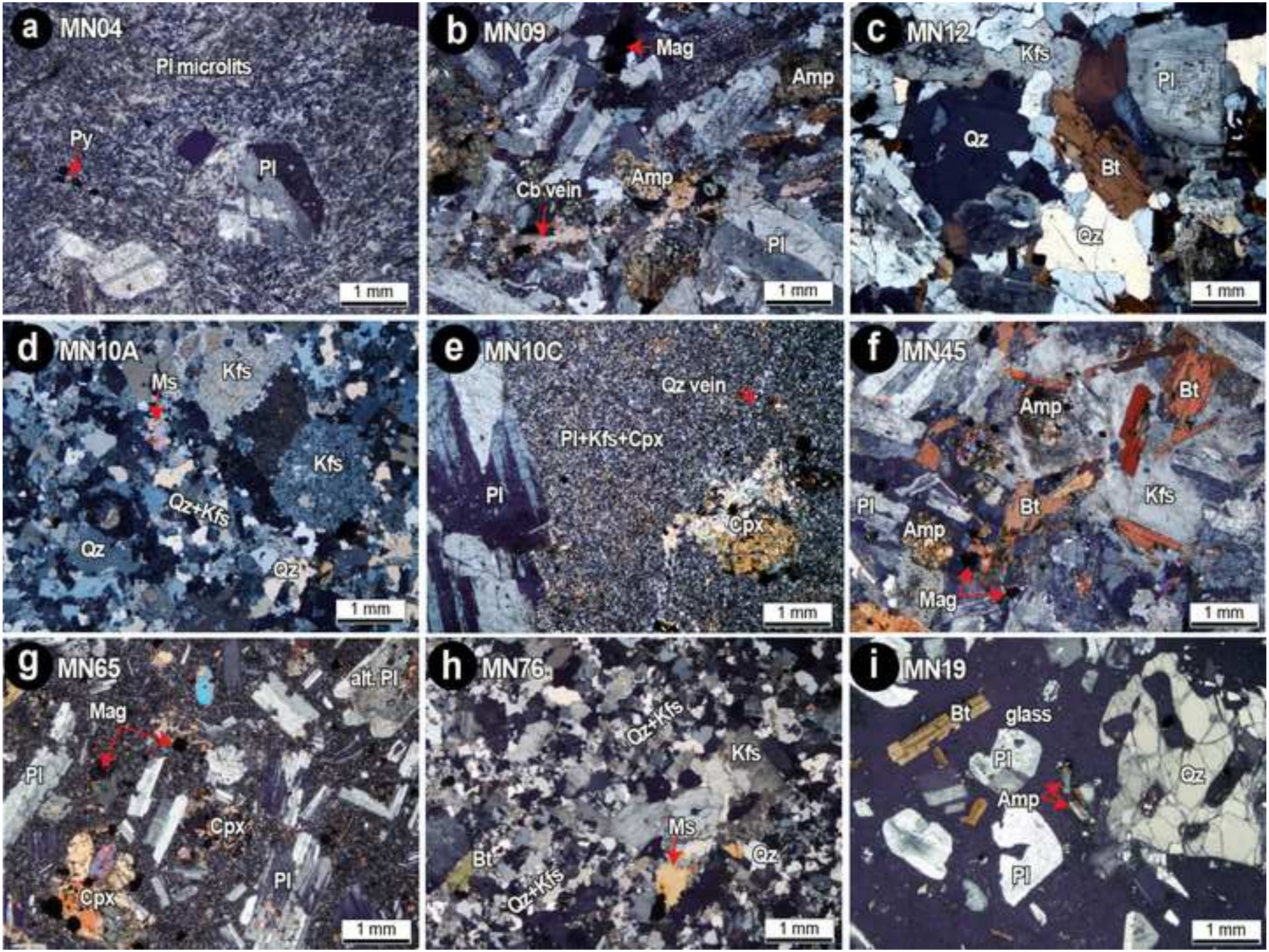

Figure 7

Click here to download high resolution image

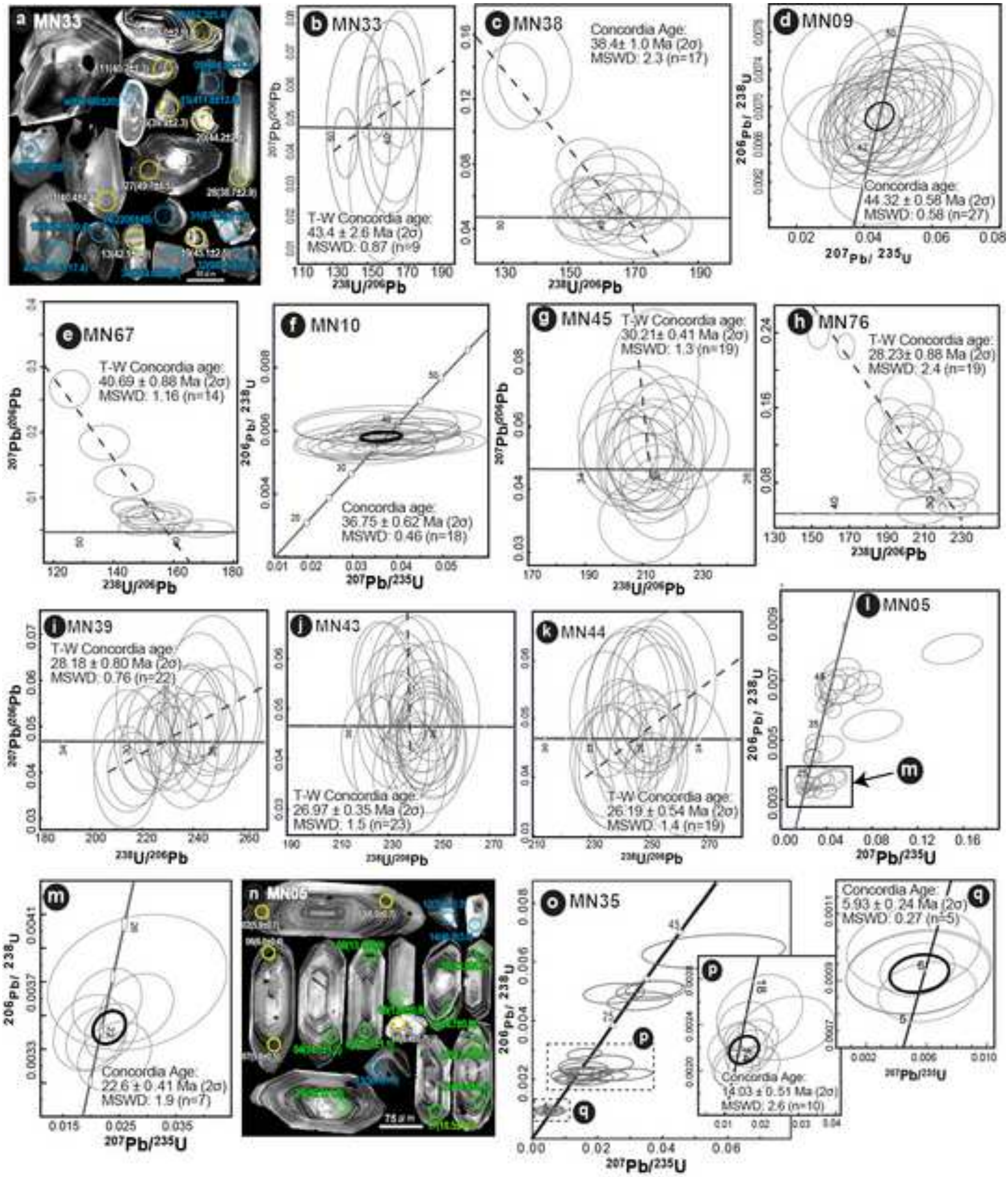

Figure 8

Click here to download high resolution image

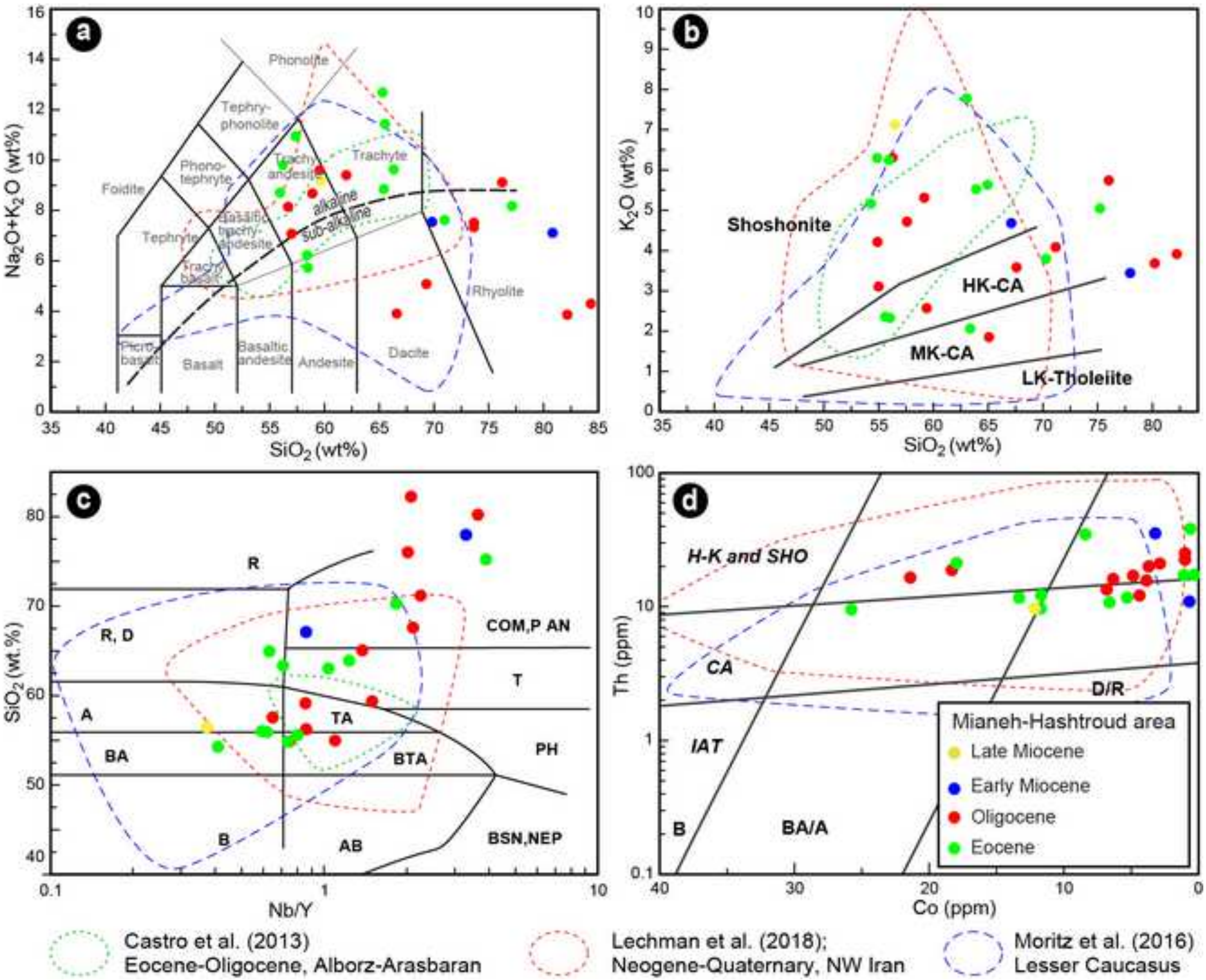

Figure 9

Click here to download high resolution image

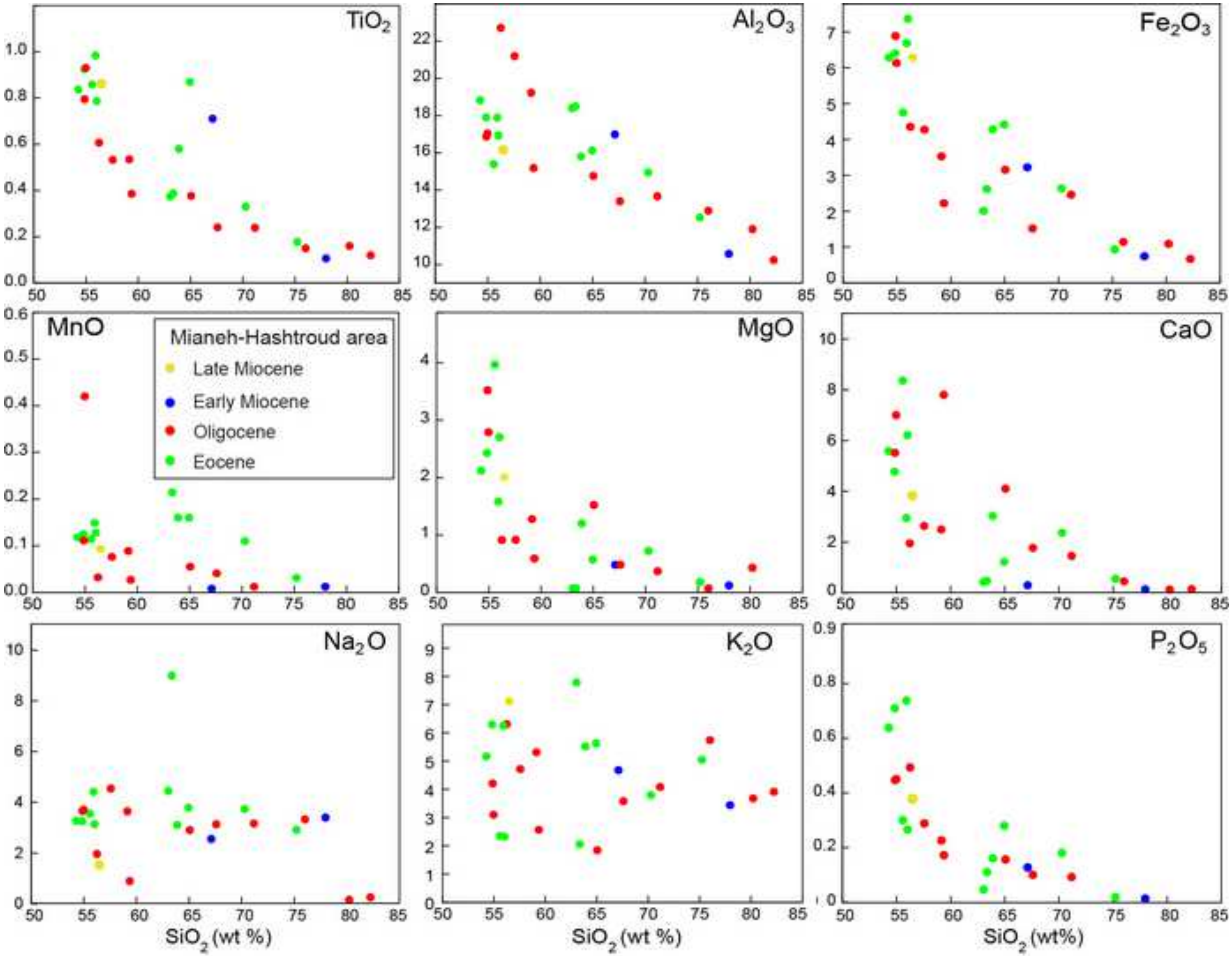

Figure 10

Click here to download high resolution image

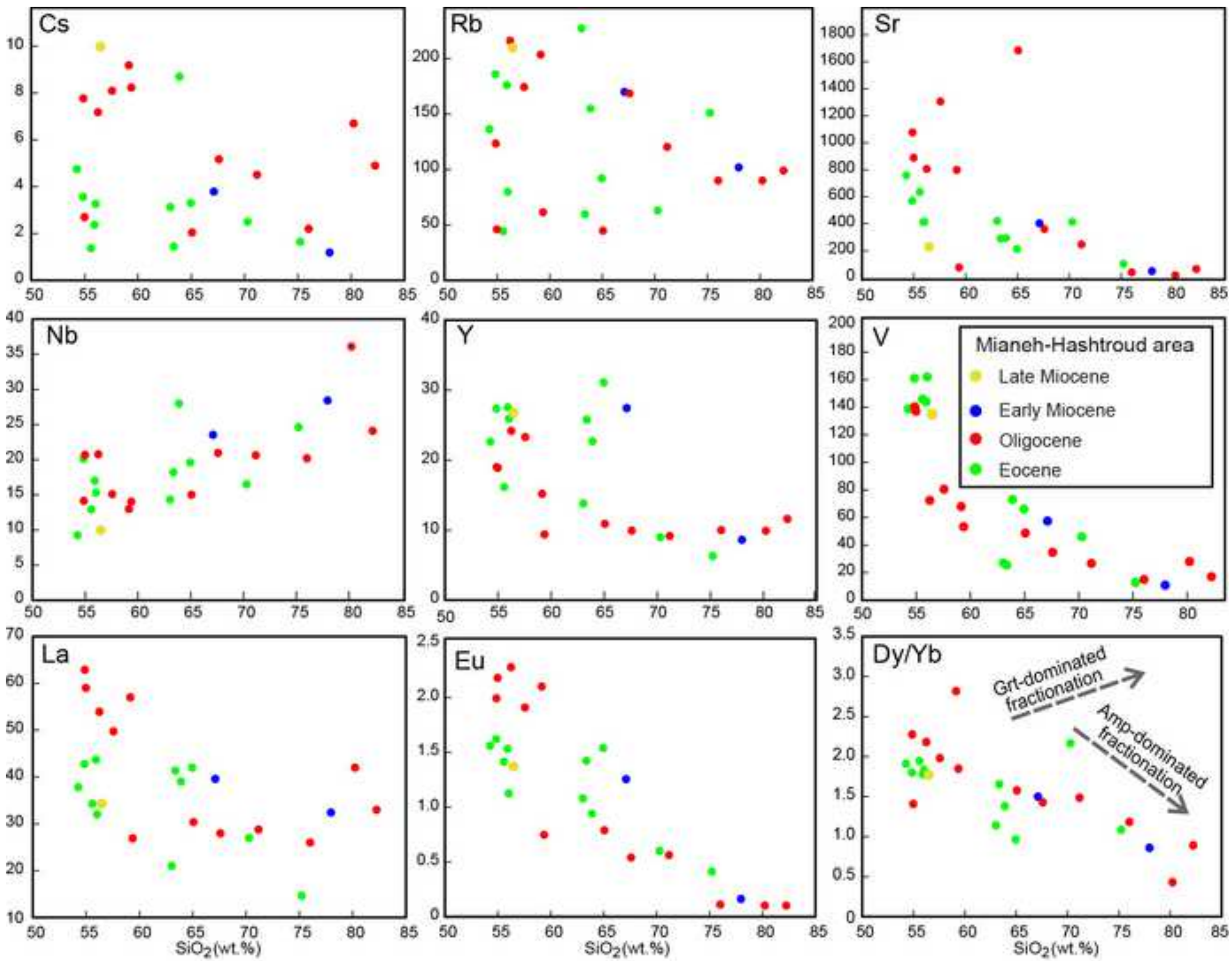

Figure 11
Click here to download high resolution image

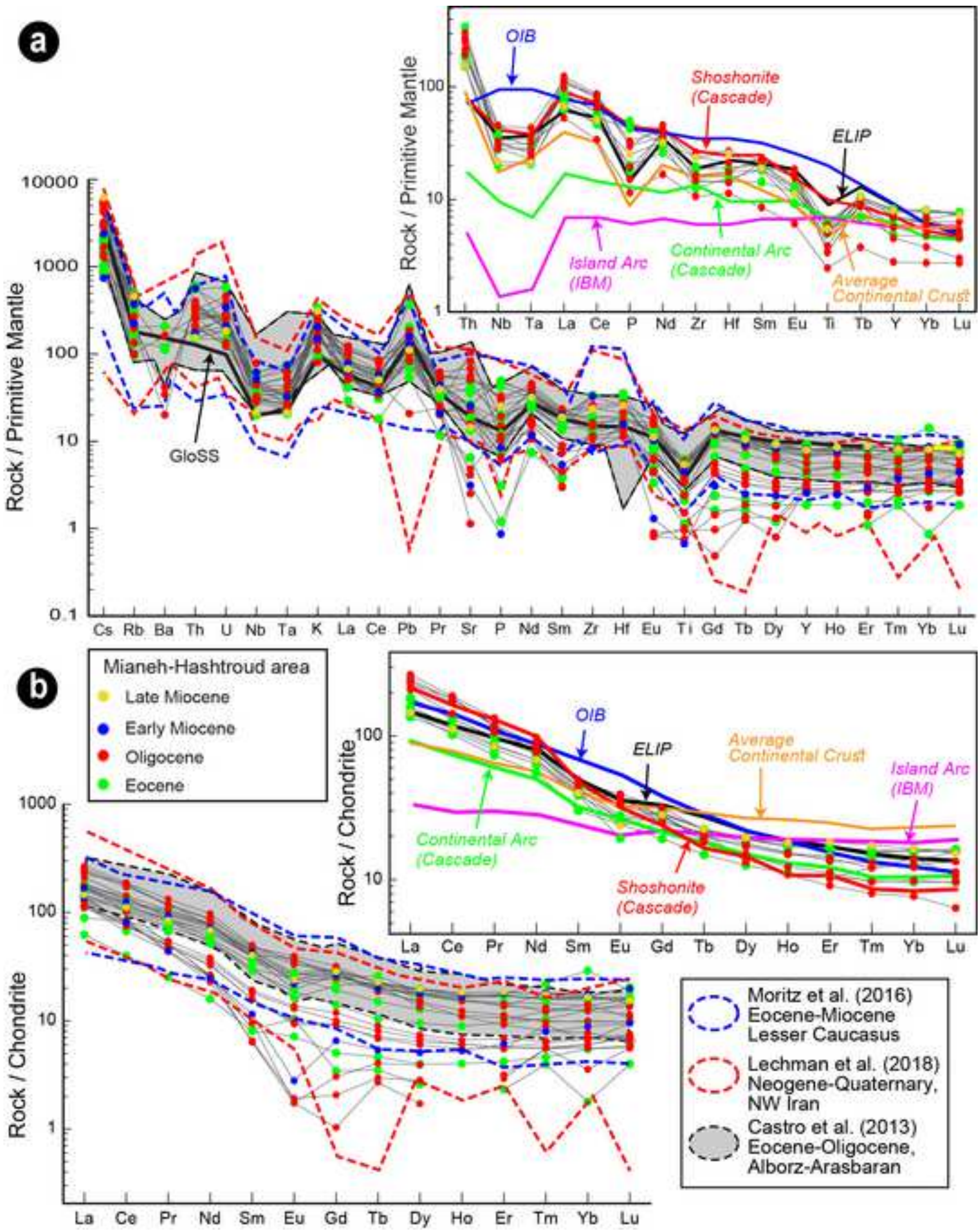

Figure 12

Click here to download high resolution image

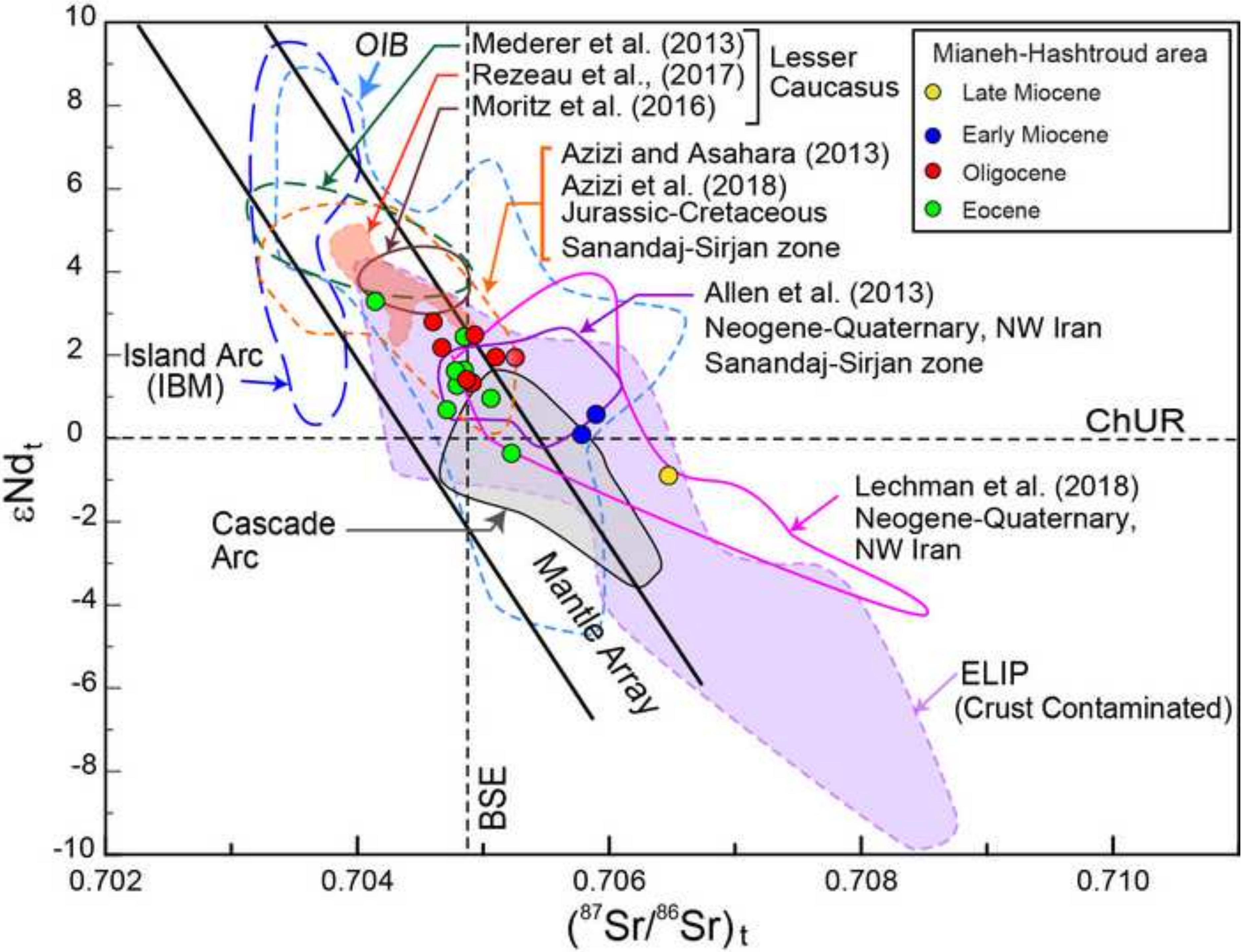

Figure 13

Click here to download high resolution image

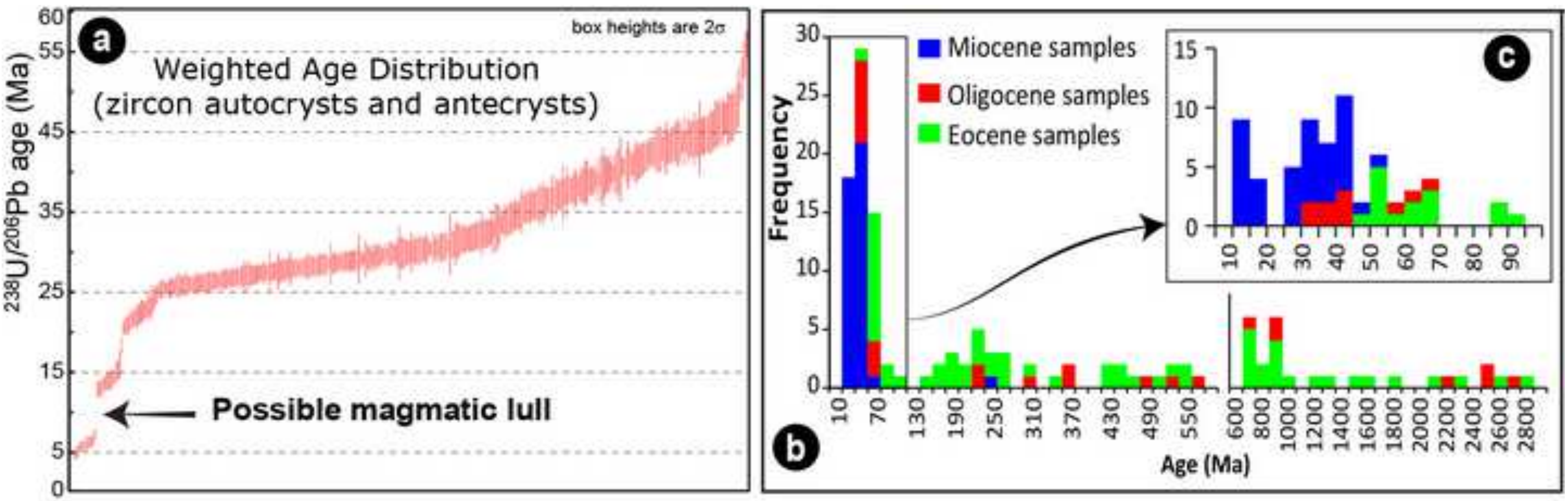

Figure 14
Click here to download high resolution image

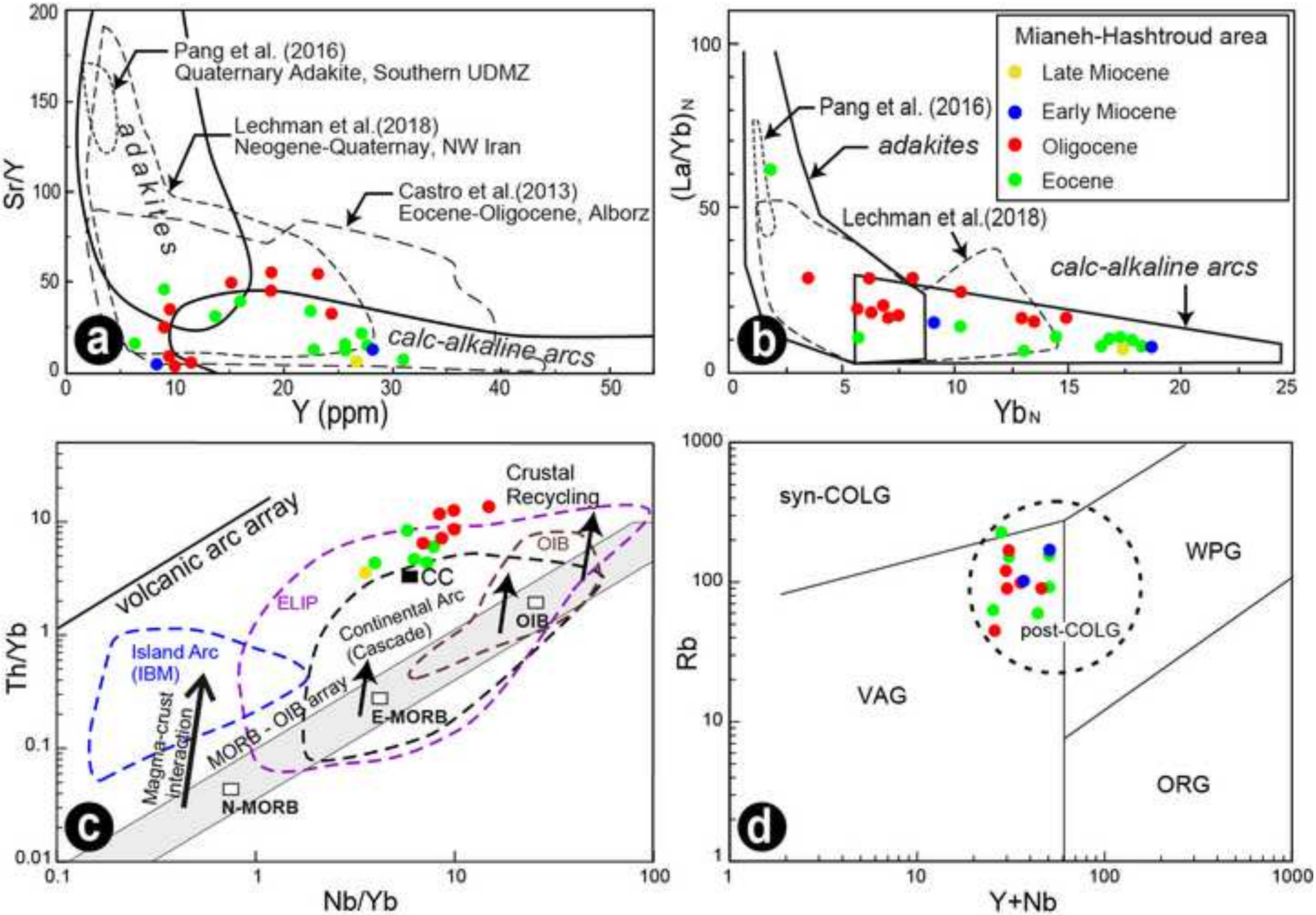

Figure 15

Click here to download high resolution image

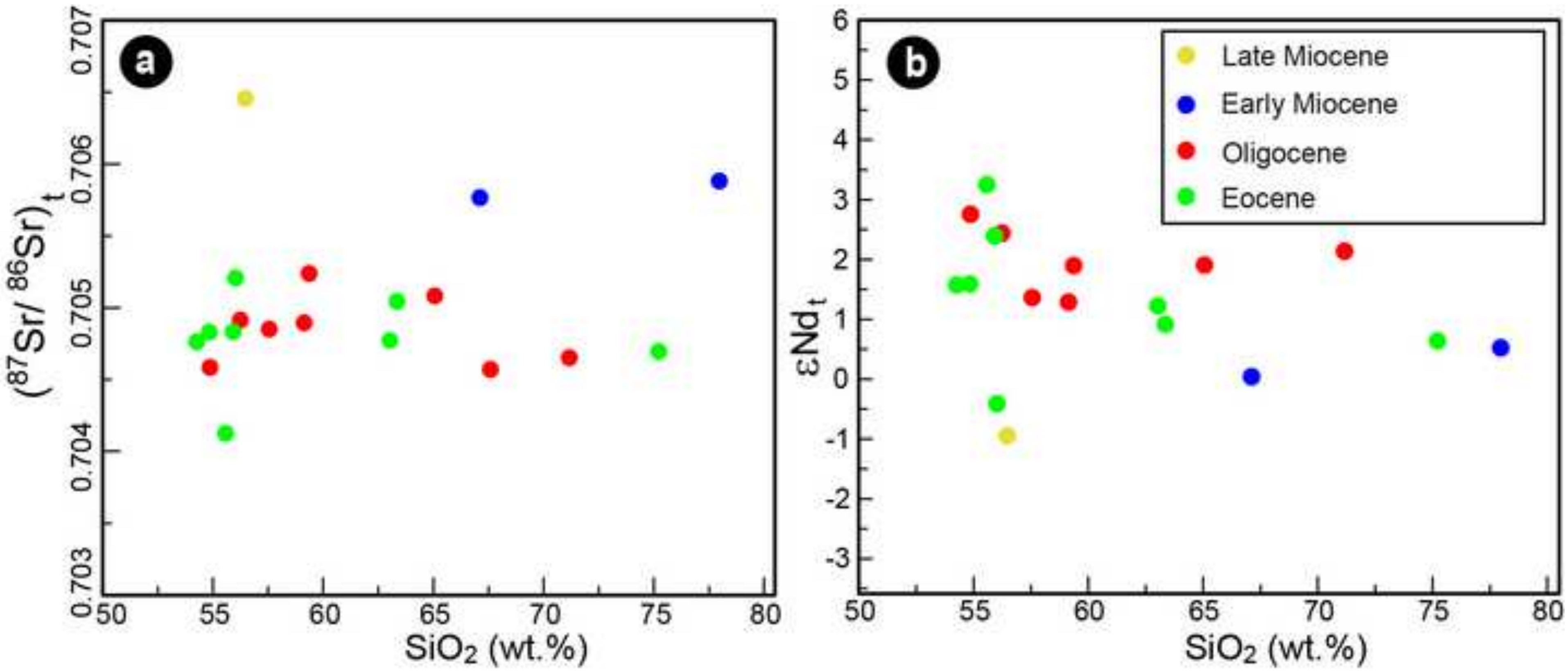

Figure 16

Click here to download high resolution image

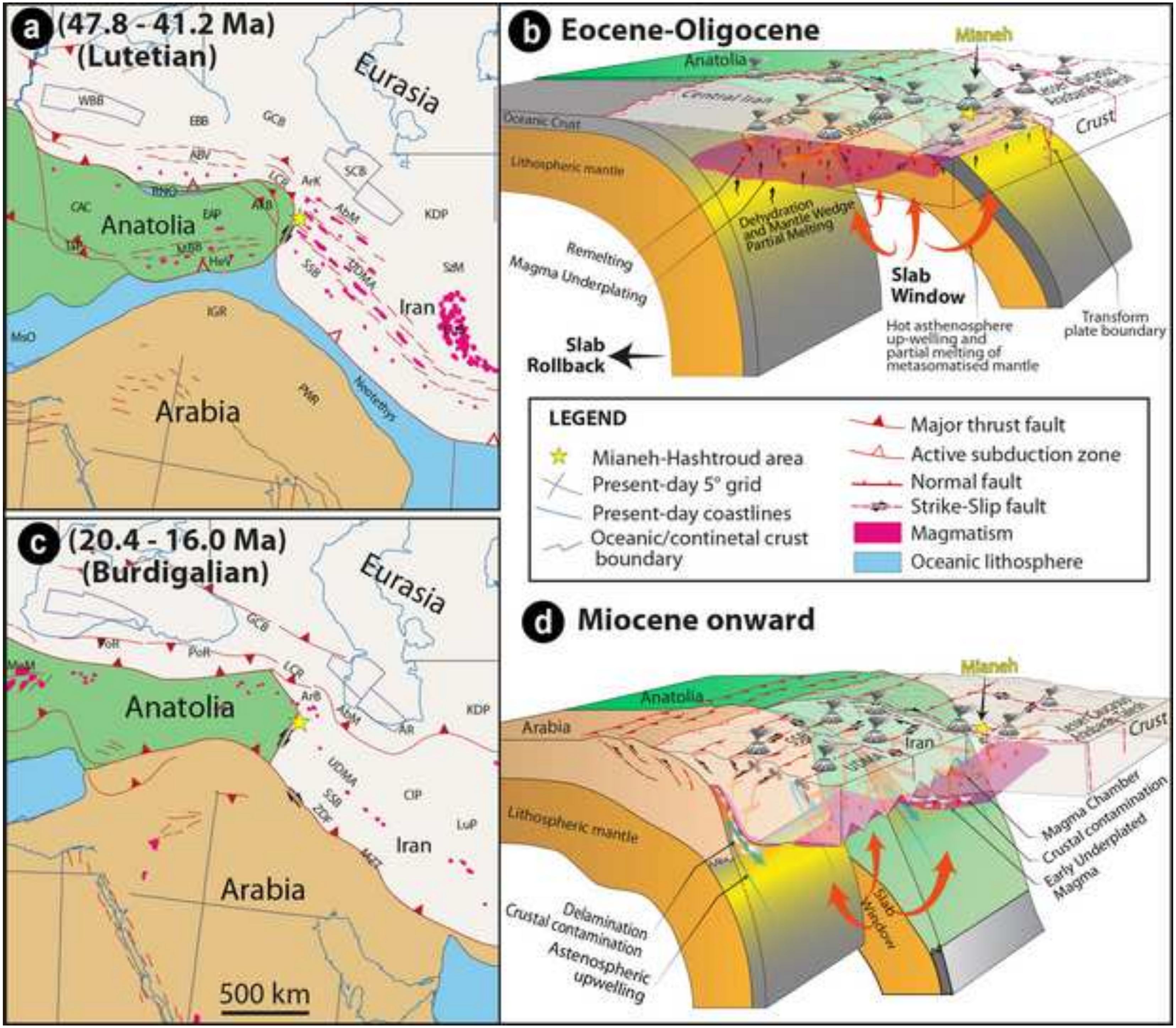

**Table 1**

**Table 1- Petrographic description of the studied samples from the Mianheh-Hashtroud, with location and ages**

| Sample | Coordinates Easting | Northing | Age[*] | Rock Type (TAS)[**] | Texture | Mineralogy |
|---|---|---|---|---|---|---|
| | | | | Country Rocks | | |
| MN04 | 47.59476 | 37.403774 | Eocene | Trachyte | Porphyritic-hypohyaline | Phenocrysts: Pl; Matrix: Pl microliths, glass<br>Accessory Minerals: Oxides, Ap, Zrn |
| MN33 | 47.59948 | 37.401769 | Eocene (43.4±2.6 Ma) | Trachyte | Porphyritic-hypohyaline | Phenocrysts: Pl; Matrix: Pl microliths, glass<br>Accessory Minerals: Oxides, Ap, Zrn |
| MN37 | 47.34281 | 37.428071 | Eocene | Trachy-andesite | Porphyritic-hypohyaline (aphanitic matrix) | Phenocrysts: Pl, Amp (mostly altered);<br>Matrix: Pl, Kfs, Amp(mostly altered), glass<br>Accessory Minerals: Oxides, Ap, Zrn. |
| MN38 | 47.59796 | 37.415256 | Eocene (38.8±1.1 Ma) | Basaltic trachy-andesite | Porphyritic-hypohyaline (aphanitic matrix) | Phenocrysts: Amp, Qz, Pl; Matrix: Pl, Cpx, Amp, glass<br>Accessory Minerals: Oxides, Ap, Zrn |
| | | | | Intrusive Rocks | | |
| MN09 | 47.37515 | 37.410123 | Eocene (44.32±0.58 Ma) | Monzodiorite | Equigranular-holocrystalline | Pl, Kfs, Qz, Amp<br>Accessory Minerals: Ap, Zrn |
| MN10A | 47.41352 | 37.426864 | Eocene (36.75±0.62 Ma) | Granite | Porphyritic-holocrystalline | Kfs, Qz, Ms, Bt (mostly altered) |
| MN10B | 47.41352 | 37.426864 | Eocene (?) | Monzonite (Enclave in MN10A) | Porphyritic-holocrystalline | Pl, Qz, Kfs, Bt, Amp (mostly altered)<br>Accessory Minerals: Oxides, Ap, Zrn |
| MN10C | 47.41352 | 37.426864 | Eocene (?) | Monzonite (Enclave in MN10A) | Porphyritic-holocrystalline | Pl, Kfs, Amp ± Cpx (mostly altered)<br>Accessory Minerals: Oxides, Ap, Zrn |
| MN12 | 47.39964 | 37.400148 | Eocene | Quartz monzonite | Equigranular-holocrystalline | Pl, Kfs, Qz, Bt<br>Accessory Minerals: Ap, Zrn. |
| MN67 | 47.40255 | 37.393276 | Eocene (40.69±0.88) | Syenite | Porphyritic-holocrystalline | Pl, Kfs, Qz, Amp (mostly altered)<br>Accessory Minerals: Ap, Zrn. |
| MN74 | 47.36233 | 37.392176 | Eocene | Syenite | Porphyritic-holocrystalline | Pl, Kfs, Qz, Amp (mostly altered)<br>Accessory Minerals: Oxides, Ap, Zrn. |
| | | | | Hypabyssal/Subvolcanic Rocks | | |
| MN02A | 47.59636 | 37.399305 | Oligocene | Syenite | Porphyritic-holocrystalline (aphanitic matrix) | Qz, Kfs, Pl, Bt, oxides |
| MN02B | 47.59476 | 37.403774 | Oligocene (32±1.30 Ma[***]) | Monzonite | Porphyritic-holocrystalline (aphanitic matrix) | Qz, Kfs, Pl, Bt, oxides |
| MN03 | 47.59476 | 37.403774 | Oligocene | Syenite | Porphyritic-holocrystalline (aphanitic matrix) | Qz, Kfs, Pl, Bt, oxides |
| MN45 | 47.20277 | 37.527598 | Oligocene (30.21±0.41) | Monzonite | Equigranular-holocrystalline | Pl, Kfs, Amp, Bt<br>Accessory Minerals: Ap, Zrn |
| MN65 | 47.58964 | 37.406518 | Oligocene | Monzonite | Porphyritic-holocrystalline | Pl, Kfs, Amp, Cpx, Oxides |
| MN76 | 47.17682 | 37.52972 | Oligocene (28.40±0.86) | Granite | Porphyritic-holocrystalline (phaneritic matrix) | Pl, Kfs, Qz, Bt, Ms<br>Accessory Minerals: Ap, Zrn |
| | | | | Volcanic Rocks | | |
| MN05 | 47.35096 | 37.42990 | Early Miocene (22.6±0.41) | Rhyolite | Porphyritic-hypohyaline | Phenocrysts: Pl , Kfs, Qz ; Matrix: Qz, Kfs, glass<br>Accessory Minerals: Ap, Zrn |
| MN07 | 47.34468 | 37.428935 | Early Miocene | Trachyte | Porphyritic-hypohyaline | Phenocrysts: Pl; Matrix: Pl, Oxides, glass<br>Accessory Minerals: Ap, Zrn |
| MN19 | 47.59745 | 37.41297 | Oligocene (28.52±0.55[***]) | Dacite | Vitrophyric | Phenocrysts: Pl, Bt, Amp, Qz; Matrix: glass<br>Accessory Minerals: Oxides, Ap, Zrn |
| MN20 | 47.62194 | 37.441021 | Oligocene | Rhyolite | Porphyritic-hypohyaline | Phenocrysts: Kfs, Qz; Matrix: Kfs, Qz, glass<br>Accessory Minerals: Oxides, Ap, Zrn. |
| MN35 | 47.58807 | 37.39960 | Late Miocene (5.94±0.24) | Trachy-andesite | Porphyritic-hypohyaline | Phenocrysts: Pl, Amp, Cpx (mostly altered); Matrix: Pl, Kfs, glass<br>Accessory Minerals: Oxides, Ap, Zrn |
| MN39 | 47.55393 | 37.405466 | Oligocene (28.18±0.8) | Dacite | Vitrophyric | Phenocrysts: Pl, Qz, Bt, Amp (mostly altered); Matrix: glass<br>Accessory Minerals: Oxides, Ap, Zrn. |
| MN43 | 47.55949 | 37.420241 | Oligocene (26.97±0.35) | Andesite | Porphyritic-hypohyaline | Phenocrysts: Qz, Cpx, Bt ; Matrix: Pl, Kfs, Cpx, glass<br>Accessory Minerals: Ap, Zrn. |
| MN44 | 47.57207 | 37.401251 | Oligocene (26.19±0.54) | Rhyolite | Vitrophyric | Phenocrysts: Pl, Qz,Bt; Matrix: glass<br>Accessory Minerals: Oxides, Ap, Zrn. |
| MN73 | 47.50650 | 37.383772 | Oligocene | Rhyolite | Porphyritic-hypohyaline | Phenocrysts: Pl, Kfs, Qz; Matrix: Kfs, Pl, Qz, glass<br>Accessory Minerals: Oxides, Ap, Zrn. |

[*]When reported, U-Pb zircon ages (this study); [**]For the intrusive rocks the nomenclature is after Middlemost (1994); [***] after Rabiee et al., (2019)

**Table 2 Supplementary data**

**Click here to download e-component: Table 2 Zircon results new.docx**

**Table 3 Supplementary data**

**Click here to download e-component: Table 3 Mianeh Table Whole Rock.docx**

**Table 4**

# Table 4: Nd-Sr isotope composition of magmatic rock samples from the Mianeh-Hashtroud magmatic district (*)

| Rocktypes | Sample | $^{87}Rb/^{86}Sr$ | $^{87}Sr/^{86}Sr_{(m)}$ | ±1SE | $^{87}Sr/^{86}Sr_{(i)}$ | $^{147}Sm/^{144}Nd$ | $^{143}Nd/^{144}Nd_{(m)}$ | ±1SE | $^{143}Nd/^{144}Nd_{(i)}$ | $\varepsilon Nd_{(t)}$ | T (DM1) (Ma) | T (DM2) (Ma) | $f_{(Sm/Nd)}$ |
|---|---|---|---|---|---|---|---|---|---|---|---|---|---|
| Standard (Andesite) | JA-1 | | 0.703547 | 0.000006 | | 0.177 | 0.512094 | 0.000005 | | | | | |
| Standard (Granite) | JG-1a | | 0.710981 | 0.000006 | | 0.133 | 0.512391 | 0.000004 | | | | | |
| Eocene country rocks | MN04 | 1.562 | 0.705726 | 0.000006 | 0.70477 | 0.111 | 0.512693 | 0.000014 | 0.512662 | 1.54 | 725 | 775.21 | -0.4357 |
| | MN33 | 1.443 | 0.705885 | 0.000007 | 0.70504 | 0.109 | 0.512675 | 0.000004 | 0.512646 | 1.18 | 732 | 799.76 | -0.4474 |
| | MN37 | 0.520 | 0.705095 | 0.000006 | 0.70476 | 0.113 | 0.512713 | 0.000004 | 0.512680 | 1.94 | 715 | 747.67 | -0.4241 |
| | MN38 | 0.201 | 0.704236 | 0.000007 | 0.70412 | 0.108 | 0.512793 | 0.000005 | 0.512766 | 3.47 | 553 | 609.07 | -0.4527 |
| Intrusive rocks | MN09 | 0.558 | 0.70556 | 0.000006 | 0.70521 | 0.121 | 0.512613 | 0.000004 | 0.512578 | -0.06 | 938 | 912.76 | -0.3864 |
| | MN10A | 4.256 | 0.706931 | 0.000006 | 0.70469 | 0.101 | 0.512656 | 0.000005 | 0.512632 | 0.81 | 699 | 819.66 | -0.4891 |
| | MN10B | 1.235 | 0.70548 | 0.000006 | 0.70483 | 0.113 | 0.512749 | 0.000024 | 0.512722 | 2.56 | 651 | 681.36 | -0.4241 |
| | MN10C | 0.943 | 0.705326 | 0.000006 | 0.70483 | 0.114 | 0.512708 | 0.000004 | 0.512680 | 1.76 | 717 | 746.99 | -0.4214 |
| Hypabyssal/ Subvolcanic rocks | MN02A | 0.738 | 0.705229 | 0.000006 | 0.70489 | 0.106 | 0.512687 | 0.000007 | 0.512665 | 1.33 | 685 | 769.39 | -0.4628 |
| | MN02B | 0.775 | 0.705266 | 0.000006 | 0.70491 | 0.110 | 0.512747 | 0.000008 | 0.512724 | 2.48 | 626 | 676.62 | -0.4418 |
| | MN03 | 0.386 | 0.705027 | 0.000006 | 0.70485 | 0.111 | 0.512692 | 0.000005 | 0.512669 | 1.40 | 715 | 764.93 | -0.4355 |
| | MN45 | 0.332 | 0.704725 | 0.000006 | 0.70458 | 0.101 | 0.51276 | 0.000004 | 0.512740 | 2.75 | 556 | 648.49 | -0.4858 |
| Volcanic rocks | MN05 | 5.972 | 0.707747 | 0.000006 | 0.70588 | 0.091 | 0.512639 | 0.000005 | 0.512626 | 0.32 | 654 | 829.70 | -0.5357 |
| | MN07 | 1.219 | 0.706147 | 0.000006 | 0.70577 | 0.118 | 0.512618 | 0.000005 | 0.512601 | -0.17 | 876 | 874.88 | -0.3993 |
| | MN35 | 2.651 | 0.706683 | 0.000006 | 0.70646 | 0.116 | 0.512555 | 0.000004 | 0.512550 | -1.56 | 940 | 955.13 | -0.4077 |
| | MN39 | 0.077 | 0.705113 | 0.000007 | 0.70508 | 0.100 | 0.512715 | 0.000005 | 0.512697 | 1.85 | 606 | 717.52 | -0.4934 |
| | MN43 | 2.340 | 0.706136 | 0.000007 | 0.70524 | 0.100 | 0.512714 | 0.000004 | 0.512696 | 1.82 | 610 | 718.54 | -0.4908 |
| | MN44 | 1.407 | 0.705172 | 0.000006 | 0.70465 | 0.097 | 0.512725 | 0.000004 | 0.512709 | 2.03 | 577 | 698.51 | -0.5068 |

*(*)The natural Nd and Sr isotope ratios were normalized based on $^{143}Nd/^{144}Nd = 0.7219$ and $^{87}Sr/^{86}Sr = 0.1194$. The CHUR (Chondritic Uniform Reservoir) values, $^{147}Sm/^{144}Nd = 0.1967$ and $^{143}Nd/^{144}Nd = 0.512638$, were used to calculate the $\varepsilon^0$ (DePaolo and Wasserburg, 1976). $f_{(Sm/Nd)} =[(^{147}Sm/^{144}Nd_{sample})/\ ^{147}Sm/^{144}Nd_{CHUR}]-1$ and $f_{(Rb/Sr)} = =[(^{87}Rb/^{86}Sr_{sample})/\ ^{87}Rb/^{86}Sr_{CHUR}]-1$. $T_{DM2} =(T_{DM1} -(T_{DM1}-t)[(f_{cc}-f_s)/(f_{cc}-f_{DM})]$, where $f_{cc}$, $f_s$ and $f_{DM}$ are the $f_{Sm/Nd}$ values of the continental crust, the samples and depleted mantle, respectively, and t is the formation age of the rock; in this calculation $f_{cc} = -0.4$, $f_{DM} = 0.086426$. $T_{DM1} =1/\lambda \ln[(^{143}Nd/^{144}Nd)_{sample}-0.51315]/\ ^{147}Sm/^{144}Nd)_{sample} -0.2137] + 1$. Detail information regarding standard samples are available in https://gbank.gsj.jp/geostandards/gsj1maine.html.*